University of Southampton

Department of Electrical Engineering

Electrostatic hazards associated with pneumatic transport and storage of powders

A thesis submitted for

the Degree of Doctor of Philosophy

by

Vahid Ebadat

August 1989

CONTENTS **Page No**

CONTENTS (contd) **Page No**

UNIVERSITY OF SOUTHAMPTON

ABSTRACT

FACULTY OF ENGINEERING AND APPLIED SCIENCE
ELECTRICAL ENGINEERING DEPARTMENT

Doctor of Philosophy

ELECTROSTATIC HAZARDS ASSOCIATED WITH PNEUMATIC TRANSPORT AND STORAGE OF POWDERS

by Vahid Ebadat

In recent years there have been many reports of dust explosions associated with industries handling particulate materials. A study has been undertaken to investigate the influence of various transporting parameters of a pneumatic conveying system on the tribo-electrification of powders. These parameters include powder transportation velocity, powder flow rate, space charge field of the powder passing through the pipes, particle size, resistivity and relative humidity. The specific charge is a linear function of the transport air velocity. The specific charge reaches a saturation level as the powder flow rate increases and falls at high powder flow rates. The saturation specific charge of powder particles is determined by a self generated space charge field during normal pneumatic conveying. The tribo-charging can hence be controlled by controlling the space charge field.

Hazardous conditions may arise when the charged powder enters a storage silo as explosible dust concentrations can result and, with the presence of an ignition source, a risk of fire and explosion exists. It is generally accepted that dispersed flammable dust clouds may be ignited by discharges from electrostatically charged conducting objects. These discharges can however be excluded if grounded conductive equipment is used. The question 'Can a flammable powder be ignited by the charge accumulated on the powder itself, even if the powder is handled in earthed conductive installation?' is investigated. The magnitude and incendivity of discharges from the surface of bulked powder and the dust cloud to probes is studied. It is possible to obtain incendive discharges which are capable of igniting a propane/air mixture with a minimum ignition energy of 0.25 mJ. The experimental results from a laboratory scale rig show that the largest probability of ignition of propane/air/nitrogen are defined for moderate streaming currents and specific charge densities.

ACKNOWLEDGEMENTS

The author would like to express his sincere gratitude to Professor A G Bailey for his guidance and encouragement throughout the duration of this project. The Marchwood silo project was managed by Dr Sampuran Singh of the Wolfson Electrostatics Advisory Unit, The University, Southampton, to whom gratitude is similarly expressed. Many thanks must also go to Mr J Smallwood of the Electrical Engineering Department, The University, Southampton, for many helpful discussions and to Mr R Ball and the staff of the Wolfson Electrostatics Advisory Unit for providing excellent technical assistance. The experimental work during the first phase and the early part of the second phase of the Marchwood silo project was carried out with major contributions by Mr D L G Thorpe and Dr P Cartwright, whose work is greatly acknowledged. Financial support was provided by the Wolfson Foundation, the Health and Safety Executive (UK), BASF (Germany), BP Chemicals (UK), British Ports Association (UK), Dutch State Mines (Holland), ICI Organics (UK), Cadbury Schweppes (UK), CPC Ltd (UK), Insurance Technical Bureau (UK), National Grain and Feed Association (USA), Nordson Corporation (USA), Shell Inter-nationale (Holland), Tate and Lyle Refineries (UK), and United Biscuits (UK), to whom the author is most grateful.

Finally, none of this work would have been possible if it had not been for the hard work and dedication of the late Professor Bill Bright in gaining the support of the above mentioned sponsors.

LIST OF SYMBOLS

A = Area of equivalent parallel plate capacitor

a = Radius of contact area

B = Geometrical constant = $\frac{\pi S_a S_b}{(S_b - S_a)}$

C = Capacitance

C_A = Capacitance per unit area

C_E = Electrometer input capacitance

C_1 = Faraday Cup capacitance

d = Distance from the centre of particle to the wall

d_c = Critical separation distance

dl = Infinitesimal pipe length

$\frac{dQ}{dn}$ = Charge exchange per collision

$\frac{dQ}{dt}$ = Rate of charge transfer or input

dq = Change of charge per unit mass

D = Electric flux density

D_s = Energy density of surface states per unit area

E = Electric field strength

e = Electron charge 1.602×10^{-19} C

E_{cl} = Electric field strength due to filling powder column

E_{cn} = Electric field strength due to powder cone

E_d = Electric field strength due to powder deposits

E_f = Electric field strength due to airborne fines

E_{max} = Maximum electric field strength

E_r = Externally applied field

E_R = Superimposed electric field strength on the pipe wall

f = Correction factor of the true area

I = Electrical current

I_s = Streaming current

J = Total current density

K = $k + 1$

k = Charge transfer reduction factor = $\frac{Af}{2\pi r^2} - \frac{NRAf}{2}$

k_1 = Charging rate

k_2 = Proportionality factor of the discharging rate

l = Charge leakage factor

L = Length

m = Solid loading (mass of powder/volume of transport air)

$\dot{m}$ = Powder mass flow rate

N = Number of particles per unit volume

n = Number of collisions by a particle

n_o = Ion pair density

n_p = Number of particles

P_E = Effective pressure at the flowmeter inlet

Q = Electrostatic charge

q = Specific charge density

Q_{max} = Maximum charge

q_{max} = Maximum specific charge density

Q_0 = Previous charge on a particle

q_o = Previous specific charge density

Q_T = Total charge on a particle

Q_1 = Charge transfer between metal and an insulating particle resulting from V_c

R = Pipe radius

r = Radius of particle

S = Radius of macrosphere formed by bulked powder

S_a = Radius of bulking point spherical shell

S_b = Radius of powder heap spherical shell

V = Voltage

v = Particle velocity

V_b = Potential difference caused by the bulk of particles

V_c = Effective contact potential

V_s = Surface potential

V_1 = Induced potential difference

W = Work function

W_i = Insulator Fermi level

W_i' = New insulator Fermi level as a result of state densities

ΔW_i = $W_i' - W_i$

W_m = Metal Fermi level

Z = Electrical resistance

Δt = Contact time

ϵ = Permittivity

ϵ_o = Permittivity of free space

ϵ_r = Relative permittivity

μ_+ = Positive ionic mobility

μ_- = Negative ionic mobility

ρ = Powder resistivity

σ = Surface charge density

σ_c = Conductivity

σ_m = Maximum surface charge density

τ = Relaxation time

χ_o = Thickness of a layer of charge on the insulator surface

Chapter 1

Introduction

CHAPTER 1

INTRODUCTION

1.1 Pneumatic Conveying - A Historical View

Pneumatic conveying could have originated when man discovered that hollow stems were suitable for blowing poison darts. The Experimental Pneumatic Railway was built in 1864 at Crystal Palace using the principle of vacuum to move a carriage which had been fitted with a sealing diaphragm through a railway tunnel [Huggett (1987)]. Although the Experimental Pneumatic Railway was not a success, the idea has been pursued, and before 1890 there was sufficient knowledge for a dock silo to be built at Millwall on the Thames in London to receive grain from ships via four fixed towers, each containing a vacuum conveying system operating at 100 tonnes per hour.

During the one hundred year history of the application of air principles, pneumatic conveying has become an essential tool in industry saving considerable manpower in laborious, dirty and dangerous operations. Pneumatic systems have a widespread application in many industries, for example, cement, minerals, power, chemicals, plastics, foodstuffs and waste handling industries.

Some of the more significant events and developments in the pneumatic conveying industry are shown in Table 1.1.

Table 1.1 **Pneumatic Conveying Historical Landmarks**
[Dixon (1981), Mason (1987), Stoess (1970)]

1864	Experimental Pneumatic Railway was built at Crystal Palace.
1910	Henry Simon installed a grain unloading system which was a combined tug and pneumatic grain discharging plant called "Garryowen II" with a capacity of 200 tonnes per hour by suction or 135 tonnes per hour by suction/blowing.
1919	A fluid solids pump, known today as the Fuller Kinyon pump, was commercially installed.
1920's	Beginning of a theoretical approach to pneumatic conveying began and the black art became more of a science.
Since 1945	The increasing productivity demanded higher conveying rates; larger factories and complexes led to longer conveying distances. Ship unloading rates have risen to over 500 tonnes per hour. Investigations are in hand for 1000 tonnes per hour.
21st Century	Expert systems will have been developed to answer, quickly and economically, the question "What is the best storage, transport and control system for a particular bulk solids handling plant?"

1.2 Advantages of Pneumatic Conveying over Mechanical Conveyors

Depending on the particular product, mechanical means are occasionally used and many comprise of belt conveyors, bucket elevators, screws or drag chain conveyors. However, mechanical transport systems are rather rare as they cannot offer the advantages of pneumatic conveying, which are as follows [Dixon (1981)]:

a) Dust free operation from totally enclosed systems.
b) Low maintenance costs and down time.
c) Minimum product contamination.
d) Routing flexibility.
e) Ease of inerting.
f) Automation.

In many installations today the pneumatic conveyor has become a necessary and integrated link within a much larger material handling function. Often there will be a series of pneumatic conveyors forming a chain of events. This is illustrated in the system diagram, shown in abbreviated form in Figure 1.1, which is totally automatic.

1.3 Pneumatic Conveying Systems

The most important features of any pneumatic conveyor are the methods of introducing the powder into the air stream and propelling the mixture of material and air down the conveying pipeline. Pneumatic conveying systems come in a number of types including: dilute phase, medium phase and dense phase systems. Each phase can be defined in terms of the mass flow ratio, which is the ratio of the mass of solids to the mass of conveying air.

Dilute phase systems, which are the oldest form of pneumatic conveying, transport the material as discrete particles. The high velocities involved cause wear on the parts of the conveyor that are in contact with the material being conveyed. In addition, there is more attrition of the conveyed material in this class of conveying than in other systems [Flain (1972)].

Figure 1.1 A Totally Automatic Material Handling Installation

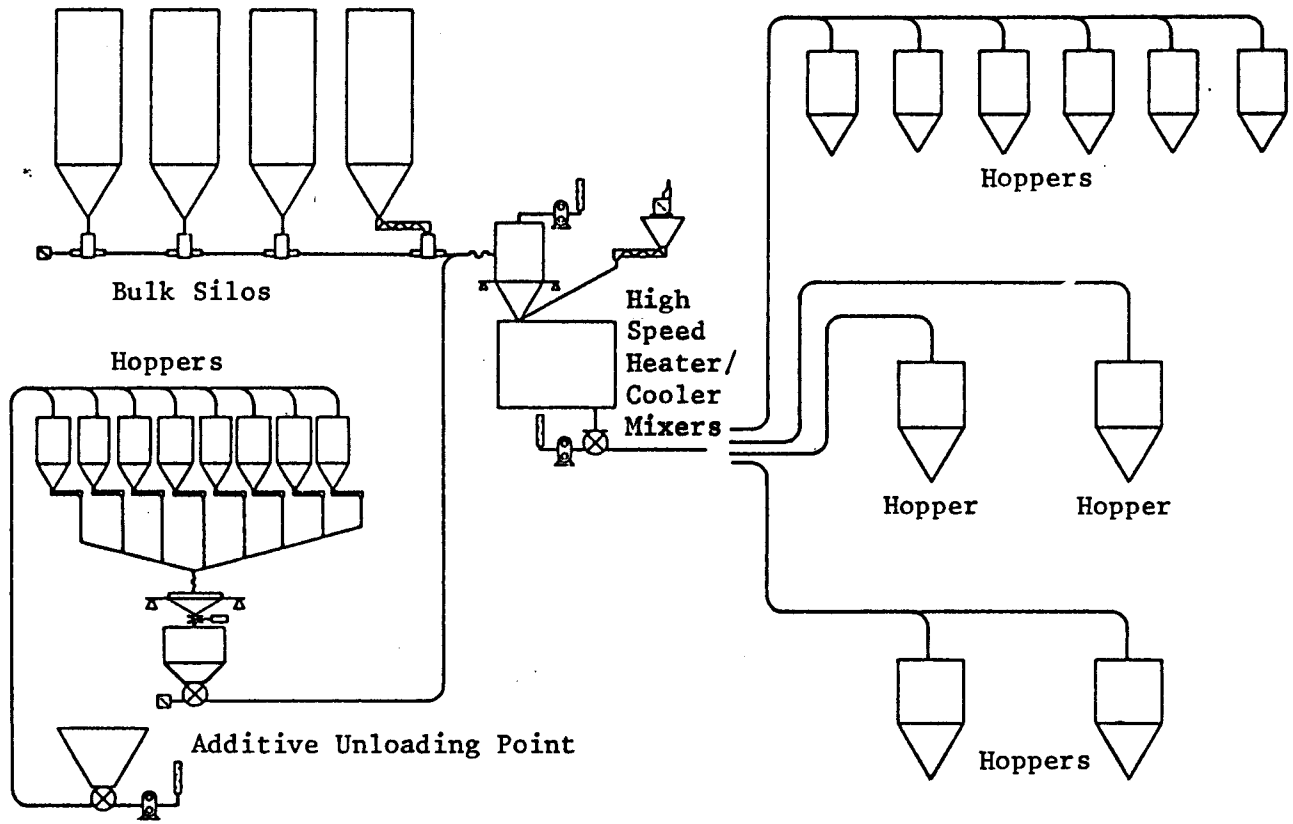

Medium phase systems operate at lower air velocities and correspondingly high solids loadings, and rely on efficient fluidisation of the material. As a result of fluidisation, the internal angle of friction decreases, thus less of the applied pressure is taken by the pipe walls and more is transmitted through the powder/air mixture. Medium phase conveyors are the most popular class of conveyor. Reduction in the angle of internal friction lessens the chances of blockage and allows longer conveying distances.

The efficiency of pneumatic transport systems increases with increasing the mass flow ratio. Dense phase conveying systems arrange for the material to be fed in the form of discrete short plugs.

A given flow regime cannot be specified in the conveying pipe by the sole definition of the loading factor. In a long conveying pipe and with a constant mass flow ratio, as the flow rate increases on expansion of highly compressed air, different flow conditions may occur. Therefore dense phase, medium phase and dilute phase conveying types can be observed along the length of the conveying pipe.

1.4 Pneumatic Conveying and Dust Explosion Hazard

The ease with which powdered products can be transported and the ever increasing transportation speeds of pneumatic conveying systems has resulted in the widespread use of such installations in many industries, for example, plastics, food, pharmaceutical and so on, as a means of transporting particulate materials into silos. In parallel with the use of pneumatic conveying, there have been many reports of dust explosions associated with industries handling particulate materials. The effects of a dust explosion can range from a small fire, resulting only in loss of production, to more devastating effects with considerable loss of life and property.

1.4.1 A Historical View of Dust Explosions

The first known reported dust explosion occurred in a Turin mill by flour dust in 1785 [Field (1982)]. The earliest explosions involving industries handling powder materials, like the coal industry and flour mills, were attributed to an inflammable gas which was thought to be produced by the dispersed dust. It was not until the latter part of the Nineteenth Century that it was realised that coal dust could ignite and explode in the absence of gas, or that flour dust alone was responsible for the increasing number of explosions in mills.

The Twentieth Century has seen an increase in the frequency of dust explosions because of the rapid expansion of powder handling industries and also the wider variety of materials. In the year 1919 the most devastating dust explosion outside the coal industry was seen with 43 people being killed in a dust explosion in a starch factory in Iowa, USA. Major dust explosions, like any other disaster involving serious loss of life, have often initiated research into the problem. An early instance of this was the independent research carried out in the USA, UK and France following 18 deaths in a Scottish mill in 1872 and 6 deaths in a French dye factory in 1978 [Field (1982)].

The two dust explosions which probably received more international coverage than any previous incident, and caused the devastating consequences of such explosions to be recognised, occurred in December 1977. As a result of grain dust explosions, in Texas 18 people died while 36 died in Louisiana.

"Little Hope of Finding Workers Alive". This is the translation of a news article from 'Le Figaro' - 20th October 1982, regarding the French grain silo explosion. After clearing the debris for 24 hours the toll of the catastrophe was four dead, one seriously injured and eight missing.

1984 witnessed another grain silo explosion with two fatalities. Extracts from an article in the Cork Examiner (Ireland) 31st October 1984:

"Second Body Found After Silo Explosion".

"The silo in which the explosion occurred consisted of 48 circular steel bins, each rising to about 100 ft and each with a capacity to hold 400 tonnes of grain. It was in one of these that the explosion was believed to have happened, blasting upwards and tearing through the eighth floor, which ran across the top of all the bins. The force of the blast blew away the top floor and the roof."

The frequency and severity of some dust explosions reported by British Materials Handling Board [Abbott (1986)] are summarised in Table 1.2.

Table 1.2 Some Dust Explosion Statistics

Country	Period	Explosions	Fatalities (Injuries)
USA	1900-1956	1120	640 (1700)
USA	1958-1977	220*	48 (500)
FGR and Neighbouring Countries	1960-1972	4000	
UK	1958-1967	247	9 (324)
UK	1967-1979	474	25** (633)

* grain industry only

** 10 in 2 incidents

1.4.2 Requirements of a Dust Explosion

The dust and also the atmosphere into which the dust is suspended require several characteristics in order for a dust explosion to take place. A number of conditions are as follows [Dixon (1981), Field (1982), Cartwright (1986), Palmer (1973)]:

i) The dust must be flammable.
Three methods of classification of dusts are usually found in the literature.

'Index of explosibility', put forward by the US Bureau of Mines, compares various explosion parameters of the dust with a standard dust, Pittsburg coal, chosen because considerable data exists on the behaviour of this material in large scale tests. The index of explosibility is defined as the ignition sensitivity multiplied by the explosion severity. If the index is greater than 1, the hazard is greater than for coal which is taken to be the borderline between a weak and a strong hazard. This method gives a useful guide to relative problems but is very complicated for the amount of information which is gained from a knowledge of the index.

The German method classifies the dust according to the damage which might be expected, ie, according to the maximum rate of pressure rise attained in a container of 1 m^3 volume. The maximum rate of pressure rise is multiplied by the cube root of the volume of the container to obtain a constant which is more or less independent of the volume of the vessel.

Although the German method of classification is becoming more general, it gives no idea of the ease of ignition of the powder.

British regulations classify powders very broadly into two groups:

a) "Group A" - Dusts which propagate flame in a vertical dust dispersion tube. The ignition source is either a continuous arc or a heated coil [Cross et al (1982)].

b) "Group B" - Dusts which do not. This does not mean that group (B) dusts never explode. If the dust is flammable at all it may well ignite at elevated temperatures in a furnace apparatus although it cannot be ignited by a spark. High air pressure or the presence of a small quantity of flammable vapour may also render a group (B) dust explosive.

ii) The oxygen content of the atmosphere in which the dust is dispersed must be sufficient to sustain combustion.

iii) The dust concentration must be above the minimum explosible concentration.

iv) The particle size distribution must be capable of supporting combustion. The particle size and shape also affect the dispersability of the dust; if this is poor due to cohesive forces or to entanglement of fibrous particles, then the explosibility limits are also modified.

v) There must be an ignition source of sufficient energy to initiate the explosion.

1.4.2.1 Factors Influencing the Explosion Violence

i) Mobility and turbulence of dust suspension.
ii) Homogeneity of dust suspension.
iii) Composition of dust and impurities.
iv) Particle size and distribution.
v) Ambient pressure and temperature.
vi) Presence of inert and diluent gases.
vii) Moisture content of dust particle.
viii) Presence of flammable gases and volatile species.
ix) Shape and size of vessel.
x) Air flow characteristics in the vessel.
xi) Internal obstructions in the vessel.
xii) Nature and location of ignition sources.

1.4.3 Ignition Sources

A combustible dispersed dust with appropriate particle size and concentration in an atmosphere containing sufficient oxygen to permit combustion requires a source of ignition of appropriate energy to cause a dust explosion. The following main sources of ignition may have sufficient energy to initiate a dust explosion [Field (1982), Cross et al (1982)]:

i) Flames
ii) Hot surfaces
iii) Welding or cutting operations
iv) Friction or impact sparks
v) Electric sparks
vi) Electrostatic discharges.

There are different opinions as to the relative importance of different ignition sources in different powder handling industries. Figure 1.2 shows the frequency of occurrence of different types of ignition sources of 84 recent dust explosions (1979-1984) in the UK [Abbott (1986)].

1.4.4 Static Electricity as an Ignition Source

Among the ignition sources with a potential risk in powder handling processes, static electricity is often regarded as the least traceable. Like any other ignition source, an electrostatic discharge can only be a hazard if the energy content present in the combustible dispersed dust has the necessary minimum value. Today electrostatics is recognised as a source of hazard or nuisance in many industries including petroleum, plastics, chemicals and electronics [Gibson (1983)].

1.4.4.1 Types of Discharge Due to Electrostatic Charging

Electrostatic discharges can be divided into five identifiable types with regard to their energy densities. The ability of these discharges to cause ignition must be investigated if the exclusion of possible ignition sources is adopted as a measure of preventing explosions and fires. The five different types of discharges are

Figure 1.2 BMHB Survey - Types of Ignition Source (Based en 84 Events)
(Abbott (1986))

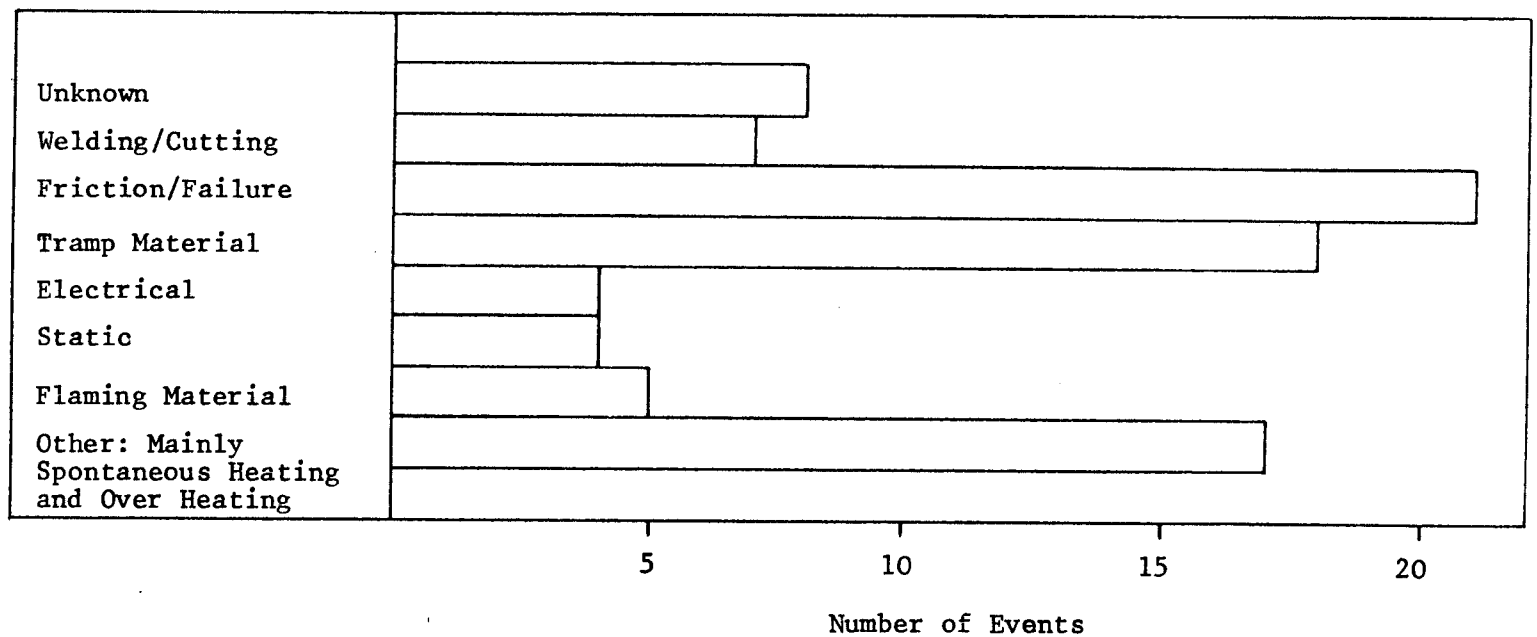

described in the following sections [Cartwright (1986), Maurer (1979), Boyle et al (1950)].

1.4.4.1.1 Spark Discharge

A discharge between conducting objects, one of which is charged and the other grounded, is termed spark discharge. The stored energy from such objects can be calculated from the expression:

$$\text{Discharge energy} = \frac{1}{2} CV^2 \qquad (1.1)$$

where C is the capacitance of the item which is raised to a voltage V by virtue of being charged.

Spark discharges are potentially the most dangerous type of discharges, because most of the energy of the charge accumulated on the isolated conducting object can often be released in a single highly incendive discharge. Since the minimum ignition energies of explosible gas, vapour and dust atmospheres are experimentally determined with the help of spark discharges, the discharge energies calculated according to the above formula can directly be compared to these values. Table 1.3 gives some examples for capacitances and spark energies from possibly insulated items in a plant.

Table 1.3 Typical Metal Items Encountered in Industry with their Capacitance and Stored Energy

Item	Capacitance (pF)	Voltage (kV)	Possible Spark Energy (mJ)
Flange	≈ 10	10	≈ 0.5
Shovel	≈ 20	15	≈ 2
Drum	100-300	20	≈ 40
Person	100-300	10	≈ 10
Road tanker	≈ 1000	15	≈ 100

Spark discharges are the cause of 95-98% of all accidents due to electrostatics [Maurer (1979)].

The incendivity of spark discharges is influenced by a number of parameters such as the length of the spark gap, shape and material of the electrode and voltage, inductance and resistance of the spark generating circuit. Boyle and Llewellyn (1950) demonstrated that the minimum capacitor energy $\frac{1}{2} CV^2$, capable of igniting dust clouds of various powders, decreased quite considerably when a series resistance was introduced in the discharge circuit. Eckhoff (1975) and Eckhoff et al (1976) have shown that the experimental minimum ignition energies for dust clouds are strongly dependent on the discharge times of the electric spark used in the ignition tests. The pressure wave of a spark with discharge time of the order of 1 μs can effectively expel an object with a mass of the order of 1 mg far beyond the distance at which the object is likely to be ignited by the hot spark channel. When the spark discharge time was increased to the order of 1 ms, the disturbance decreased. Felstead et al (1983) measured the effect of electrode characteristics on the measurement of the minimum ignition energy of dust clouds. It was found that the ignition energy increased with electrode material in the order aluminium alloy < lead < brass < stainless steel and decreased as the electrode diameter was reduced from 35 mm to 3.5 mm. The minimum energy required for ignition occurred with electrode gaps of between 11 and 13 mm. The sparks from the human body are less incendive than pure capacitive sparks for a given voltage for gases, vapours and powders [Tolson (1980), Wilson (1983), Glor (1984)].

Spark discharges can more easily be prevented compared to all other discharges, by simply earthing all conductors.

1.4.4.1.2 Brush Discharge

Brush discharges may occur in practice if earthed conducting electrodes with a radius of curvature in the range of about 5 to 50 mm, such as metallic convex bends within vessels, tanks or

silos, the fingertips of personnel or working tools approach a charged insulating surface. High field strengths can be generated in practice from highly charged non-conducting surfaces (plastic bags, walls of pipes and vessels), mists, dust clouds and bulked powders [Glor (1984)]. The field increases as the two surfaces are brought closer together and eventually the air breaks down forming a multi-channelled discharge, known as a brush discharge. Brush discharges can be incendive enough to ignite combustible mixtures of gases or vapours with air. The parameters influencing the incendivity of a brush discharge are the radius of curvature of the electrode, the polarity, the density and the area of the charged surface. Gibson and Lloyd (1965) have shown experimentally that in the range 100-225 cm^2 the charge density was independent of surface area. Above and below this range the charge density decreased. This was presumed to be due to the whole surface not being uniformly charged.

1.4.4.1.3 Propagating Brush Discharge

Another form of brush discharge with much higher energy is a Lichtenburg-like discharge or a propagating brush discharge. This type of discharge occurs when an insulating layer is backed by an earthed conducting material. Materials such as deposits of powder in dust-carrying plants, enamel, thin layers of lacquer or filter tissues, do not initiate propagating brush discharges [Maurer et al (1987)].

In the case of extended sheets of a high resistivity non-conducting material, the charge density for breakdown depends on whether there is an earthed metal either near or in contact with the side of the sheet opposite that where the charging takes place. The presence of an earthed metal behind the sheet causes a redistribution of the field so that much of it is directed towards the metal, leaving less going outwards from the surface. This causes a charge density much greater than the theoretical maximum charge density in air to be accommodated on the non-conductor before discharges occur. The maximum charge density increases as the thickness of the coating or liner decreases.

Propagating brush discharges are capable of igniting dust clouds with minimum ignition energies of several tens of Joules [Glor (1984)].

1.4.4.1.4 Lightning-like Discharge

A high energy discharge from or to a charged cloud is referred to as a lightning-like discharge or dust lightning [Maurer (1979)]. One condition for the occurrence of such discharges is that the volume in which the charged dust cloud is contained must be large. Boschung et al (1977) showed that although the conditions responsible for the initiation of lightning-like discharges in dust/air mixtures did exist, in a concrete bunker with a volume of about 60 m^3 (length x width x height ≈ 5m x 4m x 3m), for periods of 15-20 seconds, no such discharges are likely in silos of volume of less than 60 m^3 or of diameter of 3m, and of any chosen height. This conclusion is based on the assumption that the most likely path for a lightning-like discharge follows the shortest field line which connects the region of highest potential with earth. In a cylindrical vessel, except for the field near the base and at the top, the electric field strength lies in a plane perpendicular to the axis and points in a radial direction. Hence there is no possibility of obtaining lightning-like discharges from powder clouds inside cylinders having a diameter not greater than the smallest dimension of the concrete bunker, ie, 3m. The energy of lightning-like discharge is certainly sufficient to ignite combustible mixtures of gas, vapour or dust with air.

The conditions found within a VLCC (volume 24000. m^3) during tank washing have been roughly simulated on a small scale (volume 12 m^3). It was possible to scale the electric field and space potential as measured on board ship at the expense of space charge density. The space charge density on the small scale was much higher (about 10^{-6} C m^{-3}) compared to 10^{-8} C m^{-3} on board ship. This was found to be acceptable and did not affect the validity of the scaled experiments [Hughes (1980)].

1.4.4.1.5 Corona Discharge

When a high voltage is applied to or induced on a sharp electrode, a corona discharge occurs. During a corona discharge ionisation is limited to a region very close to the point where the field is high. Corona discharges are inevitable during bulking of charged powder in a container [Blythe et al (1979)]. Corona discharges are of the continuous or pulsed type and generally provide a safe way of partially removing the charge on powder. The energy density in a corona discharge is much less than in a spark and it will not ignite hydrocarbon vapours or powders. However, the ionisation of the air can enable sparks to form across much longer gaps than would normally be the case.

1.4.4.2 Effect of Electrode Size on the Time Distribution of a Discharge

The incendivity of a discharge depends not only upon the amount of energy or charge released, but also upon the time distribution of the energy. A corona discharge extended in time is less incendive than a short-lived spark discharge of the same total energy [Gibson et al (1965)]. Minimum ignition energies of powders and gases are compared with the energy of different types of electrostatic discharges in Figure 1.3 [Glor (1985)].

The electrode dimensions are the only factors, everything else being constant, that can affect the time distribution of the energy in the discharge. The variation of the transferred charge as a function of the electrode radius was studied by Berta et al (1979). Increasing the radius of the metal sphere from 3 mm to 10 mm caused the transferred charge to decrease. The transferred charge passed through a minimum and began to increase again by increasing the radius from 10 mm to 20 mm. The minimum value is explained as follows: At discharge the length of the breakdown channel is determined by the radius of the sphere, therefore the total charge in the channel is also determined by the probe radius. If the radius is larger, the channel length is less and the total charge in the channel is less. Increasing the radius of the sphere results in a larger area being discharged. These two factors in combination

Figure 1.3 Comparison of Minimum Ignition Energies with Energy of Electrostatic Discharges (Glor (1985))

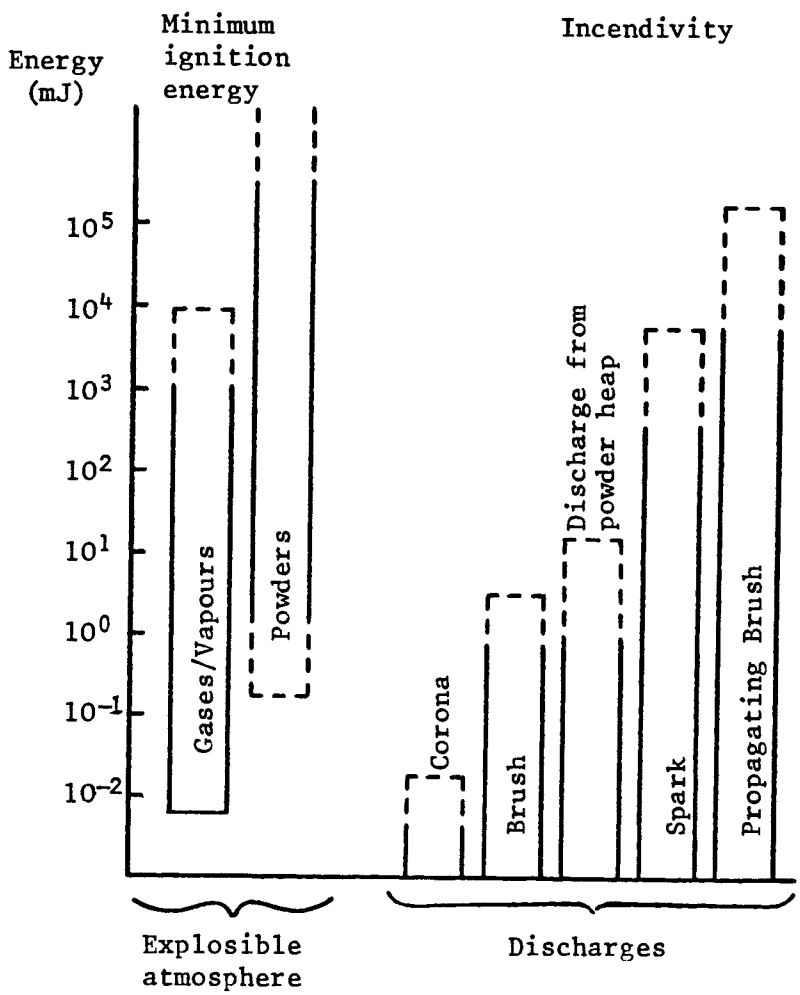

explain the minimum value in the charge transfer. Gibson et al (1965) indicated that *"Although the quantity of charge released from the polyethylene surface decreases as the electrode radius increases, the current flowing in unit intervals of time increases as the electrode size increases up to 10 mm radius"*. These authors did not find significant changes in increasing the probe radius from 10 mm to 20 mm.

1.5 Contact Electrification

Electrostatic charges are usually generated/separated whenever two materials (as webs, sheets, mouldings, powders or liquids) rub, slide or separate from each other. It is often more appropriate to describe such a contact electrification as tribo-electrification because sliding/frictional contact is involved [Bailey (1984)]. The charge transfer process in metal-metal contacts is most completely documented and understood [Harper (1967)]. Figure 1.4(a) shows the energy level diagram for electrons in two different metals which are initially uncharged and separated. In these diagrams the energy zero is taken to be the vacuum level corresponding to a stationary, isolated electron. The work function W of a metal is defined as the minimum energy that has to be expected to remove an electron from the metal and corresponds to the depth of the Fermi energy level (for a metal this corresponds to the topmost filled electronic energy state) below the vacuum level. As shown in Figure 1.4(b), when the two metals make contact with each other, electrons will flow from metal 2, which has the lower work function, to metal 1, leaving metal 2 positively charged. The flow will continue until a new equilibrium is reached, where the electrostatic contact potential difference ΔV established between the two metals just balances the difference in work function, and the Fermi energy levels are equalised [Blythe (1979)].

$$e\Delta V = W_1 - W_2 \qquad (1.2)$$

Metal work functions typically fall in the range 4-5 eV.

Figure 1.4 Energy-level Diagrams for Two Different Metals: (a) Before Contact, and (b) After Contact

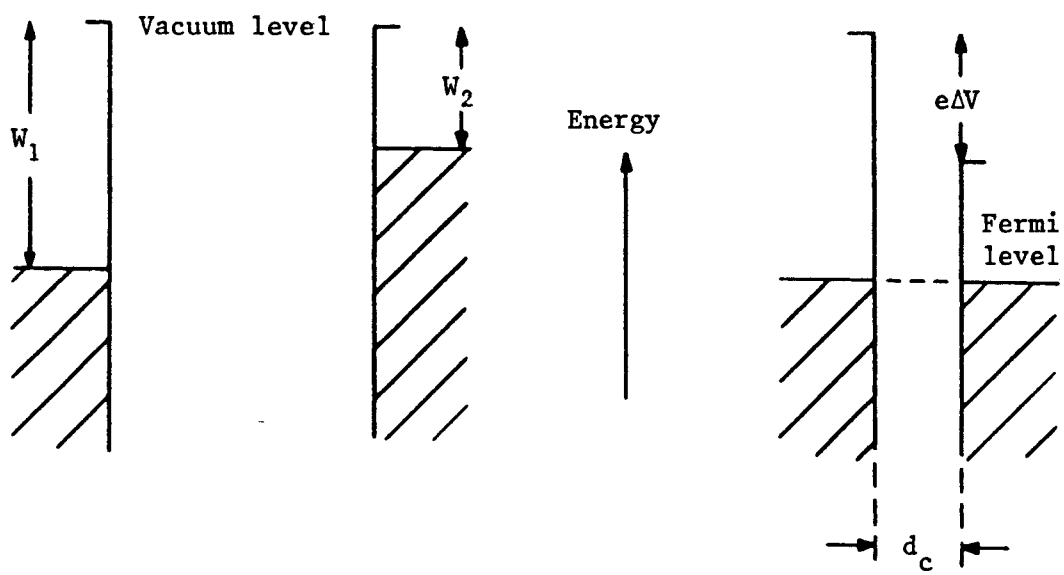

Imagine now that the two metals are slowly separated. As the gap distance between them increases, the capacitance C between the two metals decreases and less charge transfer is required to maintain the same potential difference ΔV. Consequently, as long as electrical contact is maintained through electron tunnelling, there is a back-flow of charge. At the critical distance d_c (typically $\approx$ 5 nm), the charge transfer ceases. The final charge transfer per unit area of contact is given by

$$\sigma = \frac{C}{A} \Delta V \qquad (1.3)$$

$$\sigma = \frac{\epsilon_o}{d_c} (W_1 - W_2) \qquad (1.4)$$

where A is the area of contact.

If a metal and an insulator make and then break contact it is usually found that electric charge has been transferred from one to the other. This process is, however, incompletely understood.

The essential feature of a perfect insulator is a very wide band gap which is free of any impurity levels. In that case the thermal energies would be insufficient for the necessary promotion of electrons from the valence band to the conduction band. Consequently, when a metal and an insulator are brought into contact, electrons ought not to transfer from the metal into the insulator. Similar arguments show that electrons cannot transfer from the insulator to the metal.

Bauser et al (1970) investigated the charging mechanism of insulating solids and found that for an ideal polymer in contact with a metal, the theoretical surface charge density ($\approx 10^{-31}$ C cm^{-2}) was smaller by several orders of magnitude than that obtained experimentally.

Based on the practical observation that some polymers behave as near-perfect insulators, with any charge failing to dissipate over periods of many years, it is reasonable to assume that a mechanism for contact charging which involves transfer to or from the bulk will not always apply. A satisfactory explanation for the experimental results was hence given by considering surface states.

The influence of trap levels in the energy gap of a real polymer, which are due to chemical defects on the contact electrification, was also studied by Krupp (1971).

An energy level scheme for a particular case of a simple model of metal insulator contact charging, involving only surface states on the insulator, is shown in Figure 1.5 [Blythe (1979)]. The energy density of surface states per unit area D_s is assumed to be uniform. The Fermi level in the metal W_m is lower in energy than the limit W_i (surface Fermi level) to which the surface states on the insulator are filled. Upon contact there will be an immediate flow of electrons from the insulator surface states to the metal, the charge transferred per unit area of contact being given by [Blythe (1979)]

$$\sigma = eD_s \Delta W_i \qquad (1.5)$$

where ΔW_i is the shift $(W_i' - W_i)$ to the new surface Fermi level W_i' caused by the surface charge. Denoting the consequent contact potential difference developed between the metal and insulator surfaces by ΔV, then

$$W_m - \Delta V = W_i + e\Delta W_i \qquad (1.6)$$

The geometrical capacitance per unit area between them for a separation d_c is given by

$$C_A = \frac{\epsilon_o}{d_c} \qquad (1.7)$$

Figure 1.5 Energy-level Diagrams for a Metal and an Insulator: (a) Before Contact, and (b) After Contact

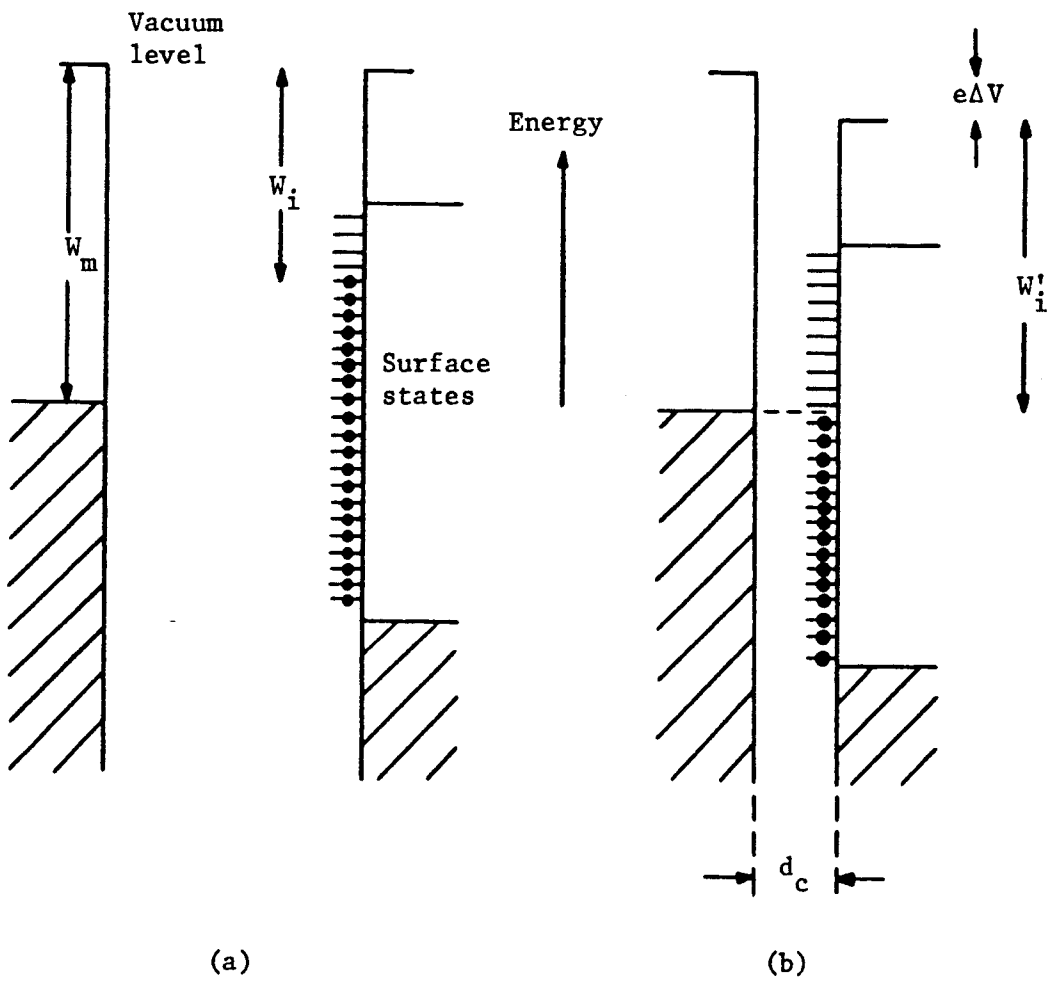

so that,

$$\Delta V = \frac{\sigma}{C_A} = \frac{\sigma d_c}{\epsilon_o} \tag{1.8}$$

Combining equations (1.5), (1.6) and (1.8),

$$\sigma = \frac{eD_s (W_m - W_i)}{1 + e^2 D_s d_c/\epsilon_o} \tag{1.9}$$

If D_s is not too large because there is no high concentration of unsatisfied chemical bonds, for example chemical defects, broken chains etc, at the surface, we may assume

$$\frac{e^2 D_s d_c}{\epsilon_o} << 1 \tag{1.10}$$

and equation (1.9) simplifies to

$$\sigma = eD_s (W_m - W_i) \tag{1.11}$$

Equation (1.11) predicts that the surface charge density imparted by metal contact to the insulator surface is directly proportional to the work function difference. The charge density is not sensitive to any critical separation at which electrical contact is lost.

In the limit of a high surface state density,

$$\frac{eD_s d_c}{\epsilon_o} >> 1 \tag{1.12}$$

Equation (1.9) simplifies and the contact charge density is given by

$$\sigma = \frac{\epsilon_o (W_m - W_i)}{ed_c} \tag{1.13}$$

The contact region is defined as the maximum area over which charge transfer can take place. For a spherical particle of radius r, the contact area A is given by (Figure 1.6)

$$A \approx \pi a^2 \tag{1.14}$$

$$\text{where } a^2 = 2r\, d_c - d_c^2 \approx 2r\, d_c \tag{1.15}$$

In practice, due to surface roughness, only a fraction of the geometric area is available for intimate contact. Loeb (1958) states that the contact area should be modified by a factor f of the order of 10^{-7}, the true contact area being

$$A \approx 2\pi\, f\, r\, d_c \tag{1.16}$$

This area is taken as the area of an equivalent parallel plate capacitor. Using equation (1.9) the charge imparted by metal contact to a spherical insulating particle is given by

$$Q_1 = \frac{2\pi\, f\, R\, d_c\, e\, D_s\, (W_m - W_i)}{1 + e^2\, D_s\, d_c/\epsilon_o} \tag{1.17}$$

When, therefore, two dissimilar materials or two similar materials of different sizes make and then break contact, charge transfer from one to the other occurs. The charge exchange tendency between similar materials is greatest when one of the particles is very small (ie, of atomic dimensions) and the other particle is comparatively large [Gallo et al (1976)].

There are three main ways in which charge can transfer from one body to another: by transfer of electrons, transfer of ions, and transfer of material carrying charge. The variation of charge transfer with metal work function, and its correlation with the chemical properties of the insulator, suggests that charge transfer is often due to electrons [Davies (1969)].

Salaneck et al (1976) showed that when metals and polymers make contact some of the metal transfers to the polymer and some of the polymer to the metal. Material transfer is of significance to

Figure 1.6 Definition of Contact Region

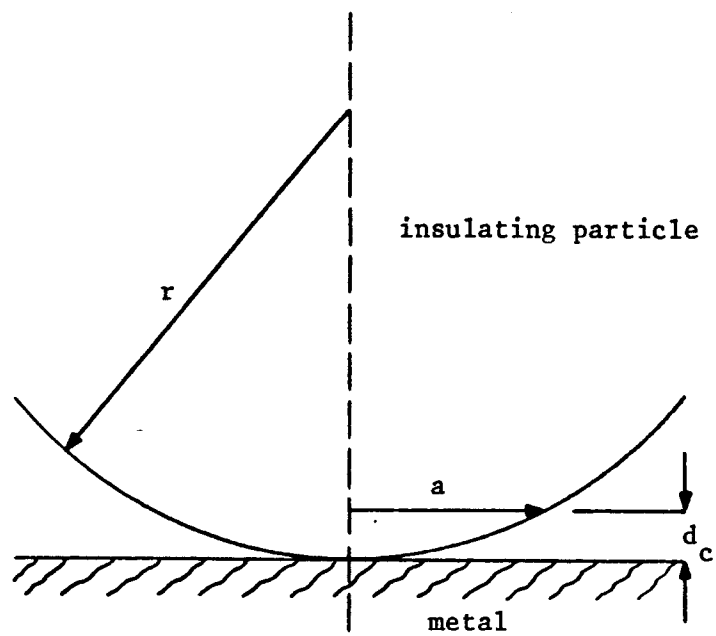

contact electrification if the transferred material carried charge, and the transferred charge per unit area exceeds the charge density observed in contact electrification. When metals slide over polymers very large amounts of polymers may transfer to the metal [Pooley et al (1972)].

Kornfeld (1976) showed that due to the presence of charged defects in the crystal lattice, solid insulators are not electrically neutral and possess their own (intrinsic) electric field. This electric field is usually compensated by ions attracted to the surface from the atmosphere. These ions together with other adsorbed molecules form the surface layer of the body. As a result of the friction of one such body against another, their surface layers are mixed and the compensation for the intrinsic field of both bodies is disturbed, ie, the bodies become electrically charged.

The overall electrical effect of a positive ion being transferred from a surface cannot be distinguished from an electron transferred to that surface to neutralise the ion.

The electrification of one insulator by another can also be predicted from knowledge of the electrification of each of the contacting insulators by metals which suggests that the electron transfer rather than ion transfer is the dominant cause of contact electrification between two insulators. Davies (1970) found that the charge transfer between two insulators can be predicted, to a certain extent, from knowledge of the charge acquired by each of the insulators on contact with metals. It is assumed that the charge on the insulators, due to contact with metals, is such as to bring the Fermi levels of the metal and the insulator into coincidence. Using the measurements of metal-insulator contact charging to deduce a Fermi level for each insulator, Davies found that the charge transfer between two insulators is correlated with their Fermi levels, the sign of the charge transfer being consistent with the hypothesis that electrons pass from the insulator with the higher Fermi level to that with the lower.

In practice polymers normally have a number of surface states within the forbidden energy range owing to chemical impurities and because of specific surface defects due to oxidation products, broken chains, and adsorbed molecules. If the charging mechanism during metal-insulator contact is due to surface states the Fermi level in the Davies' (1970) argument can be replaced by W_i (surface Fermi level) and all the conclusions will remain valid (see Figure 1.5).

Robins et al (1975) investigated the role of surface ions on charging by using insulators whose surfaces may readily be coated with a dense layer of ions of either sign. The experiments showed that surface ions had a dominant effect on the charging of pyro-electric samples. It was supposed that surface ions might also affect the charging of ordinary insulator surfaces.

Hays (1974) found that for a freshly prepared film, the mercury contact charging of polyethylene was low, 1 nC cm^{-2}. For films exposed to the laboratory air for a few hours, the contact charging increased to 20 nC cm^{-2}. Mercury was chosen as the test metal surface because a non-frictional, non-destructive and intimate but separable contact is formed. A brief exposure of the polyethylene to air near a corona, or ozone from a generator, also increased the contact charging.

The charging of clean and dirty surfaces of PTFE during contact with a spherical aluminium electrode was investigated by Homewood (1981). The clean surface of PTFE was prepared by cleaving the specimen in the ultra-high vacuum whilst the dirty surface was a similarly prepared specimen that had been exposed to air for 24 hours. Results obtained indicated no significant difference in contact charging between the two surfaces. It was concluded that for PTFE contact charge transfer is not affected by extrinsic surface states due to adsorbed impurities, which implies that the contact charge is due to electron states intrinsic to the material.

Cottrell et al (1979) showed that there is no detectable charging when perfect insulators contacted by metals. Solidified rare gases were used as 'ideal' insulating solids. Solid rare gases have an electron gap which is greater than 9 eV and the bottom of the conduction band lies close to the vacuum energy level. Because the force between atoms is weak (atoms are held together by the Van der Waals force), the atoms keep their identities in the solid and crystal defects and surface states are not expected to provide deep donor or acceptor centres. The incorporation of electronegative impurities led to negative contact electrification.

The quantity of interest in contact electrification experiments is the surface charge density, σ (charge transferred per unit area of contact). It is however very difficult to measure the actual area of contact between two bodies, and so the charge density often cannot be determined. Surfaces are nearly always to some extent rough. Consequently, the total area in actual contact is less than the apparent area of contact.

Hull (1949) mapped out the distribution of contact charge on the insulator surfaces using charged powders. Negatively charged powder settles on positively charged parts of the insulator and positively charged powder on negative parts. Uncharged portions of the specimen is freed of powder by shaking. The degree of resolution of this method is restricted by the size of the powder or dust in use. Sone et al (1974) used liquid crystal to delineate structures of residual charges on insulating surfaces. Thin films of the liquid crystal solution were applied to an ebonite plate. The solvent was then allowed to evaporate in a vacuum. Although this method does not distinguish the polarity of residual charges, it has a high resolving power ($\approx$ 1 μm) in the delineation of the surface discharges. Davies (1973) used an induction probe to determine the contact area for a range of contact loads, by measurement of the surface charge retained on the polymer surface after contact. Induction probes are limited to a spatial resolution of about 50 μm - the charge density may, however, vary on a smaller scale.

The rate at which the charge is transferred during metal-insulator contacts has an important bearing on whether the charge is transferred to bulk or to surface states. Direct measurements of the time dependence of contact electrification have shown that the total charge transferred to polyethylene and PTFE by contact to metals increased with the duration of contact [Davies (1967), Homewood et al (1979)]. The increase of charge with duration of contact was explained to be due not to any slowness in the electron transfer but to a gradual increase in contact area with time. Polymers are viscoelastic and also much softer than metals, and so will slowly deform at the contact region. Medley (1953) showed that the charge transferred to polymers by contacts to liquid mercury is independent of contact time.

Hays (1974) investigated the influence of an external electric field on the mercury contact charging of polyethylene. For freshly prepared films of polyethylene, the contact charge exchange is low and the field dependence is weak. If the polyethylene has been exposed to ozone or to the laboratory air, the contact charging and field dependence increase considerably. The field is able to modify the transfer of electron from the metal to surface states on the polymer.

External electric fields were used by Nordhage and Bäckstrom (1975) to determine the thickness of the charge layer at the insulator surface. In the absence of an externally applied electric field the thickness, χ_o, of a layer of charge on the insulator surface is such that the potential difference across it is V_c. An externally applied field E_r disturbs the equilibrium and will create a potential difference $E_r\chi_o$ across the layer. If the charge transferred is in surface states, the effective thickness of the charged layer is very small and a very large electric field will be needed to affect the charge transfer. Nordhage and Bäckstrom (1975) concluded that charge confined to states on the surface cannot be responsible for the electrification of polyethylene but must penetrate into the bulk of the insulator.

In practice, when an electric field is applied to a polymer, a shift in energy levels in the polymer relative to the metal Fermi level does not always occur. Bulk polarisation may be induced which persists for a long time after the field is removed. Many methods of charge measurements will not distinguish the polarisation charge from the contact charge.

Effect of electric fields on contact electrification of pyrex with a metal at elevated temperatures and relative humidities has been measured by Greason (1972). As the humidity and temperature increase, a large shift in the charge exchange versus electric field is observed which indicates a conductive induction electrification.

If small amounts of surface contamination, impurities or absorbed materials, rather than the basic chemical constitution of the material, significantly affect the contact charging process, it will be necessary to work under ultra-high vacuum conditions to achieve reproducible data. This is not of immediate practical relevance to many industrial situations because the solids and powders involved are not pure substances.

A basic approach for investigating the charging of powder particles transported through metal pipes is to study the charging of a particle by a single impact on a metal plate.

Masui et al (1983) studied the influence of impact speed and impact angle on the electrification of polymer (nylon 66 and PMMA) particles by impact on a metal plate. Both the impact charge and the impact area are the linear function of the vertical component of the impact speed. The impact charge and the impact area are independent of the horizontal component of the impact speed. It is also shown that the charge density (charge per unit area) is independent of the impact speed and angle and its value is only determined by the combination of the materials of the particles and the metal plate.

Yamamoto and Scarlett (1986) investigated the influence of the initial charge on a polymer (polystyrene) particle on the impact charging with metal plates of different materials. It was found that a particle which already carries more than the equilibrium value of charge will give up some or all of its charge on impact with a metal plate. On the other hand, a particle which carries a charge of the opposite sign will gain even more than a neutral particle. It was also found that the equilibrium value is almost independent of the impact conditions and depends on the particle material and size and the plate material.

John et al (1980) investigated the transfer of charge to a metal surface as a result of impacts by initially neutral particles and by initially charged particles (precharge). Three types of particles were used: methylene blue, sodium chloride and potassium biphthalate. The amount of charge transferred during a contact was dependent on the initial charge on the particle as well as the contact potential. The fraction of precharge transferred was greater for positive precharge than for negative precharge. The contact charge during these tests was positive. For a negative contact charge the dependence on the sign of the precharge reversed. John et al (1980) interpreted this effect in terms of a weakly rectifying p-n junction formed at the particle probe contact region. For positive contact charge, the particle surface material is p-type, the probe surface material n-type. When neutral particles contact the probe, electrons flow from the probe to the particle and positive charge flow from the particle to the probe until the contact potential is established. If the particle carries a positive precharge, this produces a positive bias voltage across the junction, increasing the charge transfer rate. A negative precharge on the other hand will impede charge transfer and the effects are reversed.

Kittaka et al (1977) studied the charging tendency of some synthetic high polymer pellets by charging them repeatedly by impacts in a chrome-plated chamber using a compressed air flow. The charge build-up of the pellets followed an almost exponential

growth. The initial slopes of the charging curves became steeper with increasing air pressure. This tendency was caused by an increase both in the frequency of impacts and also the contact area per impact between a pellet and the metal surface. Each charging curve had a tendency to saturate with increasing charging time. Furthermore the saturation charge was almost independent of the air pressure. In the case of spherical pellets of polyethylene, saturation charge density of -2.10×10^{-9} C cm^{-2} was obtained which is 36.3% of the maximum theoretical value assumed for an isolated sphere in free air. The difference between the theoretical and experimental saturation charge densities was explained in terms of the irregularity of the shape of the pellets, non-uniformity of the surface charge and the charging process in a small chamber.

Cho (1964) investigated the contact charging of micron-sized particles in electric fields up to 2.7×10^{8} V m^{-1}. The apparatus consists of a pair of stainless steel particle charging plates. The electric field induces a charge on a particle in contact with either plate and the resulting electrostatic force on each particle causes it to oscillate in the gap. The opposed convex plates focus the particle towards the centre of the system where they escape through a small axial exit aperture in the top plate. The properties of the emerging charged particles are then determined. It was found that conducting and semiconducting particles would continuously oscillate between the charging plates when the electric field was applied between the plates. When insulating particles were introduced in the electric field the major effect would be an induced polarisation. When a potential was first applied between the plates, there was no reaction of the insulating particles. However, with time and a small finite electrical conductivity, a few particles became charged and travelled to the opposite plate. An oscillation between the charging plates did not take place, as was the case for metal and semiconducting particles.

The charge transferred to a particle during handling will redistribute itself over the particle surface by electrostatic forces. The redistribution rate or the electrical relaxation time

of the particle material, τ, is given by the product of particle resistivity, ρ, and particle permittivity, ϵ [Bailey (1984)]. Materials with high resistivities, for example high density polyethylene, have relaxation times of hours or days.

When a static charge of electricity is uniformly distributed over a spherical surface, the field just outside the surface is normal to it. The electric field is the same irrespective of whether the sphere is a conductor or an insulator and independent of the dielectric constant of the insulator [Harper (1967)]. The electric field has a maximum intensity at the sphere surface and decays inversely with the square of distance away from the surface. Due to the highly non-uniform nature of the field in the vicinity of a small charged particle surface, electric field values much higher than that for a uniform field (3×10^6 V m^{-1}) can be supported. Harper (1967) has modified an empirical formula of Schaffer, quoted by Schumann (1923), which gives the maximum sustainable electric field on the surface of a particle in terms of the radius, r, of a spherical particle as:

$$E = 9.3 \times 10^5 \, r^{-0.3} \text{ V m}^{-1} \qquad (1.18)$$

The surface field calculated from this expression for a charged particle of radius 0.02 m is 3×10^6 V m^{-1}, the breakdown threshold for a uniform field and so, for all particles of radius less then 0.02 m, higher values of surface field may be sustained with maximum sustainable field increasing as particle size decreases, according to equation (1.18).

The static electrification of powder particles in a pneumatic conveying system is due to tribo-electrification caused by multiple collisions between powder particles and the pipe wall. An upper limit to the charge that can be acquired by the powder is reached after the powder particles are transported through a certain length of the conveying pipe. The tribo-electrification of the particles in a pneumatic conveying system is affected by changes in the conditions of collision with the pipe wall, the material of the pipe and the atmosphere.

Masui et al (1984) investigated the dependence of the electrification of polymer powders on the shape of the pipe and the transport conditions. The powder specific charge density, q, (the charge/mass ratio) increases with increasing bend angle of the elbow pipes (15-20 times for 90° elbows) because the impact area of the powder particles increases with the latter. In a straight pipe, at constant particle speed, the specific charge density, q, is constant at low solid loadings, M, (the mass of powder/volume of transport air ratio). The specific charge density increases as M increases but will decrease at very high solid loadings as the mutual collision among particles occurs very frequently and the number of particles which cannot reach the pipe wall will increase.

Boschung et al (1980) studied the tribo-electrification of powders subjected to industrial processing using a method which made it possible to determine reproducibly the influence of parameters such as powder quantity, airflow rate, length, diameter and material of the tube on the charge pick-up ability of powders. Chemical composition and surface properties of powder particles rather than the transporting conditions determined the specific charge density of powders. Specific charge densities in the range 10^{-3} - 10^{-7} C kg^{-1} were observed with the powders investigated. The extent of the specific charge densities' scatter was such that a classification of the powders' ability to pick up electrostatic charges as "low", "medium" and "high" was suggested.

The static electrification of a dilute suspension of several powders in a pneumatic conveying system were studied experimentally by Masuda et al (1976). The powders investigated were: flour, vinyl chloride, glass beads, eight grades of quartz sand and eight grades of morundum. The collision characteristics such as contact area, number of collisions per unit area and unit time and duration of contact were examined by photomicrographs of scars caused by the impact of particles on a plastic film covering the inside wall of a section of the conveying pipe. The number of scars per unit area, obtained by counting, was found to be directly proportional to the powder mass flow rate. The dimensions of the scars were, however,

independent of the powder flow rate but were proportional to the mean air velocity. The electric current generated on the wall of the conveying pipe was approximately proportional to the mean air velocity to the power 1.4 when the contact seemed to be elastic and to the power 1.9 for inelastic contacts. It was also found that the current was inversely proportional to the mean particle diameter.

Enstad (1978) investigated the influence of the conveying pipe length, pipe diameter, air velocity and the mass flow ratio on the specific charge of PVC powder. The specific charge of the powder after pneumatic conveying increases with the conveying length to a saturation value. The saturation value is in practice obtained after a conveying length of 1 to 2 m. The saturation specific charge seems to increase with the air velocity and to decrease with the tube diameter and the mass flow rate.

Cunningham (1966) investigated the relation between charge density generated on an insulating belt slipping on a grounded metal roller and work done against friction. It was shown that the charge on an insulating belt exponentially approached a limiting value as the work done against friction in slipping the belt on a grounded metal roller was increased. The limiting value increased proportionally faster as the belt tension increased. This may be due to the fact that the real contact area between the belt and roller increased proportionally faster than linearly as the belt tension was increased. It was also shown that rollers of different metals charged the belt materials differently. These differences were related to measured contact potential differences characteristic of the metals as they were used in these experiments.

Singh (1983) examined the influence of mass flow rate and relative humidity on the charging characteristics of high density polyethylene during pneumatic conveying in a full scale silo rig. Charge per unit mass was found to be smallest when the mass flow rate was at a maximum. A large relative humidity implied a large negative current and a small relative humidity implied a large positive current. Electric field measurements during and after

conveying of powder through the conveying pipes into the silo showed that high density polyethylene fines charged negatively and the coarse charging positively.

Smith et al (1983) measured the specific charge density of small quantities (between 10 and 25 g, depending on particle size) of high density polyethylene powder being transported pneumatically along a one metre length of pipe. The experimental results were consistent in terms of relative value, but approximately 100 times less than the maximum value of q_{max}.

Effects of humidity on polymer surfaces have also been studied by Sprengling (1971) who concluded that a characteristic level of surface resistivity in a humid ambient would be much less a property of a given polymer structure or composition than has been supposed. The resistivity found under such conditions was often determined to a much greater degree by the sample prehistory.

It has been reported that the humidity influences the dispersibility of the powder in the air stream [Boschung et al (1980)].

Yu (1985) observed that when some agricultural products were transported pneumatically along the conveying pipes, the charge on the powder oscillated around the saturation level as a function of the pipe length. If the powder particles were already charged to a larger level than the saturation level before entering the conveying pipework, the oscillation could contain an exponential decrease, but need not necessarily.

Ramackers (1970) found the highest specific charge density levels for silica particles during pneumatic transport to occur at low solid loadings. Specific charge density also decreases with a decrease in the transport air speed. The space charge of powder particles flowing through the pipe was used in an attempt to neutralise the charged powder by induced corona discharge from an

earthed conducting wire. This device was found to be most effective at high inlet charge levels.

The charged powder flowing through the pipe produces an electric field at the inside wall of the pipe. From this concept it appears that an additional electric field between a wire conductor mounted centrally in the pipe and the wall of the pipe can influence the specific charge [Linstrom (1978), Ebadat et al (1989)].

1.5.1 Analysis of Electrostatic Charging of Particles in Gas-Solids Flow

In a pneumatic conveying installation the powder particles become electrostatically charged due to the process of tribo-electrification. The charged powder flowing through the conveying pipe produces a radial electric field at the inner wall of the pipe. This field acts as to oppose the charge transfer between the powder particles and the inner surface of the pipe. The specific charge of powder therefore reaches a saturation limit as it flows along the pipe. Cole et al (1969-1970) presented a theory for the prediction of electrostatic charging rate of the said particles (Appendix A). The charge exchange per collision of a particle with a wall may be expressed as follows:

$$\frac{dQ}{dn} = Q_1 - k\,Q_T - 1Q_T \qquad (1.19)$$

The solution of equation (1.19) is

$$Q_T = \frac{Q_1}{K}(1-e^{-Kn}) + Q_o e^{-Kn} \qquad (1.20)$$

where $K = k + 1$.

From equation (1.20) it is clear that, given a sufficient number of collisions, a particle will always finish up with a limiting or saturation charge of $\frac{Q_1}{K}$. The influence of the space

charge field is such that even if the charge of powder is somehow made to exceed the saturation limit, the additional charge dissipates after the powder travels through a short section of the pipework.

1.6 Investigation of Electrostatic Hazards in Pneumatic Conveying and Storage of Powders

Static charges are likely to generate/separate during operations such as sieving, pouring, sliding, spraying, filtering, grinding and pneumatic transport. The specific charge densities generated during various powder handling operations are shown in Table 1.4.

Table 1.4 Charge Generated in Powder Handling Operations

Operation	Specific Charge Density ($\mu C\ kg^{-1}$)
Sieving	10^{-5} - 10^{-1}
Pouring	10^{-3} - 10^{-1}
Scroll feed transfer	10^{-2} - 1
Grinding	10^{-1} - 1
Micronising	10^{-1} - 1
Pneumatic transfer	1 - 10^{3}

In pneumatic transfer, tribo-electrification of the powder may occur in different parts of the powder processing plant. For example, it may occur in the rotary valves, conveying pipes and cyclones. It is normally only when the powder enters a silo that a significant electrostatic hazard may arise. This is because the dispersed dust cloud of the powder in the silo normally requires less amount of energy to ignite and higher energy sparks are more likely.

It is important to place the electrostatic hazard in perspective. An analysis chart of electrostatic dust explosion hazard is shown in Figure 1.7 [Singh (1983)]. There are several reasons why static electricity has become in all cases a more serious potential ignition source in powder handling and storage systems. The higher charging rates and higher levels of charge accumulation are the result of increases in the transport velocities and the construction of larger silos [Glor (1985)]. In addition, it has been realised that the values of the minimum ignition energies of certain organic powders measured are very low, overlapping with the range of values observed for pure gases (Figure 1.8) [Gibson et al (1981)].

Most powders are capable of retaining their charge when the powder resistivity lies above about $10^9 \Omega m$. The volume resistivity of dry powders processed in the organic chemical industry will, with few exceptions, exceed $10^9 \Omega m$ (Figure 1.9) [Gibson et al (1981)].

Some recent statistics reported by Glor (1985) claim that there is one dust explosion in Germany nearly every day. 9% of all these accidents are caused by static electricity. If, however, only polymeric powders are considered the percentage increases to 34%. There are on average 40 dust explosions in the UK each year and it is estimated that 10% of dust explosions are caused by static electricity [Gibson (1986)].

A dispersed dust cloud may be ignited whenever sufficient energy is supplied to initiate a runaway oxidation reaction. A kernel of hot gas must be created, in which the heat generated exceeds the heat lost, for the flame to propagate. One source of ignition in industrial fires and explosions may be electrostatic discharges. An assessment of the ignition hazard due to electrostatic discharges should not only include arguments about the occurrence and incendivity of discharges, but also about the ignition sensitivity of a given product. The ignitability of some of the common dusts in terms of various parameters is shown in Table 1.5 [Abbott (1986)]. Decreasing the particle size, in many

Figure 1.7 Electrostatic Dust Explosion Hazard Analysis (Singh (1983))

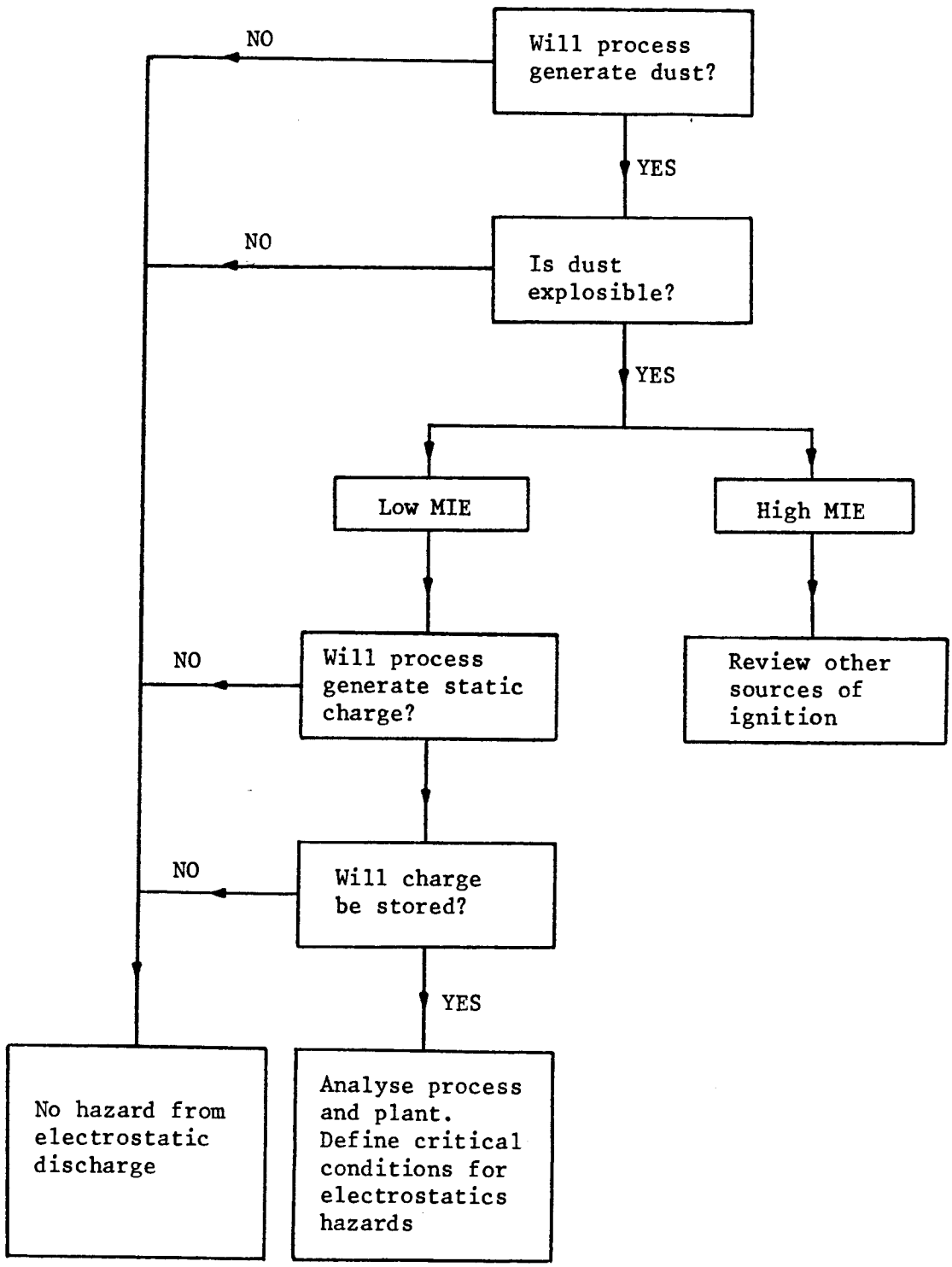

Figure 1.8 Minimum Spark Ignition Energy Data
(Gibson et al (1981))

Flammable Material	Typical MIE Values (MilliJoules)
Sensitive Detonator Explosives	0.001 - 0.1
Vapour Oxygen Mixtures	0.002 - 0.1
Vapour Air Mixtures	0.1 - 1.0
Chemical Dust Clouds	1 - 5000

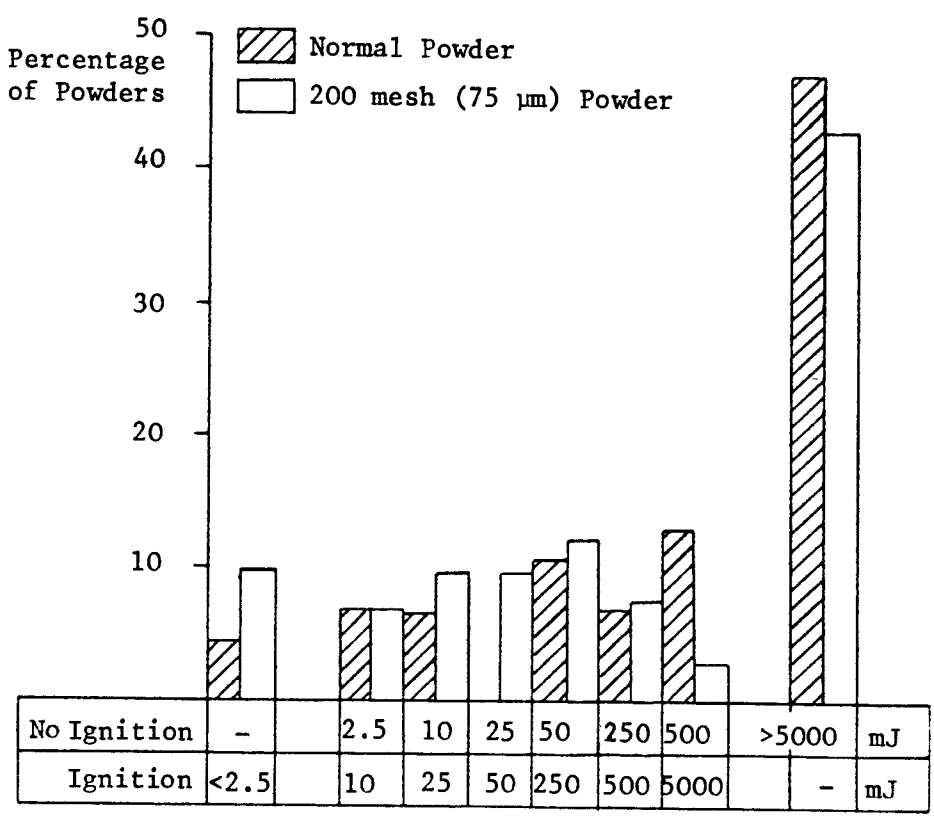

Figure 1.9 Electrical Resistivity of Powder Products
(Gibson et al (1981))

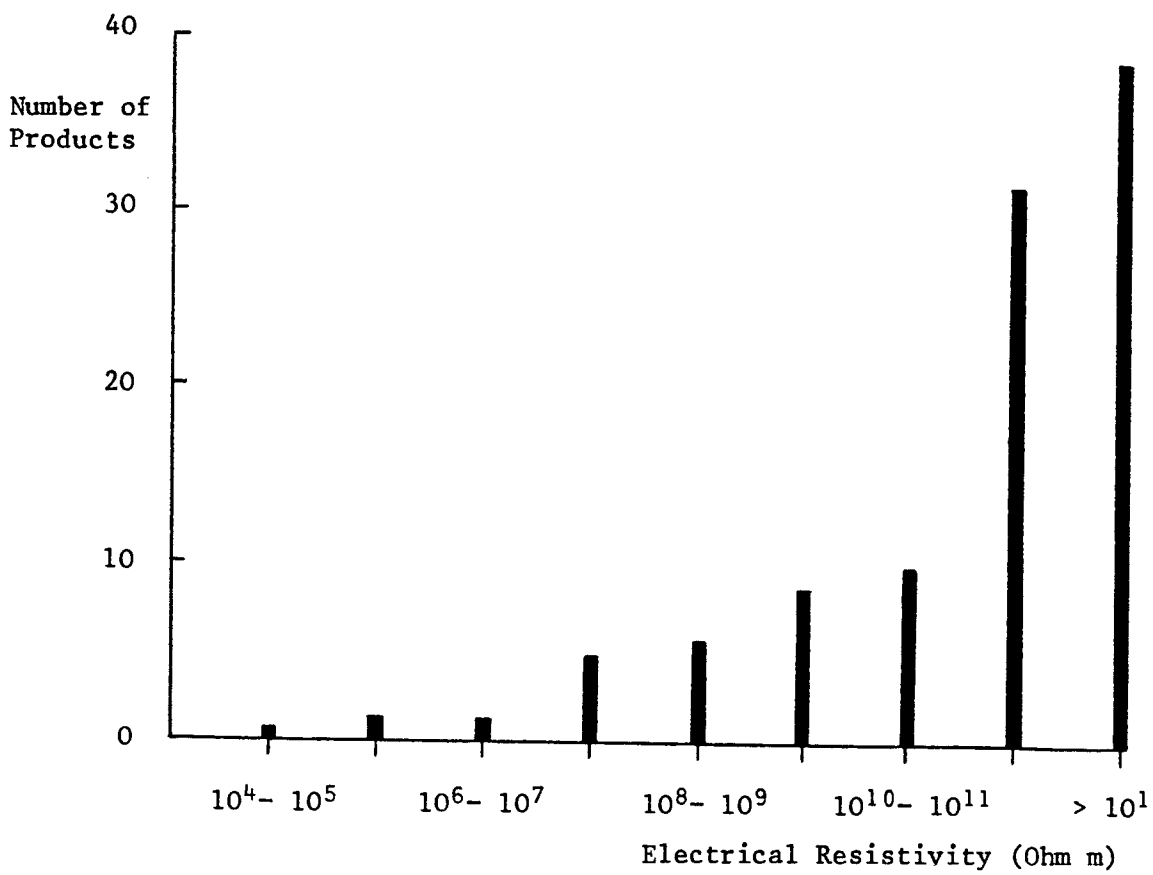

Table 1.5 - Explosion Properties of Some Dusts

	Particle Size	Typical Moisture Content	Vertical Tube Classification Test Class A/Class B	Minimum Ignition Temperature °C	Minimum Oxygen Concentration for Ignition	Minimum Ignition Energy mJ	Minimum Explosible Concentration g m^{-3}
Aluminium Powder	1-400 μm	≈ 0	A	-	12% @ 850°C	13	30
Animal Feed	-	12%	A Marginal	-	-	-	-
Bleach Precursor (organic)	< 100 μm	0.5%	A	480	-	34	50
Calcium Soap	< 100 μm	2%	A	400	-	30	-
Coal	90% <75 μm	< 1%	-	-	-	100	60
Coffee	40 μm	4%	A	410	-	160	85
Cornstarch	< 100 μm	11-12%	A	380		30	40
Diphenylol propane	-	-	-	570	12%	15	20
Fat emulsion (spray dried)	200 μm	< 1%	A	430	-	70	60
Formaldehyde resin	2-15 μm	≈ 0	-	-	-	40	30
Magnesium	-		-	610	-	-	-
Meal	-	-	-	-	-	-	-
Milk Powder	-	2.5-3.5%	-	-	-	50	?
Phenolformaldehyde	15 μm	-	A	-	-	5	20
Pigment	< 53 μm	≈ 0	A	-	-	-	-
Polyethylene	100-600 μm	≈ 0	A	390	8%	5-550	10-900
Protein (synthetic)	25-70 μm	3-5%	A	500-550	6.5-7.5% @ 800°C	250-500	30
Starch	5-32 μm	2%	A	425	-	-	60
Starch (modified)	50-125 μm	6%	A	380	-	30	20
Starch	-	-	-	-	-	-	50
Sugar	< 250 μm	<0.1%	A	350	-	30	35
Sugar	-	0.04%	-	350	-	30	20
Sugar	-	0.02%	A	400	-	30	45
Toilet Soap	< 100 μm	8%	A	500	-	-	280
Wheat	-	-	A	380	-	290	1500

cases, significantly decreases the minimum ignition energy of a powder. An example of this is given in Table 1.6 [Gibson (1986)].

Table 1.6 **Effect of Particle Size on Minimum Ignition Energy**

Particle Size Range (μm)	Minimum Ignition Energy (mJ)
710 - 1680	5000
355 - 710	250 - 500
180 - 354	50 - 250
105 - 179	10
53 - 104	10
5	10

It is generally accepted that dispersed flammable dust clouds may be ignited by discharges from charged objects such as, for example, sparks or propagating brush discharges. These types of discharges can be excluded in practice if grounded conductive equipment are used. The question that remains is: can a combustible powder be ignited by the charge accumulated on the powder itself even if the powder is handled in earthed conductive installations?

When charged non-conducting powders are pneumatically conveyed, an immense amount of charge will be released if charged particles, initially well separated from each other, are collected together into a large container [Blythe et al (1979)]. This is because the effective surface area of the whole heap will be so much smaller than the sum of individual surface areas of all the particles. In the case of earthed metal silos, the excess charge is led away to earth by low energy corona or brush ionisation of the gas space, but higher energy discharges cannot be ruled out [Thorpe et al (1985)].

Besides spark discharges from charged conductive products and corona discharges from insulating product, discharges associated

with the charge on the powder particles accumulated in a hopper have been observed by Blythe et al (1979). The discharge spreads over the surface of highly insulating powder settled in a silo forming radially directed discharge channels. Discharges across the bulked powder have been photographed, but their incendivity was not determined [Maurer (1979)]. Incendive discharges have been obtained from the surface of highly charged HDPE bulked powder. These discharges were capable of igniting a propane/air mixture with a minimum ignition energy of 0.25 mJ [Singh et al (1987)].

Results of experiments performed with dust clouds inside a 60 m^3 bunker showed that the conditions thought responsible for the initiation of lightning-like discharges in dust/air mixtures did exist but no discharges took place. Boschung et al (1977) showed experimentally that such discharges are not to be expected in silos of volume of less than 60 m^3 or of a diameter of less than 3 m and unlimited height.

A limited amount of data has been published on the incendivity of sparks from the more common forms of non-conducting surfaces found in industry. Glor (1981) showed that brush discharges from the surface of a polyethylene plate are able to ignite a number of gases and vapours. These gases were: propane, butane, acetone, 2,2-dimethylpropane, diethylether, ethylalcohol, acetic acid, ethylester and mixtures of alkanes. With the minimum ignition energy of propane air mixtures influenced by increasing the nitrogen content of the air, an equivalent energy of 3.6 mJ with an ignition frequency of 40% was achieved with brush discharges from a sphere of 35 mm radius.

Gibson (1974) chose two levels of probability as the standard for the assessment of ignition risk. A real risk of ignition will exist if discharges from a particular source are giving 50% ignitions. This measure of discharge incendivity is termed the Incendivity (0.5p) value of the discharges and is numerically equal to the minimum capacitive spark ignition energy of the atmosphere in which 50% of the discharges cause ignition. This information is

obtained relatively quickly because the relationship between probability of ignition and sensitivity of the flammable atmosphere is such that it is only necessary to carry out ignition tests with three or four different gas mixtures to accurately define the curve in the 0.5 probability region. Furthermore, a reliable value for the probability of ignition in a given gas mixture is obtained after passing only 100-200 discharges through the atmosphere. This is an arbitrary selection but it is useful in initial testing and in the establishment of situations of high risk.

The second level of probability chosen as standard is very low. When the probability of ignition becomes virtually nil then the minimum ignition energy of the gas mixture for which this occurs has special significance in that the discharges will not ignite any gas or vapour-air atmosphere whose minimum ignition energy is equal to or greater than this value. It indicates, therefore, the maximum igniting power of the discharge and has been termed its "equivalent energy". In an electrostatic risk situation a probability of ignition of less than 1 per 1000 discharges can probably be accepted as safe. It must however be said that if large numbers of discharges are occurring, then the likelihood of ignition is still significant.

When the probability of a discharge from an electrostatically charged source igniting a particular flammable atmosphere is 0.001 then it can be said to be on the threshold of ignition. The equivalent energy of a discharge defined as the minimum ignition energy of the flammable gas or vapour atmosphere, for which the probability of ignition is 0.001 (Incendivity 0.001p), is considered to represent the maximum igniting power of the discharge from that source.

The maximum surface charge density which can exist on any surface is limited by the break down strength of air above it. When a spherical earthed electrode approaches a charged insulating surface an opposite charge is induced on it. As the two surfaces are brought closer together the electric field increases

and eventually the air breaks down forming a multi-channelled discharge (brush discharge). The movement of the surface charges is determined by the surface resistivity and the tangential component of the resultant electric field strength on the surface. In the case of highly insulating materials the charge is not mobile and a small area is discharged. When an electrode is brought near the surface of a highly charged bulked powder some particles move in the direction of the tangential component of the resultant field.

The incendivity of brush discharges from positively charged surfaces are much less than from negative surfaces. Tolson (1981) found no ignition of propane with discharges from a positive surface. It was also found that a positive surface charge density of 17 $\mu C\ m^{-2}$ was required to ignite hydrogen whereas a negative surface charge density of $-3.8\ \mu C\ m^{-2}$ would ignite the same gas. Lovstrand (1981) explained this by the different character of the positive brush discharges which do not form luminous channels but only weak luminous cones at the electrode surface.

1.7 Aims of the Research

The assessment of electrostatic ignition hazards requires an understanding of the electrostatic processes liable to occur in practical situations and the ability to relate these processes to quantitative safety criteria. Since practical interest centres around the selection of actions to avoid hazards, it is important to relate electrostatic observations to features of the industrial operations [Chubb et al (1979)]. In order to define the hazard in particular pneumatic conveying installations, information is required on the magnitude and the polarity of the currents produced by the powder flow, and on the effect of changes in such parameters as flow velocity, powder resistivity, particle size distribution and atmospheric conditions on charge generation.

In spite of its long history, however, the phenomenon of contact electrification is little understood. The main difficulty with the study of tribo-electrification of powder particles in

pneumatic conveying systems, and the reason why it has not been possible to develop an exact mathematical analysis, is due to the large number of variables involved and also the fact that data is not always readily reproducible. The shortage of experimental data on the influence of these parameters adds to the already considerable problems.

Due to lack of understanding of the electrostatic explosion hazards in pneumatic conveying and storage systems, a research project was first set up in 1979. It was sponsored by fourteen inter-national companies and the Health and Safety Executive (UK). The work reported in this thesis is the continuation of the research project since 1985.

The objectives of the author's project, which would lead to a better understanding of electrostatic explosion hazards arising from pneumatic transport and storage of powders, were:

1. To study the parameters which influence the magnitude and polarity of the tribo-charging of powder particles in a pneumatic conveying installation.

2. To identify and quantify possible electrostatic ignition sources when the charged powder enters a silo.

3. To produce a code of practice for the safe handling of powders during industrial operations from the electrostatic point of view.

This should lead to a reduction in the risk of explosion, giving improved safety for personnel, and economic benefits via a reduction in maintenance costs and in some cases via a reappraisal of the need for expensive inerting.

Chapter 2

Experimental facilities and measuring procedures

CHAPTER 2

EXPERIMENTAL FACILITIES AND MEASURING PROCEDURES

2.1 Introduction

Three different pieces of experimental apparatus were used during the course of the project. A unique fully instrumented large scale silo rig was set up to investigate electrostatic charging behaviour and hazards in pneumatic conveying and storage systems. A small scale model of the rig was also constructed in an attempt to gain better understanding of the transport conditions which lead to maximum powder charging.

Magnitude and incendivity of discharges from the surface of charged powders to earthed spherical probes were investigated using a hopper rig in the laboratory as well as using the large scale silo rig.

2.2 Industrial Scale Electrostatic Hazards Investigation

Figure 2.1 shows the industrial scale experimental rig. It consists of a test silo and a storage silo with volumes of 65 m^3 and 56 m^3 and diameters of 4 m and 3 m respectively. The two silos are linked by a closed system of steel pipes of 10 cm diameter. The powder is pneumatically transported along a pipe run of 40 m from the storage silo to the test silo. The run consists of straight sections and bends. Pipe bend radii are 1.5 m and the powder is lifted over a height of 10 m before entering the test silo. The return to the storage silo takes place through a short pipe section.

The excess air in the silo is passed through a filter unit which is situated on top of the storage silo before being used for powder conveying again.

Figure 2.1a Industrial Scale Electrostatic Hazards Investigation Experimental Rig

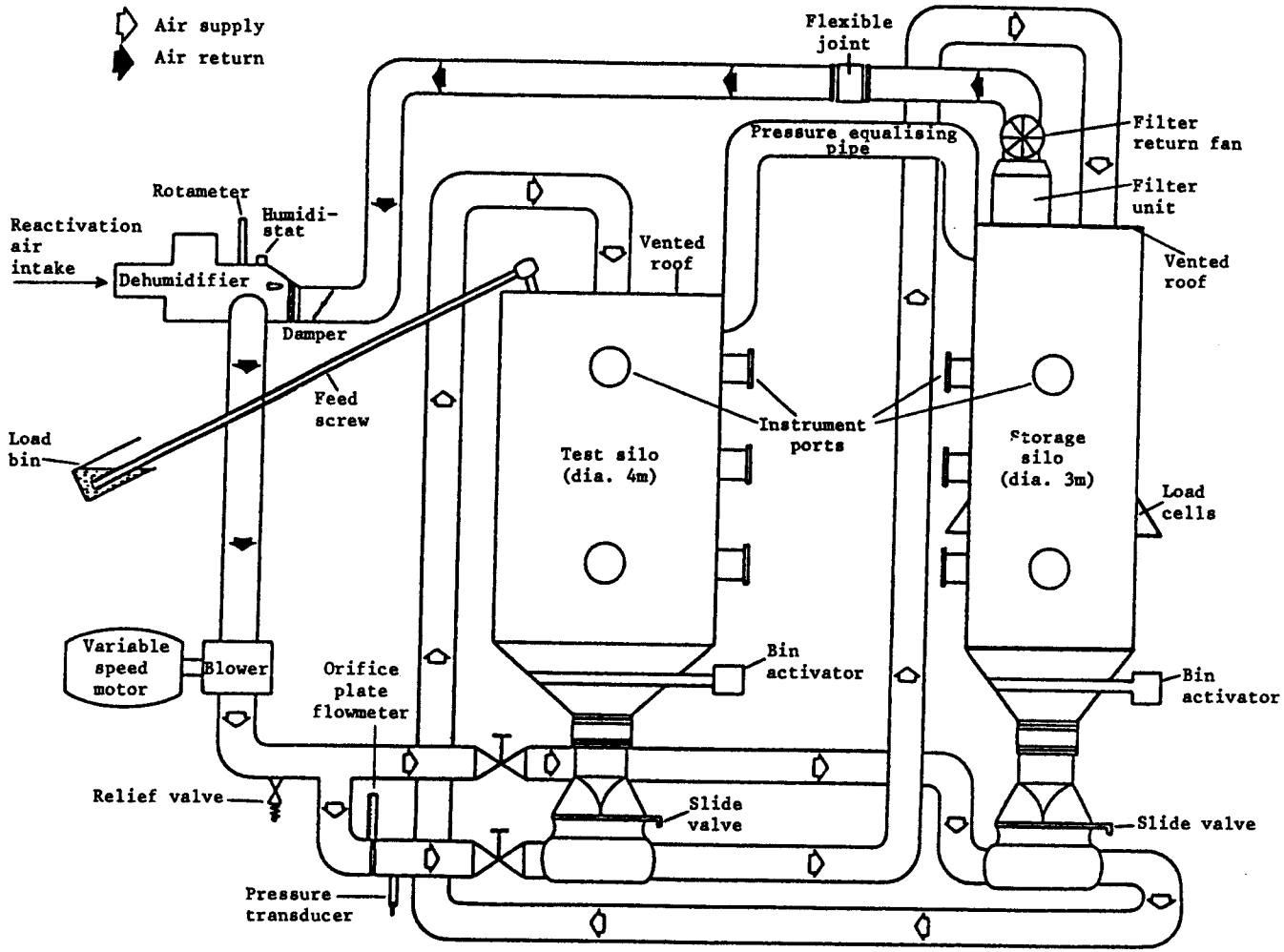

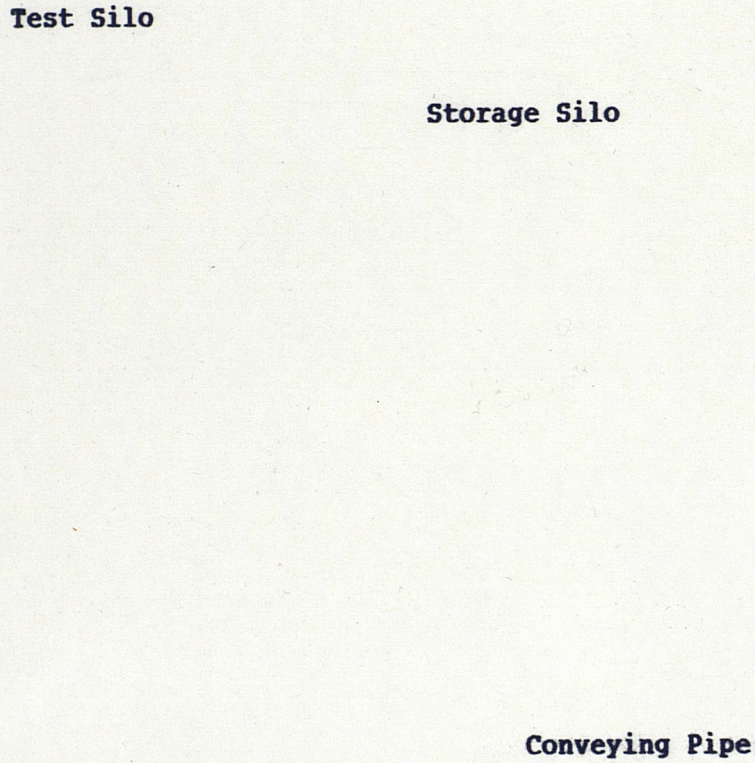

Figure 2.1b Industrial Scale Experimental Rig (Marchwood Silo Rig)

Figure 2.1b Industrial Scale Experimental Rig (Marchwood Silo Rig)

The test silo is fitted with 15 portholes to accommodate test instruments. A vibrating bin activator is fitted to each silo to ensure an even powder flow during emptying. In order to reduce the risk of any possible damage to the silo rig by dust explosions, both silos are explosion vented.

2.2.1 Instrumentation

2.2.1.1 Conveying Air Relative Humidity Control

The humidity of the transport air can be reduced by means of a dehumidifier situated in the air return line, upstream of the blower. The air to be dehumidified (process air) is drawn through a drying wheel which is capable of reducing the air relative humidity from about 80% to about 15% in less than 60 minutes.

The relative humidity of silo transport air is increased using a water spraying nozzle. The nozzle is mounted in the wall of the conveying pipe, 1.25 m from the exit of the storage silo rotary valve.

With no powder flow ($\dot{m} = 0$) the silo relative humidity was increased to the required value, the nozzle was then removed and after a few minutes the powder transfer was started. This time was allowed for any possible condensation on the inner wall of the conveying pipe to be removed by transport air. Relative humidities as high as about 80% were obtained using this technique.

The transport air relative humidity and temperature were measured using an electronic battery-powered instrument with accuracies greater than 2% RH (10-80%) and ± 0.5°C (-10 - +50°C).

2.2.1.2 Powder Mass Flow Rate Measurements

The storage silo stands on three load cells to permit continuous monitoring of powder weight. The powder feed rate from the silo is controlled using a power operated rotary feeder. This consists of an eight segment rotating wheel in a close fitting casting with top entry port and side discharge. The rotary feeder

has a variable speed of 4.5 rpm to 26 rpm with a maximum capacity of 19000 cm^3/rev. The rotary feeder causes the powder to be transported through the conveying pipes in a pulsing manner.

2.2.1.3 Transport Air Velocity Measurements

The mean air velocity is calculated from an orifice plate flowmeter reading and the inner diameter of the conveying pipe. Knowing the effective pressure, P_E, at the flowmeter inlet the flowmeter scale reading at A.T.P. is converted into the actual flow rate using equation (2.1):

$$\text{Actual Flow (Volumes at A.T.P.)} = \text{Scale Reading A.T.P.} \times \sqrt{1 + P_E \text{ bars}} \qquad (2.1)$$

A variable speed blower with a maximum air flow rate of 1140 m^3/hr enables the air velocity to be controlled.

2.2.1.4 Current Measurements

The conveying pipe consists of four bends of 1.5 m radius and 2.3 m long and a 180° bend which is 5 m long and also a number of straight pipes of different lengths. All the pipe sections are electrically isolated from each other and may be earthed through electrometers. The contribution of each pipe section to the total charge per unit time (current) generated on the powder particles can therefore be measured.

The test silo is electrically isolated from ground and is normally earthed by connection to an electrometer. The powder with a charge Q entering the test silo induces charge -Q on the surrounding enclosure and, if the test silo is connected to an electrometer of input capacitance C_E, the electrometer will indicate a voltage

$$V = \frac{Q}{(C_1 + C_E)} \qquad (2.2)$$

where C_1 is the capacitance of the enclosure to ground.

This method (Faraday Cup) is simple and gives the absolute value of the charge.

When a continuous stream of charge, for example during powder flow, flows into the cup the voltage on the capacitor will rise steadily for as long as charged material accumulates in the silo. Therefore, when making a continuous measurement of this nature, the capacitor is replaced by a resistor, Z, so that the induced charge on the test silo wall is drawn directly from earth. This continuous flow of charge constitutes a current whose magnitude, I, is equal to the rate $\frac{dQ}{dt}$, at which charge entrained in the product enters the test silo. In this situation

$$\frac{dQ}{dt} = I = \frac{V}{Z} \qquad (2.3)$$

To perform the measurements, a Keithley Model 602 electrometer was used. Although the connection of isolated pipe sections or the test silo to earth through electrometers introduced a resistance in the path of the charge relaxation (due to the internal resistance of the electrometer) no dangerous level of charge will be accumulated if the resistance to earth is less than $10^6\Omega$ [Gibson (1983)].

2.2.1.5 Electric Field Measurements

Electric field meters were used to measure the radial component of electric field at different heights in the silo wall and on the wall of the conveying pipe [Pollard et al (1975)]. The field mills were air purged to prevent powder deposition on their surfaces.

All field meters were calibrated similarly using parallel plates. A diagram of the calibration parallel plates is shown in Figure 2.2. Since the electric field mills were most sensitive to the fields from charged powder particles in their immediate vicinity, it was suspected that the mill near the test silo top would read fields due principally to the finest powder carried in the air amid the general air turbulence.

Figure 2.2 Schematic Representation of Field Meter Calibration Parallel Plates

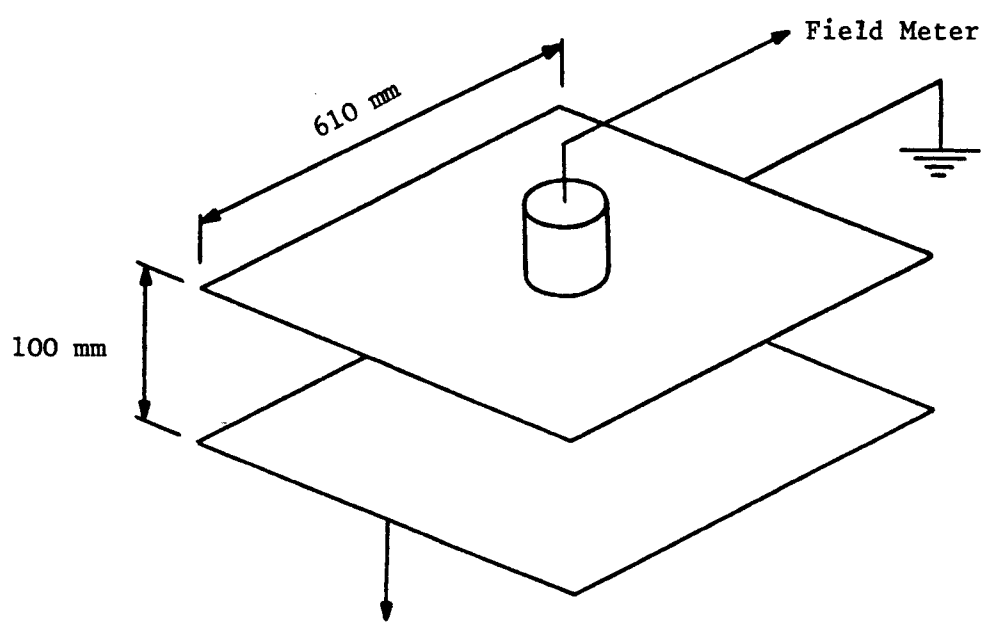

Throughout this project, a distinction has been drawn between powder 'fines' and the 'coarse' (larger particles) for HDPE. There is, of course, no clear division to be made between fines and coarse from a size point of view, but it is nevertheless true that fine particles are more likely to be found in the gas space above the bulked powder than coarse particles.

2.2.1.6 Electric Space Potential Measurements in the Dust Cloud

A rotating vane field mill mounted flush with the surface of a spherical shroud of approximately 40 cm diameter was used to perform the measurements. The vane was driven by compressed air which was also used to purge the vanes and detection plates to keep them free from dust. The spherical shroud was used to increase the range of the field meter. The field meter was calibrated to enable the space potential (in the absence of the mill head) at the measurement point, to be inferred. The calibration was obtained by suspending the spherical shroud containing the field mill in a metal drum which was connected to a high voltage d.c. generator. With the spherical shroud connected to earth the field meter readings were recorded for a range of potentials on the drum (see Figure 2.3).

The field mill was suspended at different heights in the dust cloud and the field measurements were translated into the potential at which that point would have been in the absence of the mill.

2.2.1.7 Measurement of Electrostatic Discharges

2.2.1.7.1 Detection of Discharges by Radio Frequency Method

Electrostatic sparks are detected through their emission of electromagnetic radiation. The presence of discharges in the test silo was monitored using a radio frequency detection system at radio frequencies of 38 MHz with a bandwidth of 2 MHz. This method of detection provided a high sensitivity to low energy electrostatic sparks, combined with a low sensitivity to corona discharges. The latter were unlikely to cause ignition [Butterworth (1979), Chubb (1974), Chubb et al (1973)].

Figure 2.3 Schematic Representation of Field Meter Calibration for Space Potential Measurement

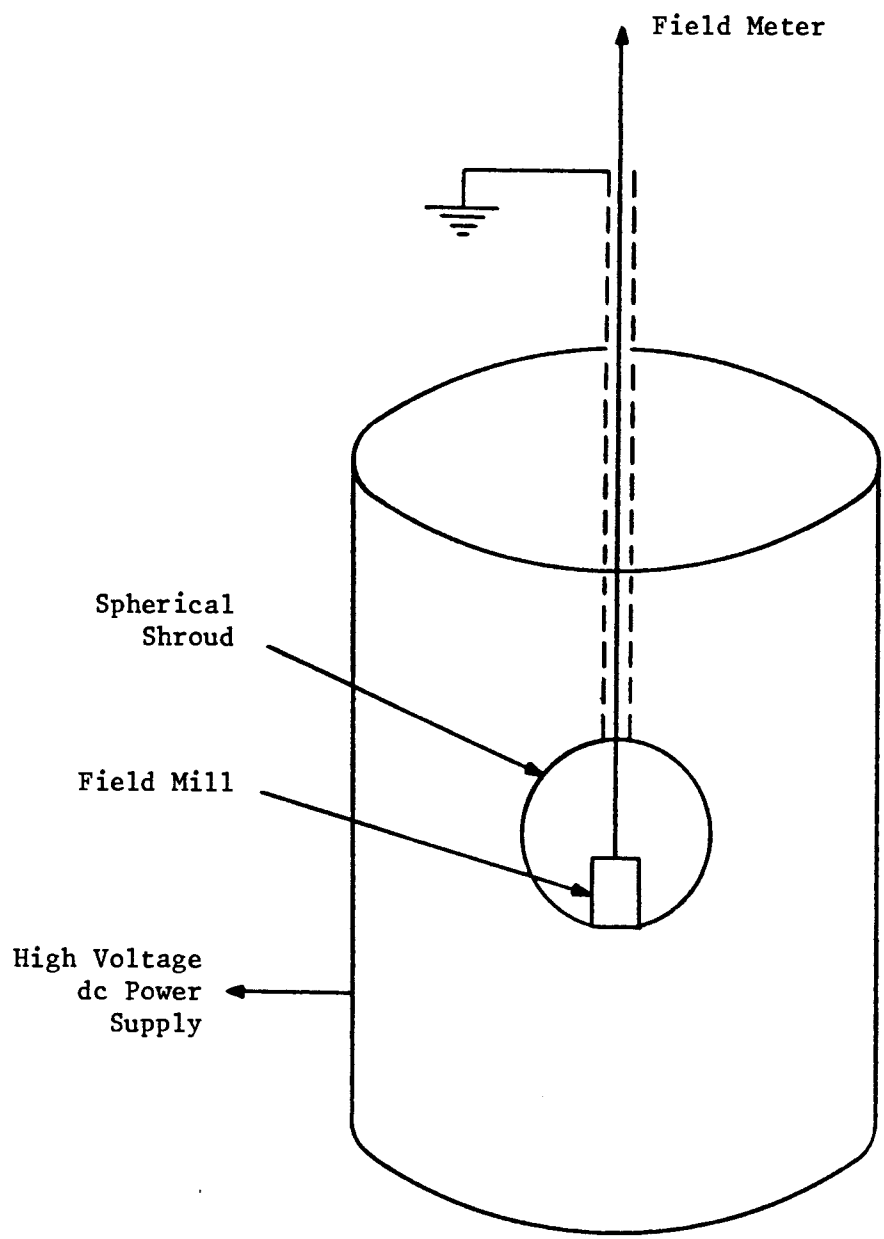

Two aerials were mounted inside the test silo and one outside. Signals from three receivers passed to coincidence and anti-coincidence circuits which ensured that signals originating within the silo were counted as significant only if detected by both internal aerials in the absence of a signal from the external aerial. This arrangement eliminated interference from external sources and the effect of local events very close to either aerial. A discriminator was included in each radio channel which could be set to distinguish significant events from low level background signals. A schematic is shown in Figure 2.4.

2.2.1.7.2 Measurement of Charge Transfer in a Discharge

A metal sphere of diameter 19 mm, which is connected to earth through an oscilloscope by a length of coaxial cable with a capacitance of 4.8 nF, is shown in Figure 2.5. The probe was either suspended in the air space above the bulked powder or was lowered towards the bulked powder in an attempt to promote discharges.

The total charge transfer to the probe is given by equation (2.4).

$$\text{Charge transfer} = CV \qquad (2.4)$$

where C is the total capacitance of metal sphere, coaxial cable and the internal capacitance of the oscilloscope. V is peak voltage rise seen on the oscilloscope [Wilson (1985), Kramer et al (1979)].

Brush discharges between a negatively charged insulating liquid and an earthed conducting electrode were studied by means of the charge transfer measurement technique shown in Figure 2.5 [Mills et al (1982)]. It is shown that with brush discharges the error due to the pre-breakdown charge induced on the electrode is small in relation to the discharge magnitude. Providing the electrode geometry does not approach plane parallel, the error will be in the order of 5%.

Figure 2.4 Schematic of Radio Frequency Spark Detection Equipment

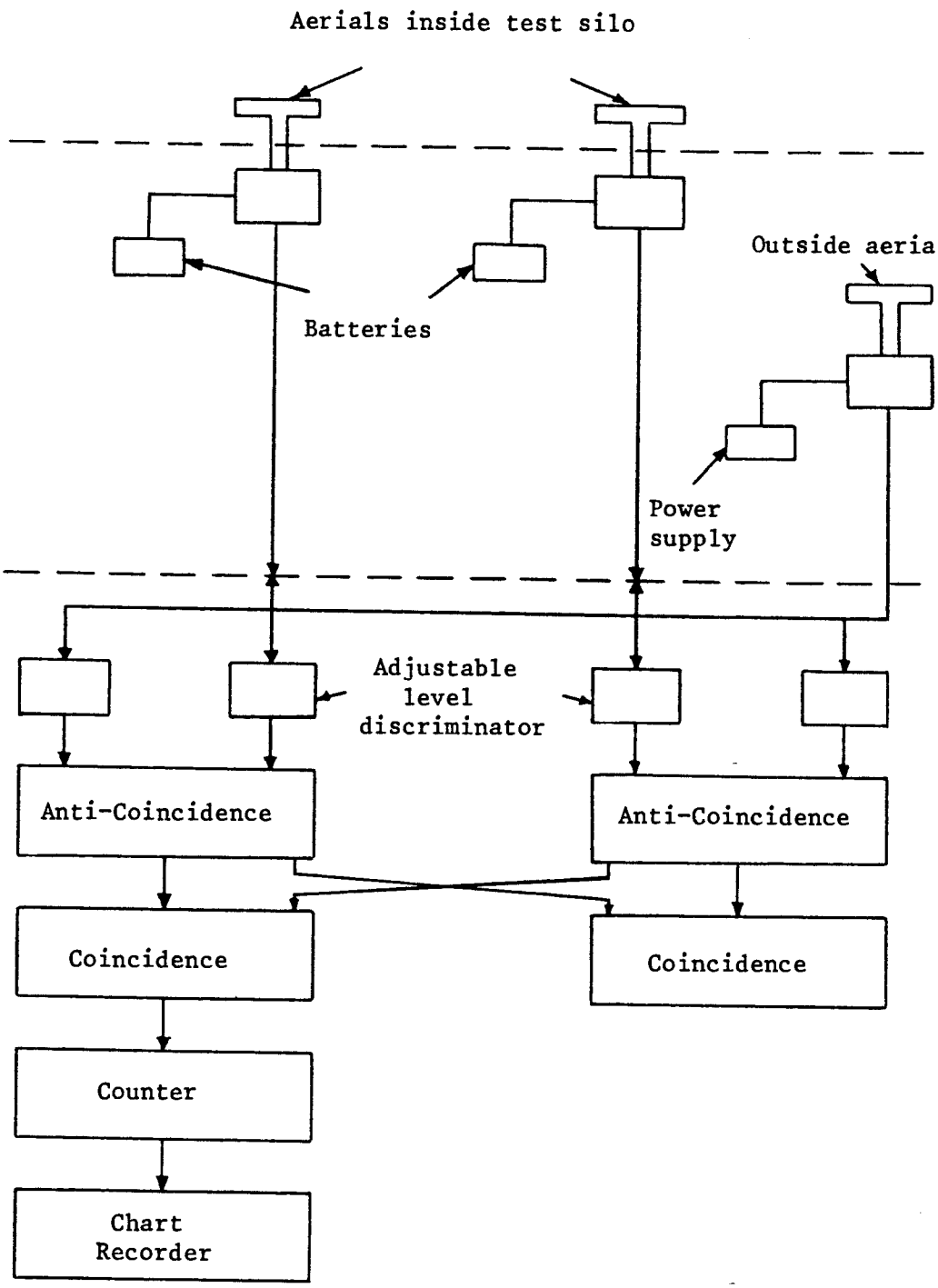

Figure 2.5 A Charge Transfer Measurement Diagram

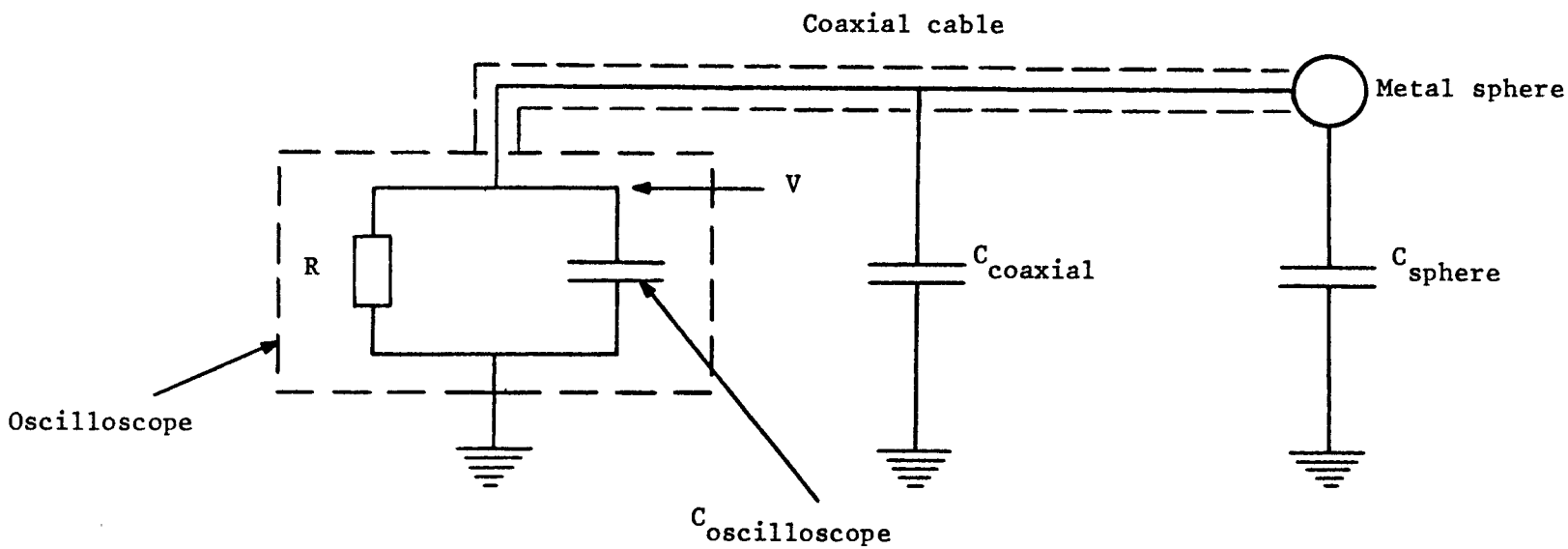

$C_{coaxial} + C_{sphere} = 4.84$ nF

2.2.1.7.3 Measurement of the Incendivity of Discharges

A gas shrouded probe was used to measure the incendivity of discharges from the surface of the bulked powder or from the powder dust cloud. The probe comprised a 19 mm diameter metal sphere which was immersed in a localised environment of propane/air of known ignition energy. The size of any discharge to the probe was measured on the oscilloscope as described in section 2.2.1.7.2. The construction of the probe was based on a design by Gibson and Lloyd (1965).

The minimum ignition energy of the propane/air mixture used in our experiments was 0.25 mJ [Lewis et al (1961)]. Any electrostatic discharge from the surface of the bulked powder or from the powder dust cloud, which was capable of igniting this propane/air mixture, was considered to have an equivalent electrical energy of at least 0.25 mJ [Gibson et al (1965)].

A diagram of the gas emitting probe is shown in Figure 2.6. The probe was connected via a coaxial cable to a parallel resistor/ capacitor circuit. All other metal parts of the probe (gas fittings and the metal gauze needed for sealing of the glass beads) were earthed via the outer screen of the coaxial cable. The main body of the probe was made of nylon.

The probe was arranged to insert into the silo from directly above one of the explosion vents which could be opened remotely. The gas flow rates were controlled using gas flowmeters and the gas/air mixture was sent along a flexible airline to the gas probe. A Riken type 18 gas indicator was also used to check the fractional propane percentage at the gas probe outlet. The Riken type 18 instrument functions on the basis of the variations in the refractive index due to the changes in the propane concentrations in air.

Figure 2.6 Gas Emitting Probe

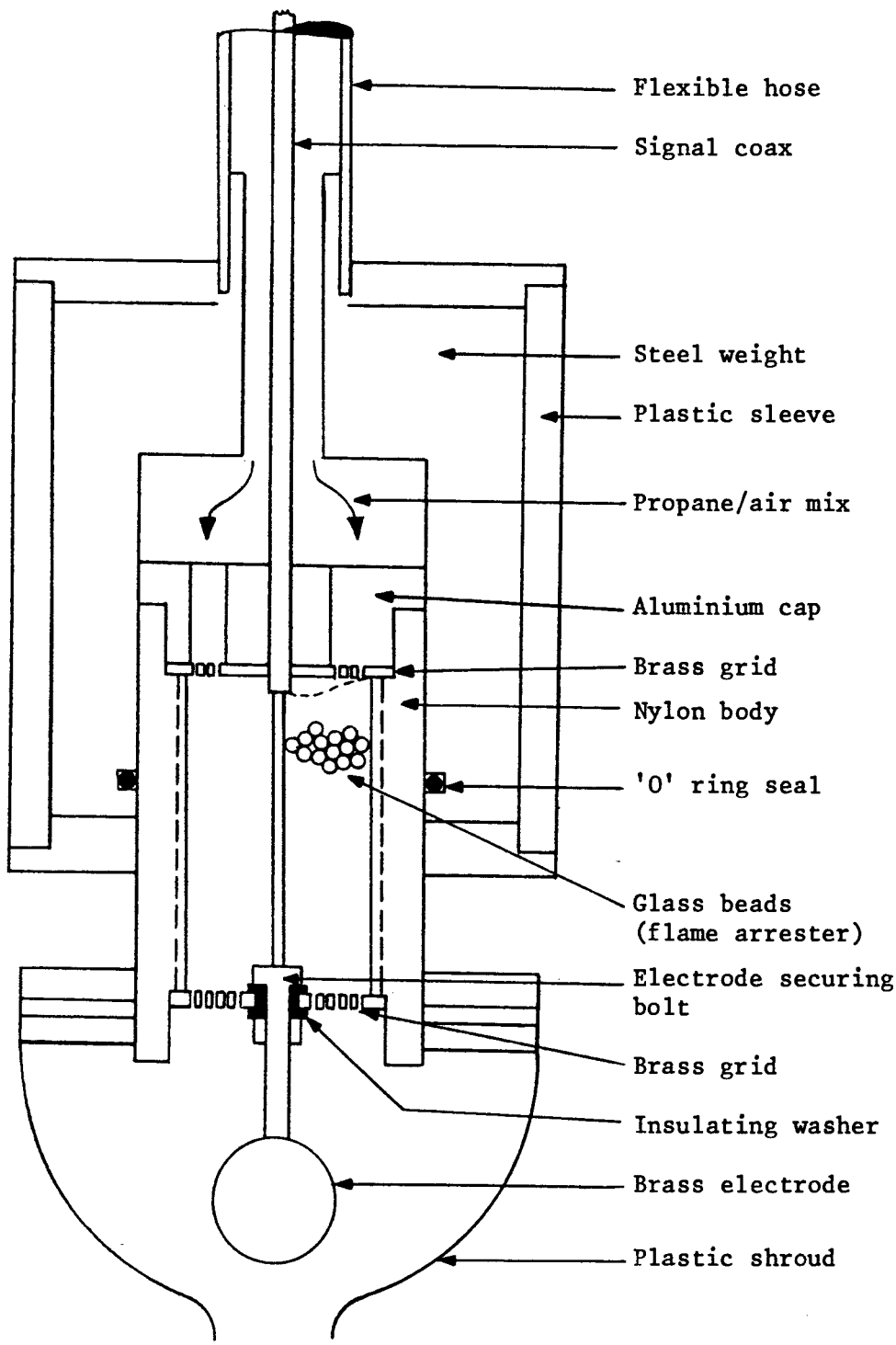

2.3 Powder Charging using a Corona Charge Injector

During some experiments the natural charging levels of powders were increased with the aid of a corona discharge injector. The aim of this practice was to create extreme conditions under which electrostatic discharges could happen.

The corona charge injector, which comprises a solid rod with protruding needles mounted along the axis of a 45 cm section of the conveying pipe, can supply charge at a rate of up to 200 $\mu C\ s^{-1}$ at 30 kV. The corona charge injector could be positioned at different points in the conveying pipe.

The use of unipolar corona discharge for particle charging is a very reliable method of charging particles. A high voltage applied to a sharply curved electrode will ionise the air in the vicinity of the electrode when the field reaches a critical value. Complete breakdown of the gap is prevented by the rapid divergence of the electric field away from the electrode.

A corona discharge that occurs when the discharge is negative (positive) in potential with respect to its surroundings is termed a negative (positive) corona. Large kinetic energies are acquired by electrons which are accelerated in the high field region and frequently liberate other electrons by collision with air molecules [Coventry (1984)]. Electron avalanches are developed in the high field region. Their trajectories, however, are directed away from the discharge electrode. In a positive corona, electron avalanches develop towards the discharge electrode, leaving positive ions in their wake. As ionic mobilities are less than electron mobilities, a slowly moving positive space accumulates.

A particle of radius r placed in the ion stream will intercept and trap ions on its surface and will continue to charge to a value Q given by equation (2.5).

$$Q = 4\pi \epsilon_o r^2 \left(\frac{3 \epsilon_r}{\epsilon_r + 2} \right) E \qquad (2.5)$$

where ϵ_r is the relative permittivity of the particle and E the applied electric field.

2.4 Control of Powder Specific Charge by Means of Superimposed Electric Field

A steel conducting rod of diameter 5 mm and length 300 mm was mounted coaxially in the centre of a steel pipe section of length 500 mm and with the same diameter as the rest of the steel conveying pipes. The rod was insulated from the pipe wall and supported by two PVC bars. The pipe section containing the rod (superimposed electric field device) replaced a 500 mm section of the transport loop on top of the test silo.

An HV power supply was used to establish an electric field between the conducting rod and the earthed pipe wall. The tribo-electrification currents resulting from the collision of powder particles with the conducting rod were measured by an electrometer. The diameter of the conducting rod was sufficiently large to prevent the onset of corona discharge from the rod when potentials as high as about 30 kV were applied to it.

2.5 Silo Scale Model

Figure 2.7 shows a schematic diagram of the small-scale experimental rig. It consists of a powder rotary feeder, a Faraday cup and a conveying metal pipework which links the two together. Pneumatic transport is used to transfer powder through the conveying pipe from the rotary feeder to the Faraday cup. Powder is fed at a fairly constant rate from a vibratory feeder into a small hopper located above the rotary feeder. The rotary feeder is a variable speed, eight segment device which is an approximate scale model of the rotary feeders at Marchwood silo rig. A DC motor whose speed is varied by a Variac is used to drive the rotary feeder.

Figure 2.7 Schematic Diagram of Laboratory Pneumatic Transport Apparatus

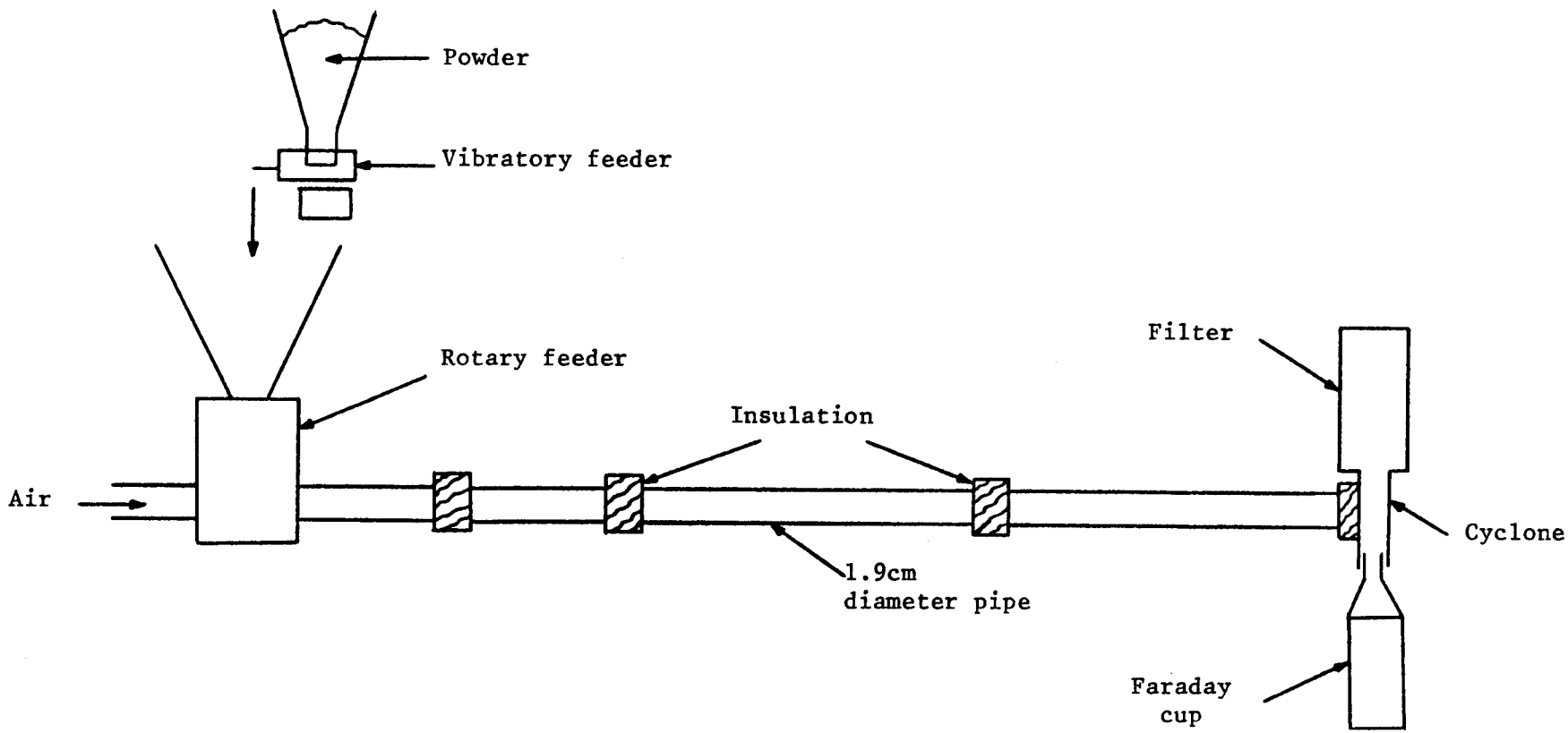

A segmented transport pipe of variable length and geometry is used. Each segment is electrically insulated from its neighbour to enable current measurements to be performed to ascertain the location of powder charging in the system.

2.5.1 Cyclone Faraday Cup

The total specific charge on the powder is measured in a Faraday cup at the end of the conveying pipe. The Faraday cup consists of two concentric aluminium cups which are electrically insulated from each other. The inner cup is connected to an electrometer to enable measurements of charge on powder. The external cup which is electrically earthed is used for screening the inner cup from any external electrical noise sources, for example mains or other charged objects, such as the experimenter.

A cyclone is connected on the top of the Faraday cup which is basically a spiral plate system situated in a pipe [Dixon (1981)]. Its function is to separate the powder from air upwards to a filter. The cyclone is most efficient when used with coarse powder.

A Keithley Model 602 electrometer was used for the current measurements, as explained in section 2.2.1.4.

2.5.2 Transport Air Velocity Measurements

The mean air velocity is calculated from an orifice plate flowmeter with a scale accuracy of ± 3% FSD. The flowmeter has a non-linear scale of from 40 to 440 litre/min, so knowing the effective pressure, P_E, at the flowmeter inlet the flowmeter scale reading at ATP is converted into actual flow rate using equation (2.1).

2.5.3 Measurement of Mass Flow Rate

An accurate method of mass flow rate measurement is to weigh the net mass of powder collected in the Faraday cup for a known period of time. This method takes into account the powder rejected out of the vacuum outlet pipe in the rotary feeder case during high mass flow transportations and also at low air flow speeds.

The balance used for weighing the powder is a Sartorious electronic balance with an accuracy of 10 mg.

2.6 Spiral Conveyor and Electrostatic Powder Handling Rig

Figure 2.8 shows the schematic diagram of the laboratory rig used to study the characteristics and incendivity of electrostatic discharges from the surface of bulked materials. Due to the relatively small load of materials required for testing, it is possible to test products that are available in small quantities.

The rig consists of two storage metal hoppers each of 50 cm diameter and volume of 0.10 m^3 placed one above the other and isolated from the metal frame. The top hopper can be adjusted at any height from the top of the bottom hopper. The powder falls from the top hopper into the bottom hopper under gravity. A pipe section of inside diameter 10 cm connects the two hoppers together. The amount of powder leaving the top hopper is controlled by a lever-operated valve. The powder in the bottom hopper is transferred back into the top hopper by a flexible spiral conveyor.

2.6.1 Current Measurements

The hoppers are electrically isolated from the metal frame of the rig and earthed by connection to electrometers to allow measurement of charge per unit time on the powder entering the hoppers. Because no significant tribo-electric charging took place during the gravitational feed of HDPE powder, the corona charge injector device described in section 2.3 was positioned inside the pipe connecting the hoppers to charge the powder particles. Variation of the corona potential and the mass flow rate of powder resulted in a range of streaming currents and therefore specific charge densities.

A Keithley Model 602 electrometer was used to perform the current measurements as explained in section 2.2.1.4.

Figure 2.8 Spiral Conveyor and Electrostatic Powder Handling Rig

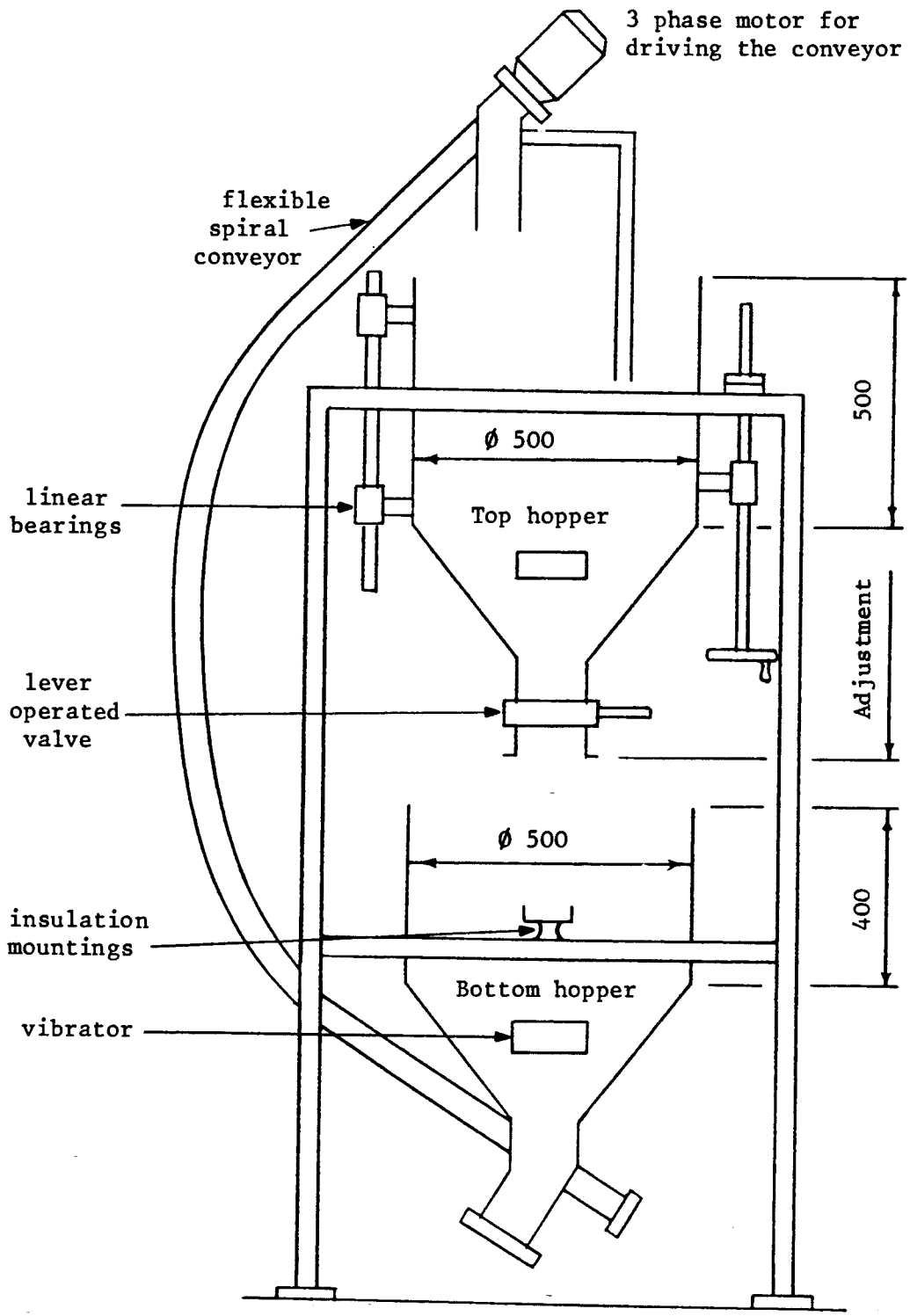

2.6.2 Powder Mass Flow Rate Measurements

The mass of powder entering the bottom hopper per unit time (mass flow rate) is controlled by a lever-operated 100 mm diameter diaphragm valve connected to the bottom of the top hopper. The valve was calibrated to give five different mass flow rates. The calibration was carried out by weighing small batches of powder collected for known periods of time, for each valve setting.

2.6.3 Current Transients for Brush Discharges

A discharge was produced by lowering the probe onto the surface of charged bulked powder. The magnitude of the charge transfer was determined by measuring the rise in potential across a capacitor, as shown in Figure 2.5. Alternatively, the current transients were monitored using the circuit diagram shown in Figure 2.9.

The current transients were monitored with a fast Tektronix 7912 AD transient digitiser, as the voltage developed across the 50 Ω characteristic impedance of the coaxial cable. The transient digitiser was used with a sweep rate of 100 ns/division and had a sweep accuracy of 1.5%.

The data were presented as a graph by a Nimbus computer which took the data from the transient digitiser. The graph had vertical and horizontal resolutions of 128 dots and 512 dots respectively. The print-out was the direct copy of the screen display.

2.6.4 Measurement of Total Charge Transfer from Bulked HDPE Surface

The total charge transfer during each probe insertion onto the surface of bulked HDPE pellets and fine powder is determined using the circuit diagram shown in Figure 2.10. The total charge transfer from the discharges to the probe is measured by connecting the gas emitting probe to earth via a low leakage 10 μF poly-carbonate capacitor. The voltage rise on the capacitor is measured by connecting the capacitor to an oscilloscope via a

Figure 2.9 Experimental Arrangement for Current Transient Experiments

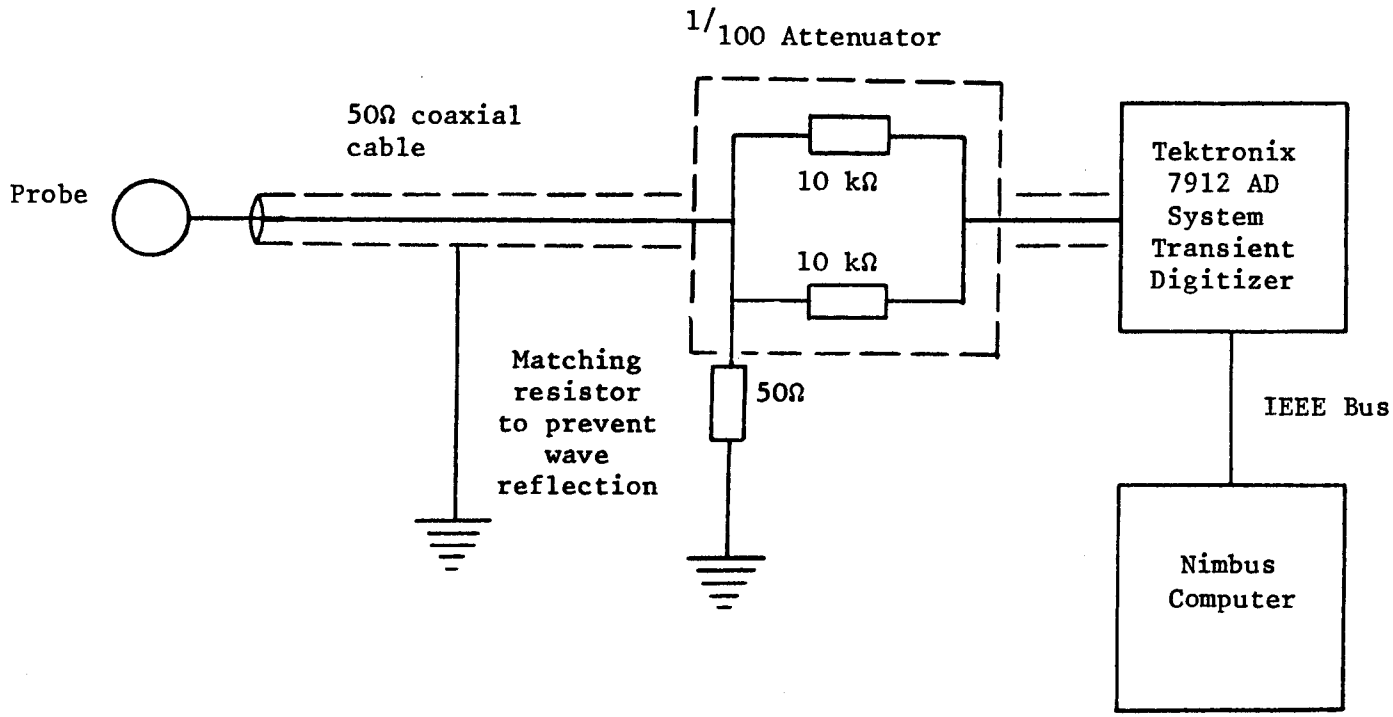

Figure 2.10 Circuit Diagram for Total Charge Transfer Measurements

C_1 = 10 μF Polycarbonate

C_2 = 47 pF

R_1 = 1 kΩ

R_2 = 1 MΩ

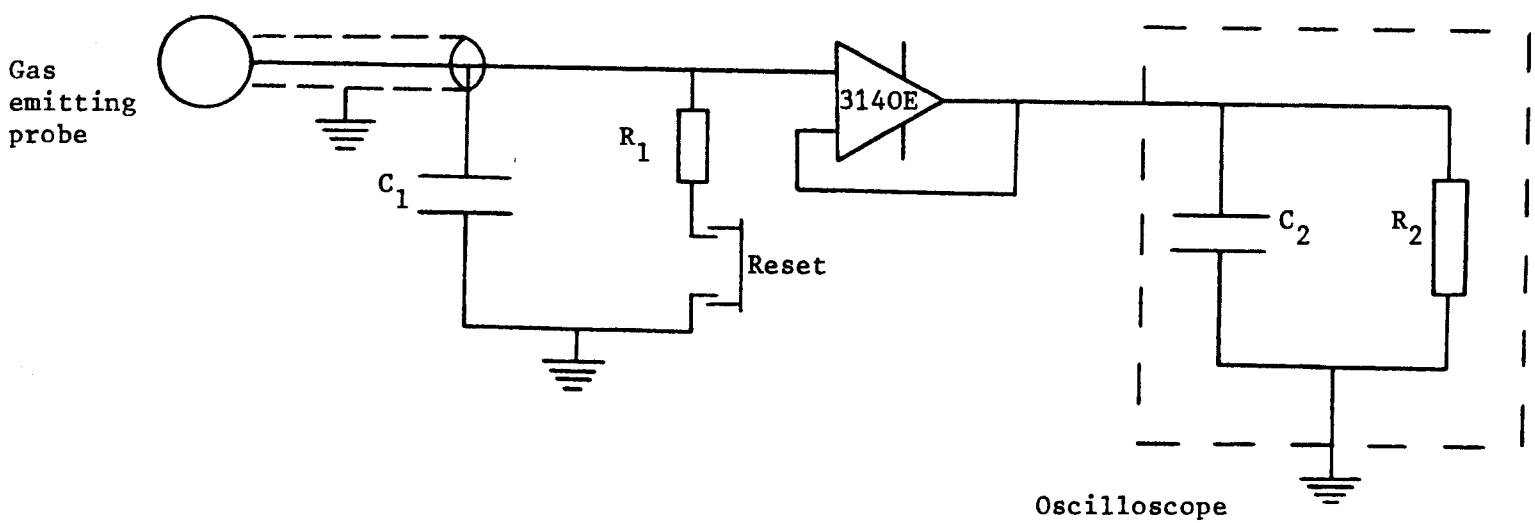

voltage follower. The voltage follower has a characteristic input impedance of 1.5×10^{12} Ω.

The capacitor can be discharged by pressing the reset button.

2.6.5 Measurement of Incendivity of Discharges from HDPE Pellets

A gas emitting probe similar to the probe used at the Marchwood silo rig was used (see section 2.2.1.7.3). A perspex tube of length one metre connected the gas emitting probe to the flexible propane/air/nitrogen mixture line. The gas emitting probe fixed to the perspex tube slid in an adjustable sliding fit PVC support pipe which was mounted onto the hopper rig metal frame. This arrangement ensured that the gas emitting probe could be directed repeatedly to any fixed point on the surface of bulked HDPE in the bottom hopper.

The minimum ignition energy of the propane/air/nitrogen mixture used during this part of the project was slowly raised by increasing the additional nitrogen content while keeping the propane concentration fixed at 4.2%. The concentrations of propane are given in volume percent in respect to the total propane/air/nitrogen content. The additional amount of nitrogen in the mixture is given in volume percent in respect to the total nitrogen/air content.

$$\frac{\text{propane} \times 100}{\text{propane} + (\text{air} + \text{nitrogen})} = 4.2\%$$

The minimum ignition energies of propane/air/nitrogen mixtures determined with capacitive spark discharges are shown in Figure 2.11 [Glor (1981)].

Figure 2.11 Minimum Ignition Energies of Propane/Air/Nitrogen Mixtures, Determined with Capacitor Spark Discharges (Glor (1981))

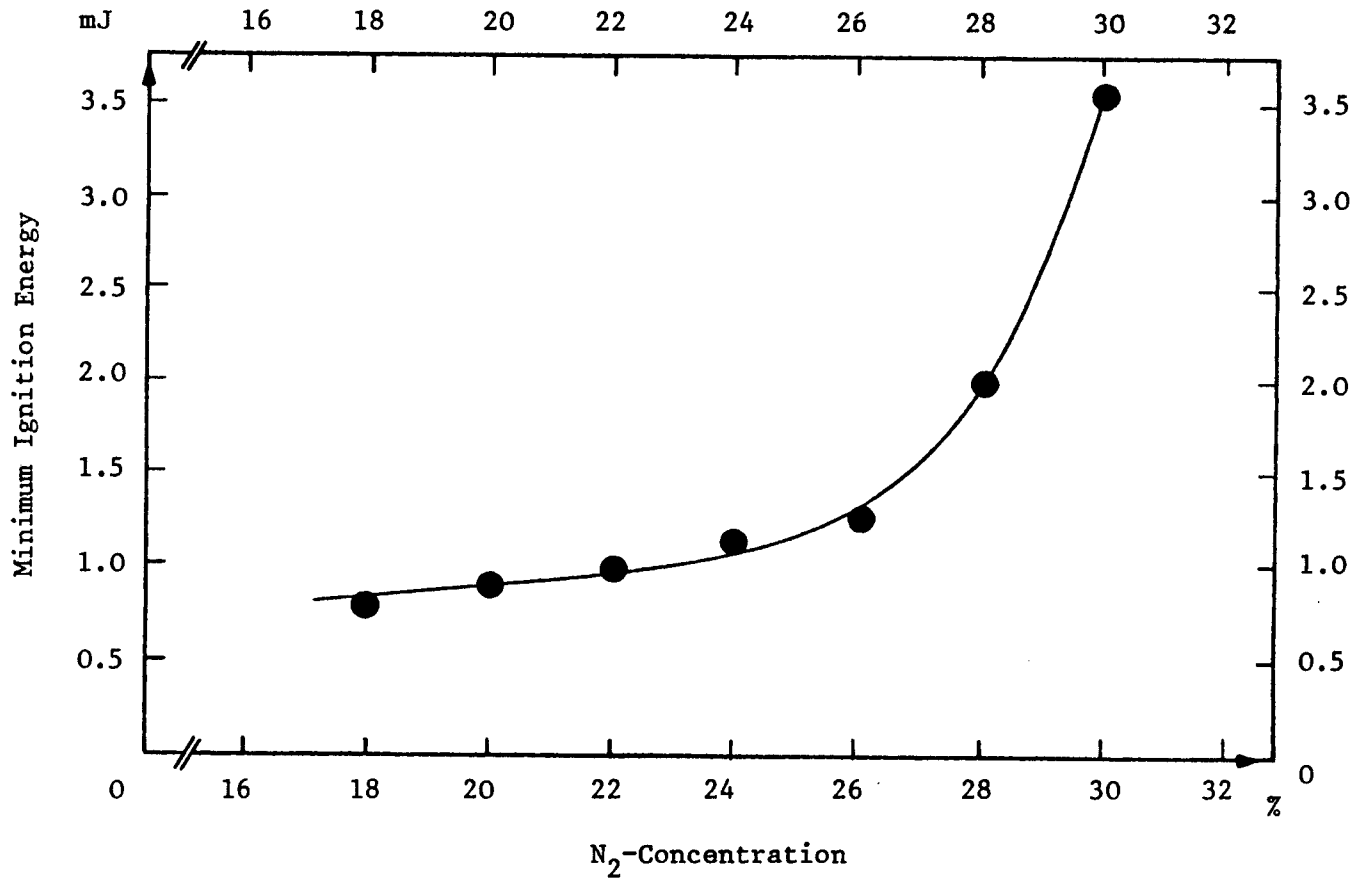

Chapter 3

Tribo-electrification of powders by pneumatic conveying

CHAPTER 3

TRIBO-ELECTRIFICATION OF POWDERS BY PNEUMATIC CONVEYING

3.1 Introduction

In order to most effectively control and eliminate hazards which arise from contact electrification or to devise new applications and optimise present applications it is necessary to understand the mechanisms responsible for charge transfer and the accompanying dissipation processes.

The experimental work during this part of the project is concerned with examining some of the transporting parameters which influence the charge build-up on the powder.

In a pneumatic conveying system, the powder particles become charged at a constant rate until a saturation limit is reached. The saturation specific charge is obtained after a conveying length of a few metres. In the regions where the charge on the particles somehow causes the space charge field to exceed the saturation limit, the particles lose some of their charge at a rate which probably is proportional to the charge. The influence of space charge field on tribo-electrification is investigated by applying a superimposed electric field to control the charging of powder particles colliding with the pipe wall in the presence of such a field.

The effect of the conveying air velocity, powder mass flow rate and conveying air relative humidity on the magnitude and polarity of specific charge of powder is studied. Two powders, high density polyethylene (HDPE) and maize starch, which have different electrical properties and particle sizes, are tested. Where necessary the results of work carried out by other workers on different powders is also reported in order to draw comparisons. Some of the results obtained from the full scale rig at Marchwood

are compared with the results obtained from the laboratory tests in an attempt to gain better understanding of the electrostatic charging characteristics during pneumatic conveying and storage of powders.

3.2 Theory

a) Microscopic Considerations

Cole et al (1969-1970) presented a theory for the prediction of the electrostatic charging rate of the solid particles (see Appendix A). In the absence of charge leakage the contact potential is $V_c-(V_1- V_b)$ and the charge added to a particle per collision with the wall can be expressed as

$$\frac{dQ}{dn} = \frac{\epsilon A f}{d_c} \left(V_c - \frac{Q_T\, d_c}{2\pi\, r^2 \epsilon} - \frac{Q_T\, NR\, d_c}{2\epsilon}\right) \qquad (3.1)$$

It is considered that the initial charge, taken to be effectively at the centre of the particle, will induce a mirror charge on the particle surface. The resulting potential, V_1, at the point of contact will tend to transfer charge. V_1 is given by

$$V_1 = \frac{Q_T\, d_c}{2\pi\, r^2 \epsilon} \qquad (3.2)$$

However, if this expression is evaluated for typical parameters ($d_c = 1 \times 10^{-9}$m, $r = 100$ μm, $Q_T = 1.64 \times 10^{-11}$C), the result will be $V_1 = 0.003$V. Since V_c is of the order of 1V, V_1 is negligible. Evidently, only charge in the vicinity of the contact area affects the charge transfer.

When a charged particle approaches the earthed pipe wall, opposite charges will be induced on the pipe wall before impact. A field is established acting in the opposite direction to that producing the initial charge transfer. There is also a second electric field which is due to the space charge of particles being conveyed through the pipework. In the absence of any charge leakage

the charge added to a particle per collision with the wall was expressed by equation (3.1). The first term on the right hand side of equation (3.1) represents the charging effect due to contact potential. The other two terms represent the counter-charging effects of the image-charge field (2nd term) and the space-charge field (3rd term).

To examine which one of the above mentioned electric fields is the dominant one in a pneumatic conveying system, the potential difference between an initially charged particle and the earthed pipe wall at the distance d_c can be compared with the potential difference between the particle and the wall in the presence of an electric field caused by the charged particles flowing through the pipe. The ratio of the second and third terms puts the relative importance of these two effects into perspective:

$$\frac{\dfrac{Q_T\, d_c}{2\pi\, r^2 \epsilon}}{\dfrac{Q_T\, NR\, d_c}{2\epsilon}} = \frac{1}{\pi r^2\, NR} \qquad (3.3)$$

The following assumptions have been made:

i) The initial charge of a particle is uniformly distributed on the surface of the particle. In the case of resistive powders with very high resistivities, it is assumed that particles have had many collisions at different points on their surfaces.

ii) The particles are uniformly distributed in the conveying pipe.

Equation (3.3) suggests that for a fixed number of particles per unit volume and fixed pipe radius, the larger the particles, the more dominant will be the effect of the space charge field on the charge added to a particle per collision with the wall of the conveying pipe.

The relaxation time, τ, and duration of contact, Δt, are not introduced in Cole et al (1969-1970) theory. Masuda et al (1976) showed that the factor $(1 - e^{-\frac{\Delta t}{\tau}})$ multiplied by the right hand side of equation (3.1) would greatly alter the charge added to a particle per collision. As a consequence, a particle would require many more collisions to reach its saturation charge limit than shown by Cole's theory. In fact, if the relaxation time is very long compared to the contact time, equation (3.1) may be written as

$$\frac{dQ}{dn} = \frac{\epsilon A f}{d_c} \left(V_c - \frac{Q_T d_c}{2\pi r^2 \epsilon} - \frac{Q_T NR d_c}{2\epsilon}\right) \frac{\Delta t}{\tau} \qquad (3.4)$$

The duration of the contact calculated by John et al (1980) is of the order of 10^{-8} seconds for typical conditions.

Therefore a particle with a charge of Q_0 before the onset of charging by collisions with the pipe wall, after a number of collisions, acquires a total charge

$$Q_T = Q + Q_0 = \frac{Q_1}{K}(1 - e^{-Kn}) + Q_0 e^{-Kn} \qquad (3.5)$$

where

$$Q_1 = \frac{\epsilon A f V_c \Delta t}{d_c \tau}$$

$$K = k + 1 \text{ and } k = \frac{Af \Delta t}{2\pi r^2 \tau} + \frac{NR\, Af\, \Delta t}{2\tau}$$

The role of contact potential, V_c, between the particle and the pipe wall, image charge, space charge field of particles passing through the pipe, charge leakage, effective contact area, contact time, electrical relaxation time of particle material, particle size and the critical separation distance in electrostatic charging of particles in pneumatic conveying, are highlighted by equation (3.5). Most of these parameters are however very difficult if not impossible to measure.

In section b) a model is presented to explain the tribo-electrification of powder particles which considers the macroscopic parameters of a pneumatic conveying system.

b) Macroscopic Considerations

The specific charge of powder particles in a conveying pipe reaches a saturation limit after travelling through a length of pipe. The phenomenon can be divided into two counteracting processes, ie, charging and discharging [Enstad (1978)]. Charging occurs when powder particles collide with the pipe walls; discharging occurs between the powder and the tube wall when specific charge exceeds the saturation limit.

Enstad (1978) suggested that the powder charges at a constant rate, whereas the rate of the discharge of the powder probably increases with the increasing charge of the powder. The change of the charge per unit mass through an infinitesimal tube length, dl, is thus given by

$$dq = k_1\, dl - qk_2\, dl \tag{3.6}$$

Integration of equation (3.6) gives

$$q = \frac{K_1}{K_2}\,(1 - e^{-K_2 l}) + q_o e^{-K_2 l} \tag{3.7}$$

The specific charge of the transported powder particles approaches a saturation limit (q_{max}) which is already virtually achieved when

$$K_2 l \geq 5 \tag{3.8}$$

For the saturation charge limit we may consider the electric field at the boundary of a transport pipe of radius R and length l which carries powder with uniform charge per unit volume, and uniform powder density in the pipe.

The field E at the boundary of a volume containing charge Q enclosed by surface S is given by equation (3.9)

$$\iint_S E \, dS = \frac{Q}{\epsilon_o} \tag{3.9}$$

For a cylindrical pipe of radius R, the charge per unit length $\frac{Q}{L}$ is given by

$$\frac{Q}{L} = 2\epsilon_o \pi R E \tag{3.10}$$

The current leaving the pipe is given by equation (3.11)

$$I = \frac{Qv}{L} \tag{3.11}$$

Substituting equation (3.10) into equation (3.11), the maximum current leaving the pipe is therefore given by equation (3.12)

$$I_{max} = 2\epsilon_o \pi \, Rv \, E_{max} \tag{3.12}$$

Equation (3.12) can also be expressed in terms of the saturation specific charge on the powder q_{max} leaving the pipework.

$$q_{max} = \frac{2\epsilon_o \pi \, Rv \, E_{max}}{\dot{m}} \tag{3.13}$$

q_{max} in equation (3.13) is equal to $\frac{K_1}{K_2}$ in equation (3.7), therefore

$$q = \frac{2\epsilon_o \pi \, Rv \, E_{max}}{\dot{m}} (1 - e^{-K_2 l}) + q_o e^{-K_2 l} \tag{3.14}$$

Equation (3.14) shows that the specific charge of powder particles flowing through conveying pipes reaches a saturation limit after travelling a certain length. The second term in equation (3.14) shows that even if q_o is larger than the saturation specific charge which can be acquired by powder, it will be dissipated after travelling through a short section of pipe.

If equation (3.14) is applied to straight sections of Marchwood silo transport pipes the following considerations are necessary:

i) The mass flow rate at a point in the pipe during transport is not uniform but is pulsed. If the charge is localised in a small patch, the saturation electric field strength, E_{max}, on the pipe wall will be reached at a lower specific charge density.

ii) The irregularity of the shape of the powder particles, and non-uniformity of the particle surface charge, will lead to a decrease in the calculated q_{max} [Kittaka et al (1977)].

Linstrom (1978) suggested that a saturation specific charge density is achieved when the sum of the electric field at the wall of the pipe produced by the bulk of the charged powder and that due to the contact potential between the particle and wall of pipe produces the value zero. A superimposed electric field applied between a conducting rod mounted centrally in the conveying pipe and the wall of the pipe can therefore be expected to influence the specific charge of the powder particles colliding with the inner wall of the pipe.

Equation (3.14) can be rewritten as

$$q_{max} = \frac{2\pi \epsilon_o Rv}{\dot{m}} (E_{max} + E_R) \qquad (3.15)$$

3.3 Results and Discussion

3.3.1 Properties of Test Powders

The tests reported here were carried out using high density polyethylene (HDPE) powder and maize starch. Some of the electrical and physical properties of these powders are shown in Table 3.1. The cumulative mass distribution of HDPE powder and maize starch used during the experiments are shown in Figure 3.1 and Figure 3.2 respectively.

Figure 3.1 Cumulative Mass Distribution (HDPE)

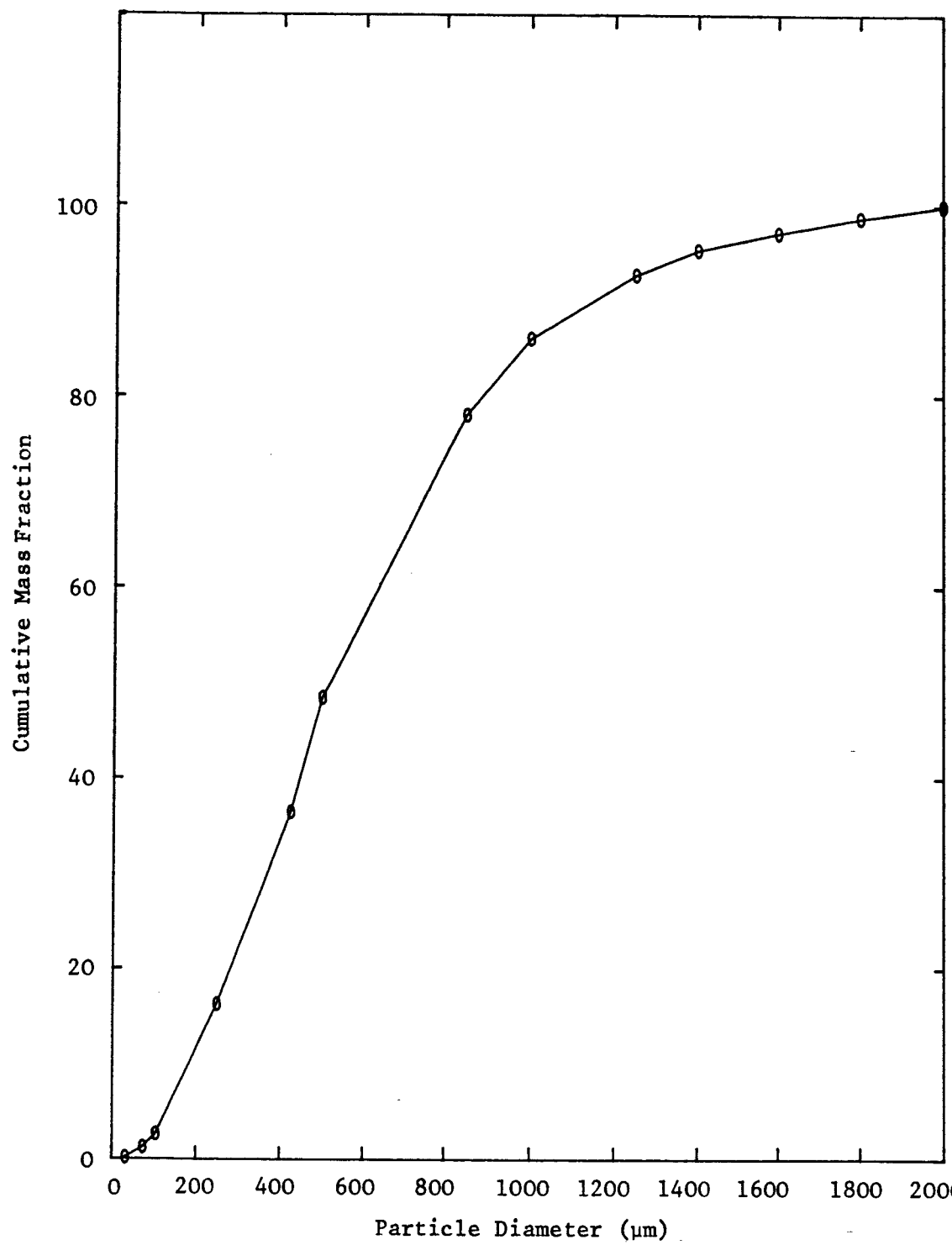

Figure 3.2 Cumulative Mass Distribution (Maize Starch)

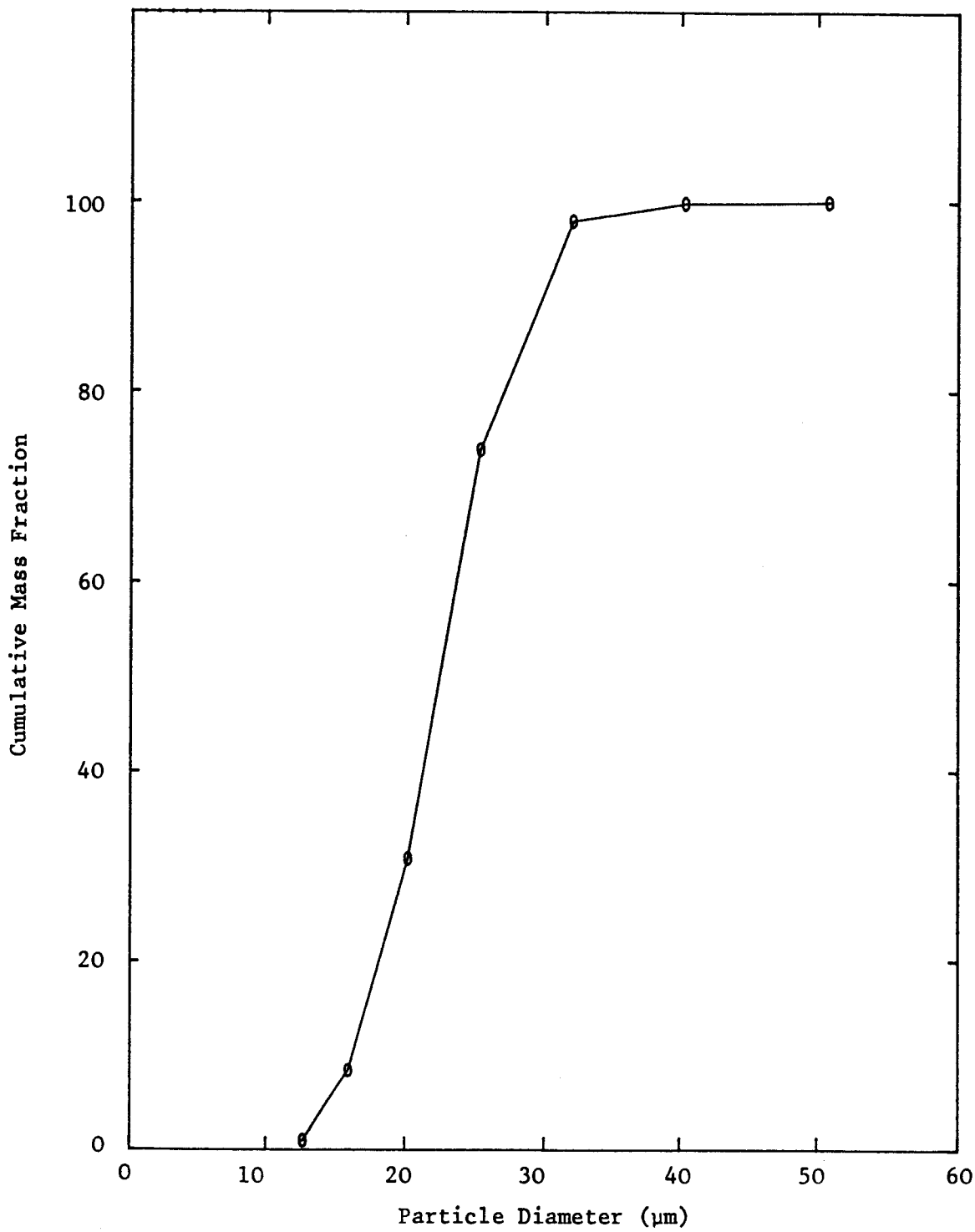

Table 3.1 Properties of Test Powders

Test Material	Volume Resistivity (Ωm)	Density (kg m^{-3})	Mass Median Diameter (μm)
HDPE	$> 10^{15}$	950	500
Maize Starch	$(0.3 - 1.0) \times 10^{9}$	625	22

3.3.2 Experiments Carried out Using the Full Scale Marchwood Silo Rig

3.3.2.1 Correlation of the Theory of the Electrostatic Charging of Powders by Pneumatic Conveying

In an attempt to verify equation (3.12), an electrostatic field mill was positioned in the wall of the conveying pipe, 0.25 m upstream of the test silo. The radial electric field of the charged powder on the wall of the conveying pipe was measured for various silo currents.

Figure 3.3 compares the measured space charge field with the one calculated using equation (3.12) as a function of the silo current, knowing the silo streaming current, powder velocity in the pipework and the radius of the conveying pipes. The largest difference between the calculated and measured values of the space charge field occurred at a silo current of -5.0 μA. This difference could be due to the influence of high space charge fields of the dust cloud inside the test silo near the fill pipe, on the field meter readings, especially at high silo currents [Lees et al (1980)].

Referring to equation (3.13), two of the factors of a pneumatic transportation installation influencing the saturation specific charge of powder entering the test silo are the powder transport velocity and the powder feed rate.

Figure 3.3 Space Charge Field on the Wall of Conveying Pipe as a Function of Silo Current (HDPE)

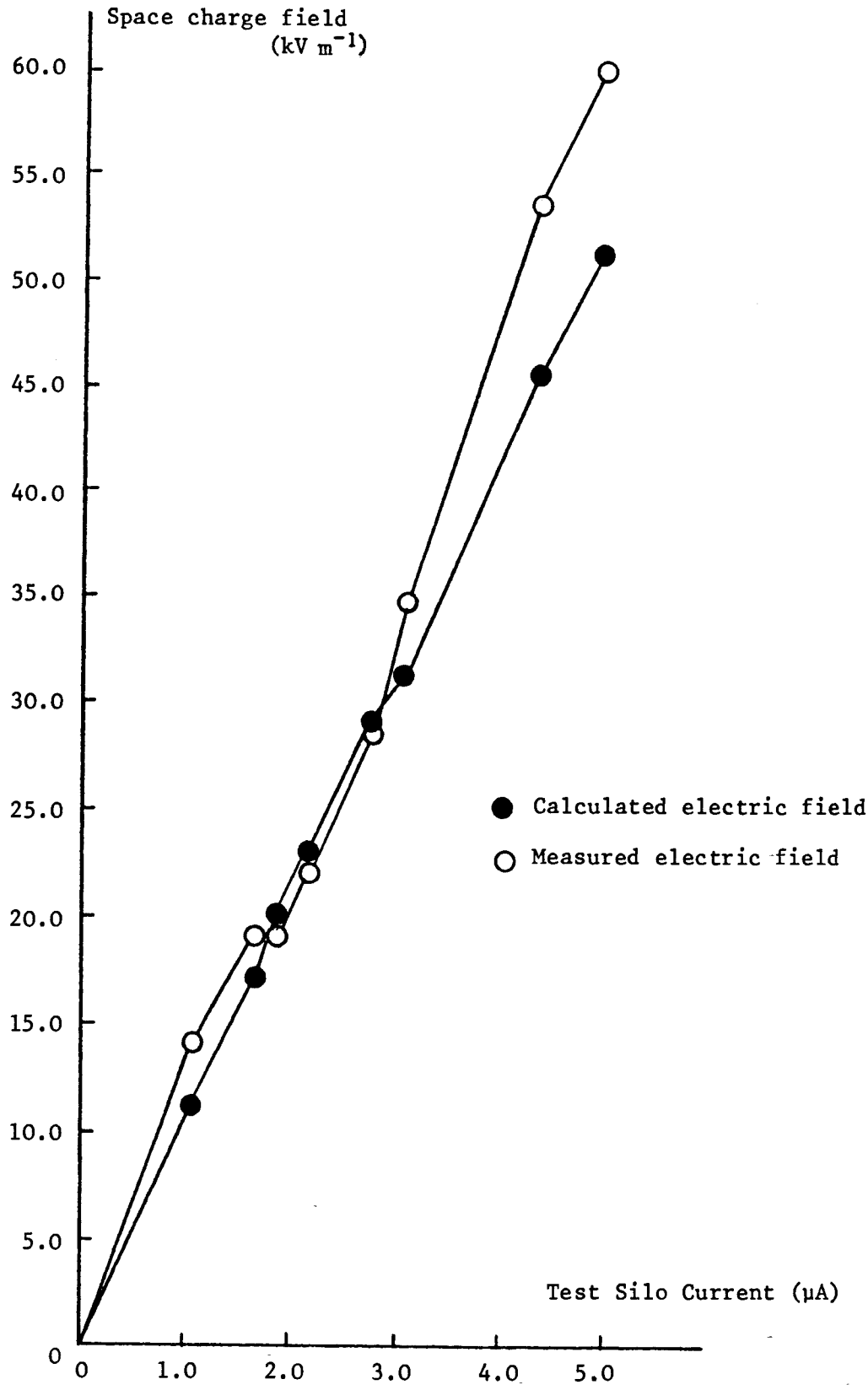

Figures 3.4 and 3.5 show the variations of the specific charge of powder entering the silo as a function of mean transport air velocity for high density polyethylene (HDPE) and maize starch respectively. The influence of air velocity on the specific charge of maize starch has been illustrated for minimum (0.4 kg s^{-1}) and maximum (3.2 kg s^{-1}) mass flow rates. These tests were carried out for the minimum powder mass flow rate at two slightly different relative humidities.

From the results, a linear dependency of the specific charge on the transport air speed is apparent. Equation (3.13) suggests that, everything else being constant, the maximum specific charge of powder entering the silo is a linear function of powder speed. What was also apparent from Figures 3.4 and 3.5 was that the powder was charged before entering the conveying pipework (the regression lines do not pass through the origin, suggesting a charge independent of the particle velocity on the powder particles). This can be explained using equation (3.14) which shows that for $v = 0$ and $L = 0$, $q = q_o$.

In these experiments it was assumed that the powder particles travelled at the same speed as that of the transport air.

Figure 3.6 illustrates the dependence of powder specific charge on mass flow rate during testing of HDPE. Although there is not a clear relationship between the specific charge and the powder feed rate the results, however, suggest that a higher specific charge is obtained at lower mass flow rates while mass flow rates of about 3.6 kg s^{-1} give lower specific charge densities.

Figure 3.7 shows the specific charge density of maize starch as a function of mass flow rate. The figure shows a clear trend with the specific charge decreasing as powder feed rate increases.

During powder handling operations, particles become electrically charged due to the process of sliding/frictional contact. As the mass flow rate increases, the number of particles

Figure 3.4 Specific Charge of HDPE Entering Test Silo as a Function of Transport Air Speed

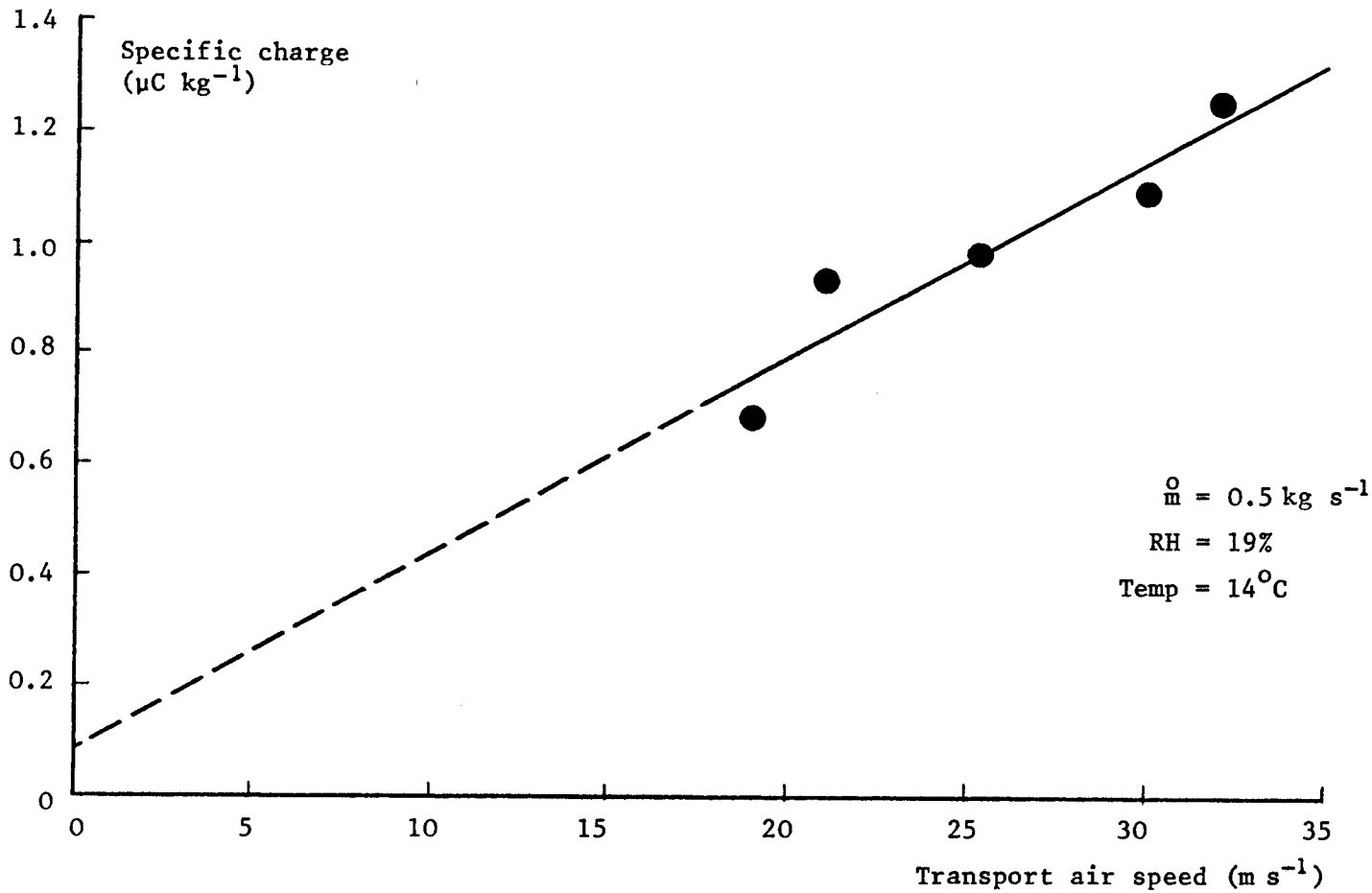

Figure 3.5 Specific Charge of Maize Starch Entering Test Silo as a Function of Transport Air Speed

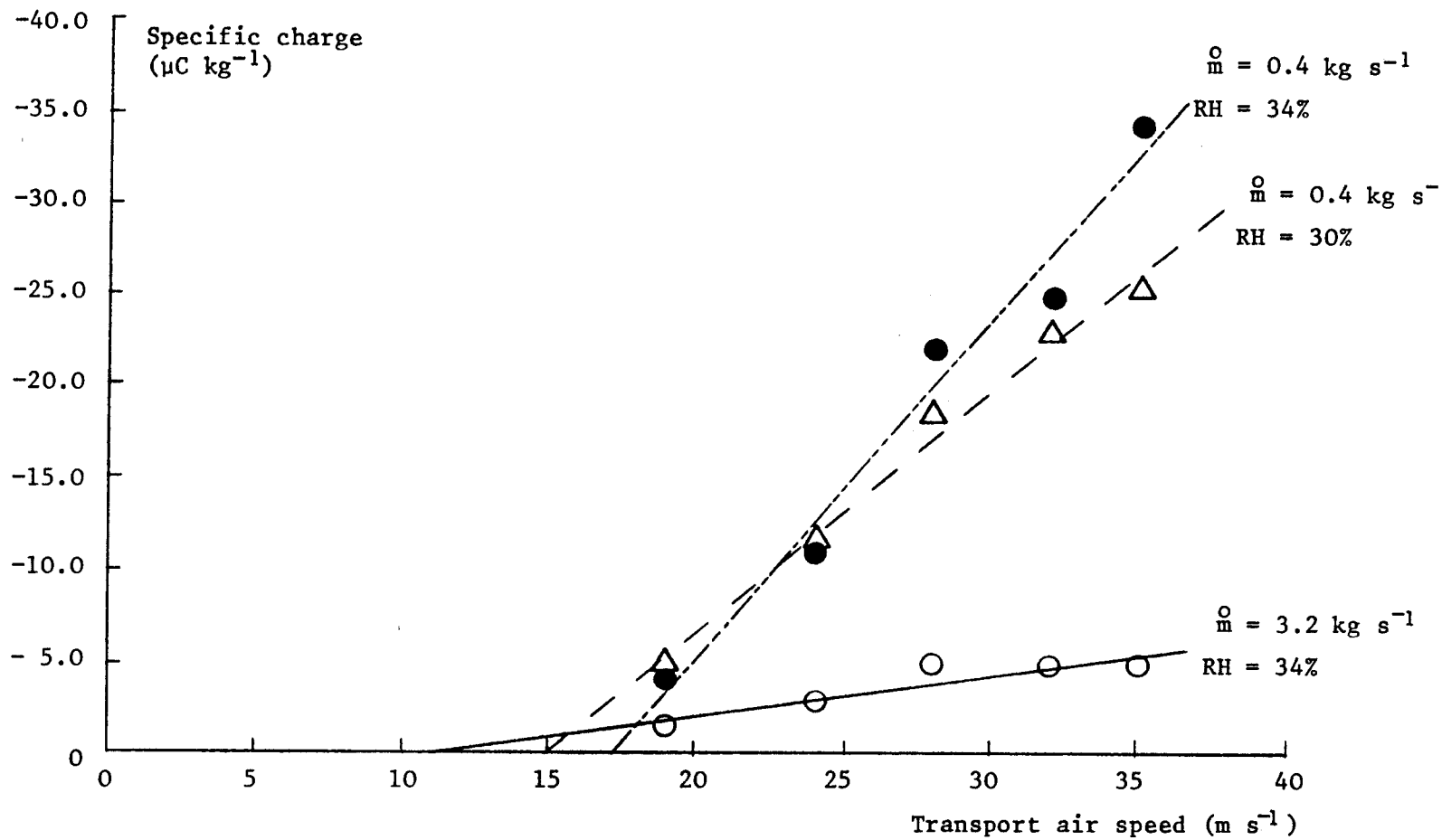

Figure 3.6 Specific Charge of HDPE Entering Test Silo as a Function of Powder Feed Rate

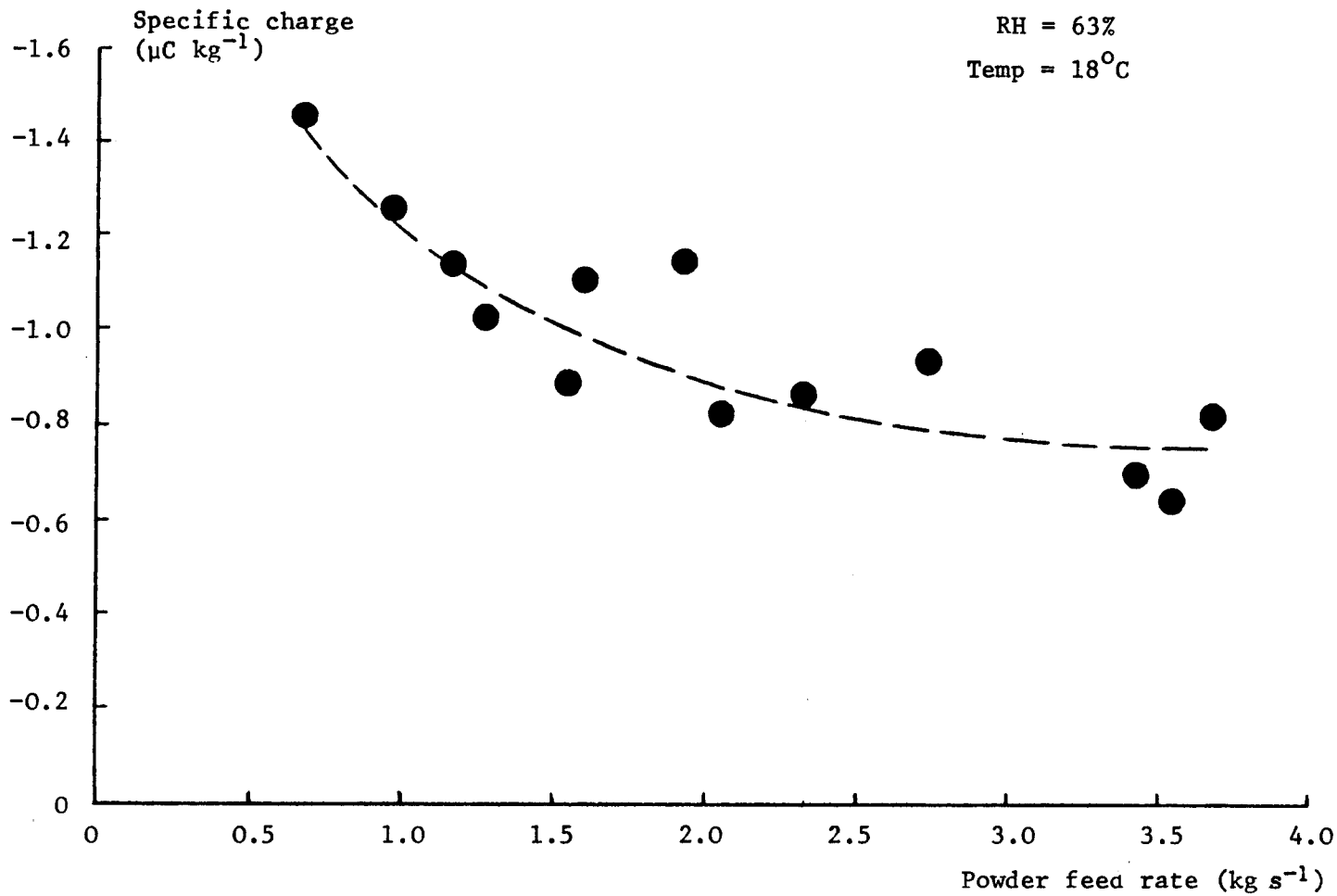

Figure 3.7 Specific Charge of Maize Starch Entering Test Silo as a Function of Powder Feed Rate

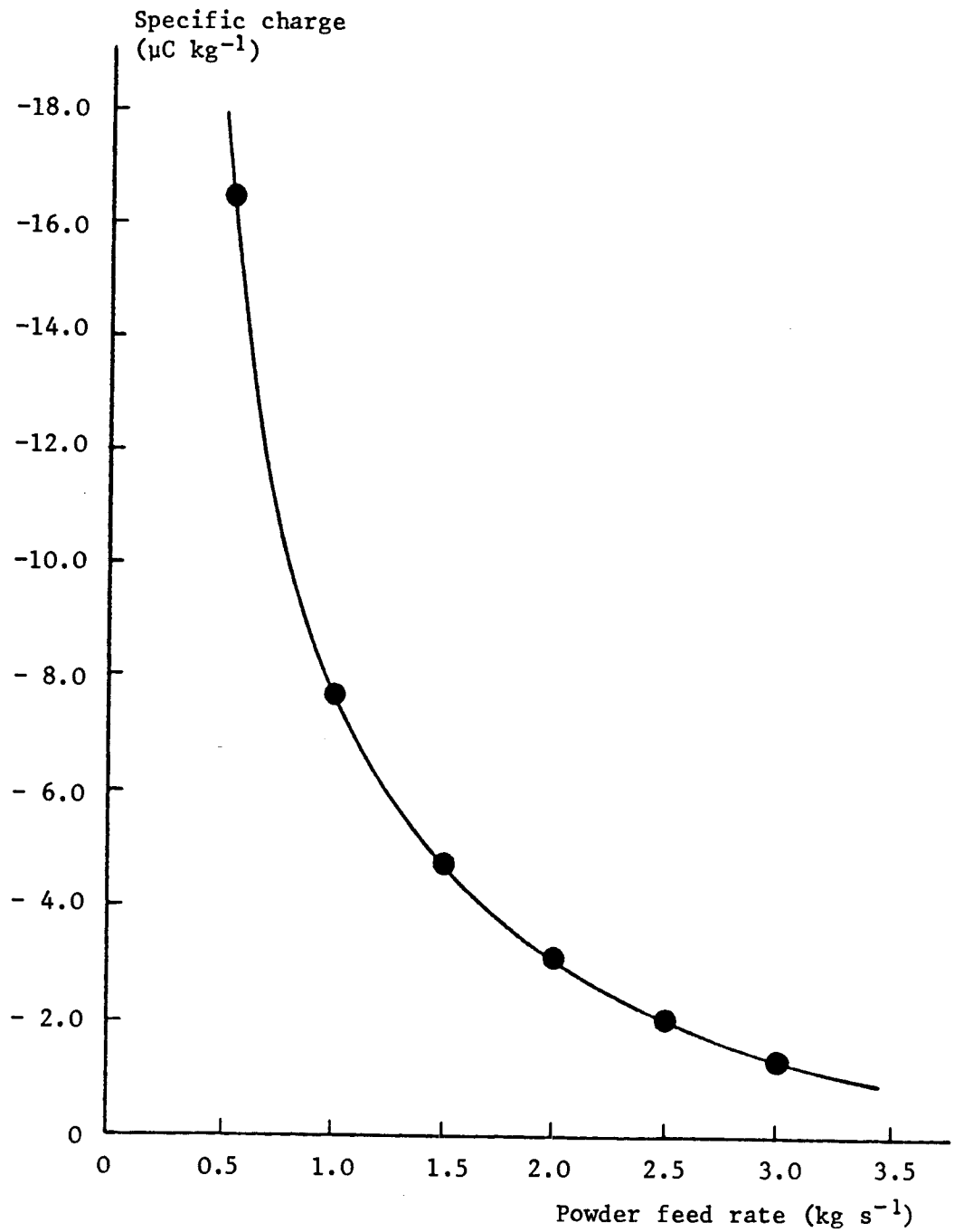

which cannot reach the pipe wall increases, therefore charge per unit mass decreases with an increase in mass flow rate.

The maximum specific charge of powder entering the silo is also shown by equation (3.13) to be inversely proportional to the powder mean flow rate (everything else being constant).

3.3.2.2 Influence of Space Charge Field on the Tribo-Electrification of Powder Particles in Pneumatic Conveying

The space charge field produced by the bulk of the charged particles passing through a pipe has an influencing effect on the maximum specific charge which can be obtained by the particles colliding with the pipe wall [Cole et al (1969-1970)].

In this section, observations made during various experiments on the influence of space charge field on tribo-electrification is discussed.

The results of the experimental work which has been carried out on HDPE, wheat, sugar and maize starch at Marchwood silo rig are shown in Table 3.2. These results were obtained by placing the corona charge injector device (see section 2.2) upstream of the first bend. When the HT DC power supply was on, all first bend currents had a high value and of the same polarity as that of the corona current which means that a large portion of corona charge on the particles is lost when the particles collide with the inner wall of the first bend. Subsequent pipe sections were observed to discharge the corona charged powder by decreasing amounts. The extra charge placed on maize starch, sugar and wheat powder particles was discharged almost completely by the time the particles had passed through the second bend.

The charge on the HDPE powder particles entering the silo per unit time (current) increased from -0.6 μA to -6.0 μA when the corona charge injection was used. However, the current measured was not greater than the maximum current measured with HDPE powder.

Table 3.2 - Results of Experimental Work Carried out on HDPE, Wheat, Sugar and Maize Starch at Marchwood Silo Rig

Current (μA)	6.2 T Batch HDPE Fines		Wheat		Sugar		Maize Starch	
	HT off	HT on	HT off	HT on	HT off	HT on	HT off	HT on
1st bend	+0.1	-24	-1.2	+12.0	+1.5	+30	-9	-22
2nd straight	+0.02 ↔ -0.02	-1.8 ↔ -2.7	-	-	-	-	+4.5	+4.5
2nd bend	+0.04	-0.75	-0.92	-0.15	-0.3 ↔ +0.3	-0.3 ↔ +0.3	-2.8	-2.8
3rd bend	-	-	-0.6	-0.02	-	-	-0.8	-0.8
4th straight	-	-	-	-	-	-	-2	-2
Top 180° bend	0	-0.3	-1.6	-1.6	-0.8	-0.8	+2	+2
Silo	-0.6	-6	+7.5	+7.5	+0.6	+0.6	-10	-10

Currents as high as -6.0 μA were measured for short periods immediately after pipe bends had been cleaned without using the corona charge injector.

The results of Table 3.2 suggest that the space charge field of charged powder flowing through the conveying pipes at Marchwood silo rig can have an infuencing role on the saturation specific charge of powder. The influence of the space-charge field is such that even if the charge of powder is somehow made to exceed the saturation limit, for example, by corona charging, the additional charge dissipates after the powder travels through a short section of the pipework.

3.3.2.3 The Influence of a Superimposed Electric Field on Tribo-Electrification of Powder Particles in a Pneumatic Conveying System

In this section the influence of space charge field on tribo-electrification of powders during pneumatic conveying is studied by applying a superimposed electric field to control the charging of powder particles colliding with the pipe wall in the presence of such a field.

a) High Density Polyethylene (HDPE) Powder

Figure 3.8 shows the variation of the specific charge of HDPE particles in the field pipe section as a function of a superimposed electric field obtained by monitoring the pipe section wall current to ground, which arises due to charge exchange with colliding powder particles. The superimposed field was calculated using the usual expression for the radial field within an infinitely long coaxial electrode arrangement. The specific charge of powder particles as a result of collisions with the inner wall of this field pipe section increases sharply after the applied electric field on the surface of the inner wall exceeds a value of about 100 kV m^{-1}. The variation of specific charge of powder entering the silo as a function of superimposed electric field within the field pipe section is shown in Figure 3.9. As can be seen from Figure 3.9, the polarity of the specific charge of powder entering the silo is opposite to the

Figure 3.8 Specific Charge of HDPE Powder as a Result of Collisions with the Wall of the Field Pipe Section as a Function of the Superimposed Electric Field at the Wall

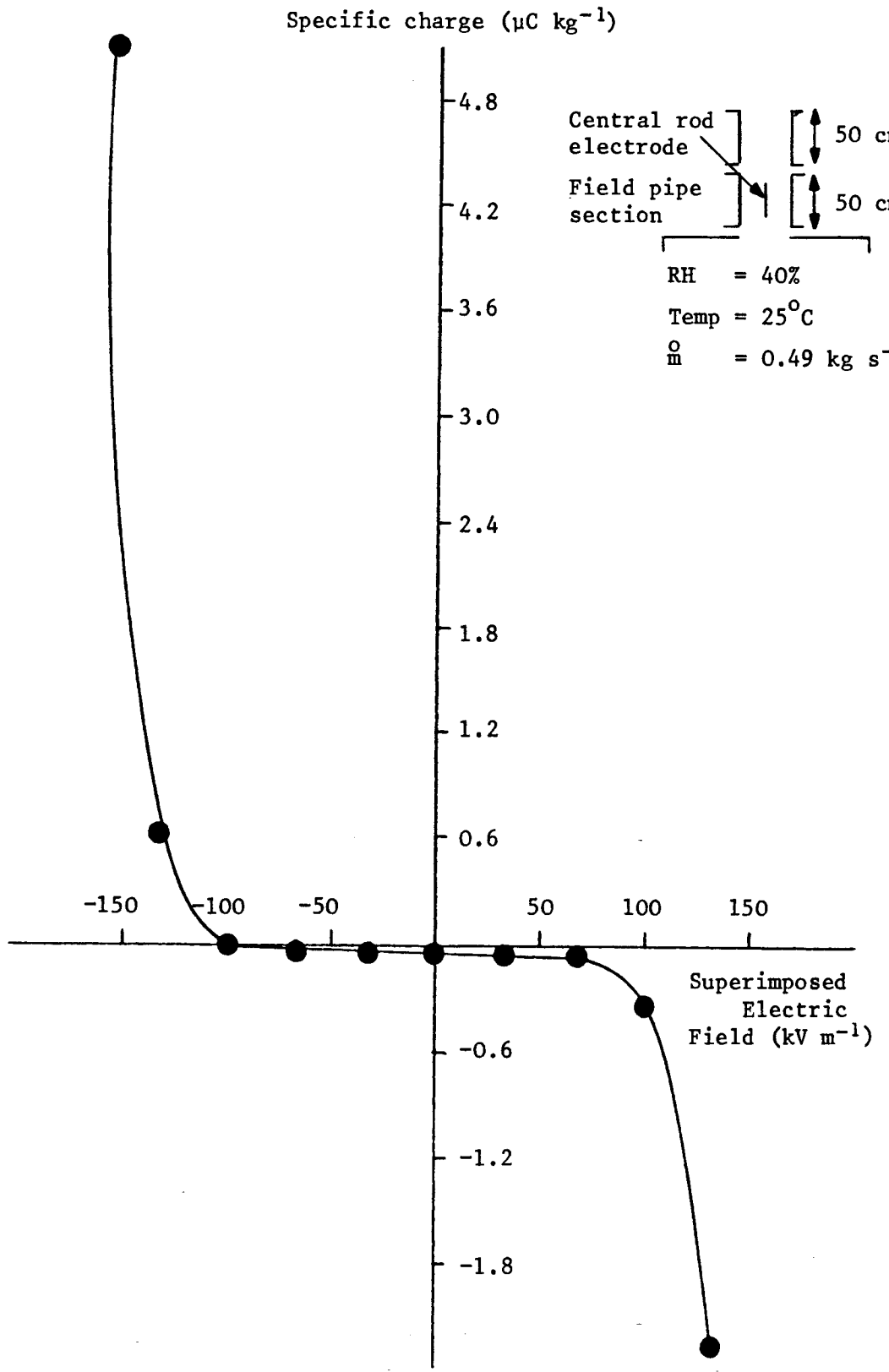

Figure 3.9 Specific Charge of HDPE Powder Entering Silo as a Function of the Superimposed Electric Field at the Wall of the Field Pipe Section

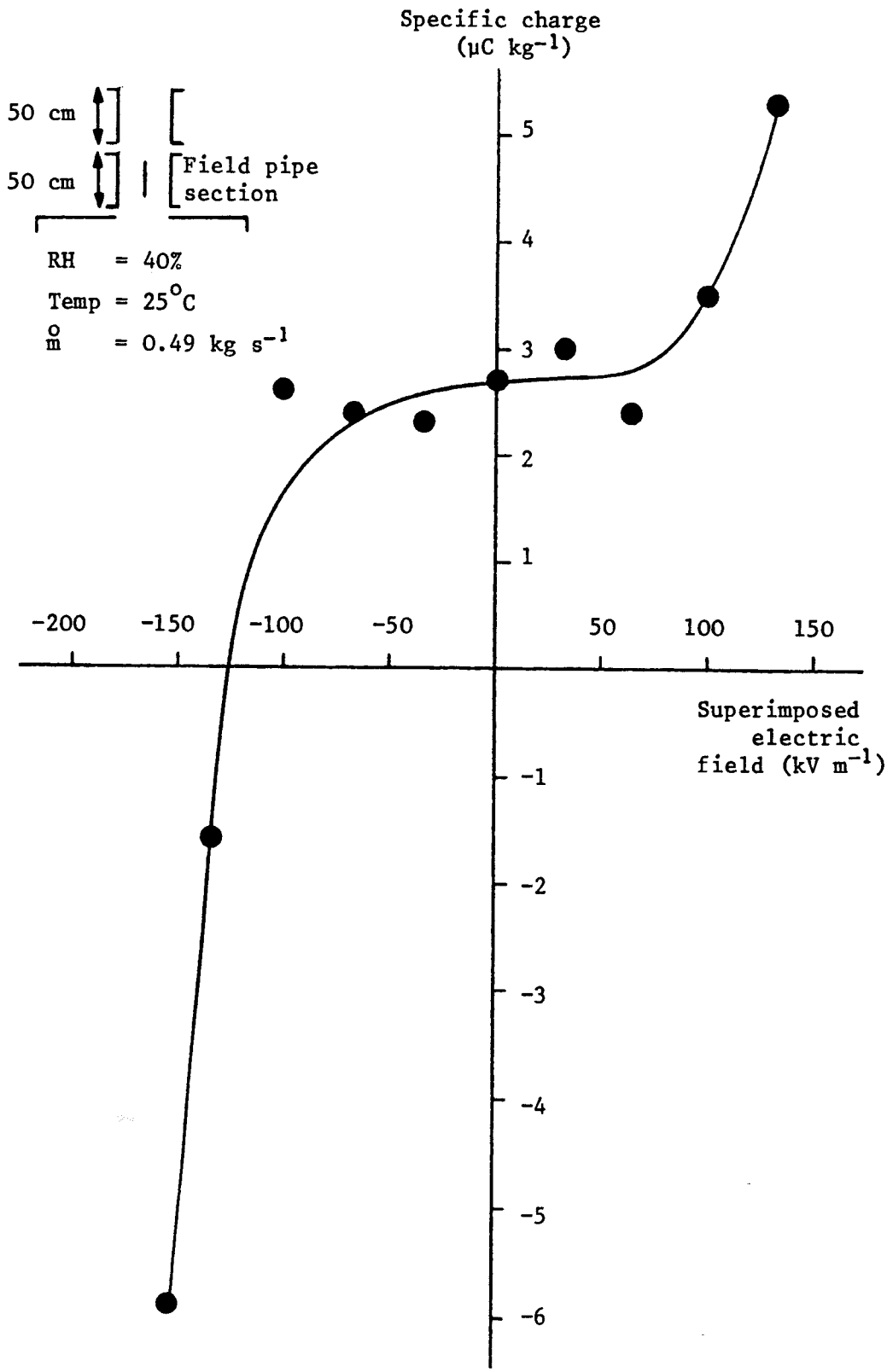

specific charge of powder in the field pipe section and also its magnitude is larger. This infers that the dominant charge transfer process within the field pipe section occurs at the central rod electrode rather than at the pipe wall (see Fig. 3.12).

Figures 3.10 and 3.11 shows traces of the silo current and also the electric field strength readings of the dust cloud at a point 2.5 m from the roof of the test silo. In Figure 3.11 the central rod conductor of the field pipe was at a potential of -23 kV. Comparison of Figures 3.10 and 3.11 indicate the effectiveness of the superimposed electric field in reducing the space-charge field of the dust cloud inside the test silo and the silo current.

Figure 3.12 shows the specific charge of HDPE powder as a result of collisions with the conducting rod as a function of the applied electric field at the inner wall of the conveying pipe. The other set of values on the x-axis of Figure 3.12 corresponds to applied potentials on the conducting rod. Comparing Figures 3.9 and 3.12 indicates that specific charge of powder entering the silo was due primarily to the tribo-electrification of powder particles with the conducting rod, rather than the inner wall of the field pipe section when the superimposed electric field was applied.

The ratio of the area of the inner surface of the field pipe section to the surface area of the central conducting rod was calculated to be about 33. Considering this ratio one would expect that, in the absence of an applied field, the current due to the collisions of powder particles with the conducting rod would be about 33 times smaller than the tribo-charging current of particles colliding with the inner wall of the field pipe section.

Figure 3.13 illustrates the tribo-charging currents (no applied field) of the field pipe section and central conducting rod as a function of mass flow rate of HDPE. For this experiment the central rod conductor was earthed through an electrometer. The maximum ratio of field-pipe section current to the central conducting rod current is 10 from Figure 3.13. The difference

Figure 3.10 Traces of the Silo Current and Electric Field Strength at the Silo Wall. Central Rod Grounded.

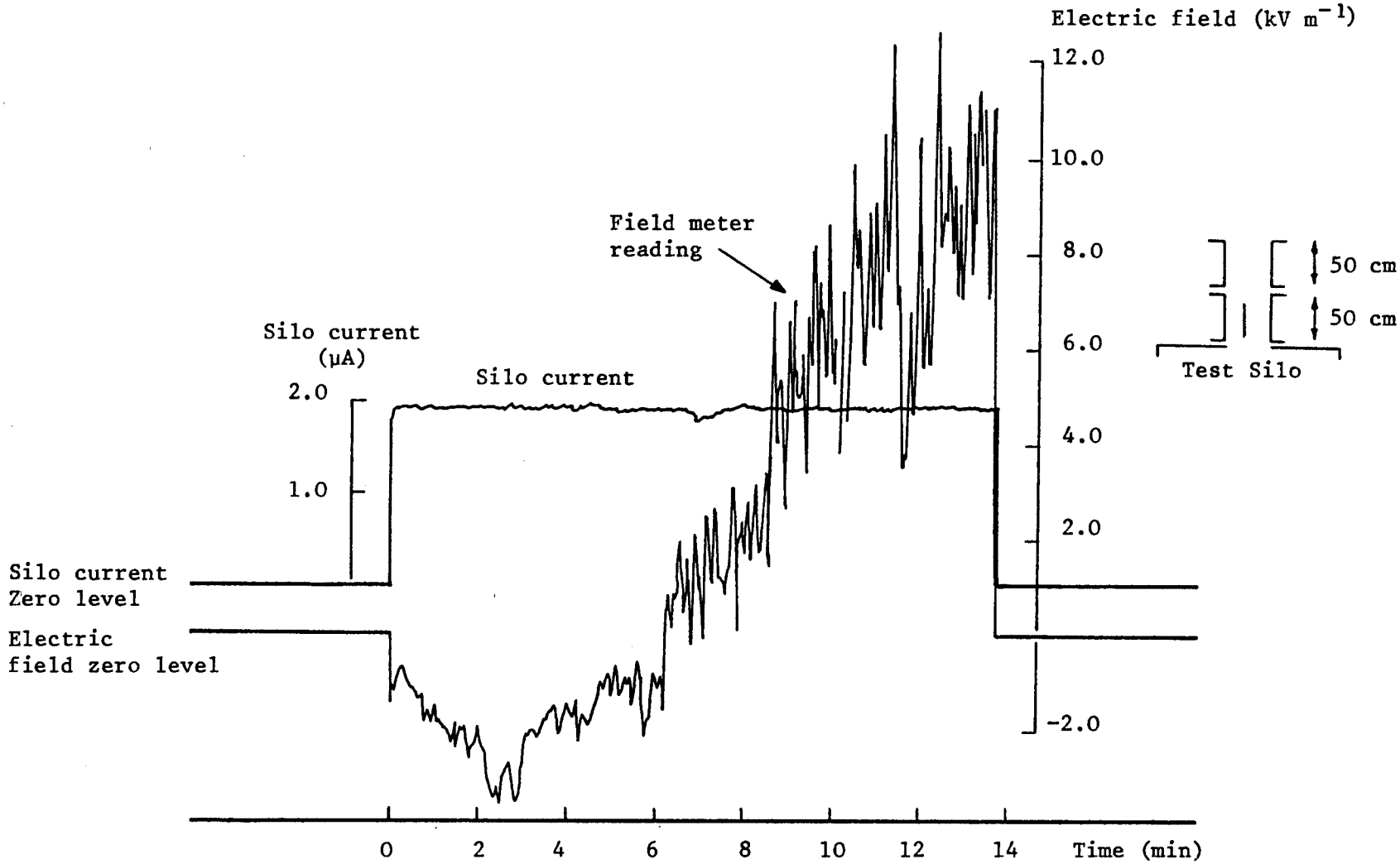

Figure 3.11 Traces of the Silo Current and Electric Field Strength at the Silo Wall. Central Rod at a Potential of -23 kV.

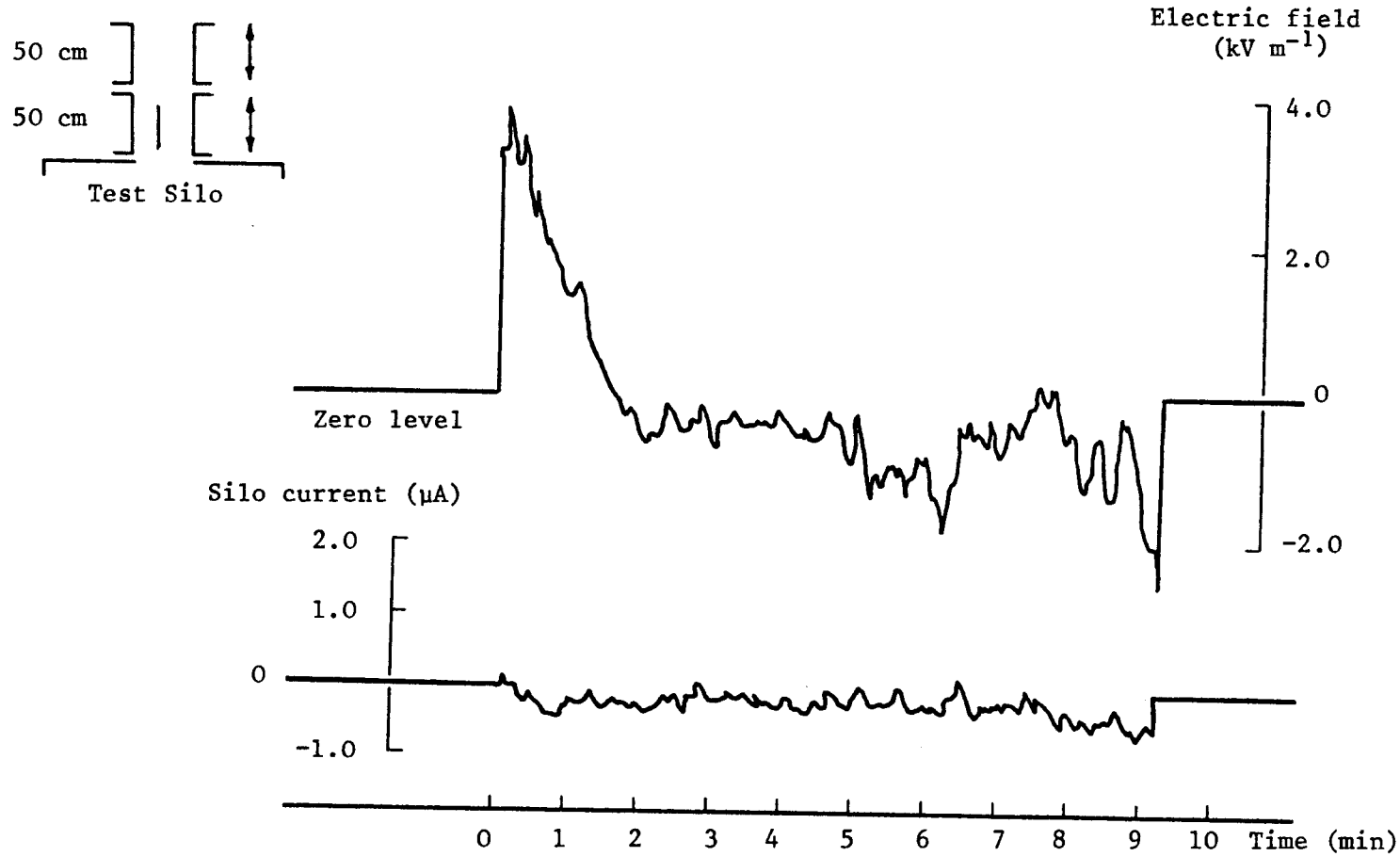

Figure 3.12 Specific Charge of HDPE as a Result of Collisions with the Conducting Rod as a Function of the Superimposed Electric Field at the Inner Wall of the Conveying Pipe

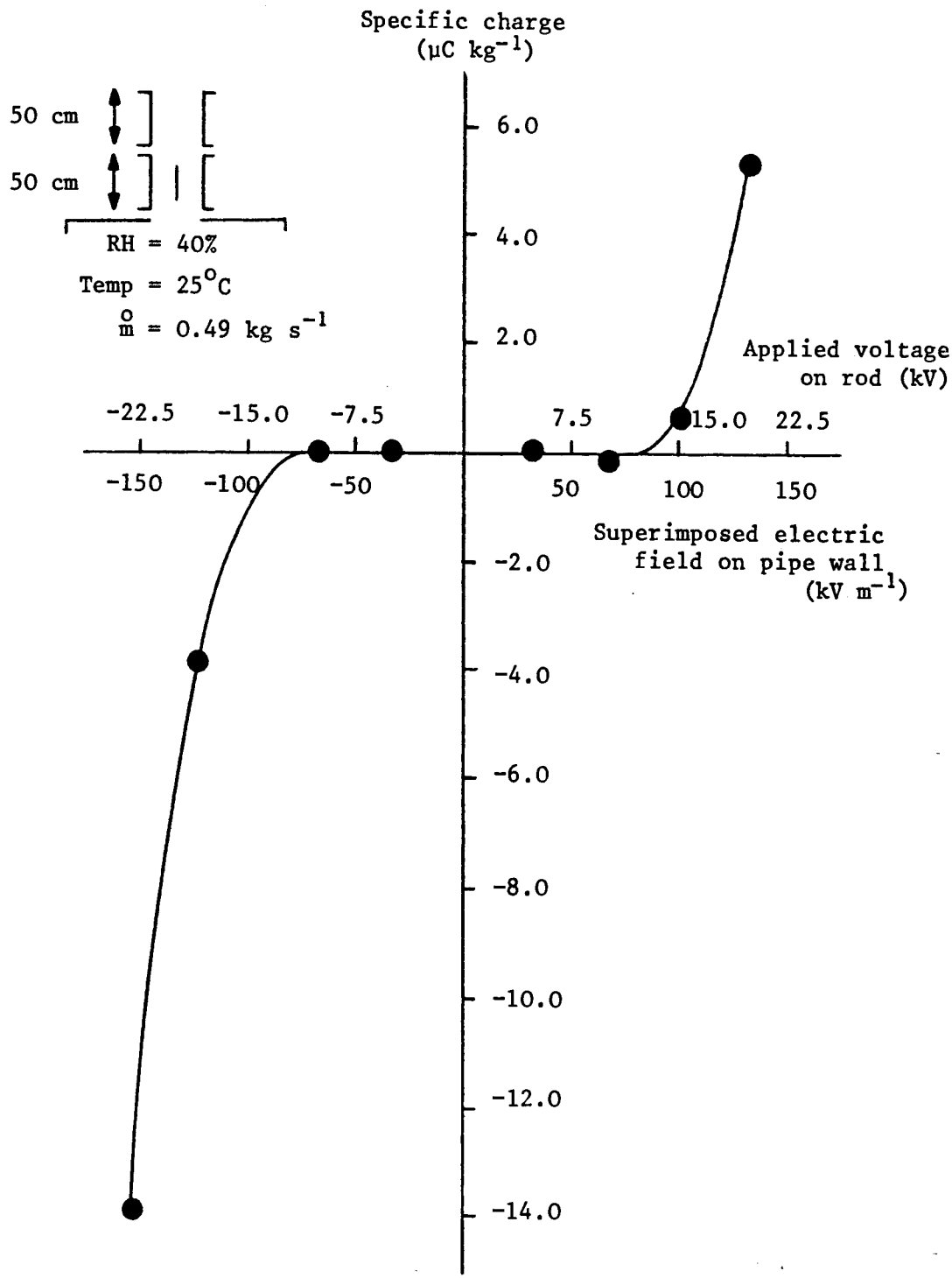

Figure 3.13 Currents of Field Pipe Section and Central Pipe Rod Conductor Due to Powder Tribo-charging as Functions of Powder Mass Flow Rate

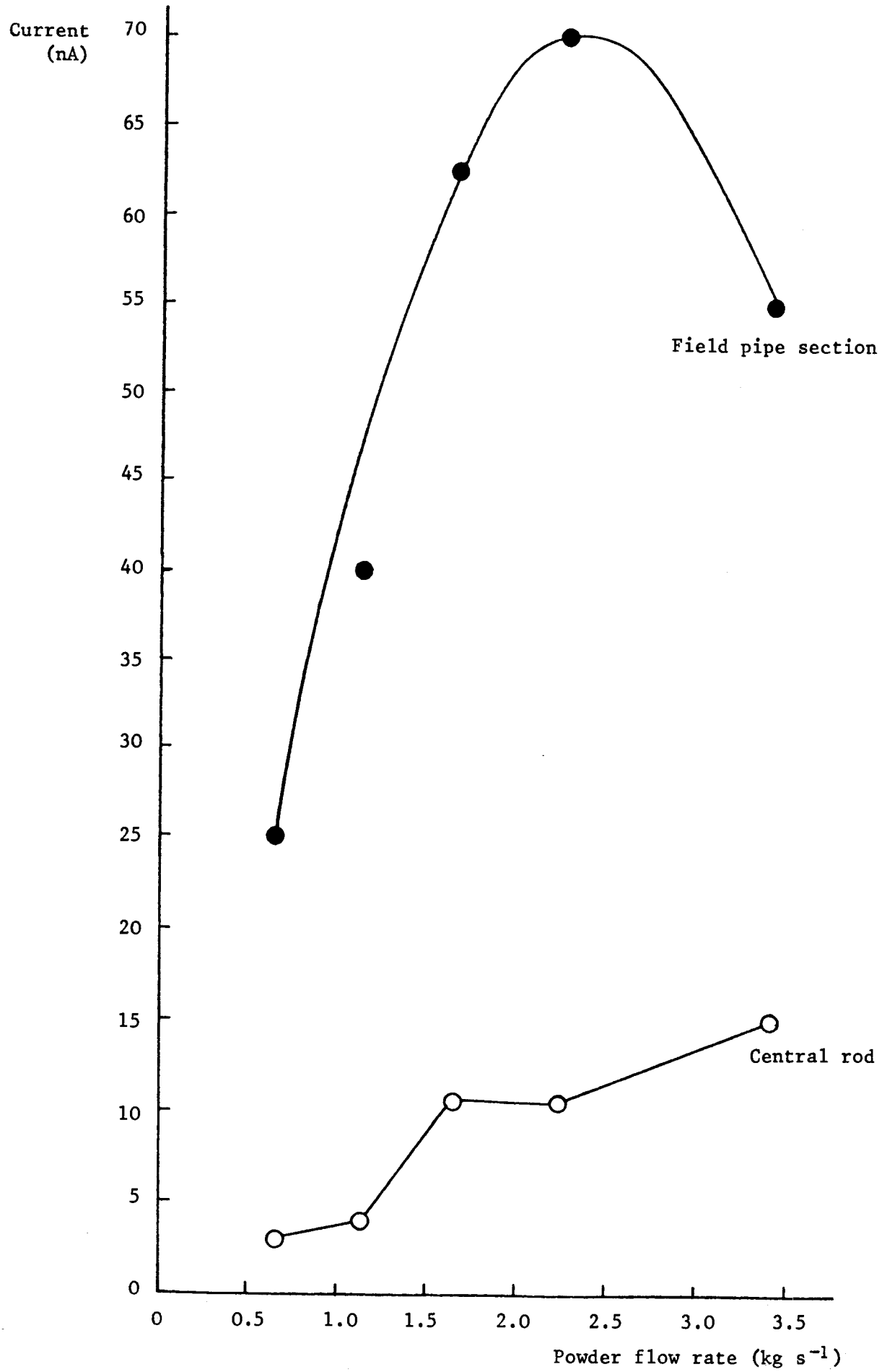

between the expected and experimental values possibly may be due to the flow characteristics of powder particles.

When the conducting rod is raised in potential, because its radius is small compared with the radius of the conveying pipe, the electric field is highly divergent. Electric field intensity decreases rapidly with distance ($E \propto \frac{1}{R}$) from the surface of the conducting rod, see Figure 3.14. Hence a particle approaching the conducting rod experiences an electric field which is opposite in direction and also much larger in magnitude than the electric field on the inner surface of the pipe wall. For example, with a potential of 25 kV on the central rod electrode the ratio of the electric field on the surface of the conducting rod to the electric field on the inner wall of the conveying pipe is 10. This probably accounts for the difference both in magnitude and sign of the specific charge of powder entering the silo and that due to the collision with the inner wall of the field pipe section.

The saturation specific charge of powder in a pneumatic conveying system results from large numbers of energetic collisions between the particles and the pipe wall. The superimposed electric field is applied inside the conveying pipe of length only 300 mm. Therefore this field must be much larger than the powder space-charge field in order to compensate for the relatively small number of collisions which take place between the particles and the pipe wall in the presence of the superimposed field. Consider for example Figure 3.9 with the additional electrical field equal to zero, the saturation specific charge entering the silo is $+2.7\ \mu C\ kg^{-1}$ for a powder velocity of $35\ m\ s^{-1}$, mass flow rate $\dot{m} = 0.49\ kg\ s^{-1}$ and a pipe radius $R = 5$ cm, using equation (3.14)

$$E_{max} = +\ 13.6\ kV\ m^{-1}.$$

In practice (Figure 3.9) the additional electric field for HDPE was required to be larger than about $100\ kV\ m^{-1}$ before any significant change in the specific charge on the powder entering the silo was observed.

Figure 3.14 Radial Electric Field as a Function of Pipe Radius

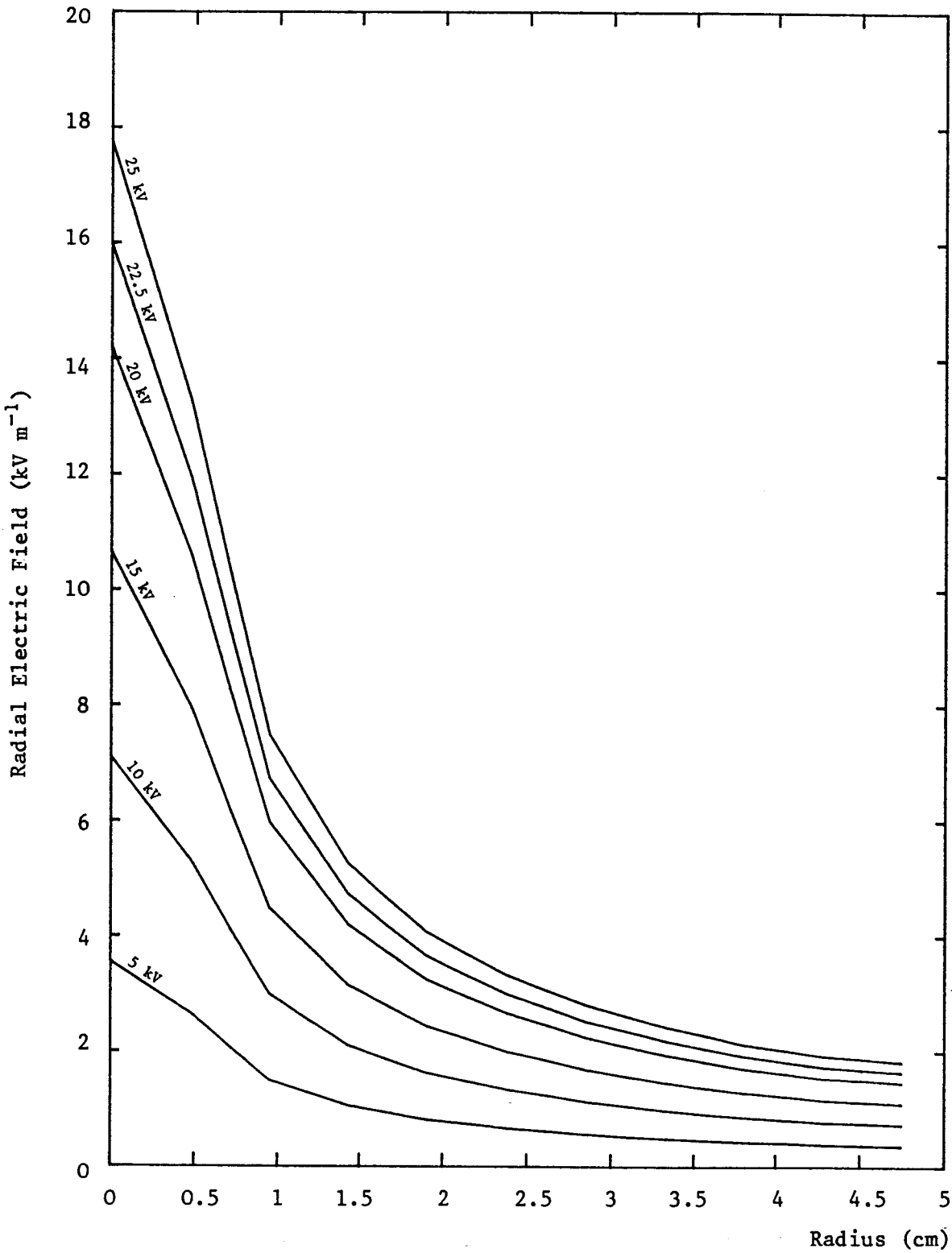

The fact that the contact charge of HDPE powder does not vary linearly with applied electric field may be explained as follows:

Assuming the energy density of surface states per unit area, D_s, is not too large, then the surface charge density of an insulator is given by equation (3.16)

$$\sigma = eD_s (W_i - W_m) \qquad (3.16)$$

We see from equation (3.16) that the surface charge of the insulator after contact with a metal is directly proportional to its surface state density D_s and to the work function difference. It is expected that $W_i > W_m$ and by an order of magnitude $(W_i - W_m) \approx 1$ eV, so $\sigma \approx -eD_s$. This relationship is only valid if the energy distribution of the surface states is uniform.

In the presence of an applied field, E, the electronic energy levels of the insulator shift relative to those of the metal. In describing the effect of the applied field on contact charging, equation (3.16) may be generalised to [Hays et al (1971)]:

$$\sigma(E) = e \int_{W_m^*}^{W_i} D_s (E)\, dE \qquad (3.17)$$

where $W_m^* = (W_m + Ed_c)$

In equation (3.17), $D_s(E)$ is a function which describes the surface state density. According to this model, the change in the contact charging by the applied field is proportional to the surface state density at an energy of $(W_i + Ed_c)$ eV below the vacuum level, ie,

$$\frac{d\sigma(E)}{dE} \propto D_s (W_m^*) = D_s (W_m + Ed_c) \qquad (3.18)$$

For a uniform surface state density, equation (3.17) becomes

$$\sigma(E) = eD_s (W_i - W_m - Ed_c) \qquad (3.19)$$

In the limit of a high surface state density ($\frac{eD_s d_c}{\epsilon_o} \gg 1$)

$$\sigma(E) = \frac{\epsilon_o}{ed_c} (W_i - W_m - eEd_c) = \sigma(0) - \epsilon_o E \qquad (3.20)$$

Equation (3.20) predicts that in the limit of a high surface state density, the slope of the contact charging against applied field should approach the value of the permittivity.

The fact that the relationship between contact charging and the applied electric field is not linear may therefore be due to the non-uniform energy distribution of the surface states.

b) Maize Starch Powder

Figure 3.15 shows the variation of the specific charge of maize starch powder particles in the field pipe section as a function of superimposed electric field. With no potential on the rod electrode, the maize starch powder was negatively charged by colliding with the inner surface of the field pipe section. Application of a positive potential on the rod electrode with respect to the pipe wall (positive superimposed electric field) increased the powder specific charge whereas a negative potential on the rod electrode of about -4.8 kV ($E \approx -32$ kV m^{-1}) neutralised all the charge of the particles colliding with the inner wall of the field pipe section (curve 1 of Figure 3.15).

In the experiments with maize starch, for some tests a series of steel baffles were introduced into the conveying pipe preceding the superimposed field pipe section. By this means the tribo-electric charging of the powder was significantly increased.

With the HV supply to the rod electrode of the field pipe section switched off, the maize starch powder would normally lose

Figure 3.15 Specific Charge of Maize Starch Powder Passing Through the Field Pipe as a Function of Electric Field at Wall of Field Pipe Section

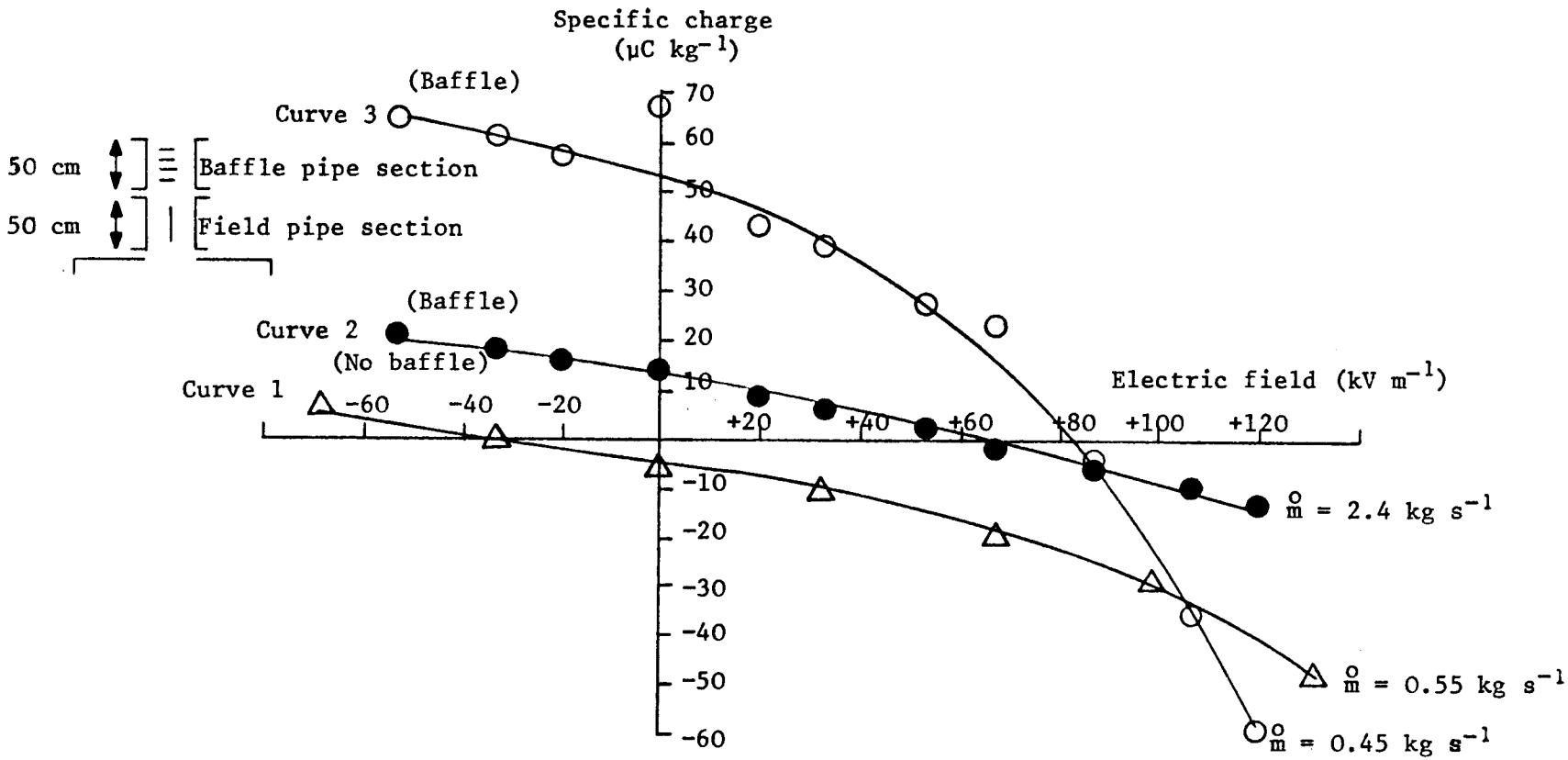

most of its charge after colliding with the inner wall of the field pipe section after becoming highly charged negatively in the baffle pipe section. Application of a positive DC potential on the conducting rod resulted in the powder losing less charge by collisions with the inner wall of the field-pipe section. At a particular level of superimposed electric field, charged maize starch particles passed through the field-pipe section without losing any charge. A further increase in the superimposed electric field caused the maize starch particles colliding with the inner wall of the field pipe to become negatively charged (curves 2 and 3 in Figure 3.15).

3.3.2.4 Effects of Relative Humidity on Tribo-Electrification of HDPE

It has long been thought that a high relative humidity causes the charge of bulked powder to discharge to ground relatively rapidly. An early but comprehensive paper by Field (1946) concluded that:

a) Surface resistivity of plastic dielectrics reached an equilibrium value in times from 10 minutes to not more than one hour.

b) The equilibrium value was a strong exponential function of ambient humidity in the range 70% to 100% RH.

c) Regain of high resistance on subsequent exposure to an atmosphere of 0% RH is generally as rapid as the initial drop at 100% RH.

Figure 3.16 illustrates the results of work carried out by Field (1946) on the effect of relative humidity on the surface resistivity of polyethylene.

High density polyethylene is very resistant to water. Increase in weight after immersion in water at 20°C for a year more is generally less than 0.2%. At higher temperatures oxidation may result in polar groups and increased water absorption. A few

Figure 3.16 (Left) Effect of Relative Humidity on Magnitude of Exposure Curve for Polyethylene

(Right) Relation of Equilibrium Surface Resistivity to Relative Humidity for Polyethylene (Field (1946))

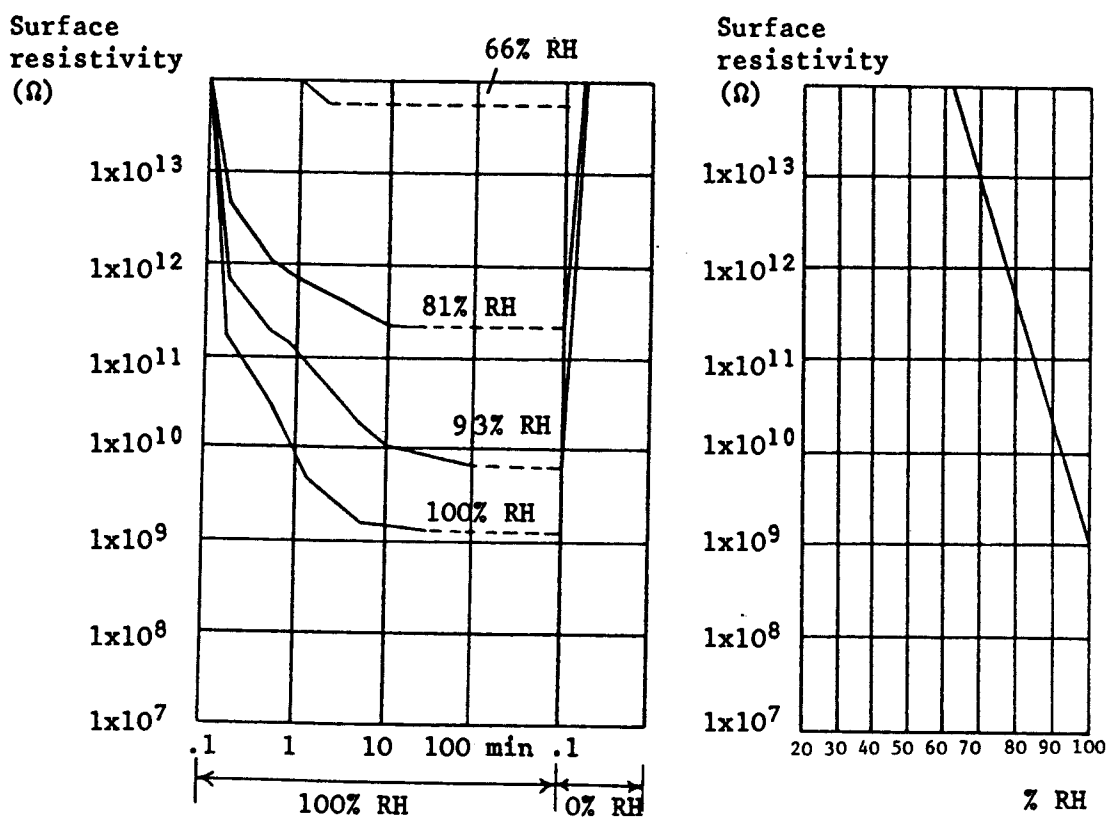

parts per million of impurity or moisture in a hydrocarbon fuel is sufficient to give appreciable charging during flow through a pipe [Bailey (1986)]. Incorporation of carbon black in high density polyethylene tends to increase absorption. Water absorption after 28 days at 70°C is 0.15 mg cm^{-2}. The rate of oxidation varies from sample to sample and increases as the amount of oxygen absorbed by the polyethylene increases [Roff et al (1971)].

During earlier work on different batches of HDPE powder it was noticed that the transport air relative humidity had a noticeable effect on tribo-charging. A plot of the RH of the transport air against silo current showed that a large RH corresponded to a large negative current and a small RH corresponded to a positive current (see Figure 3.17) [Cartwright et al (1985)]. This graph was plotted using the values of silo current obtained at different occasions for different relative humidities.

Similar results were obtained for the HDPE powder using a water spraying nozzle to increase the relative humidity of silo transport air. With no powder flow ($\dot{m} = 0$) the silo relative humidity was increased to a high value ($\approx$ 70%). The nozzle was then removed and after a few minutes the powder transfer was started. The silo transport air relative humidity was then allowed to fall gradually to the ambient level and then the dehumidifier was used to decrease the RH further.

Figure 3.18 shows the variation of transport air relative humidity and also specific charge of HDPE entering the silo against time. A decrease in relative humidity resulted in a large decrease in specific charge of HDPE powder. Figure 3.19 is a plot of transport air relative humidity as a function of specific charge of HDPE entering the silo. The trend was similar to the work reported by Cartwright et al (1985). Figures 3.20 and 3.21 are the results of similar experiments carried out with a powder mass flow rate of 2.5 kg s^{-1}.

Figure 3.17 Mean Relative Humidity as a Function of Mean Silo Current

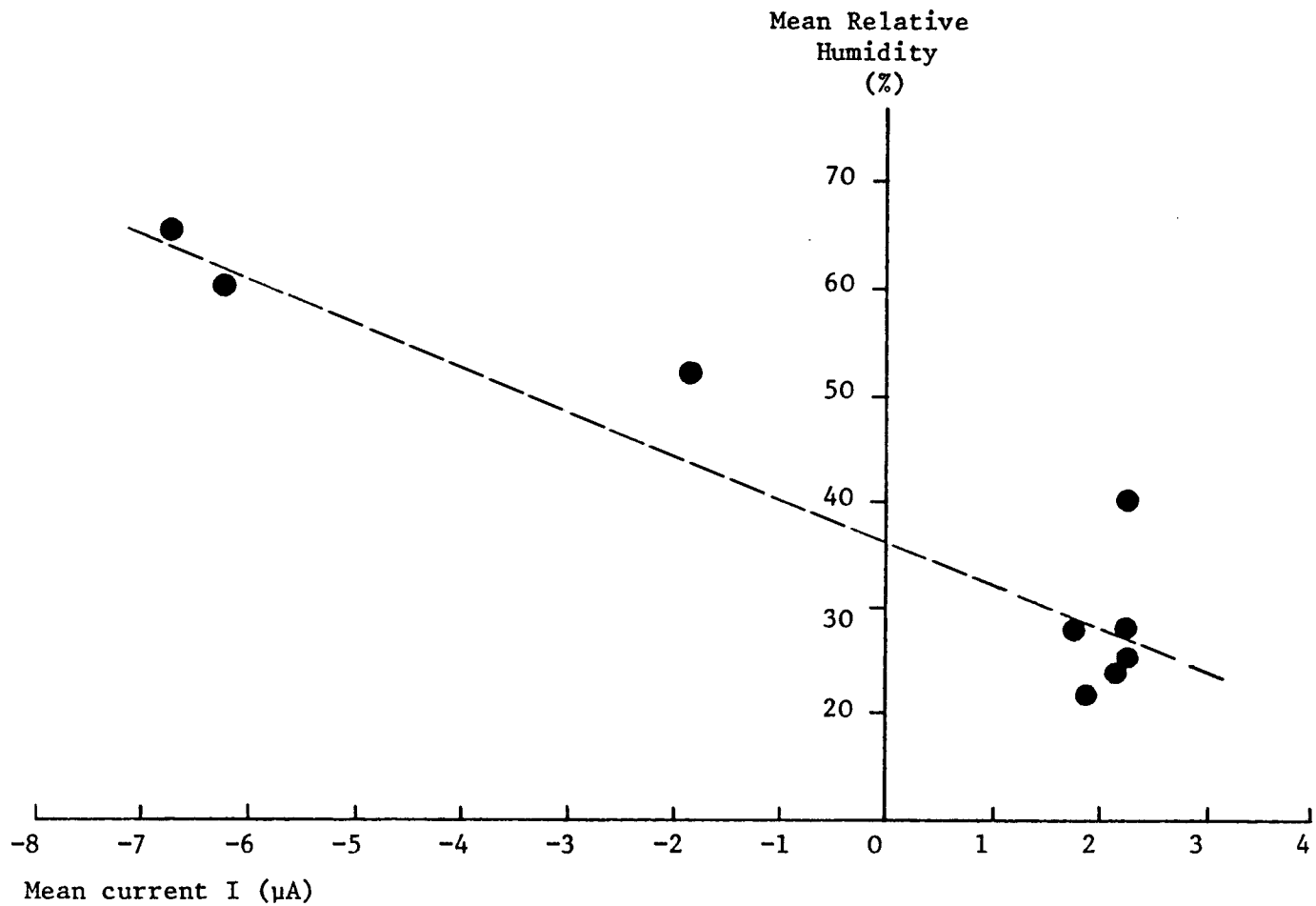

Figure 3.18 Transport Air Relative Humidity and Specific Charge as a Function of Time

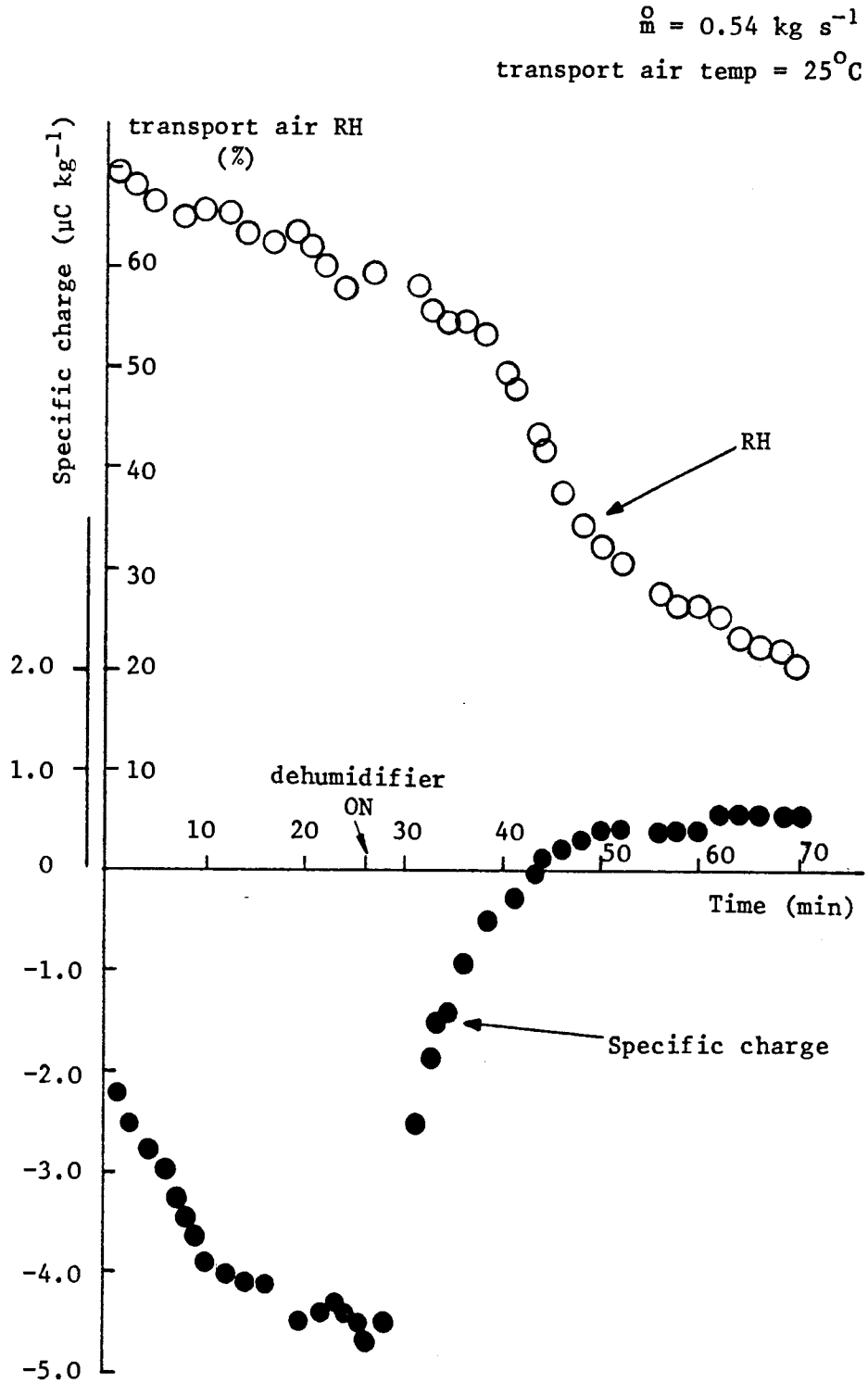

Figure 3.19 Transport Air Relative Humidity as a Function of Specific Charge

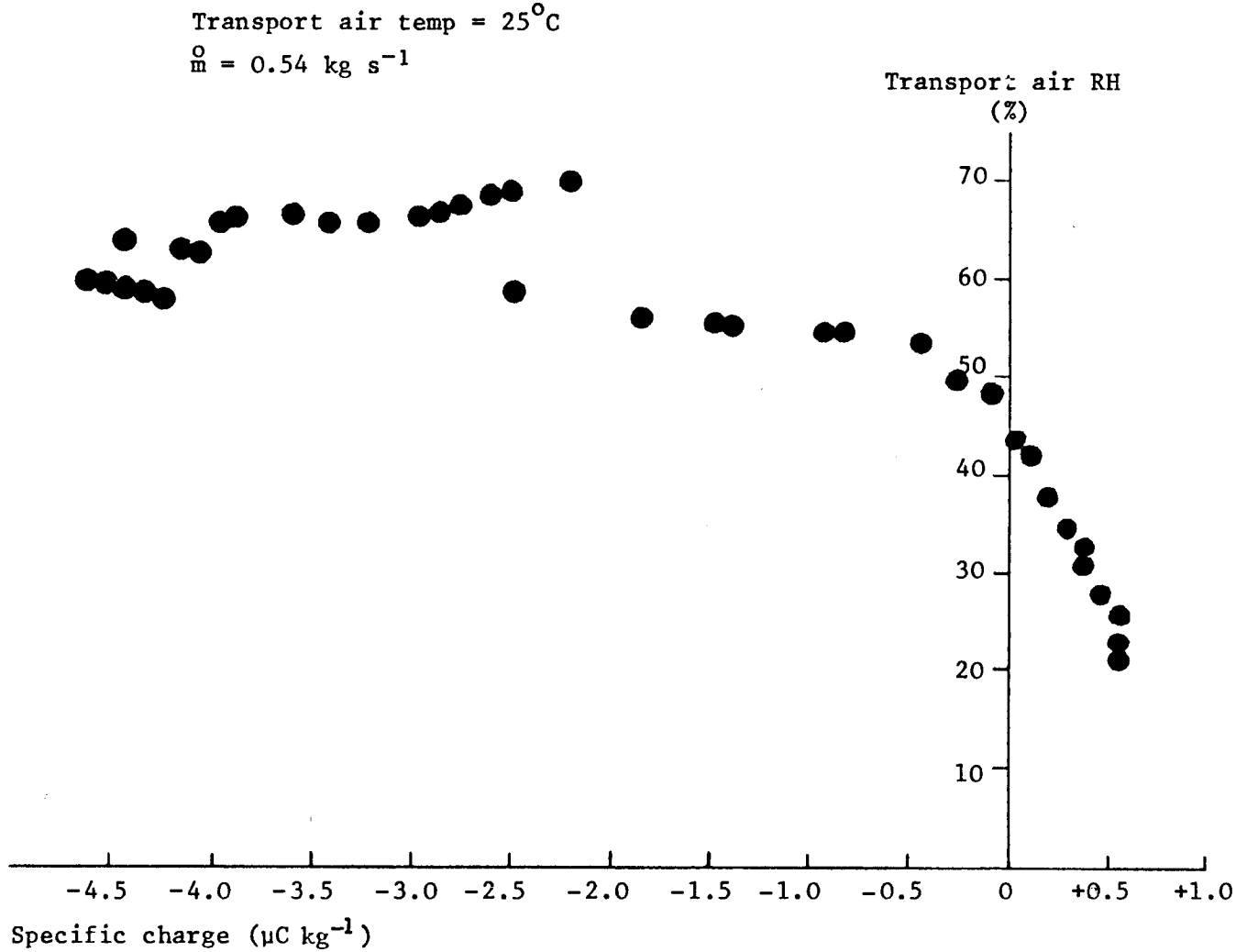

Figure 3.20 Transport Air Relative Humidity and Specific Charge as a Function of Time

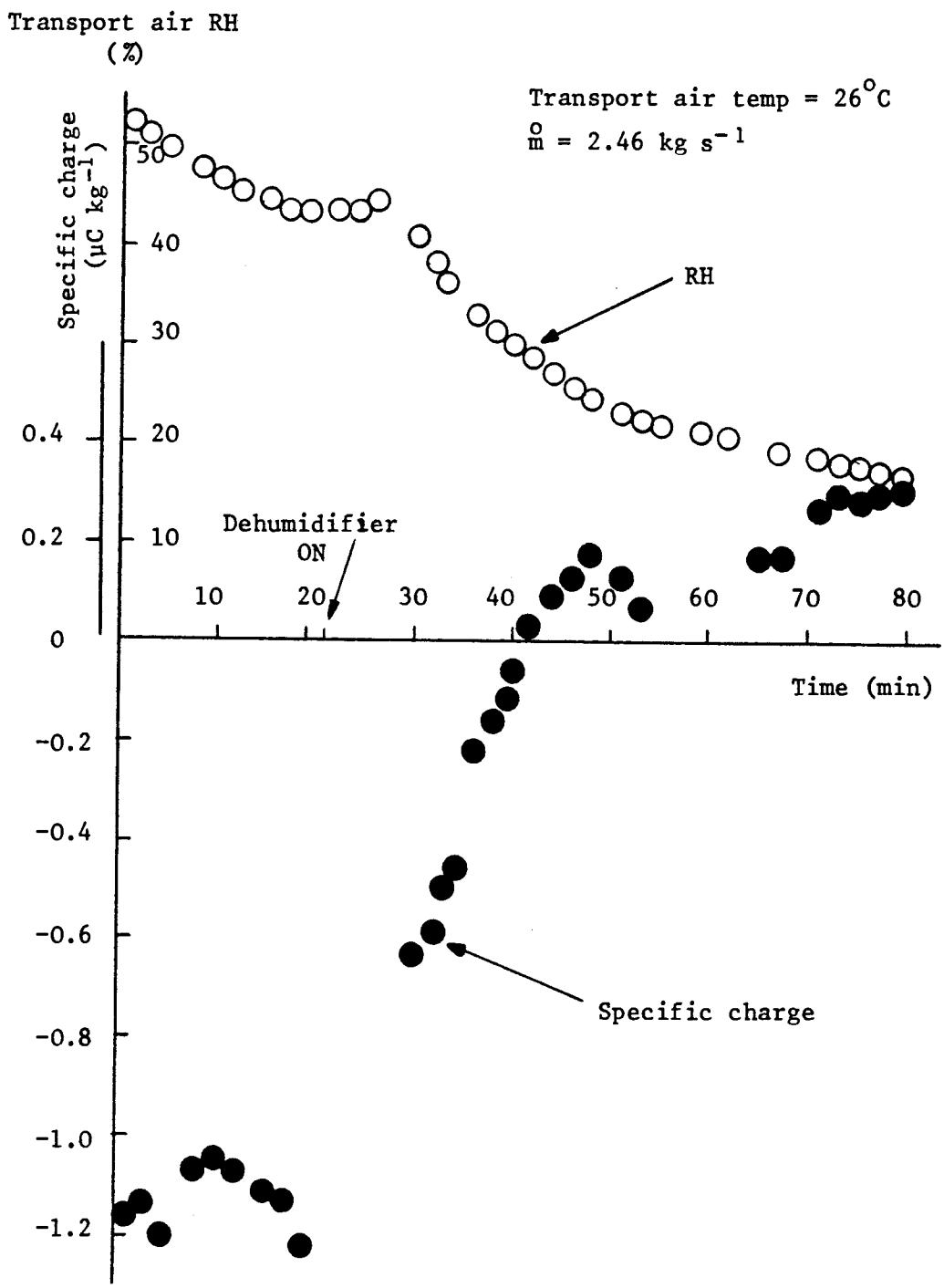

Figure 3.21 Transport Air Relative Humidity as a Function of Specific Charge

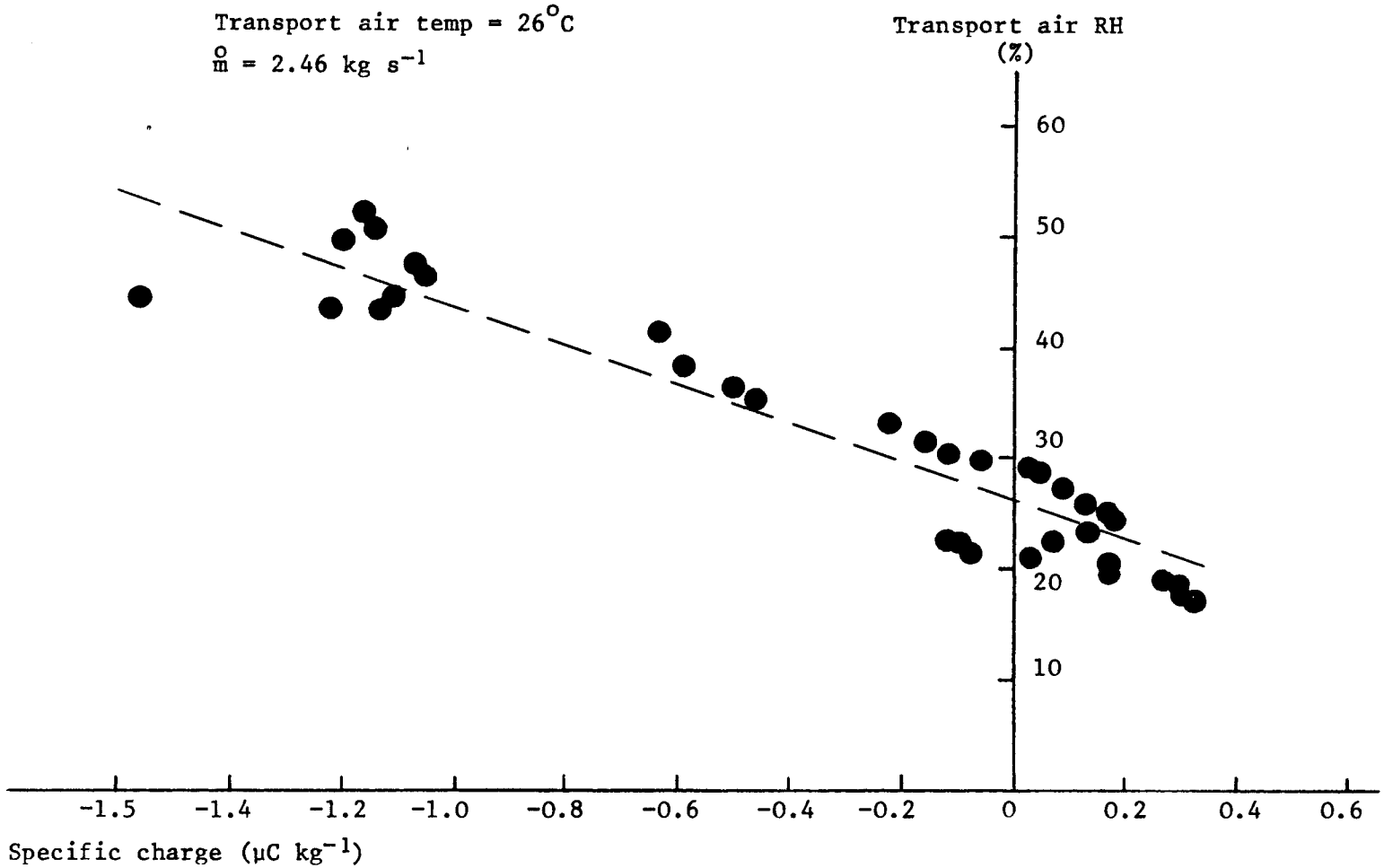

The variations of specific charge of HDPE entering the silo as a function of time at two relative humidities of 25.5% and 63.5% for powder flow rates of 3.1 kg s^{-1} and 3.3 kg s^{-1} respectively is shown in Figure 3.22. This experiment confirmed that the changes in the specific charge of HDPE powder were indeed as a result of changes in the transport air relative humidity, everything else being constant.

3.3.3 Silo Scale Model

In this section, the dependence of specific charge of powder particles leaving the pipe on the transport speed and the mass flow rate is examined for two batches of high density polyethylene (HDPE) powder having different particle size distributions. The particle size distribution histograms for the two batches of HDPE powder are shown in Figure 3.23.

Figure 3.24 shows a schematic diagram of the experimental rig. The internal diameter of the mild steel conveying pipe is 19 mm. Section 2.4 describes in detail the operating and measurement methods of the small scale rig.

3.3.3.1 Powder Specific Charge as a Function of Transport Air Speed

From the Figures 3.25 and 3.26 of charge per unit mass as a function of powder velocity for fines and coarse HDPE powder respectively, it can be seen that the charge to mass ratio is a linear function of the powder transport speed. This relationship can be explained using equation (3.13) which suggests that the specific charge of powder is a linear function of the powder speed for a fixed mass flow rate.

As discussed earlier (section 3.3.2.1), the charge on powder particles at zero transport speed suggests that the powder was charged before it entered the conveying pipework.

Different values of specific charge for the same transport air speeds in both Figures 3.25 and 3.26 may be due to small variations in the flow characteristics of powder particles during pneumatic transport.

Figure 3.22 Specific Charge against Time for Two Transport Air Relative Humidities

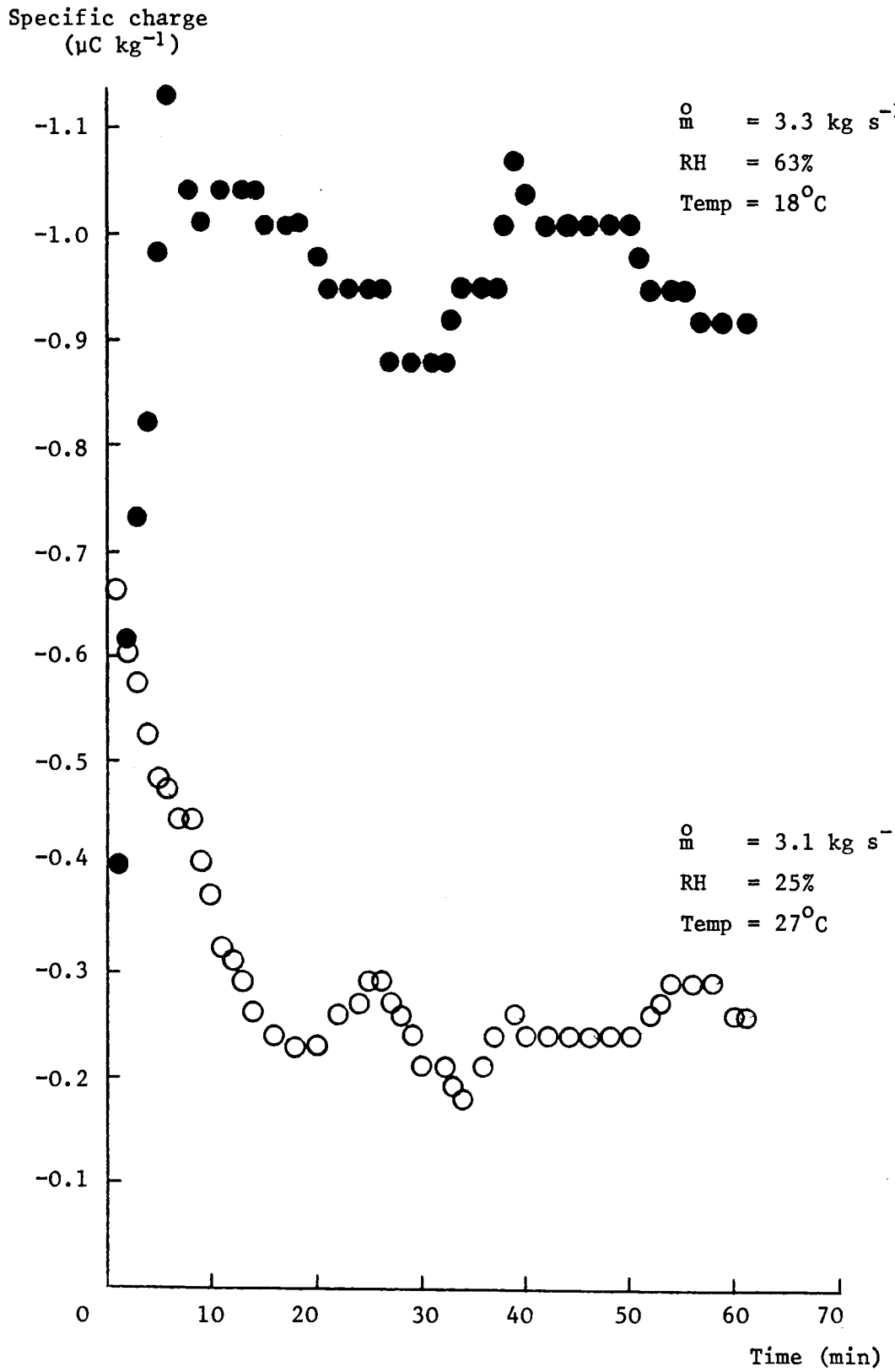

Figure 3.23 Particle Size Distribution Histograms for HDPE Powder

Size Band	Size Range (μm)
1	790 - 1600
2	500 - 790
3	295 - 500
4	250 - 295
5	212 - 250
6	150 - 212
7	125 - 150
8	125

Size Band	Size Range (mm)
9	1.6 - 3.18
10	0.79 - 1.60
11	0.50 - 0.79
12	0.25 - 0.50
13	0.25 - 0

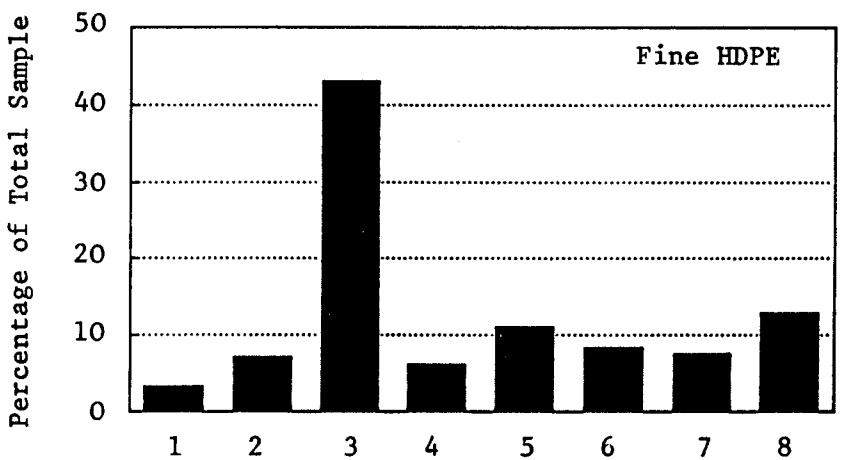

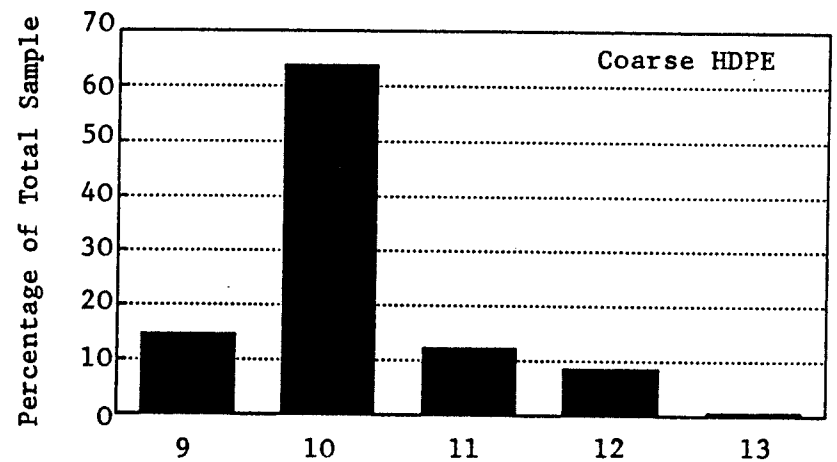

Figure 3.24 Scaled Down Model of Marchwood Silo Rig

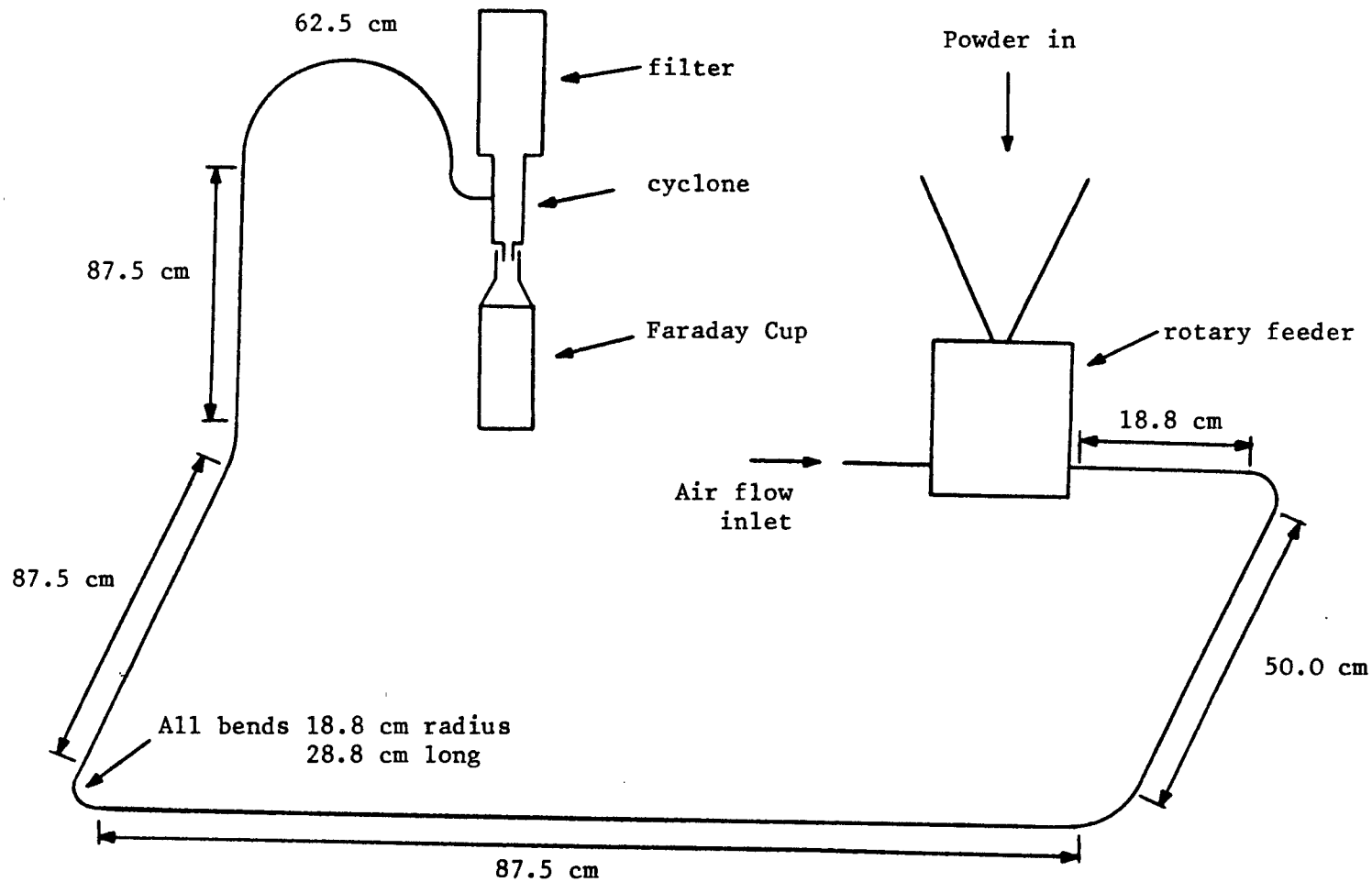

Figure 3.25 Variation of Specific Charge of HDPE (Fines) Entering Faraday Cup as a Function of Transport Air Speed for Silo Scale Model

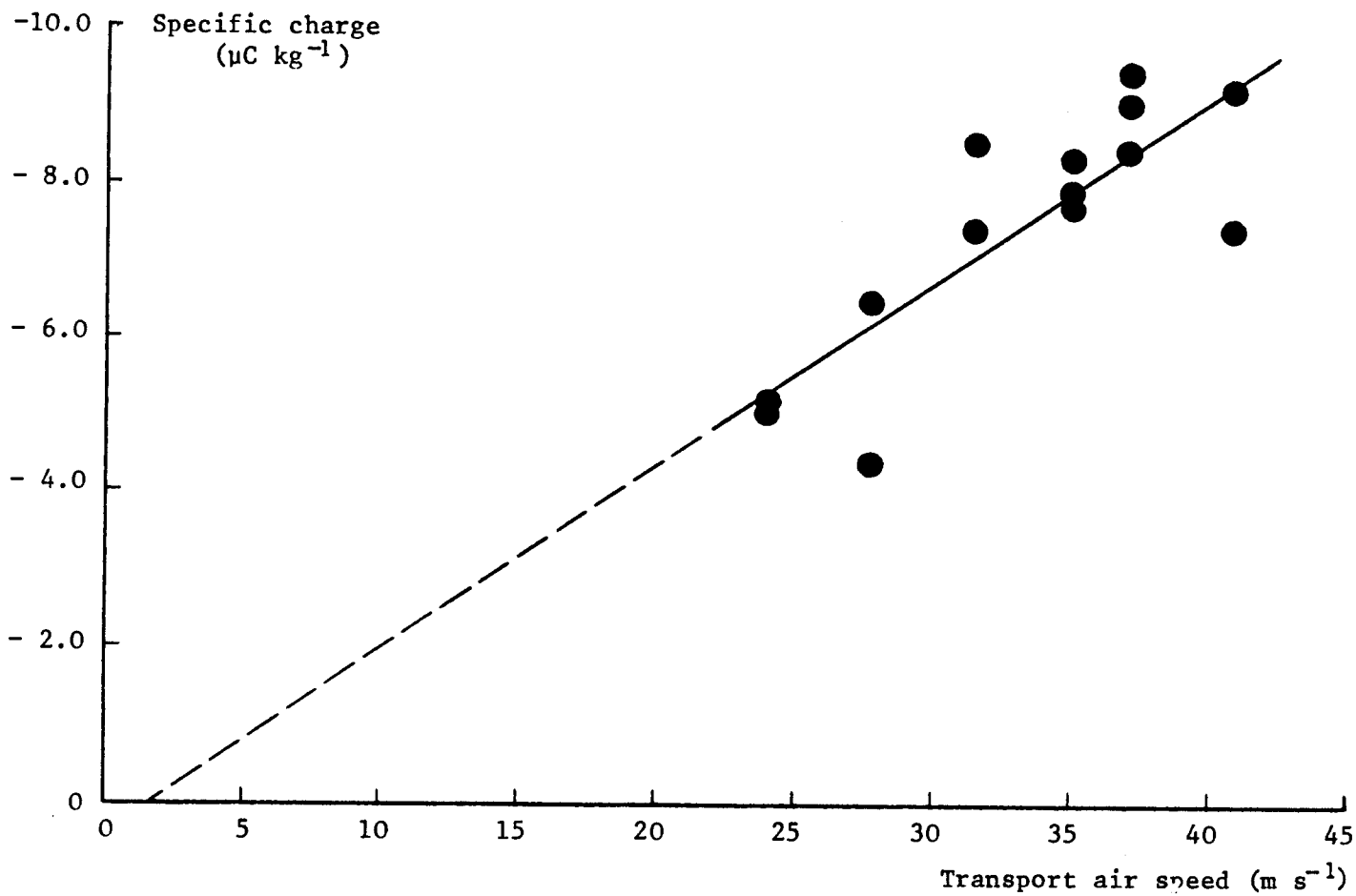

Figure 3.26 Variation of Specific Charge of HDPE (Coarse) Entering Faraday Cup as a Function of Transport Air Speed for Silo Scale Model

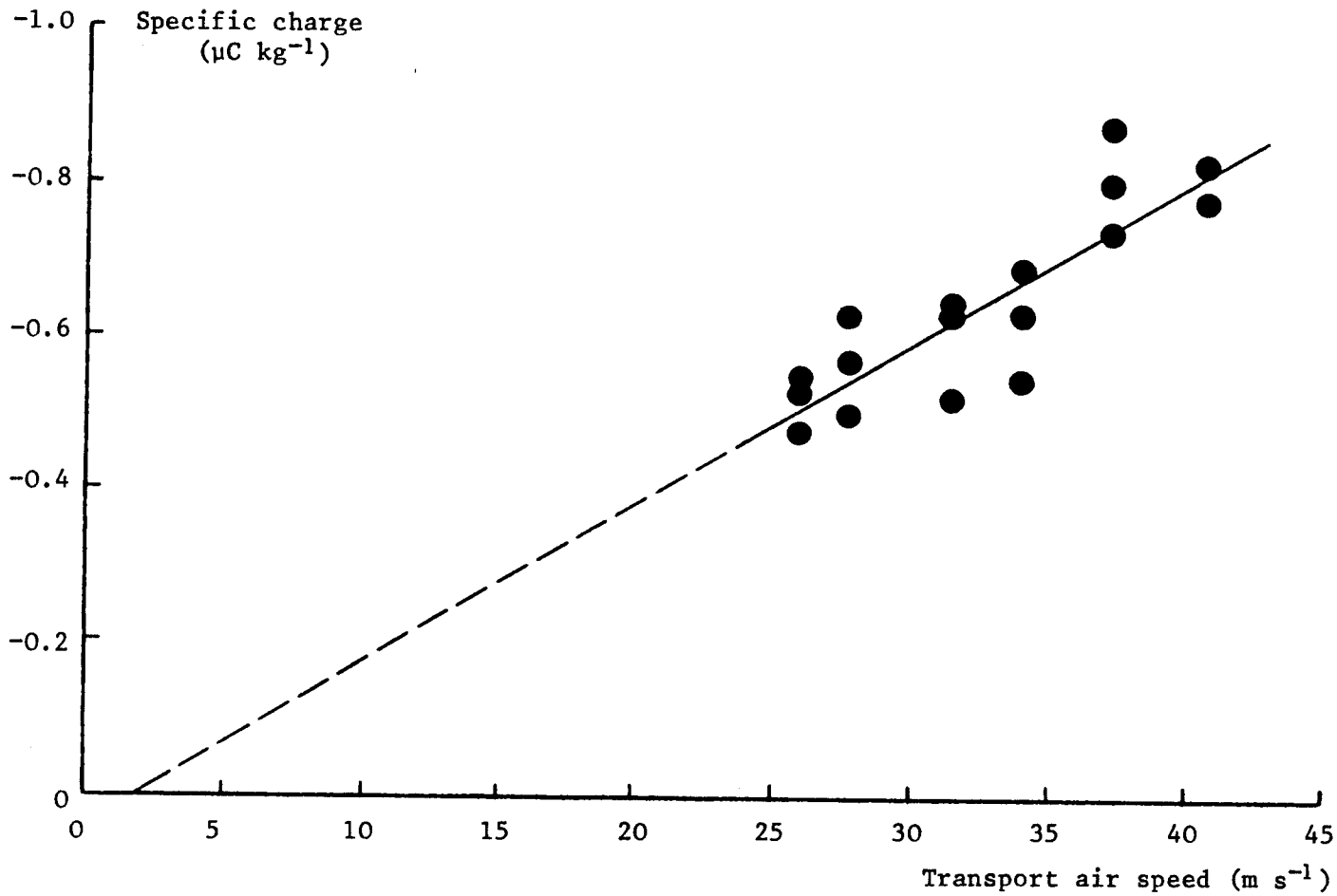

3.3.3.2 Powder Specific Charge as a Function of Mass Transfer Rate

The influence of powder feed rate on the specific charge of fines and coarse HDPE powder particles are shown in Figures 3.27 and 3.28 respectively. Both figures show a peak in the specific charge values measured at mass flow rates less than 0.5×10^{-3} kg s^{-1}. At higher mass flow rates, the characteristic fall off of specific charge with mass flow rate is observed.

At low mass flow rates, because of slight turbulence of particle flow, some of the particles collide with the pipe wall. Since at low mass flow rates hardly any mutual collisions between particles take place it can be assumed that the total charge on the powder is proportional to the mass flow rate. As mass flow rate increases, the chance of mutual collision among powder particles increases gradually, but at the same time the number of particles colliding with the pipe wall will increase as well.

At high mass flow rates, the number of particles colliding with each other increases. The number of particles which cannot reach the pipe wall will also increase with an increase in the mass flow rate because of extremely short average path lengths between particles, and therefore most of the powder charge will be generated by collision between the pipe wall and the particles flowing in the vicinity of the pipe wall. Therefore charge per unit mass will decrease with increase in mass flow rate.

3.3.3.3 Variations of Specific Charge of HDPE Powder as a Function of Conveying Pipe Length

In this experiment a horizontal conveying pipe of total length 3.5 m and internal diameter 19 mm connected the rotary feeder to the Faraday cup. The conveying pipe was divided into four 25 cm, three 50 cm and one 100 cm sections. The system was designed such that a pipe section of length 25 cm and with the same diameter and material as the rest of the conveying pipe, but with a series of baffles inside it, could replace the 25 cm length pipe section connected to the outlet of the rotary feeder. The purpose of the baffle pipe was

Figure 3.27 Specific Charge of HDPE (Fines) as a Function of Powder Feed Rate for Silo Scale Model

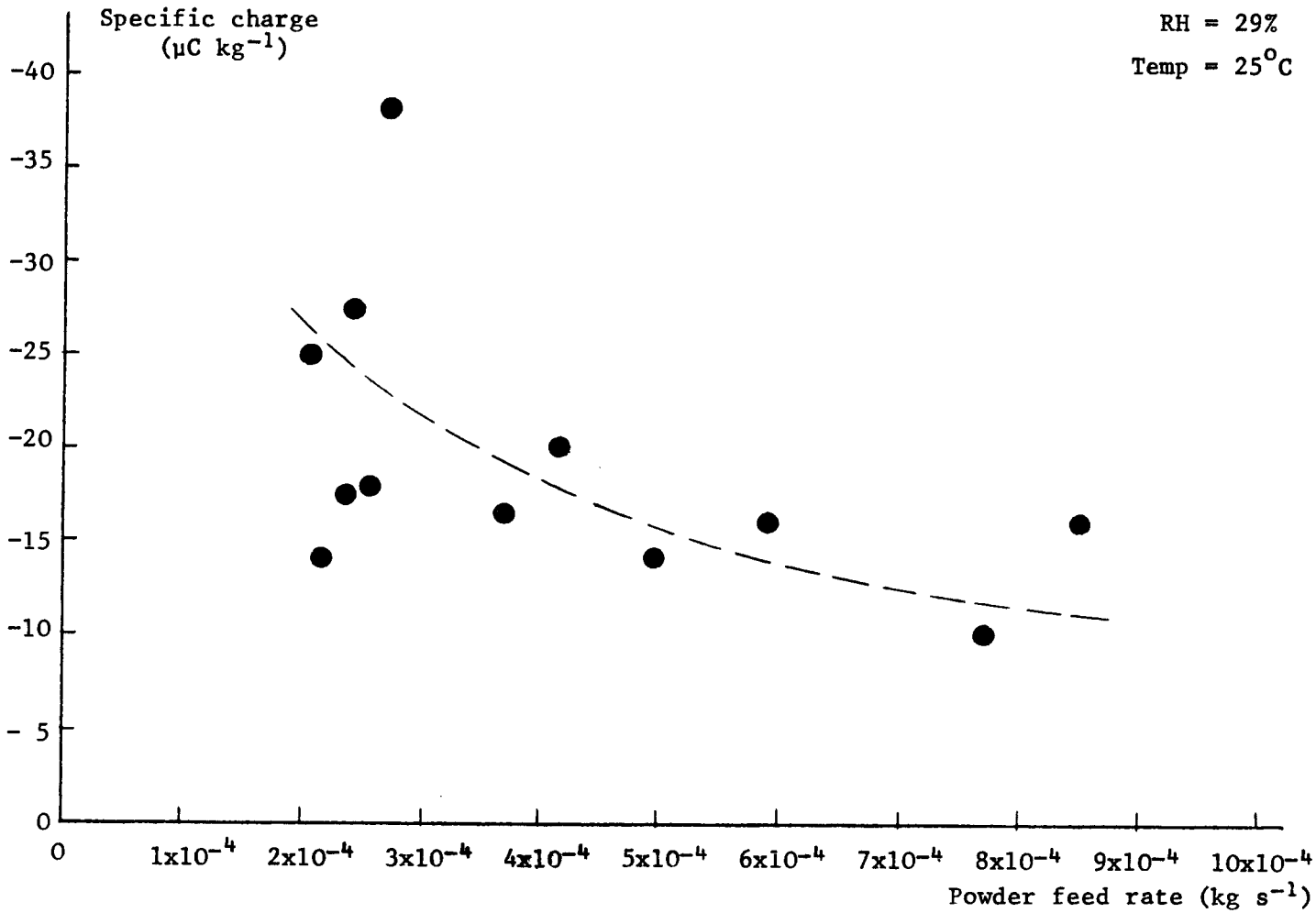

Figure 3.28 Specific Charge of HDPE (Coarse) as a Function of Mass Flow Rate for Silo Scale Model

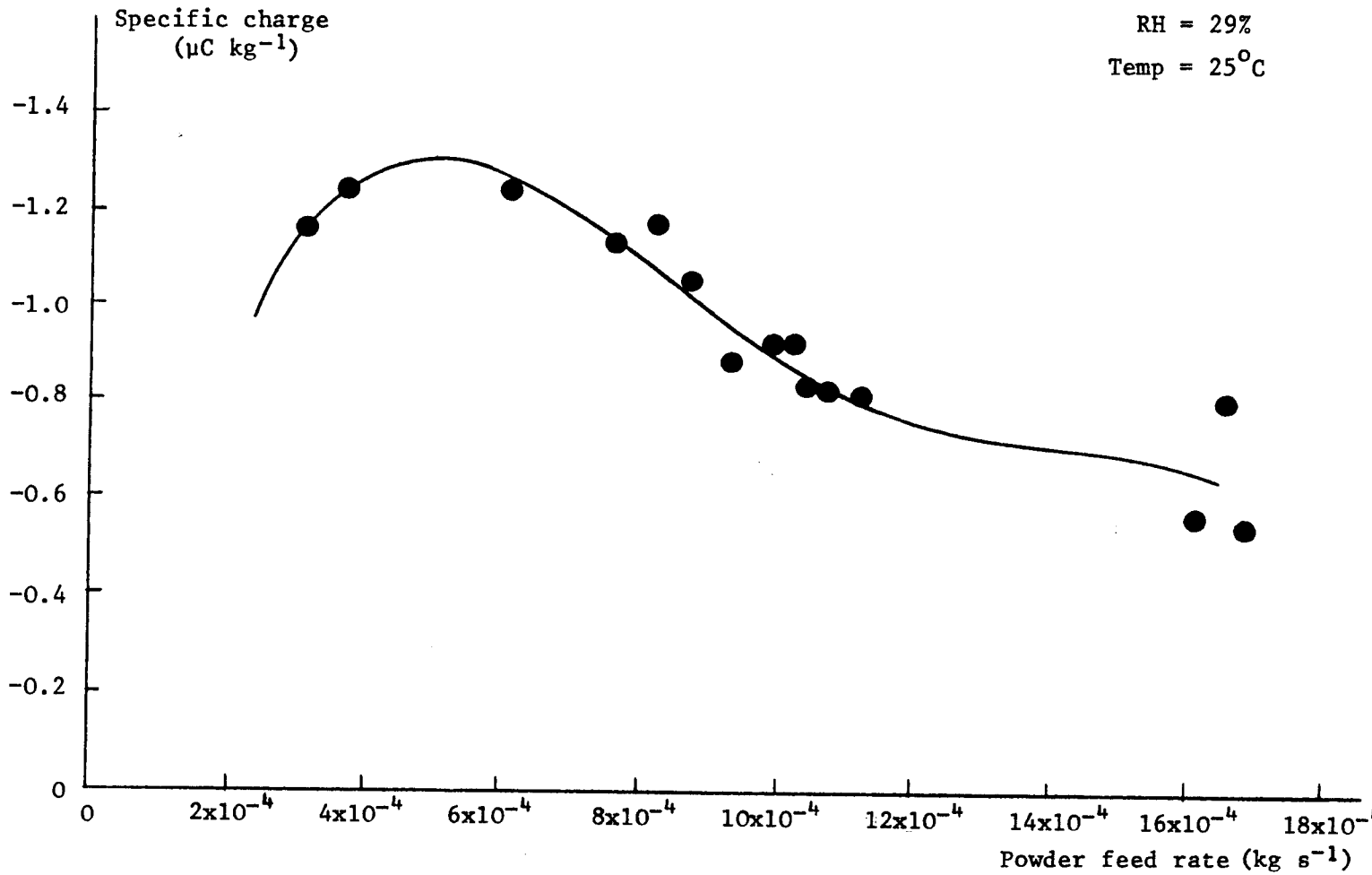

to increase the specific charge of powder by tribo-electrification. Each pipe section was electrically isolated from the next section and was earthed through an electrometer.

Figure 3.29 shows the variation of specific charge of powder as a function of conveying pipe length. As was discussed in section 3.2, the powder specific charge approaches a saturation limit after travelling through a short section of the conveying pipe. When the first 25 cm pipe section was replaced with the baffle pipe, a new saturation limit was reached.

This is not in agreement with the mathematical model presented by Cole et al (1969-1970) and also the experimental model discussed in section 3.2.b. They predicted that even if the initial specific charge on the powder particles is larger than the saturation specific charge which can be acquired by the powder, it will disappear after travelling through a short section of pipe.

This discrepancy between the experimental results and the theoretical predictions may be explained by considering equation (3.13)

$$q_{max} = \frac{2\epsilon_o \pi R v E_{max}}{\dot{m}} \qquad (3.13)$$

From curve 1 of Figure 3.31, $q_{max} = 4.2\ \mu C\ kg^{-1}$, $v = 24.6\ m\ s^{-1}$, $R = 9.5\ mm$, $\dot{m} = 5.1 \times 10^{-4}\ kg\ s^{-1}$. Substituting these values into equation (3.13) gives $E_{max} = 164\ V\ m^{-1}$.

The magnitude of the electric field due to the space charge of particles being conveyed through the pipe is clearly far too small to have any influence on the saturation specific charge of powder.

If a particle is charged after a previous impact, then, as it approaches the pipe wall, opposite charges will be induced on the pipe wall before impact, and a field is established acting in the opposite direction to that producing the charge transfer. In the

Figure 3.29 Specific Charge of HDPE Powder Entering Faraday Cup as a Function of Conveying Pipe Length

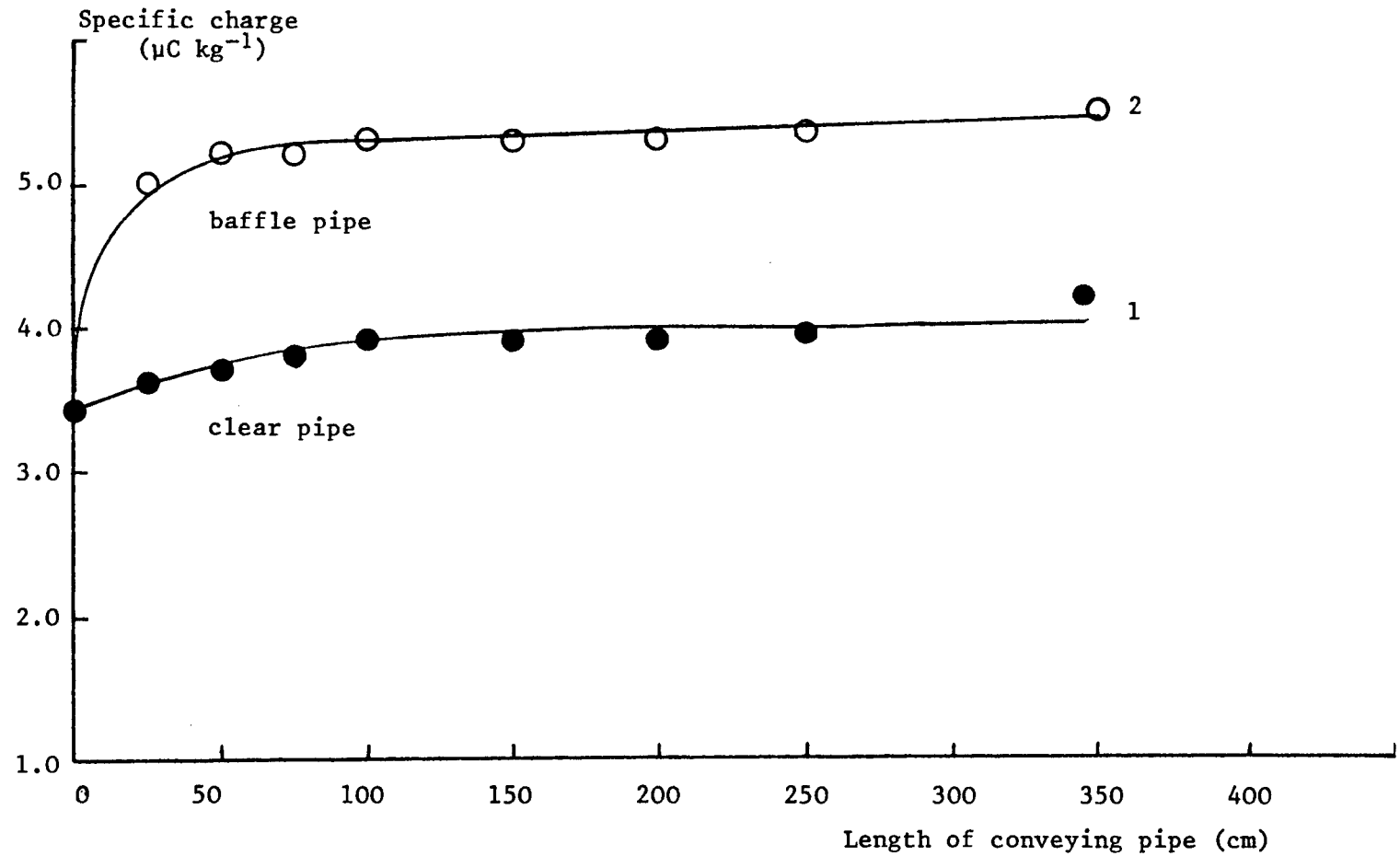

absence of a large space charge field, this electric field determines the saturation limit of the charge.

A specific charge of 4.2 μC kg^{-1} is below the maximum charge that individual particles can sustain, therefore larger charge to mass ratios will be obtained when particles have very energetic collisions with the steel baffles.

3.3.3.4 Influence of Powder Particle Size on the Specific Charge Density

Comparison of Figure 3.25 with Figure 3.26 and Figure 3.27 with Figure 3.28 clearly indicate that the fine powder particles are charged to much higher levels than the coarse powder.

It was earlier stated that the impact charging of a particle depends on only the vertical component of the impact velocity and that the impact area is a linear function of the vertical component of the impact velocity [Masui et al (1983)]. Field (1982) showed that a reduction to one eighth of the original particle size results in an 800 per cent increase in surface area (Figure 3.30) [Field (1982)].

For a small charged particle, the surface electric field is highly divergent and its intensity decreases rapidly with distance from the surface. Since the surface charge density (charge per unit area) produces the maximum electric field over only a small region near the surface, a higher surface charge density than that for a large particle may be sustained [Blythe et al (1979)]. The specific charge density on two hundred different powders was measured by Boschung et al (1980) using an apparatus designed to simulate pneumatic transport. The wide range of charge densities (10^{-7} to 10^{-3} C kg^{-1}) obtained under the same experimental conditions could be attributed to differences in the surface area and the chemical composition of the powder.

For some powders the polarity of charge acquired by friction is a function of the particle size [Cross et al (1982)]. Field

Figure 3.30 Increase in Surface Area Resulting from Particle Size Reduction

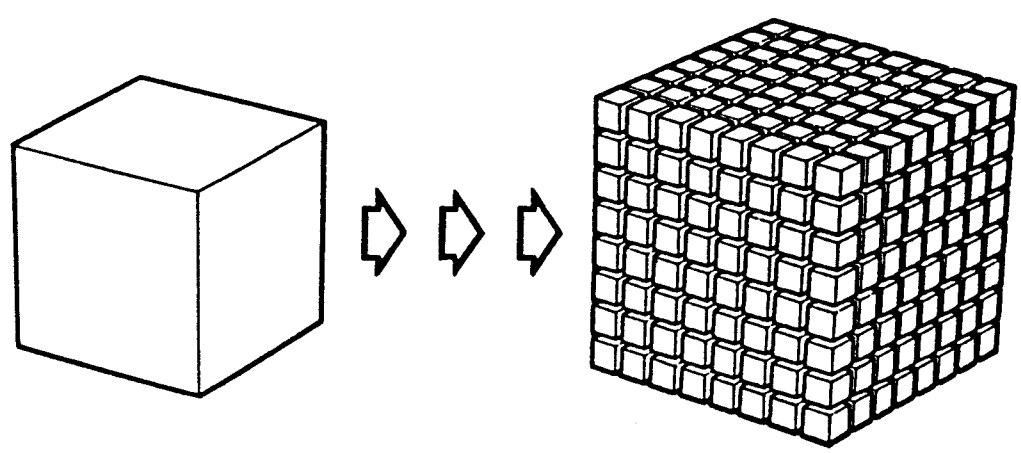

measurements showed that both the bulked coarse HDPE powder and the fine powder dust cloud were negatively charged for a negative silo current. When the silo current was positive the coarse particles were charged positively and fine particles negatively. It has also been observed both in industrial installations and in laboratory tests that the polarity of the electric field reverses as the coarse particles settle out of a dust cloud [Cross et al (1982)].

In terms of flammability and explosibility, a material generally becomes more hazardous as the particle size is reduced.

3.4 Summary

A theoretical model of the electrostatic charging of powders by pneumatic conveying is presented and verified experimentally. The phenomenon of electrostatic charging of powder particles during pneumatic conveying is divided into two counteracting processes, charging and discharging. Charging occurs when powder particles collide with the pipe walls, discharging occurs between the particles and the pipe walls in regions where the electric field exceeds the saturation limit and pre-impact effect. The model shows that even if the specific charge of the powder entering the pipework is larger than the saturation specific charge which can be acquired by powder, it will be dissipated after travelling through a short section of the pipe. Experimental investigations supporting this model show that the tribo-electrification of powder particles reaches a saturation level after travelling through a short length of conveying pipe. An additional charge on the powder entering the pipework will discharge after flowing through a short distance.

The dependence of saturation specific charge of powders flowing through pipes on various influencing parameters of the pneumatic conveying installation, such as powder transport speed and powder feed rate, is investigated using both the Marchwood silo rig and the silo scale model. The charge to mass ratio is a linear function of the transport air speed. The specific charge of powder particles at Marchwood silo rig shows a trend with

the specific charge decreasing as powder mass flow rate is increased. The specific charge of HDPE reaches a saturation level at mass flow rates less than 5×10^{-4} kg s^{-1} using the small scale rig. At higher mass flow rates, the characteristic fall off of specific charge with mass flow rate is observed.

Charged powder flowing along a pipe sets up a space-charge field at the pipe walls so that the charging process during particle/wall collisions occurs under the influence of a self-imposed field. It is concluded that the limiting or saturation specific charge of powder particles transported along the pipework is determined by this "self-generated" space-charge field during normal pneumatic conveying. For the silo scale model, the saturation specific charge is found to be larger than the maximum saturation specific charge obtained at Marchwood silo rig under normal operating conditions. The space charge field of powder flowing through the silo scale rig is calculated to be too small to have any influence on tribo-electrification of HDPE.

The charge build-up in a silo is related directly to the charge exchange that occurs in the powder feed pipework, so that controlling the tribo-electric charging in the pipework offers a solution to the problem of charge build-up in silos. To this end the role of the space charge field on the tribo-electrification process is investigated.

A section of standard pipework is modified by mounting a rod electrode along the axis, enabling a radial electric field to be set up between the rod surface and the inner walls of the pipe either aiding or in opposition to the natural space-charge field of the powder. The measurements on HDPE powder and maize starch show that the tribo-electric charging of powder can be controlled by a superimposed electric field. As the radial field at the surface of the rod electrode is higher than the field at the pipe wall, the charge exchange between colliding particles and the rod surface are greater than charge exchanges at the pipe wall, the particle-rod

exchange being dominant for the geometry and test conditions reported here. By controlling the magnitude and sign of the voltage on the rod any charged powder entering the field pipe section may be charged more highly, have its polarity reversed or may be neutralised. When powder is neutralised the space-charge field and the current of the silo drop to negligible levels.

Transport air relative humidity has a noticeable effect on tribo-electrification of HDPE powder. Experiments on the effects of relative humidity on the specific charge of HDPE powder suggest a relation between the two, such that a large RH implies a large negative specific charge and a small relative humidity implies a small positive specific charge.

Chapter 4

Electrostatic hazards in storage silos

CHAPTER 4

ELECTROSTATIC HAZARDS IN STORAGE SILOS

4.1 Introduction

In Chapter 3 it was shown that static electricity is generated during pneumatic conveying of powders. It is normally only when the powder enters a silo that a significant electrostatic hazard may arise. This is because the dispersed dust cloud of the powder in the silo normally requires less amount of energy to ignite. A sudden sugar slide initiated an electrostatic discharge which was believed to be the ignition source in a 20,000 tonne sugar silo explosion [Muller-Hillebrand (1963)]. Spark and propagating brush discharges, although potentially the most dangerous type of discharges, can however be excluded by using grounded conducting equipment or avoiding plant items fabricated from non-conducting materials. The igniting power of charged combustible powders which may enter an earthed conducting installation is however still unknown. In order to evaluate the risk of ignition of a fine particle dust cloud in a grounded conducting silo, the amount of charge accumulated on and the incendivity of discharges from the surface of bulked powder and the dust cloud must be studied.

During pneumatic conveying and storage of a conducting powder, the electrostatic charge on the bulked powder is conducted to earth very quickly. The charge on the suspended particles in the dust cloud can however give rise to very high space potentials and electric fields. In the case of highly insulating powders a more serious ignition hazard may arise when the highly charged particles settle into bulk form because the increase in volume charge density increases the probability of discharges. When the space charge density of a dust cloud or the surface charge of a bulked powder reaches a level at which the electric field strength associated with the charge exceeds the dielectric breakdown strength of the

surrounding atmosphere, an electric discharge will occur. The electric field strength of air at atmospheric pressure and temperature is approximately 3×10^6 V m^{-1}. In any particular situation the possibility of an electrical discharge from a dispersed dust cloud or from the surface of bulked powder can be assessed from measurements and calculation of the electric field strength and the potential.

When an earthed electrode approaches a charged insulating surface it acquires an opposite charge by induction. The field increases as the two surfaces are brought closer together and eventually the air breaks down forming a multi-channelled discharge known as a brush discharge. The charge is not mobile on the insulating surface and only a small area is discharged, releasing a limited amount of energy. It is therefore more realistic to measure the incendivity of discharges directly by bringing an earthed sphere surrounded by a flammable atmosphere of known minimum ignition energy to the charged surface. A discharge from the charged surface is said to have an ignition energy equivalent to that of the flammable atmosphere, if it is just able to ignite it [Gibson et al (1965)].

In this chapter, electrostatic activity during storage of two powders, maize starch (ρ = (0.3 to 1.0) x 10^9 Ωm) and high density polyethylene ($\rho > 10^{15}$ Ωm), are studied using the full scale Marchwood silo rig. These studies include the space and surface potential and electric field measurements and determination of existence and incendivity of discharges. The influence of such parameters as specific charge of powder and relative humidity on the above measurements are also determined. A laboratory scale rig is also used to study the effects of streaming current, specific charge density and powder flow rate on the probability of ignition and incendivity of discharges from the surface of bulked HDPE pellets under more controllable conditions.

4.2 Electrostatic Effects During the Bulking of Charged Powder

Thorpe et al (1985) presented a model to describe the potential distribution of charged bulked powder. In this model the charge per unit time on the particles entering the silo is seen as a streaming current, I_s, which produces a constant surface potential, V_s, across the resistance of the bulked powder (see Figure 4.1).

Assuming that the base of the bulked powder heap is a spherical shell (radius b) and is at earth potential, and also that the bulking point has a spherical shell (radius a), then the capacitance, C, between the shells is approximately given by

$$C = 4\pi \epsilon_o \epsilon_r \frac{S_a S_b}{(S_b - S_a)} \times \frac{1}{4} \qquad (4.1)$$

The decay time constant for charge on the inner spherical shell is given by equation (4.2)

$$\tau = zC = \epsilon_o \epsilon_r \rho \qquad (4.2)$$

The resistance, z, between the shells is thus

$$z = \frac{\epsilon_o \epsilon_r \rho}{C} = \frac{\rho (S_b - S_a)}{\pi S_a S_b} \qquad (4.3)$$

The maximum surface potential directly below the fill pipe entrance is given by equation (4.4)

$$V_s = I_s z = \frac{I_s \rho}{B} \qquad (4.4)$$

where ρ is the powder resistivity and B is a geometrical constant which for the partly filled silo is approximated by the expression

$$B = \frac{\pi S_a S_b}{(S_b - S_a)} \qquad (4.5)$$

Figure 4.1 The Bulked Powder Heap

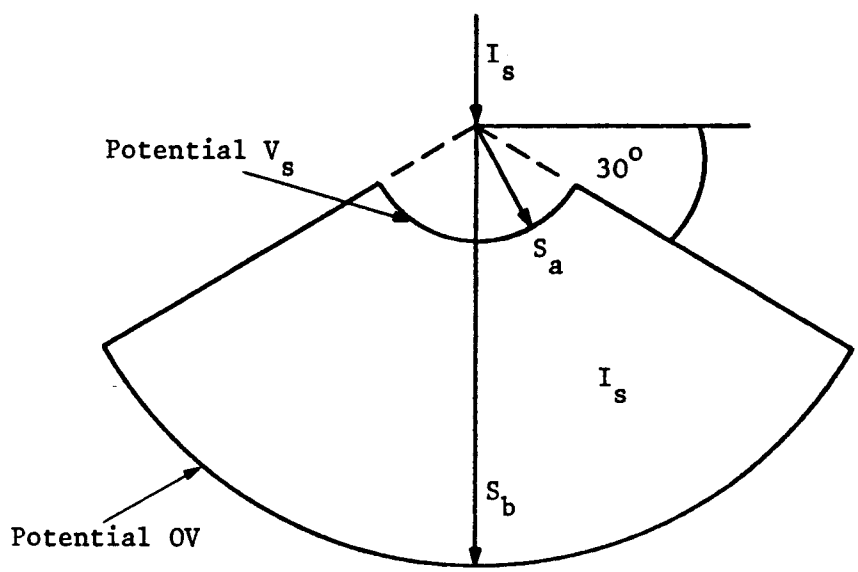

The approximate maximum silo currents, maximum surface potential, and resistivities of all the powders so far tested at Marchwood silo rig are shown in Table 4.3.

Table 4.3 **Broad Summary of Test Results**

Product	Powder Resistivity, ϱ, (Ωm)	Maximum surface potential, V_s, (no charge injection) (kV)	Approx. max. silo currents (no charge injection) (μA)
HDPE (fines)	$> 10^{15}$	-	+ 3.5
Wheat	$(4 \text{ to } 6)\times10^{7}$	≈ 0	+11.0
Sugar	10^{8} to 10^{10}	+16.5	+ 3.5
Phenol	10^{13} to 10^{15}	-16.0	- 8.0
Starch	$(0.3 \text{ to } 1.0)\times10^{9}$	- 5.0	-13.5

The geometrical constant, B, is a function of silo height, width, angle of repose of bulk powder, and fill depth, which was given by a simplified equation (4.5). From experimental observations, $a \approx 0.3$ m and $S_b \approx 2$ m and the angle of repose of the bulked powder in the silo was measured to be approximately 30°, but if $S_a \ll S_b$, then,

$$B = \pi S_a \approx 1 \text{ m} \qquad (4.6)$$

Equation (4.4) then becomes

$$V_s = I_s \varrho \qquad (4.7)$$

From this equation the relationship between the maximum theoretical surface potential of the bulk powder and the volume resistivity was plotted for a range of silo streaming currents between 1.0 μA and 30.0 μA (Figure 4.2).

Figure 4.2 Maximum Theoretical Surface Potential as a Function of Volume Resistivity

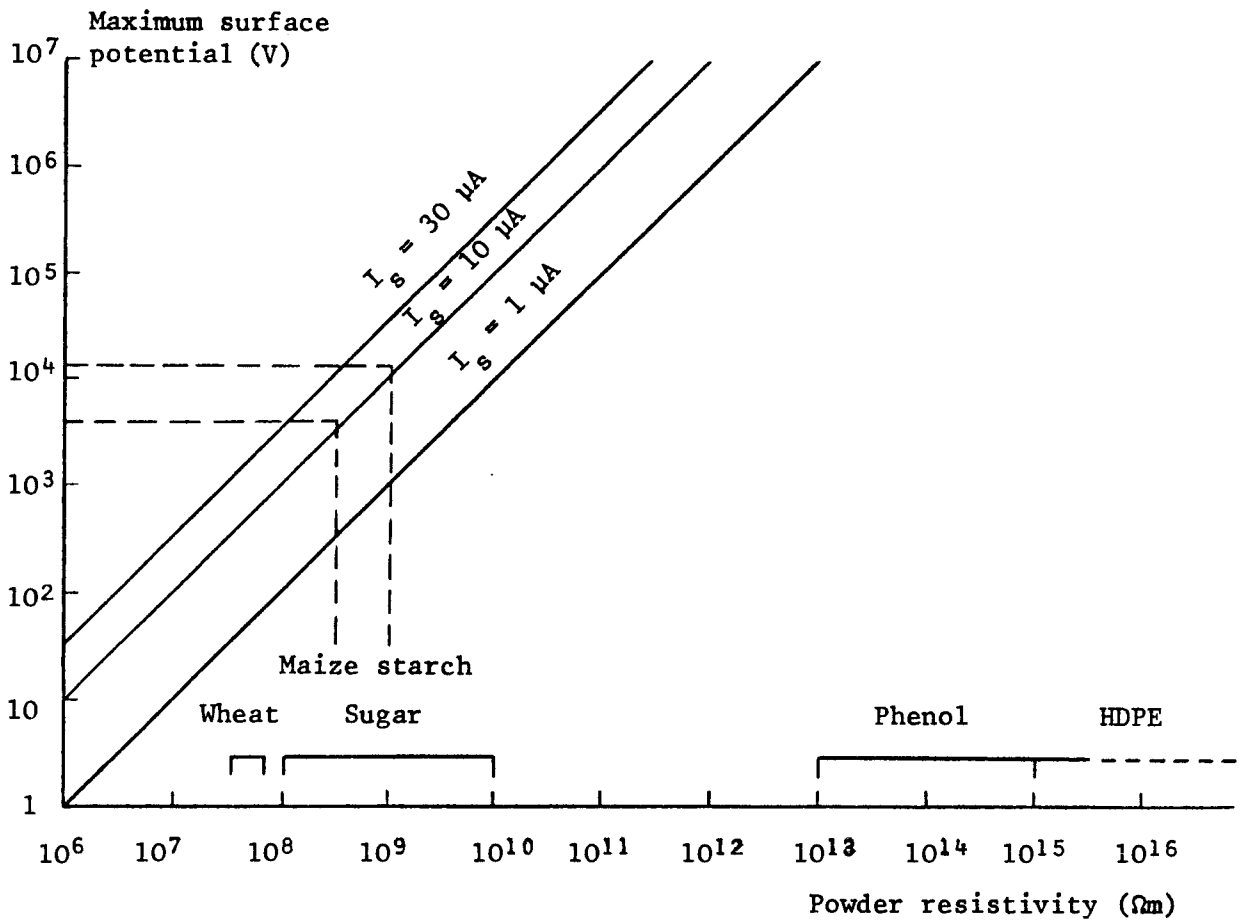

The limit of streaming current, I_s, indicated in Figure 4.2, represents the range of values of I_s obtained in previous experiments at the silo (refer to Table 4.3).

Using the graph in Figure 4.2, the maximum surface potentials on bulk powder can be predicted if the powder resistivity and streaming current are known. For example, in the case of maize starch with a resistivity between (0.3 to 1.0) x 10^9 Ωm, the maximum measured streaming current (I_s) was found to be -13.5 μA. From Figure 4.2, this gives a maximum surface potential of (-4 to -13.5) kV. The measured value of surface potential for maize starch was -5 kV (Table 4.3).

The surface potential for powders having resistivities larger than about 10^{13} Ωm is not possible to predict using this model because the excess charge is lost by low energy corona or brush ionisation of the gas space. This is because when highly charged powders are bulked, provided the rate at which the charge enters the silo is larger than the charge relaxation time of the powder, the electric field on the surface of bulked powder will increase and eventually will exceed the breakdown limit causing ionisation of the air.

Blythe et al (1979) considered the hypothetical case where a stream of charged insulating particles of radius r, initially well separated from each other, is collected together into a macrosphere of radius S, see Figure 4.3. If the original particles are charged to the maximum, then the cumulative electric field generated in the air around the conglomerate will exceed the breakdown limit, causing ionisation of the air.

The charge Q released from the powder by bulking is given by

$$Q = n_p 4\pi r^2 \sigma_m - 4\pi S^2 \sigma_m \qquad (4.8)$$

n_p is the number of powder particles.

Figure 4.3 The Bulking Effect

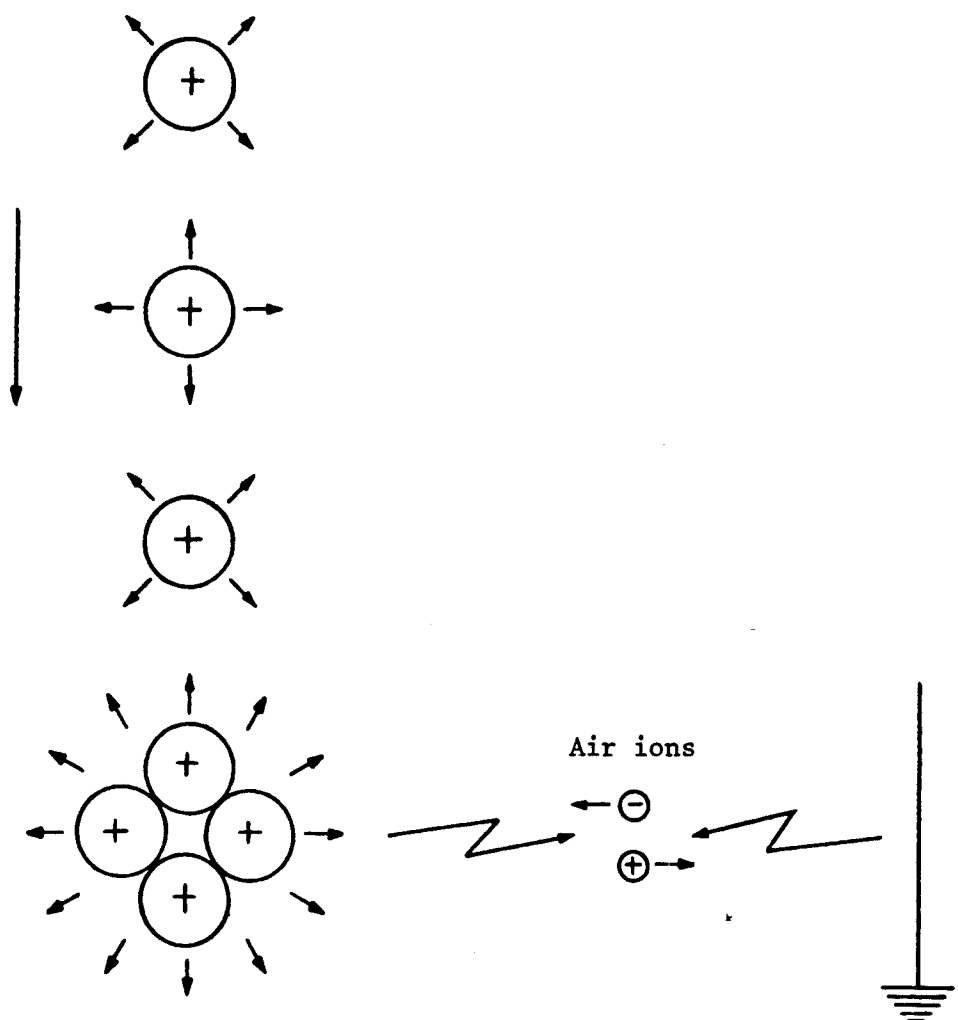

As a result of such bulking effect, a large amount of charge will be released, because the effective surface area of the whole heap is much smaller than the sum of the individual surface areas of all the incoming small particles, ie, $S^2 << n_p r^2$ in equation (4.8). If the container is metal and is earthed, the air discharges are led away to earth. Figure 4.4 shows the charge release when particles having a maximum theoretical surface charge density ($\sigma_{max} = 8.22 \times 10^{-6} \; r^{-0.3}$ C m^{-2}) are collected together into a macrosphere of radius S, using equation (4.8). Bulking densities of 600 kg m^{-3} and 470 kg m^{-3} were considered for particles with a radius 1.7 mm and radius of 0.5 mm or smaller, respectively.

Although this model gives an account of the quantity of charge released as a consequence of bulking, the particles in practice are not spherical and, furthermore, the number of particles, radius of each particle and the specific surface charge density, are not practical parameters to work with.

Experimentally, the total charge on the powder entering the silo can be measured. By Gauss's theorem, the electric field due to a sphere of charged powder (see Figure 4.5) is given by

$$\iint_A \epsilon_o \, E \, dA = Q \qquad (4.9)$$

Therefore, at a radius S

$$Q = \epsilon_o \, E \, 4\pi \, S^2 \qquad (4.10)$$

Thus

$$Q_{max} = 4\pi \, \epsilon_o \, S^2 \, E_{max} \qquad (4.11)$$

where Q_{max} is the maximum charge on powder allowed by the dielectric strength of air.

The difference between the total charge entering the silo and the maximum charge predicted by equation (4.11) will give the amount of charge released by the bulking effect.

Figure 4.4 Charge Release as a Function of Bulked Powder Radius

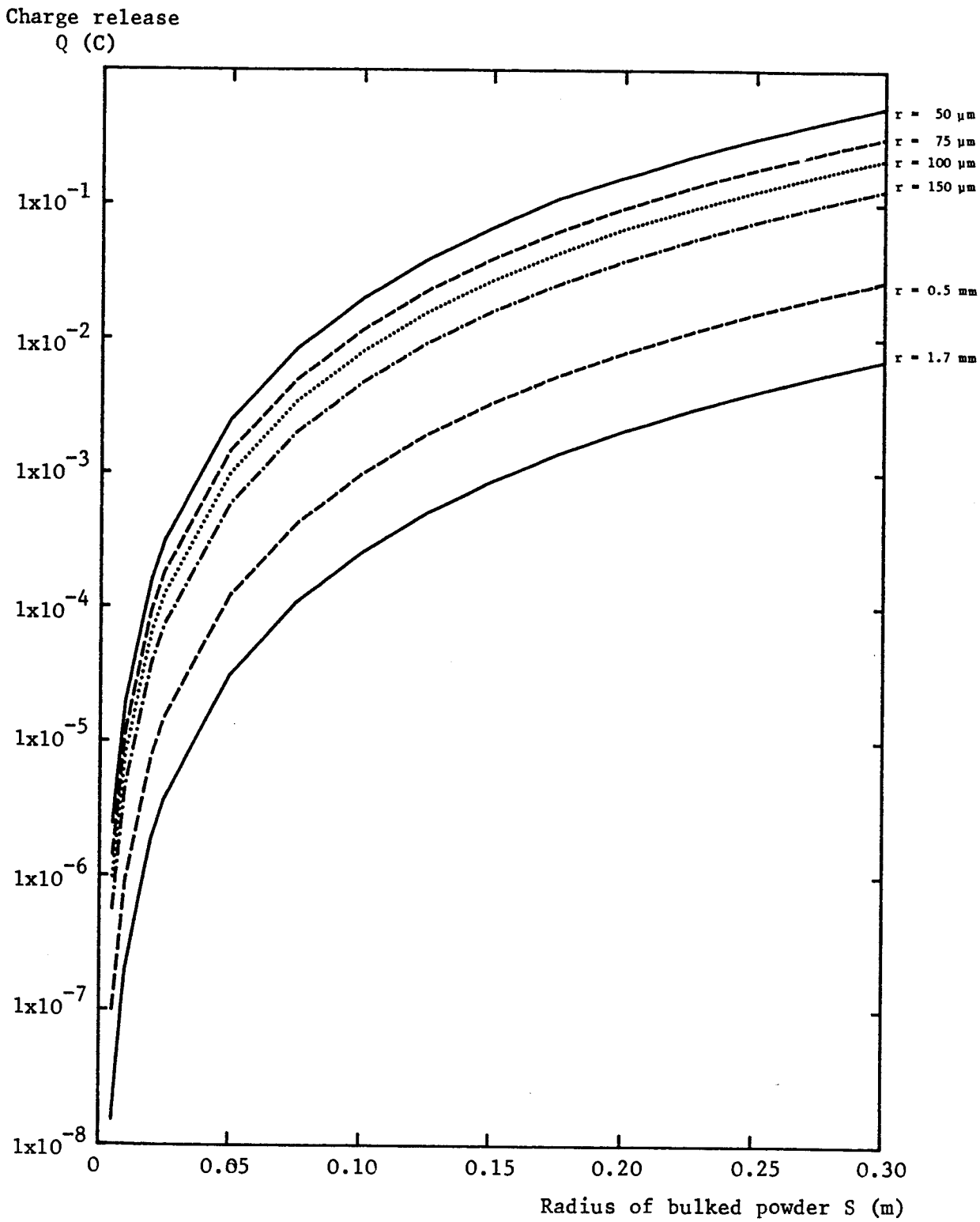

Figure 4.5 The Bulking Effect at Marchwood Silo

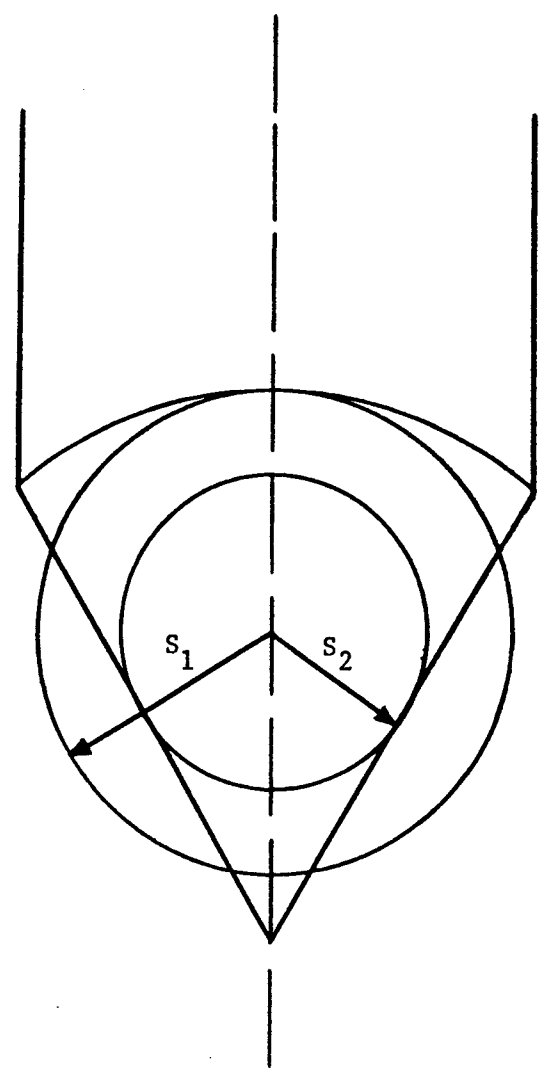

S_1 = 1.0 m
S_2 = 1.5 m

Using equation (4.11), for $E_{max} = 3 \times 10^6$ Vm^{-1} and for:

$S = 1.0$ m $\quad Q_{max} \approx 334$ μC

$S = 1.5$ m $\quad Q_{max} \approx 750$ μC.

Experimentally, for a typical run of 6.2×10^3 kg of HDPE fines with a specific charge of 2 μC kg^{-1}, the total charge entering the silo is:

$$Q_{max} = 6.2 \times 10^3 \text{ kg} \times 2 \times 10^{-6} \text{ C kg}^{-1}$$
$$Q_{max} = 12400 \text{ μC}.$$

This value is greater than that allowed theoretically, which suggests that electrostatic discharges must take place on every occasion that the powder is collected together in the silo, provided the rate at which charged powder enters the silo is greater than the charge relaxation time of the bulked powder.

Figure 4.6 shows the silo filling current and silo emptying current as a function of time for a 6.2 tonne batch of HDPE fines. The emptying process started as soon as the filling of the silo was completed. Comparison of the two currents shows that electrostatic discharges occur during the bulking process. The excess charge may be released in the form of low energy corona discharges.

Considering an emptying current of 0.2 μA (see Figure 4.6), the total remaining charge on the powder is given by

$$Q = 0.2 \times 10^{-6} \text{ C s}^{-1} \times 28 \text{ min} \times 60$$
$$Q = 336 \text{ μC}$$

The maximum charge on powder allowed by the dielectric breakdown of air was earlier calculated to be 334 μC and 750 μC for spheres of radius 1 m and 1.5 m respectively. Allowing for the inaccuracy inherent in the calculations, these values are comparable to those observed experimentally.

Figure 4.6 Graph of Silo Current as a Function of Filling Time for 6.2 Tonne of HDPE

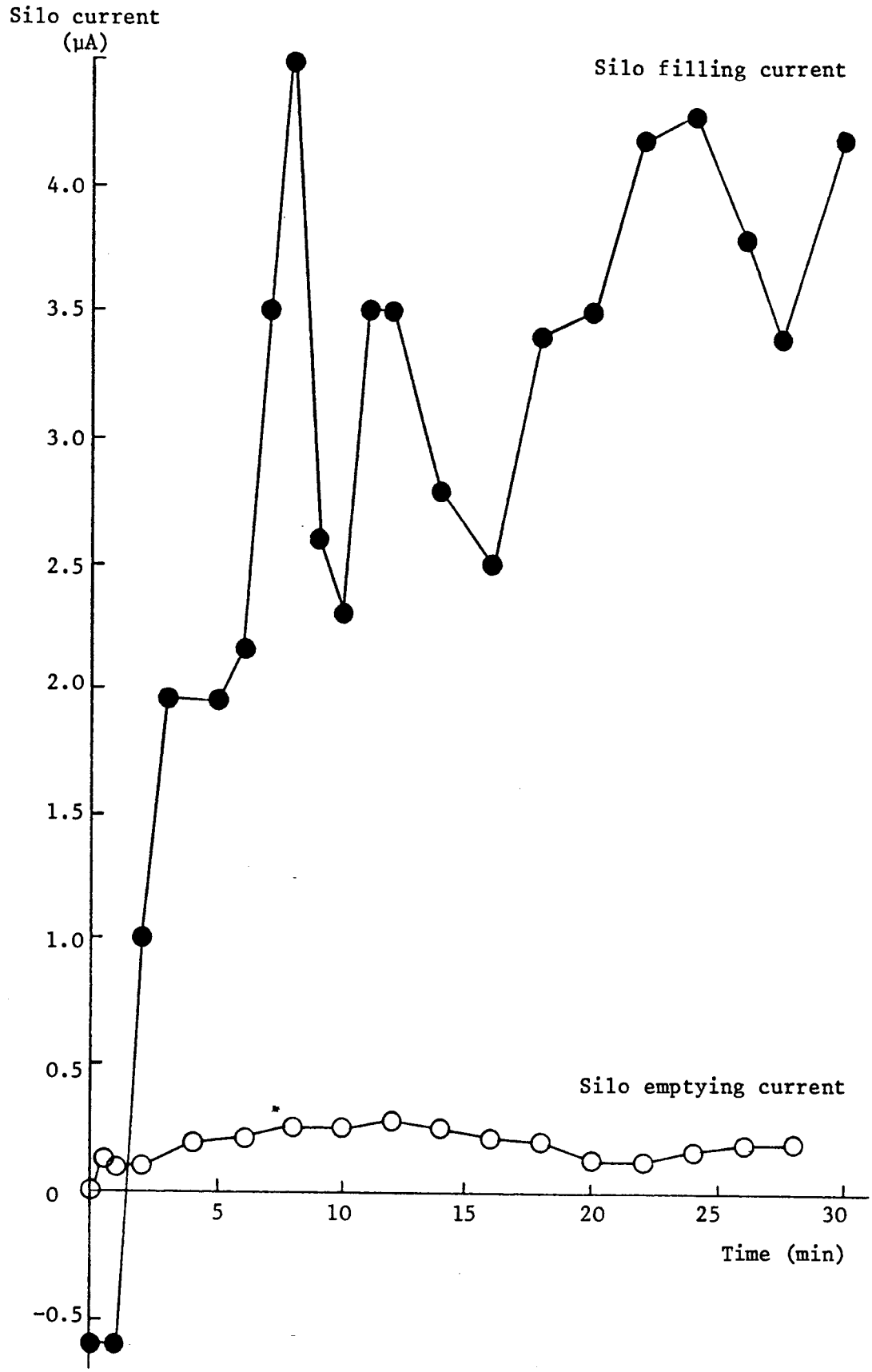

4.3 Experimental Results from the Full Scale Marchwood Silo Rig

4.3.1 Electric Field Measurements for Fine HDPE Powder

At approximately 20 minutes after the end of a run, a field mill was lowered through one of the explosion vents to the powder cone surface. Figure 4.7 shows a series of field strength readings taken across the cone surface, with the millhead close to the powder. The silo current and the transport air relative humidities were +0.46 μA and 33% respectively.

Figure 4.7 shows that the strongest fields were positive and occurred near the silo wall. Towards the centre of the silo, however, the fields measured were negative and much smaller [Cartwright et al (1982)].

Field measurements of the dust cloud (to be discussed later) showed that the powder charging which took place during pneumatic conveying was bipolar; when the silo current was positive the dust cloud (fine particles) in the silo was charged negatively and the coarse particles positively. When the silo current was negative, the charge on both the coarse and fine particles was negative. The difference in the polarity of the measured electric fields near the silo wall and towards the centre of the bulked HDPE surface could be due to the negative fines settling on top of the positive bulked powder, but predominantly in the centre of the silo.

Figure 4.9 shows the electric field measurements of the powder dust cloud. The experimental data during this part of the experiment was obtained during consecutive runs from a field mill positioned at porthole numbers 3, 4 and 5 (see Figure 4.8). The field mill was mounted in the portholes of the test silo and flush with the inner wall.

Trace 1 shows the electric field measurements at position 5. The electric field was positive and peaked at about +150 kV m^{-1}. There were some field fluctuations in the vicinity of the field mill which could possibly be due to powder particles hitting the

Figure 4.7 Electric Field Strength Across HDPE Powder Surface (Cartwright et al (1982))

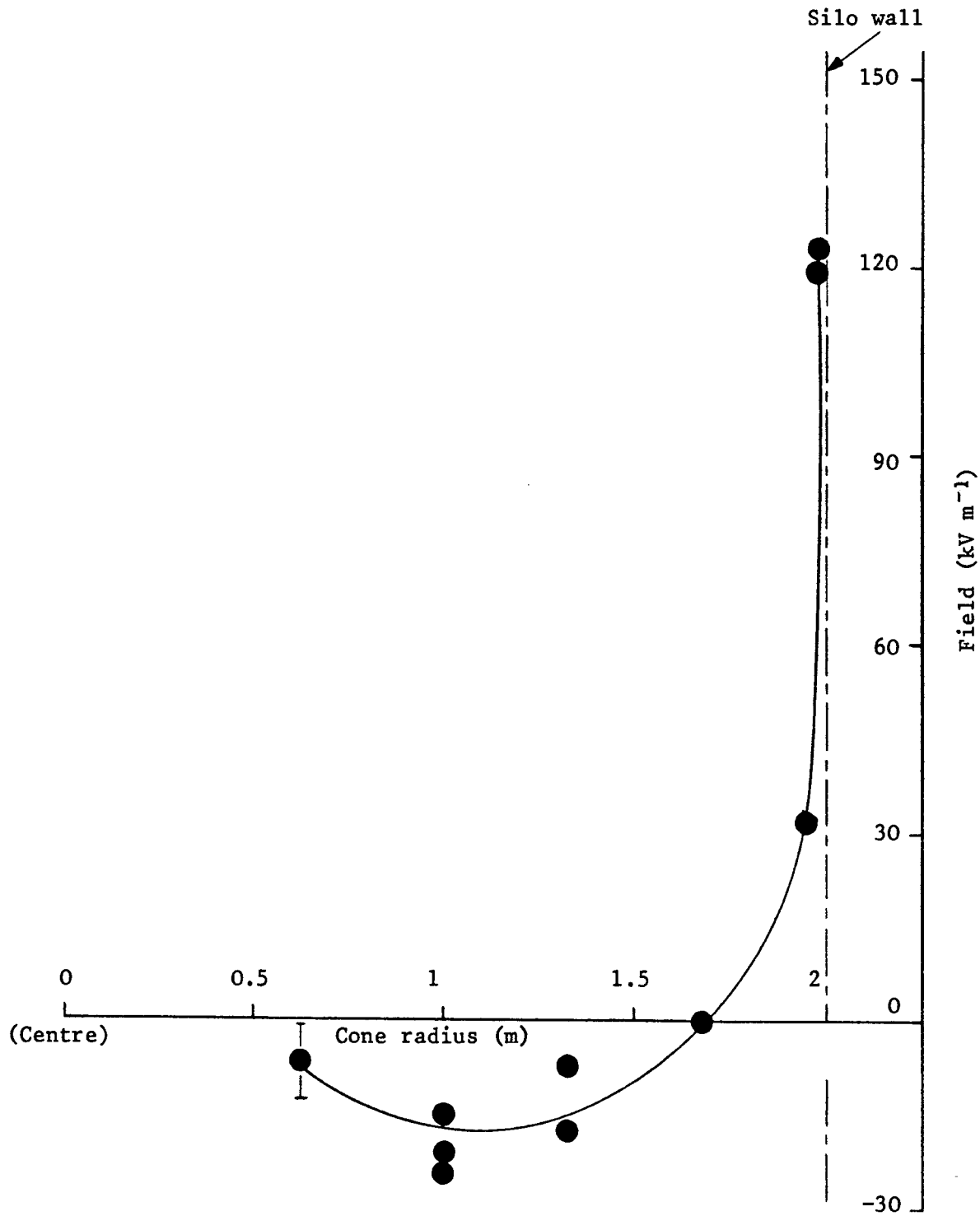

Figure 4.8 Port-hole Labelling Scheme

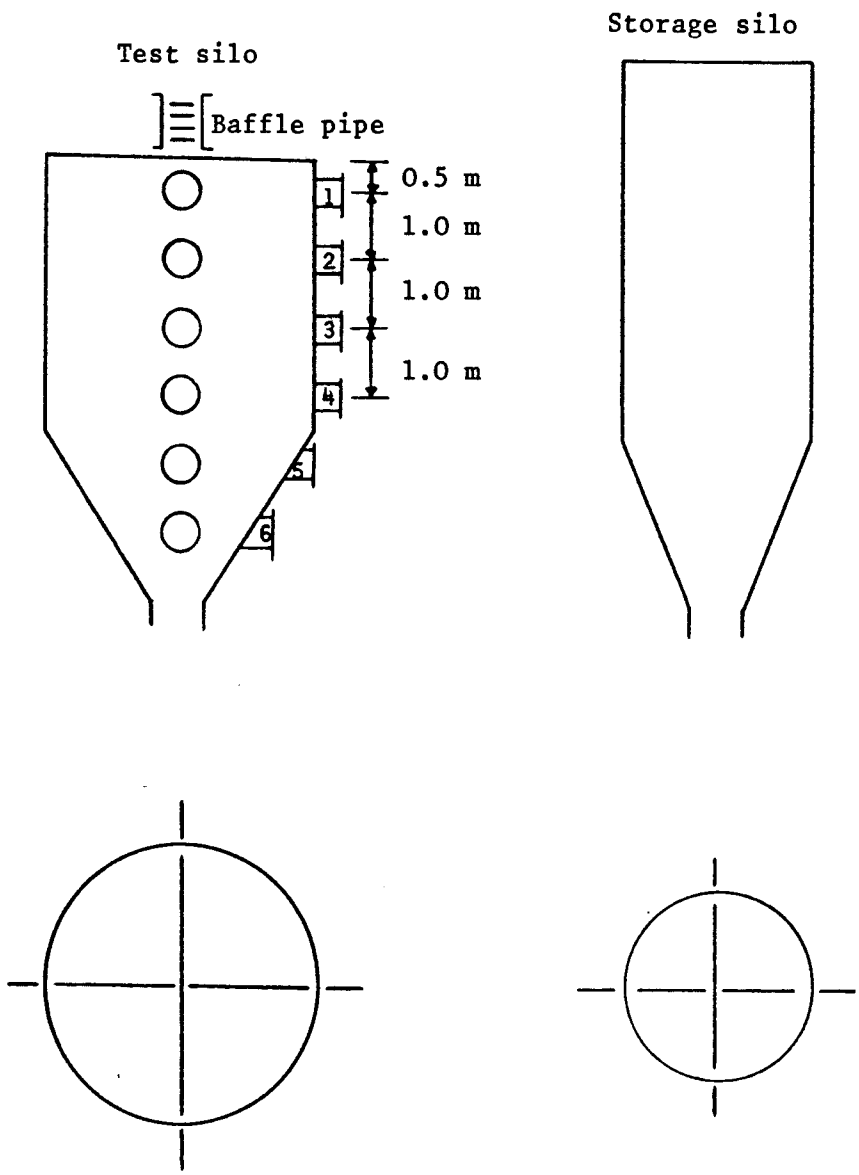

Figure 4.9 Electric Field Strength of HDPE Dust Cloud
(Cartwright et al (1982))

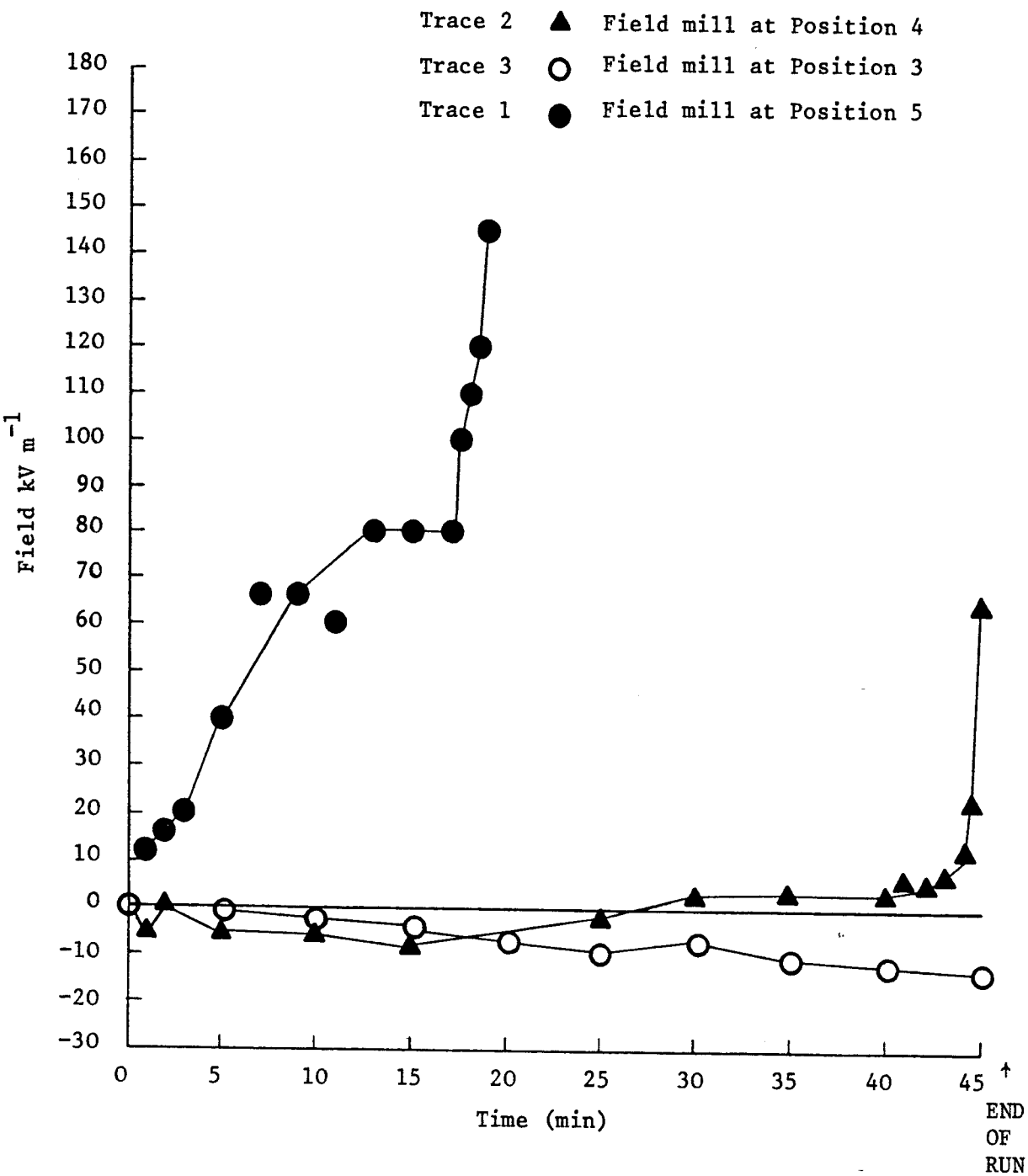

millhead. The field mill became covered with powder 19 minutes after the start of the run. The rapid rise in the magnitude of the electric field 16 to 19 minutes into the run was due to the proximity of the surface of the powder cone to the field mill.

Trace 2 (field mill at position 4) shows an initial negative swing and after 27 minutes a positive electric field which rapidly increases at the end of the run when the powder cone surface comes very close to the millhead. The initial negative electric field is due to the negatively charged fine dust cloud. After 15 minutes, the level of the positively charged bulked powder is sufficiently high in the silo to influence the electric field measurements. At 27 minutes from the start of the run the magnitude of the negative dust cloud is equal to the magnitude of the positive bulked powder and therefore the electric field reading is zero.

The electric field measurements at position 3 (trace 3) is negative throughout the run. The electric field strength at this position is largely due to the negatively charged dust cloud [Cartwright et al (1983)].

The normal component of the electric field detected at each mill has components from several sources.

$$E_{total} = E_f + E_d + E_{cl} + E_{cn} \qquad (4.12)$$

For a field mill at position 3 the normal component of the field due to settled bulk powder cone, E_{cn}, is small because E_{total} does not change when the test silo is emptied. The normal component of the field due to the powder column during filling, E_{cl}, can be calculated approximately given the silo current measurements and the powder transport velocity. The charge per unit length on the powder column entering the silo is thus given by $\frac{I_{silo}}{v}$. With a typical current value of 2 μA and a calculated filling velocity of 32 m s^{-1}, this gives $\frac{Q}{L}$ = 62.5 nC m^{-1}. Assuming the powder column as a long, thin cylinder, the field at the silo wall is given by Gauss's theorem:

$$E_{cl} = \frac{Q}{2\pi \epsilon_o R L} \qquad (4.13)$$

which gives $E_{cl} \approx 0.5$ kV m^{-1}. R is the radius of the test silo.

The dust cloud in the silo, acting as a dielectric, would reduce the E_{cl} value by up to a factor of 2.3. It can therefore be concluded that E_{cl} is generally small and equation (4.12) is reduced to

$$E_{total} = E_f + E_d \qquad (4.14)$$

E_f and E_d are the normal components of the electric fields due to airborne fines and powder deposits in proximity to the millhead respectively. The contribution of E_d to E_{total} can be estimated by periodically switching off the powder flow and monitoring the field meter reading after a short time.

For mill locations near the powder heap, equation (4.12) should be considered.

4.3.2 Electric Field Observations at Silo Wall for Maize Starch

The intensity of electric field of maize starch dust cloud was recorded simultaneously at three of the portholes in the silo wall. A series of baffles was placed inside the conveying pipe immediately before the entrance to the silo to increase the powder specific charge density.

Variation of the electric field strength at the individual measurement locations in the course of the filling is illustrated in Figure 4.10. The numbers on the graphs in Figure 4.10 correspond to the positions of the field mills in Figure 4.8. The bulk powder level rose above field mill number 3, 50 minutes after the start of the filling process. Field mills 1 and 2 never became covered with the powder.

From one evaluation of the field strength measurements it may be deduced that in the test silo without inserts, the maximum electric field due to the charged dust cloud occurred at about

Figure 4.10 Variation of Electric Field Strength with Time

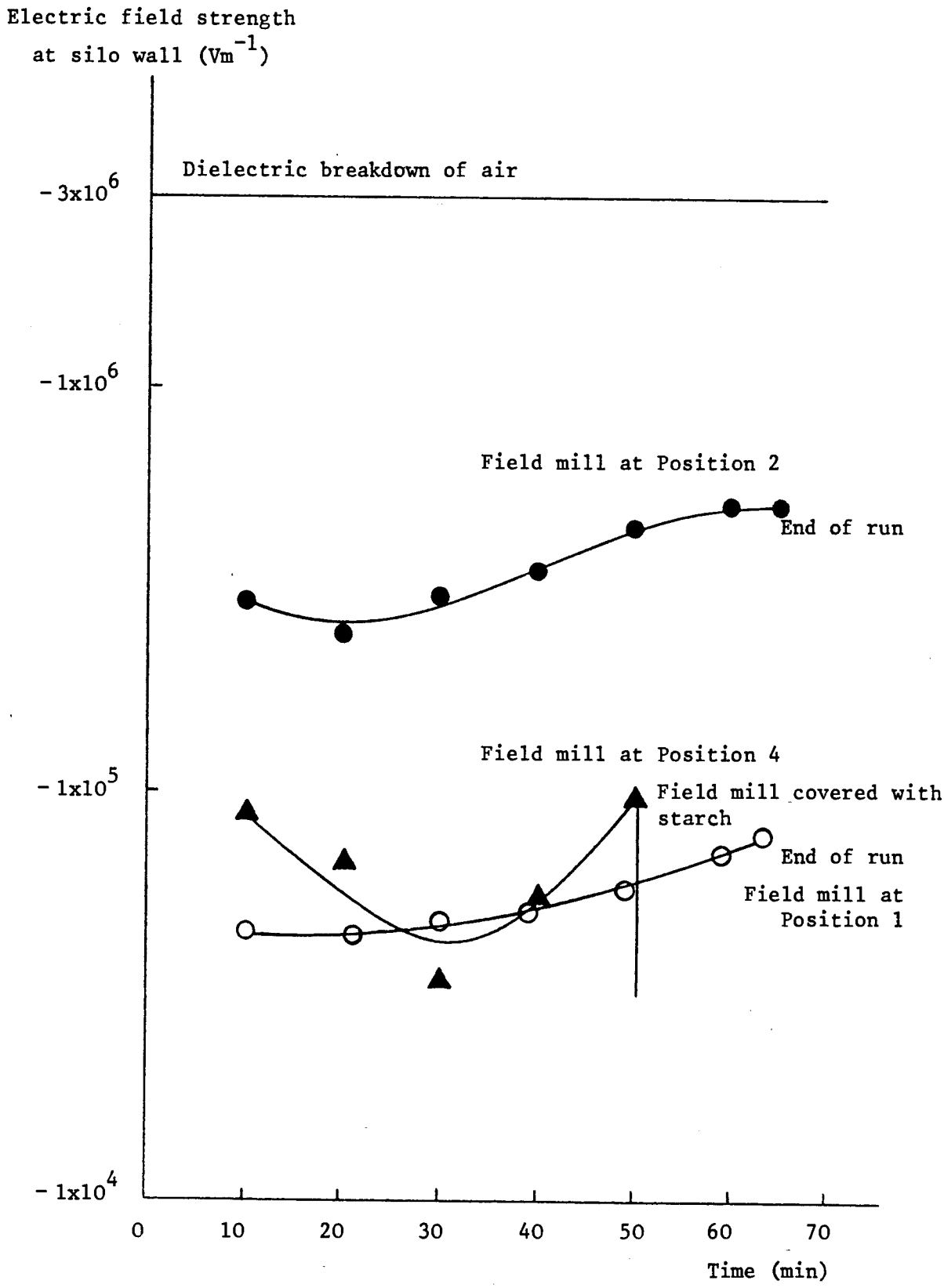

1.5 metres from the top of the silo. High electric fields were produced at the beginning or end of the filling process.

During this experiment, the powder flow rate and silo current were 2.9 kg s^{-1} and about -10 μA respectively. The relative humidity of the conveying air was ≈ 88%.

4.3.3 Space Potential Measurements for HDPE Powder

The potential in the gas space above the powder heap was measured using a field mill. Figure 4.11.a shows the readings obtained at grid points along a radial plane in the test silo. Figure 4.11.a also shows the equipotential lines which are sketched at 100V intervals, assuming rotational field symmetry about the silo axis.

As shown in Figure 4.11.a, the field lines start from the edges of the powder cone and move towards the centre of the silo and upwards to the relatively clean explosion vents and perhaps to the centre of the powder cone [Cartwright et al (1982)]. Field lines cross equipotential lines at right angles.

Figures 4.11.b and 4.11.c show the potential measurements taken 70 minutes and 17 hours after the end of the same run respectively. Changes both in the magnitude and the shape of the equipotentials is apparent, which may suggest that more field lines originating at the edge of the powder cone terminate at the powder cone centre.

The field line distribution obtained when the test silo was empty is shown in Figure 4.11.d. About halfway up the silo the space potential was zero. The shape of the equipotentials indicates that the powder deposits on the lower part ofthe silo wall was positively charged while the deposits near the silo top were charged negatively. The magnitude of the space potentials in Figure 4.11.d are higher than for Figure 4.11.c, which could be due to the effect of the negatively charged fines which were disturbed by the emptying process.

Figure 4.11 Space Potential of HDPE Powder
(Cartwright et al (1982))

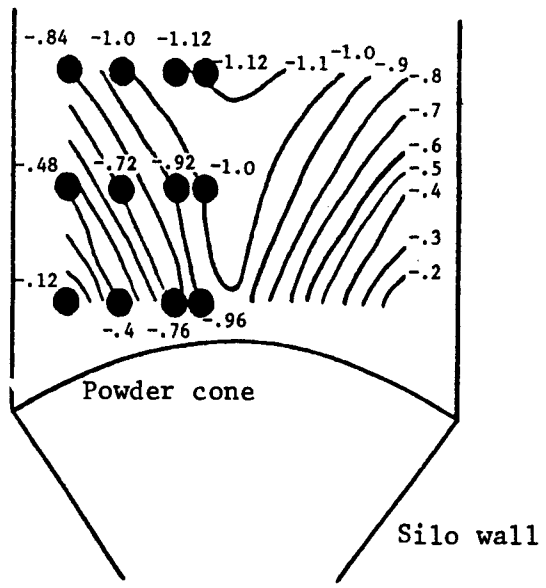

a) Reading taken 10 minutes after end of run. Equipotential lines at 0.1 kV Division

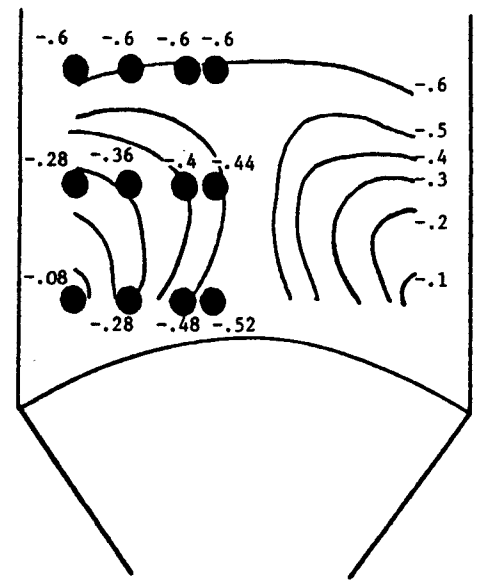

b) Readings taken 70 minutes after end of run. Equipotential lines at 0.1 kV Divisions

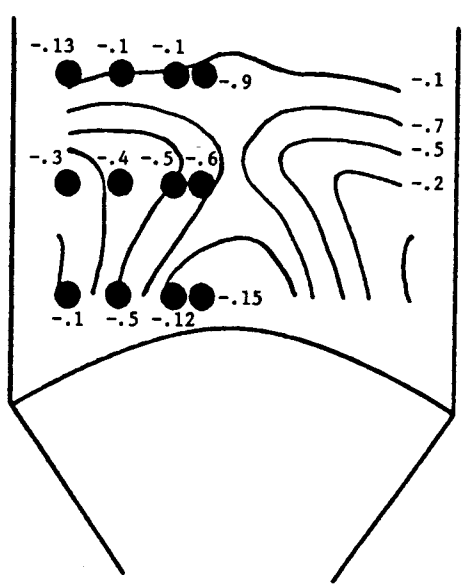

c) Reading taken 17 hours after run. Equipotential lines at 0.025 kV intervals

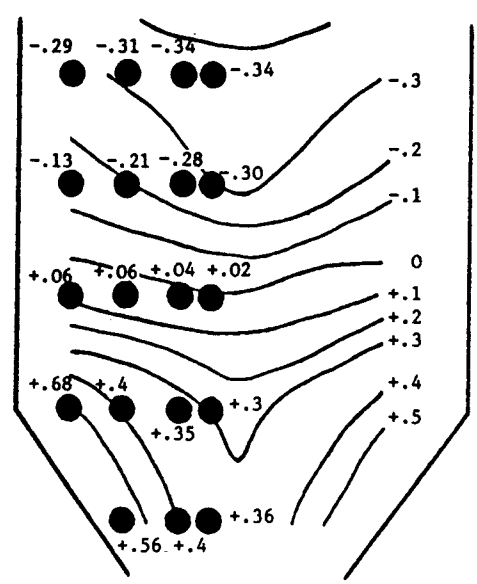

d) Silo empty. Equipotential lines at 100 V intervals

Space potential measurements could not be taken near to the silo wall or the powder cone due to their effect on the field lines by introducing the mill.

4.3.4 Potential Measurements for Maize Starch

Figure 4.12 illustrates the space potential of the charged cloud of maize starch powder. The measurements were taken at grid points along a radial plane in the silo. A series of baffles were placed inside the conveying pipe to enhance the powder tribo-charging. The measurements were carried out for two currents of -12 μA and -35 μA.

As can be seen from comparison of Figures 4.11 and 4.12, the space potentials for maize starch are much larger than those for HDPE. This could be due to the fact that maize starch powder particles are very fine and therefore very airborne. This, together with higher electrostatic charges on the powder particles, give rise to larger space potentials.

The largest space potentials were obtained towards the centre of the silo and about 1 m to 2 m from the top of the silo.

Also shown in Figure 4.12 is the dust cloud density measurements at grid points along a radial plane in the test silo, measured simultaneously with the space potential measurements. A suction Faraday cup was used for these measurements. The largest dust cloud density was measured about 3 metres from the top of the silo and about 50 cm from the silo wall. The measured value was 143.5 g m^{-3} when the mass flow rate was 2.8 kg s^{-1}. The largest dust cloud density for the minimum mass flow rate of 0.59 kg s^{-1} was 40 g m^{-3}. This value was obtained at a point 2 m from the top of the silo and 50 cm from the wall.

The minimum explosible concentration (MEC) for maize starch is 20 g m^{-3}. The maximum explosible concentration has not been defined although a figure of 2000 g m^{-3} has been reported by CPC (UK) (1985).

Figure 4.12 Space Potentials Inside Test Silo for Maize Starch

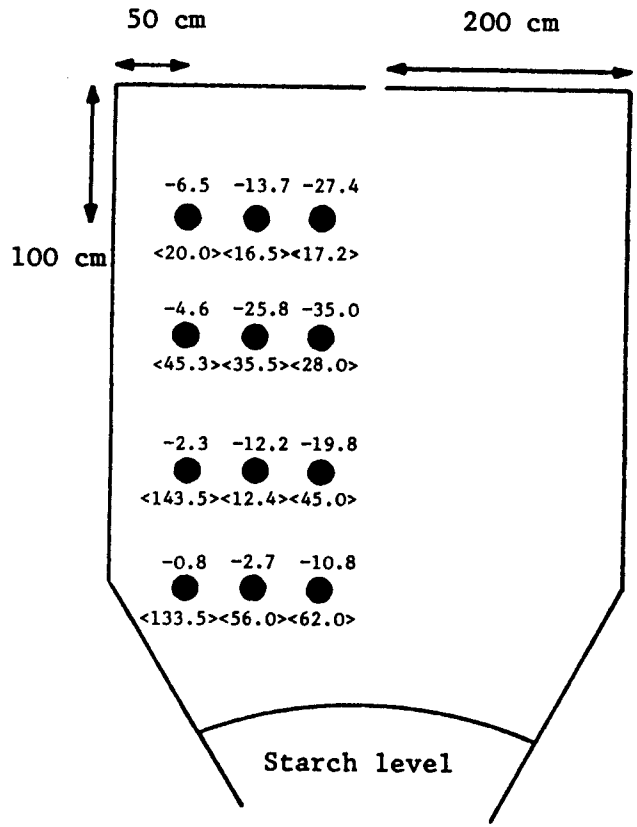

(a) RH = 35%
Silo current = -12 μA
Mass flow rate = 2.8 kg s^{-1}
Space potential (kV)
<Cloud density g m^{-3}

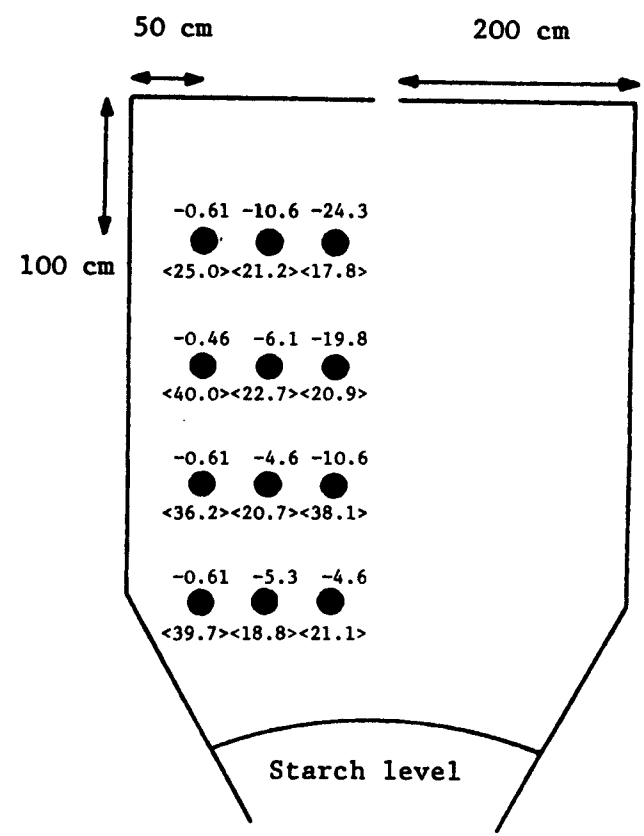

(b) RH = 31%
Silo current = -35 μA
Mass flow rate = 0.59 kg s^{-1}
Space potential (kV)
<Cloud density g m^{-3}

Surface potential measurements were also made by lowering a plate connected to an electrostatic voltmeter onto the powder surface.

With no corona charge injection the surface potentials were always less than -2 kV. With corona charge injection at the outlet of the conveying pipe surface potentials up to -15 kV were obtained. The surface potentials were not influenced by powder flow rate variations between 0.8 kg s^{-1} and 2 kg s^{-1} [Thorpe (1984)].

With the corona charge injection device positioned at the filling pipe outlet some free ions could enter the test silo. Therefore no accurate silo currents could be obtained.

4.3.5 Measurements of Electrostatic Discharges

4.3.5.1 Radio Frequency Technique

a) HDPE Powder

Figure 4.13 shows the variation of the spark count frequency as a function of time throughout four separate runs. For these tests charge injection was used and the specific charge on the powder entering the silo was controlled by variation of the mass flow rate. The figure shows that when the mean powder specific charge was about -1.2 μC kg^{-1} (this corresponds to a silo current of about -5 μA and a powder flow rate of 4.2 kg s^{-1}), only one r.f. emission was detected. When the mean specific charge on the powder was increased to -4.3 μC kg^{-1} by decreasing the mass flow rate, eight r.f. emissions were detected.

With a powder specific charge of -8 μC kg^{-1}, the spark detection rate increased to nearly 30 discharges per minute at about 25% in the run, whereas for a powder specific charge density of -17 μC kg^{-1}, up to 120 discharges per minute were detected [Cartwright et al (1983), Bailey (1987)].

Discharges were also sometimes detected during emptying the test silo. These discharges coincided with sudden slipping of powder from the silo wall. Discharges sometimes coincided with the

Figure 4.13 Radio Signal Count Rate and Frequency for Various Mass Flow Rates During the Testing of HDPE Fines. (Bailey (1987))

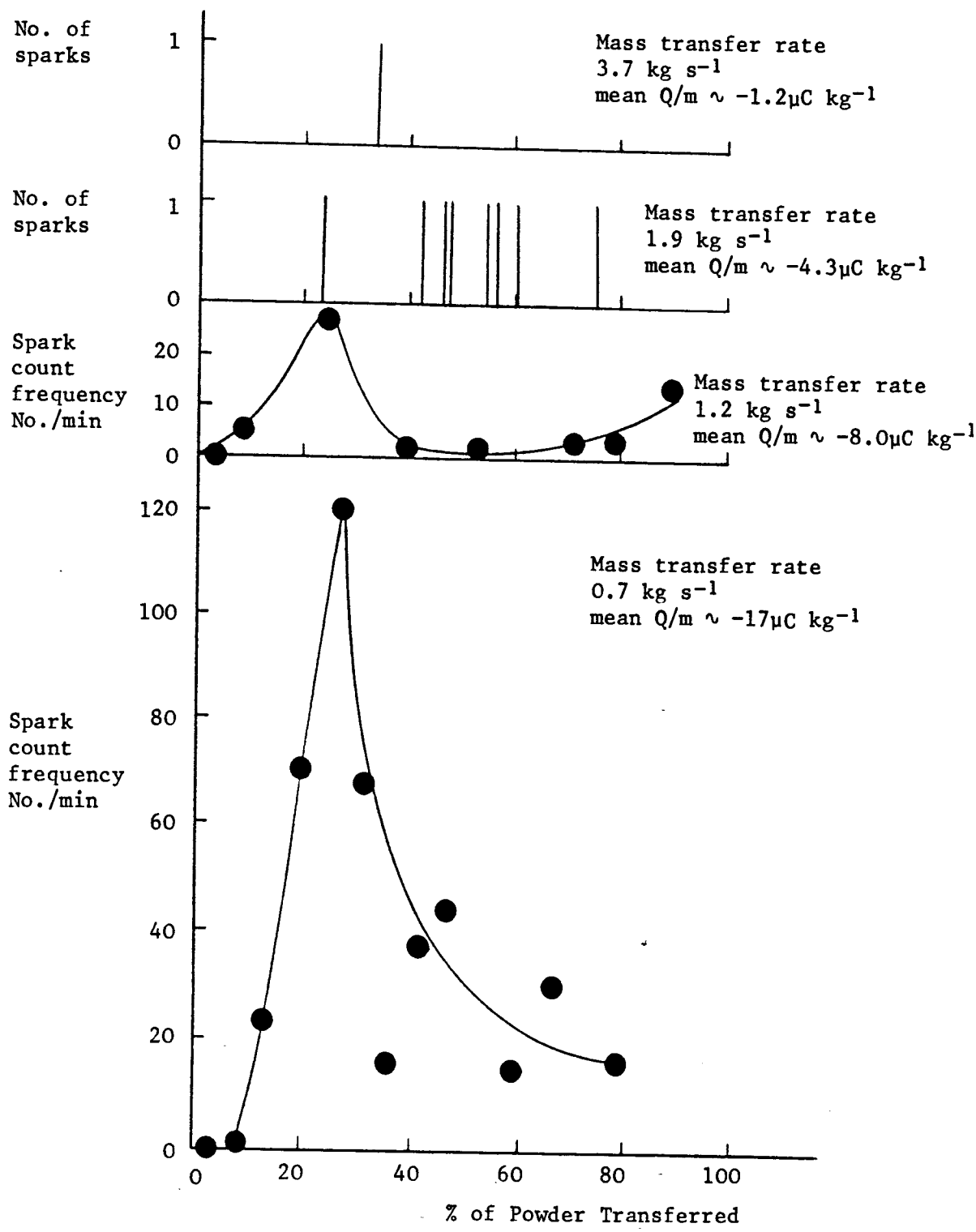

clearing of small blockages which occasionally occurred during test silo emptying.

It is not possible to separate r.f. emissions as originating from the heap of the bulked powder or the charged dust cloud. It is probable that some or all of the discharges were in or from the dust cloud.

b) Maize Starch Powder

The average rate of detection of discharges during loading the test silo with maize starch as a function of powder mass flow rate is shown in Figure 4.14. The frequency of spark detection increases as the mass flow rate is increased. Figure 4.15 illustrates the dependence of silo current on mass flow rate during r.f. measurements. Comparison of Figure 4.14 with Figure 4.15 clearly shows that frequency of discharge detection increases as the rate of input of charge into the test silo decreases.

The r.f. detection method provides a high sensitivity detection to low energy discharges, combined with a low sensitivity to corona discharges. It may be possible that, at high silo currents, the charge is dissipated in the form of corona discharges whereas at low silo currents higher energy discharges may be produced. Thorpe (1984) reported no clear increase in frequency of spark detection when charge injection was used to increase the silo current. It ranged from 20 per minute to approximately 100 per minute.

4.3.5.2 Probes Lowered to the Surface of HDPE Powder

The experimental work on the incendivity and the magnitude of the charge transfers to the gas emitting probe and spherical probe from the surface of the bulked powder has mainly been divided into three sections:

i) Charge transfers to probes suspended in the powder dust cloud for various powder charge densities and also at different stages during the silo loading.

Figure 4.15 Silo Current as Mass Flow Rate was Varied

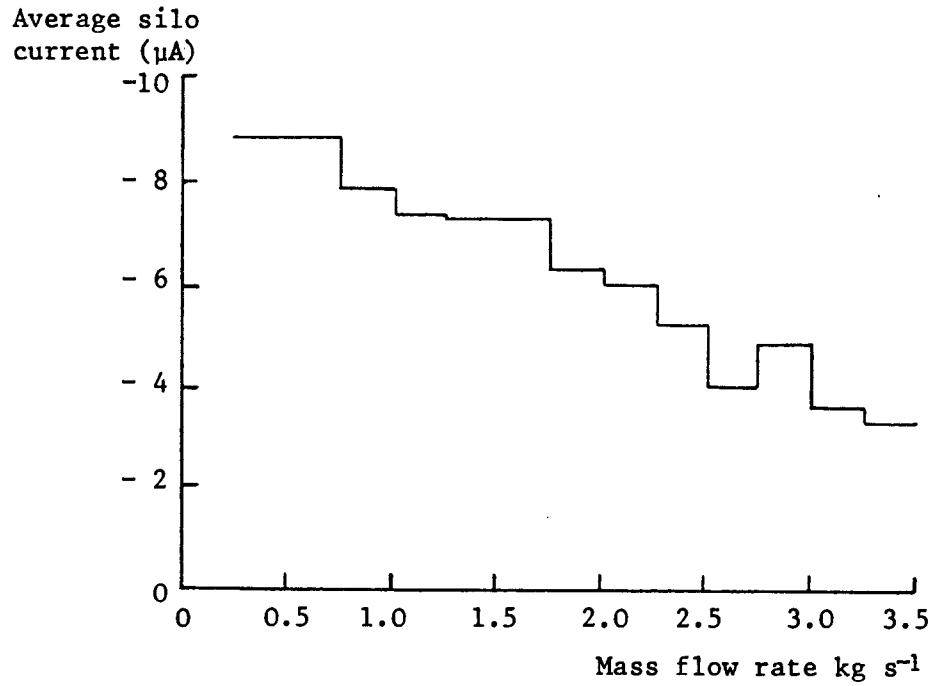

Figure 4.14 Rate of r.f. Detection of Sparks as Mass Flow Rate was Varied (Thorpe (1984))

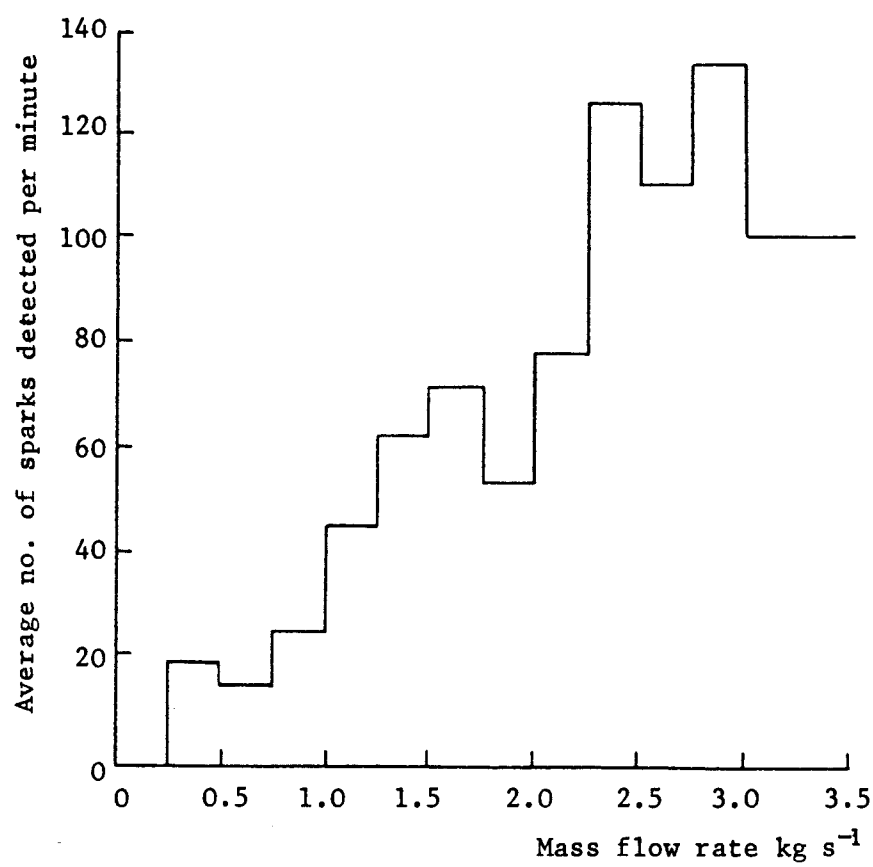

ii) Charge transfers to probes from the surface of the HDPE heap at high transport air relative humidities.

iii) Charge transfers to probes from the surface of a depression made in the bulked powder inside the test silo.

Spherical probes connected to earth through the electric circuit shown in Figure 2.5 were suspended in the powder dust cloud to draw discharges at various locations. The probes were also located near to the powder filling column. The largest discharges were however obtained when the probes were located a few centimetres above the surface of the powder heap. The frequency of discharges would drop greatly if the probes were lifted above about one metre from the heap surface.

Figure 4.16 shows a plot of electrostatic discharges to both the gas emitting probe and spherical probe as a function of percentage of powder transported into the test silo. Some of the tests were carried out using the corona charge injector within the conveying pipe upstream of the test silo. With the corona charge injection positioned so close to the silo, some free ions could enter the silo; as a result accurate measurements of silo current and hence the specific charge of the transported powder were not possible. Maximum specific charge density was however obtained when the mass flow rate of the powder was at a minimum. Data with corona charge injector positioned before bend 4 (see Figure 2.1) is also included. At this position no free ions could enter the test silo. The maximum charge transfer of about 96 nC was obtained with a minimum mass flow rate when about 80% of the run had been completed. No discharges were obtained below about 30 per cent of the total powder transferred into the test silo.

The data shown in Figure 4.16 were supplemented with data from other charge transfer experiments to produce Figure 4.17. As can be seen the charge transfer to both the gas emitting probe and the spherical probe are plotted as a function of the HDPE specific charge density. Again a number of tests were carried out with the

Figure 4.16 Charge Transfers to Spherical Probe

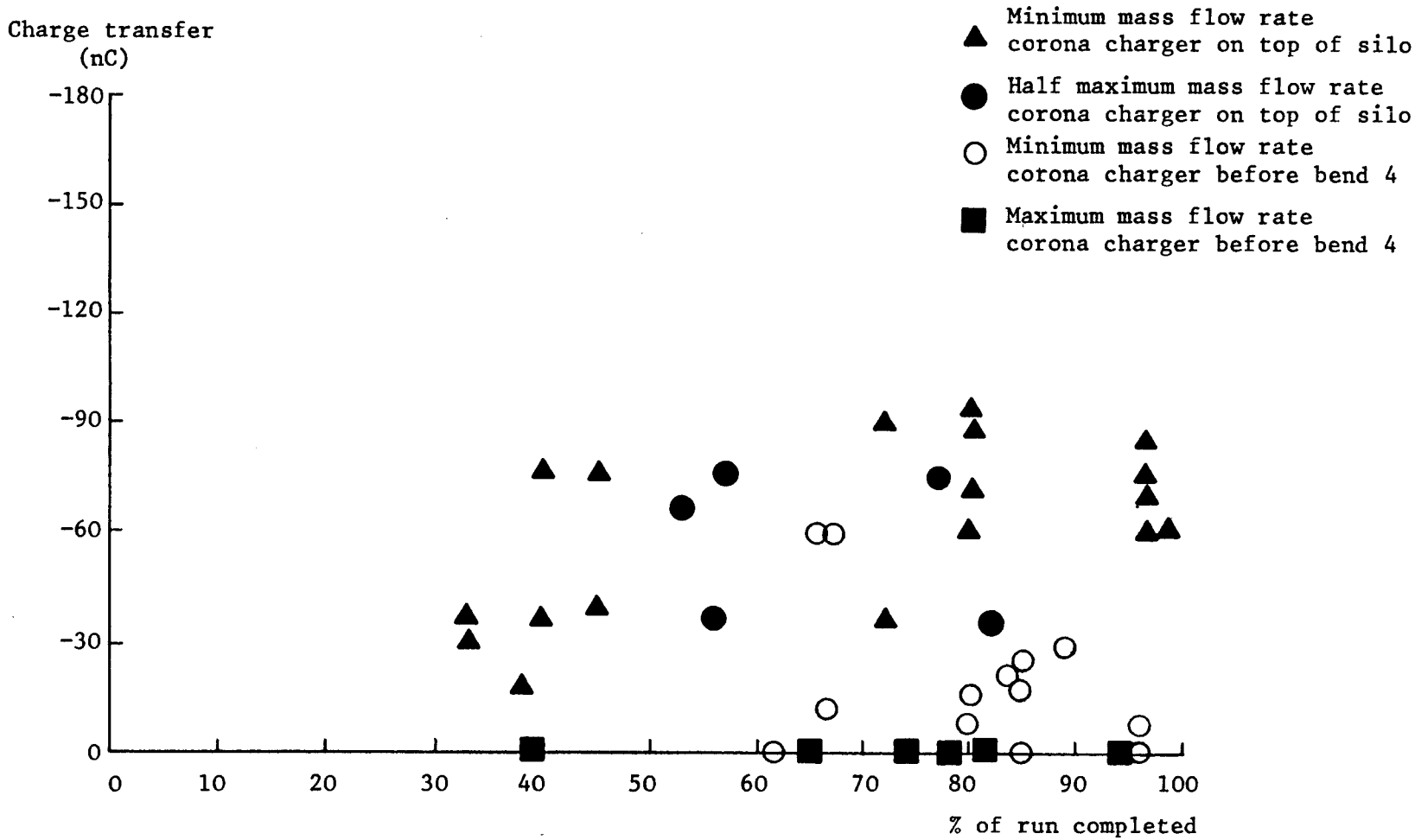

Figure 4.17 Size of Charge Transfers to Both Gas Probe and Spherical Probe Plotted Against Charge per Unit Mass of the Powder

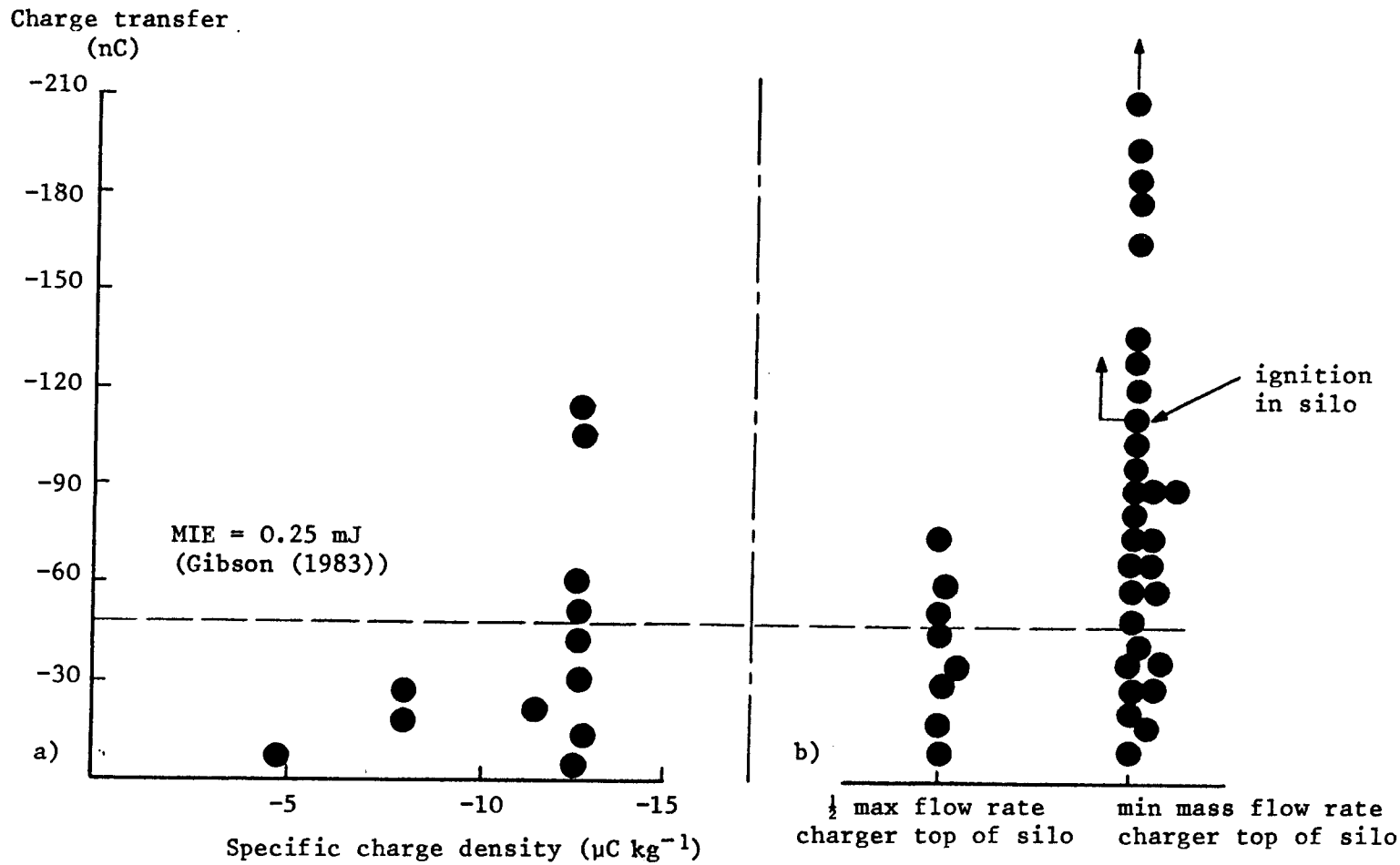

corona charge injector very close to the test silo and therefore the specific charge of powder could not be measured. The charge transfer to the probes increased as the specific charge of powder transported into the silo increased [Bailey (1987)]. At specific charge densities of below -5 $\mu C\ kg^{-1}$ no discharges to the probes were observed. Discharges greater than -230 nC were detected with a minimum powder flow rate and the corona charge injection in use.

During one run with the mass flow rate at a minimum and the corona charge injector connected very close to the silo, a propane/air ignition occurred when the probe was lowered to the surface of the powder heap. A large discharge in excess of -120 nC was detected to the gas emitting probe. The equivalent electrical energy of this discharge was greater than 0.25 mJ. The dust cloud in the test silo failed to ignite [Cartwright et al (1982-1983)]. Immediately after the probe ignition, as a safety precaution, the propane supply was shut off and the powder transfer stopped. The gas emitting probe was then raised from the silo and the plastic shroud was observed to be partially melted and charred.

The spherical and gas emitting probes were also lowered towards the bulked powder in the test silo at high transport air relative humidities. Figure 4.18 shows a plot of discharges to the probes as a function of the specific charge of powder entering the test silo. The specific charges of -3.1 $\mu C\ kg^{-1}$ and -4.7 $\mu C\ kg^{-1}$ were obtained using the corona charge injection device. These tests were carried out with the charge injection located in the pipework 50 cm from the silo inlet. All free ions were lost to the earthed pipe walls under these circumstances and so only charged powder entered the silo.

As the probe approached the surface of the bulked powder, a series of multiple discharges were followed by a very large charge transfer ($\approx > -650$ nC) to the probe. This coincided with a decrease in the silo current (see Figure 4.19). Although the magnitude of the charge transfers to the gas emitting probe were very high, they failed to ignite a propane/air mixture with an equivalent electrical

Figure 4.18 Discharges to the Gas Emitting Probe and Spherical Probe as a Function of Silo Specific Charge

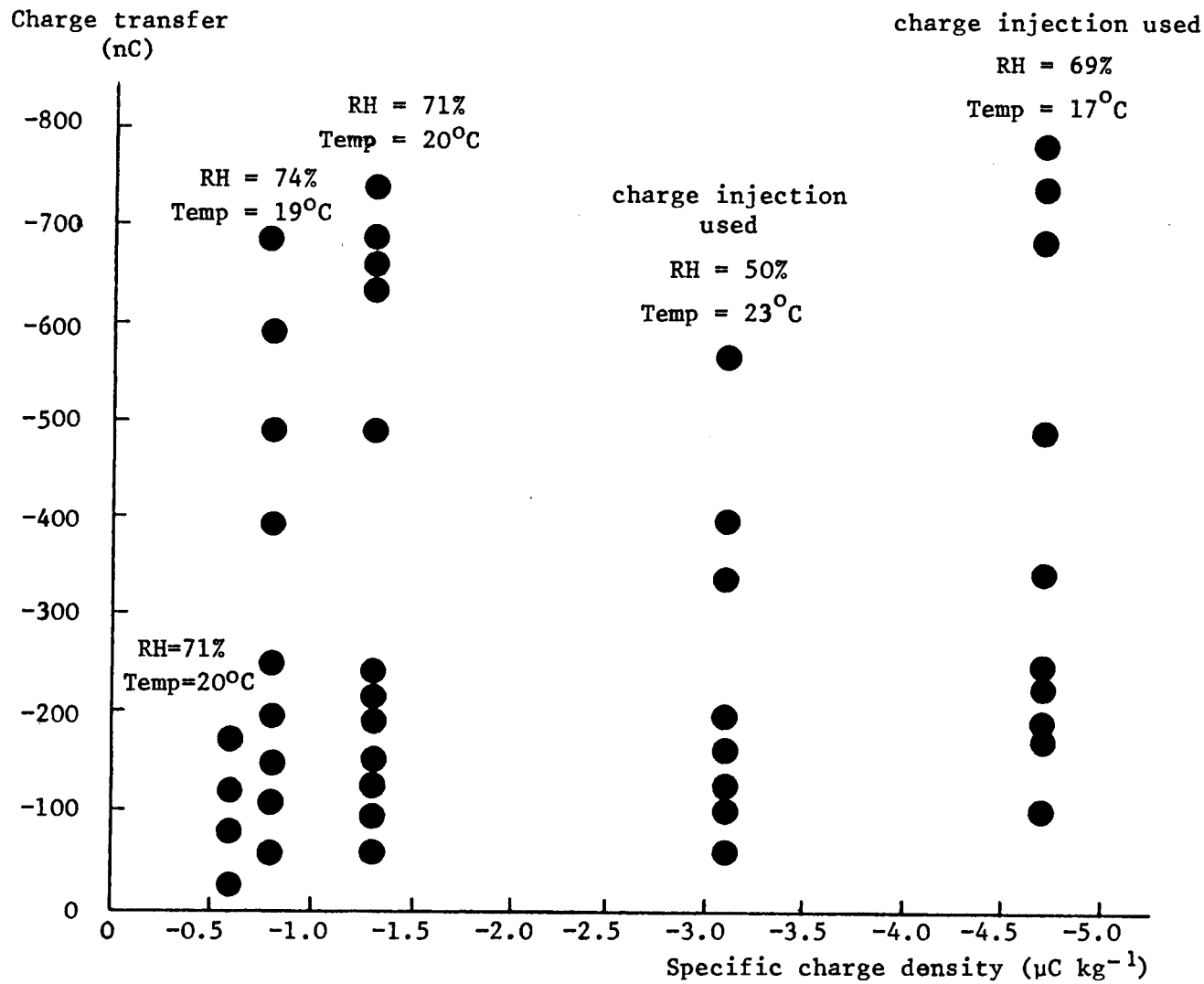

Figure 4.19 Silo Current Monitor During Probe Insertion at High Transport Air Relative Humidities

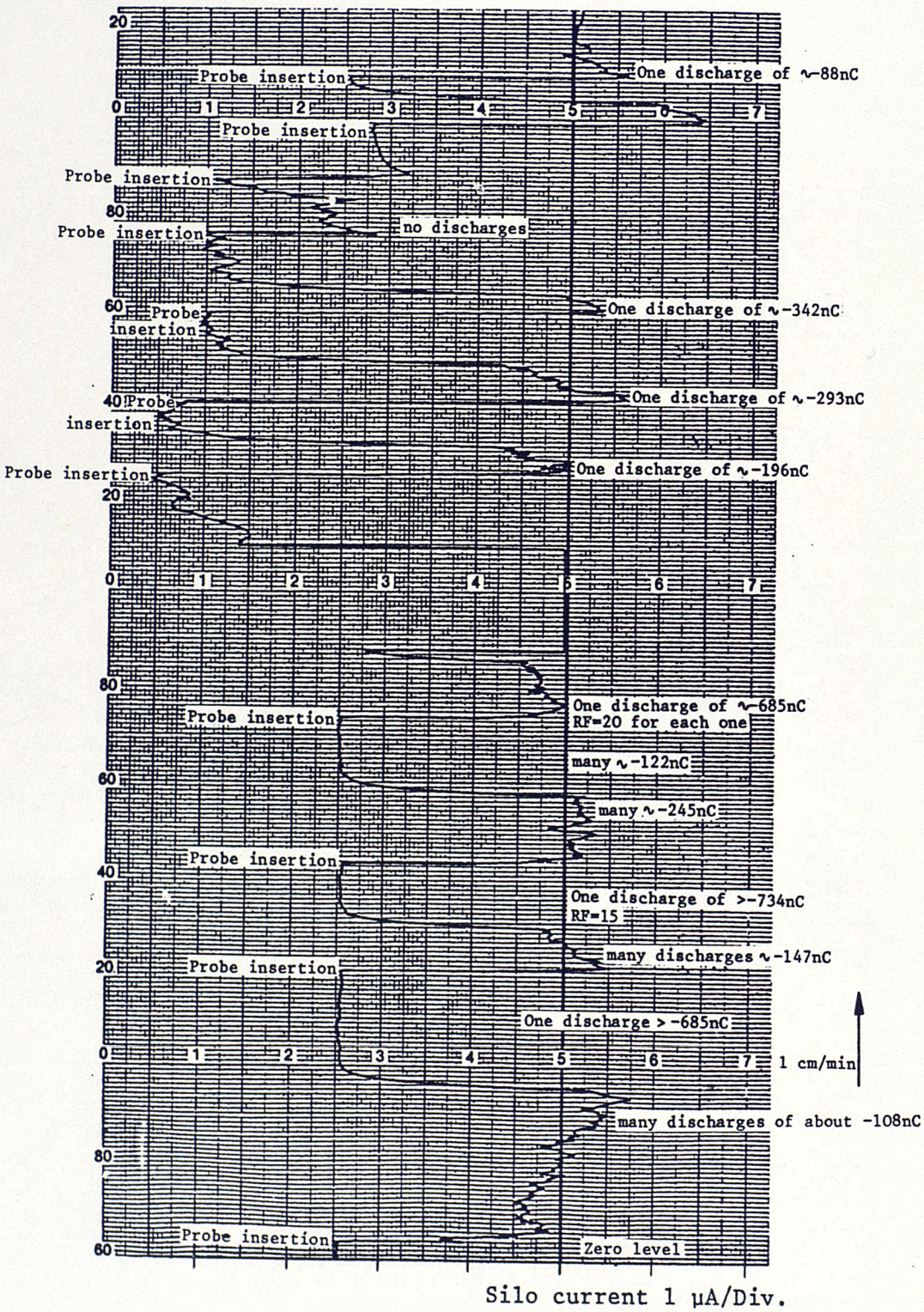

energy of 0.25 mJ. Gibson et al (1965) found that brush discharges from charged insulator surfaces to a grounded metal sphere, transferring 130 nC of charge, can ignite inflammable vapours with a minimum ignition energy of 0.25 mJ with an ignition probability of about 50%. More recent results indicate an ignition threshold of 20-50 nC [Gibson (1983)].

The decrease of the silo current to zero when the probes touch the surface of the bulked powder (Figure 4.19) indicated that the silo current is dissipated as low energy electrostatic discharges and is conducted to earth through the probe when it is touching the surface of bulked powder. These discharges are produced as a result of the bulking effect of the highly charged powder.

Volume resistivity and charge decay measurements for HDPE powder showed no dependence on the ambient relative humidity even for RH values as high as about 80%.

In practice during partial emptying of silos, sometimes powder flow occurs within a channel surrounded by non-flowing (dead) material, thus creating a depression. In order to investigate the magnitude and incendivity of electrostatic discharges to probes when such a depression is filled with charged powder, a depression was created in the bulked powder inside the test silo by partially transferring back some of the powder into the storage silo. The depression was then filled with charged HDPE powder. Discharges to either the gas emitting probe or the spherical probe from the depression during filling were monitored. The charge transfers to probes under these circumstances are compared with the charge transfers to the probes when the silo was being filled under normal operating conditions (no depression) in Table 4.4.

The largest charge transfers were obtained seconds after the filling started, while the smaller charge transfers were obtained towards the time when the depression was nearly full.

Table 4.4 Charge Transfers to Probes

	Mass flow kg s^{-1}	Specific charge μC kg^{-1}	No. probe insertions	Average charge transfer nC
Depression	2.9	-4.4	18	-88.5 ± 42.9
No Depression	2.9	-4.6	19	-48.2 ± 29.3

Comparison of the results indicate that the charge transfers from the surface of a depression made in the bulked powder are larger than the charge transfers from the surface of powder cone to the probes. There is however no evidence that the ignition risk increases if such a depression is filled with charged powder.

4.3.5.3 Discharges to Probes from the Maize Starch Dust Cloud

Having found out the points where the space potential was the highest for both minimum and maximum flow rates (refer to section 4.3.4), the spherical and gas emitting probes were lowered to these points. For only one insertion, the number of discharges to the probe were more than 1000 with a magnitude of about 100 nC, as indicated in Table 4.5.

Table 4.5 Charge Transfers to Probes

Mass flow rate (kg s^{-1})		0.6	2.8
Silo current (μA)		-40	-12
Specific charge density (μC kg^{-1})		-66.7	-4.3
Spherical probe	No. of probe insertions	1	1
	No. of discharges	>1000	>1000
	Max. charge transfer for each discharge (nC)	≈ -100	≈ -100
Gas Emitting Probe	No. of probe insertions	-	1
	No. of discharges	-	> 50
	Max. charge transfer for each discharge (nC)	-	≈ -50

The gas emitting probe was only inserted at a mass flow rate of 2.8 kg s^{-1} in order to have a higher space potential and also a higher dust cloud density.

No discharges were obtained when the probes were lowered down to the surface of the maize starch heap.

Among all the powders tested at the Marchwood silo, only discharges from the dust cloud of maize starch ignited the propane/air mixture. The equivalent electrical energy of this discharge was equal or greater than 0.25 mJ. At the time of propane/air ignition, the gas emitting probe was suspended 0.8 m from the silo central axis and about 2 m from the top. A charge transfer of about -220 nC was observed to the gas emitting probe [Thorpe (1984)]. The powder feed rate was 0.9 kg s^{-1} and the transport air relative humidity and temperature were 26% and 27°C respectively. Ignition of the propane/air mixture occurred only once, despite many attempts. There was no dust explosion.

During this experiment the corona charge injection device was positioned on top of the test silo to enhance the charging levels.

4.4 Experimental Results from the Laboratory Scale Powder Handling Rig

The operation of the rig used in this part of the project was described in section 2.6. The aim of these experiments is to study electrostatic activity of HDPE during bulking. HDPE pellets and fine HDPE powder are tested. An attempt is made to compare the behaviour of electrostatic discharges to spherical metal probes of different sizes from the surface of bulked HDPE pellets and HDPE fine powder. Because of safety reasons and in order to prevent any dust explosion in the laboratory, only HDPE pellets are used to study the incendivity of electrostatic discharges. The average diameter of pellets is 3.4 x 10^{-3}m and each have a mass of 1.9 x 10^{-5} kg. The solid density and bulk density of the HDPE pellets are 950 kg m^{-3} and 599.2 kg m^{-3} respectively. Since no energetic collisions occur during the gravitational feed of HDPE, a corona

charge injector device is used to vary the streaming current and hence the specific charge density of the pellets entering the bottom hopper. The position of the corona injector in the pipe is such that no free ions can enter the bottom hopper.

Figure 4.20 shows the variation of streaming current (charge on the HDPE pellets entering the bottom hopper per unit time) as a function of mass flow rate. There was an increase in the current as the mass flow rate increased. The maximum current obtained was -3.6 μA for a mass flow rate of 0.15 kg s^{-1} when the corona injector needles were at -20 kV. Further increases in the corona injector potential did not result in larger currents. This value is ten times smaller than the maximum theoretical current obtained by using equation (3.12) for an average pellet velocity of 4.3 m s^{-1} and a pipe radius of 5 cm.

The variation of the specific charge density of pellets as a function of mass flow rate is illustrated in Figure 4.21. The specific charge densities did not change with powder flow rates between 0.03 kg s^{-1} and 0.15 kg s^{-1}. The largest specific charge density was obtained with the corona charge injector at a potential of -20 kV.

The igniting power of electrostatic discharges were measured directly by passing discharges from the surface of bulked HDPE pellets through flammable propane/air atmospheres of different sensitivities. The minimum ignition energy of the propane/air mixture was increased by partially inerting it with nitrogen (see section 2.6.5). Each test (every point on the graphs) was repeated 50 times and the probability of ignition was measured. For example, if 10 out of 50 probe insertions ignited the propane/air/nitrogen mixture, then the probability of ignition for that particular gas mixture was 20%.

The dependence of the probability of ignition on the streaming current, specific charge density and the pellets flow rate was examined. Three spherical brass electrodes with diameters

Figure 4.20 Current as a Function of Mass Flow Rate

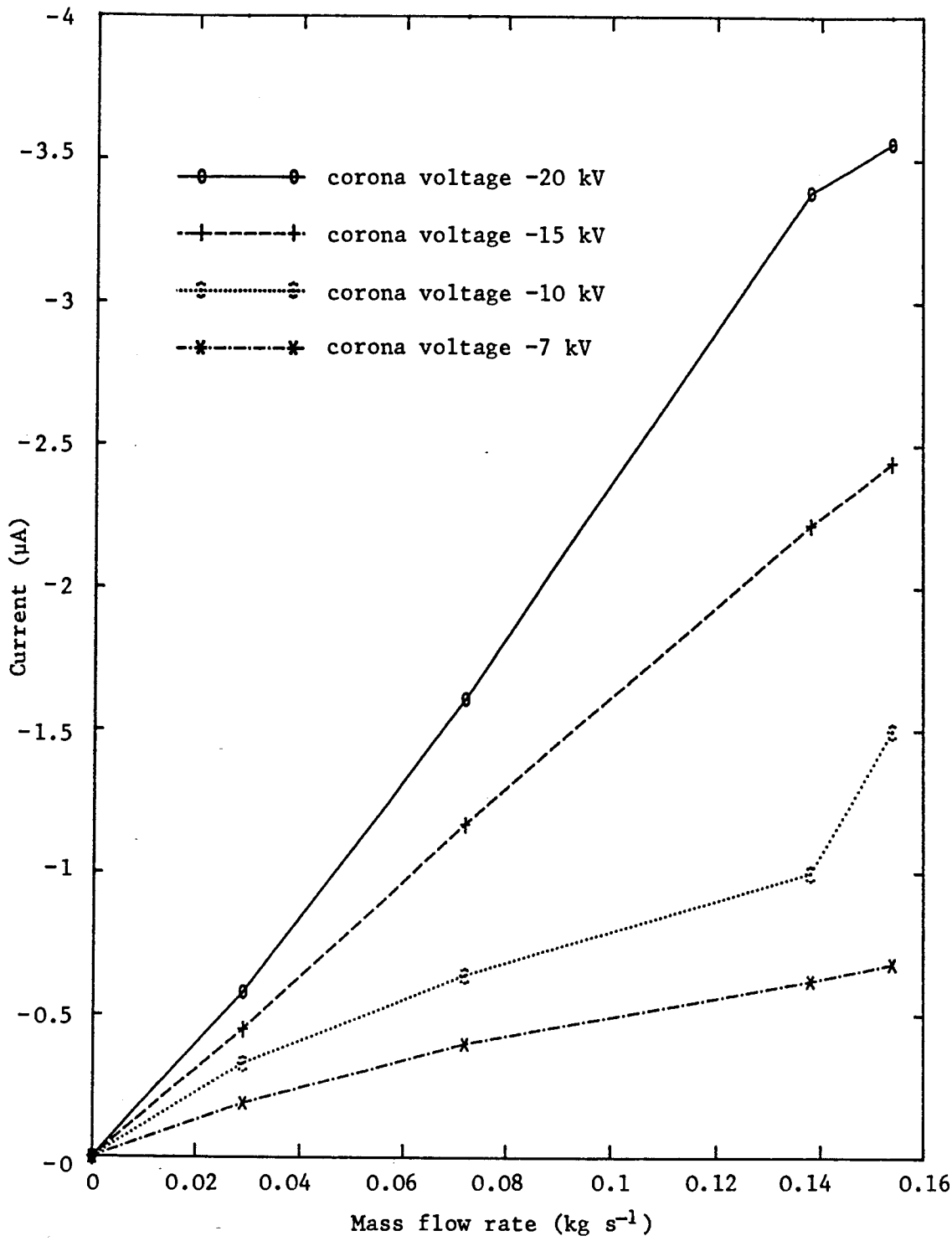

Figure 4.21 Specific Charge Density as a Function of Mass Flow Rate

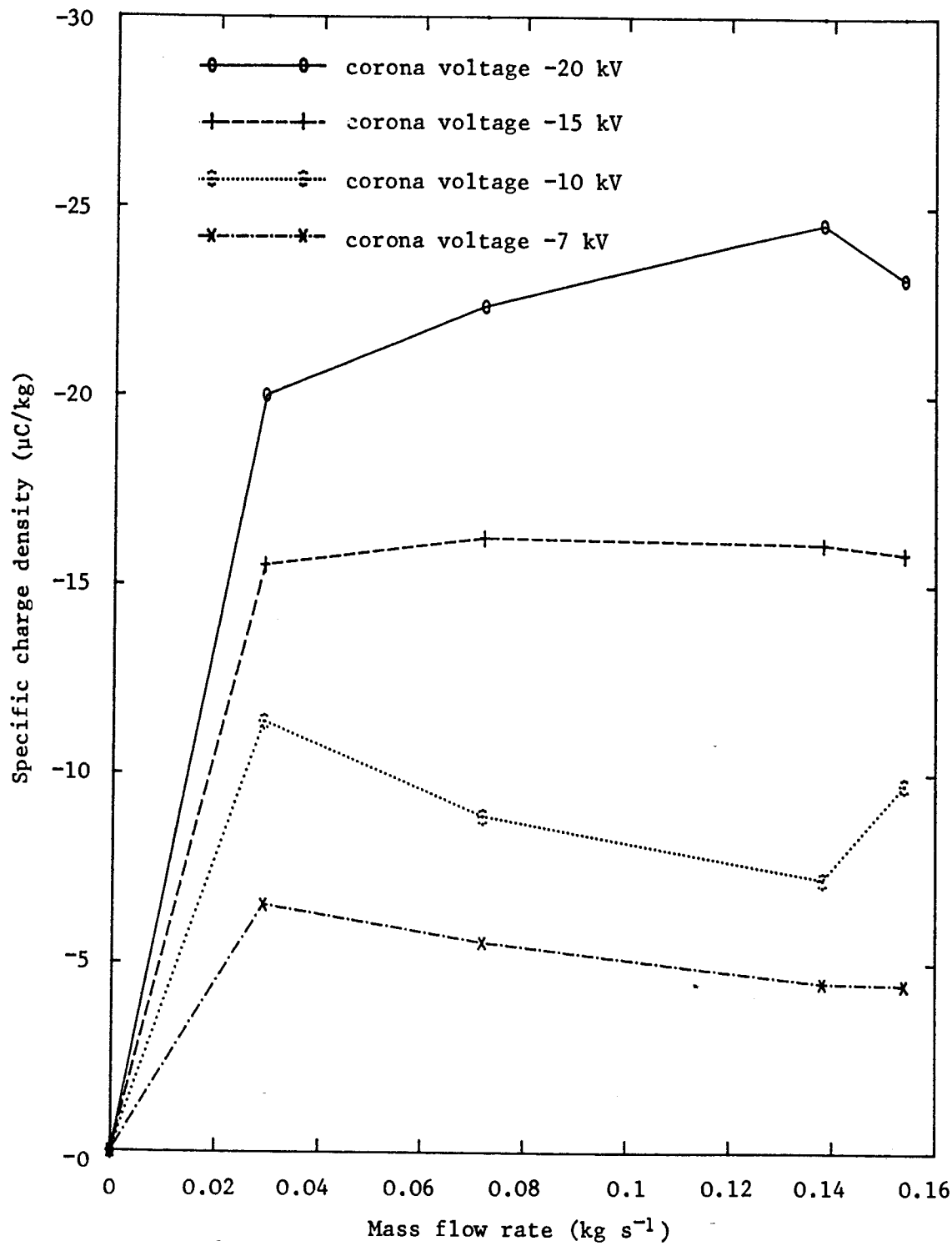

of 28.6 mm, 22.2 mm and 12.7 mm were used in the gas emitting probe for these experiments. Propane/air/nitrogen mixtures with minimum ignition energies between 1.0 mJ and 4.4 mJ allowed an exact determination of the equivalent energy of electrostatic discharges from the surface of bulked HDPE pellets to the gas emitting probe.

The ambient relative humidity and temperature during these experiments were below 35% and 27°C respectively.

4.4.1 Discharges to Probes from Surface of HDPE Pellets

When a discharge is initiated by lowering an earthed electrode towards the surface of a charged bulked powder, the potential across the gap between the electrode and charged surface drops sharply and a current rises. The total charge transferred in a discharge can be obtained by measuring the area of the current/time trace. A reasonable approximation to the discharge energy can also be obtained by multiplying the area of the current trace by the voltage across the discharge gap at the point of breakdown.

Figure 4.22 illustrates transient digitiser traces of some typical current transients. These were obtained using three electrodes of diameter 12.7 mm, 22.2 mm and 28.6 mm. The pellets flow rate and streaming current were varied to obtain a range of specific charge densities betwen zero and about -23 $\mu C\ kg^{-1}$. Each test was repeated three times. For most of the discharges the total duration of the current flow was about 350 nano seconds with a rise time of about 50 nano seconds. With a few exceptions the discharges to the electrode with a diameter of 12.7 mm were the smallest in magnitude. The largest discharges occurred with pellets charge densities of less than -15.9 $\mu C\ kg^{-1}$ and an electrode of diameter 22.2 mm.

Close observation of the brush discharges caused by the approach of a spherical electrode towards the charged surface of bulked powder showed that the discharges have several foot-points with a tendency of a stem close to the surface of the sphere.

Figure 4.22 Traces of some Typical Current Transients

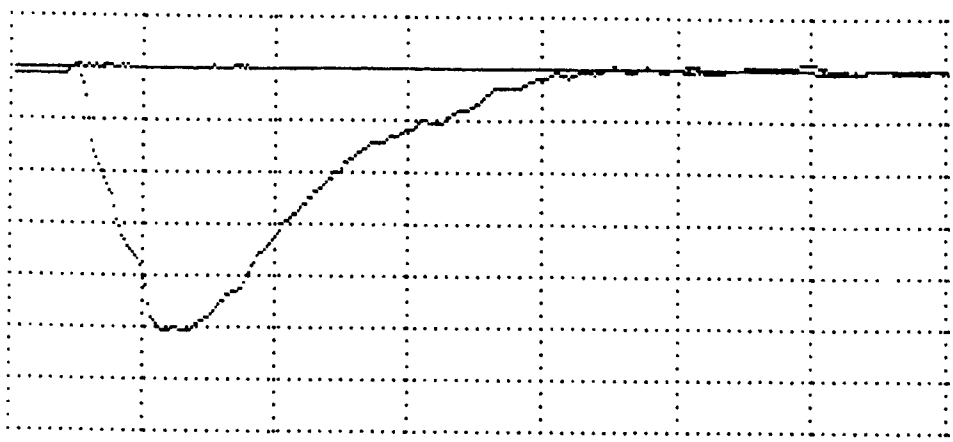

a)

Vertical	0.4 A/Division
Horizontal	100 nano seconds/Division
Streaming current	-0.62 μA
Specific charge	-5.3 μC kg^{-1}
Probe diameter	22.2 mm

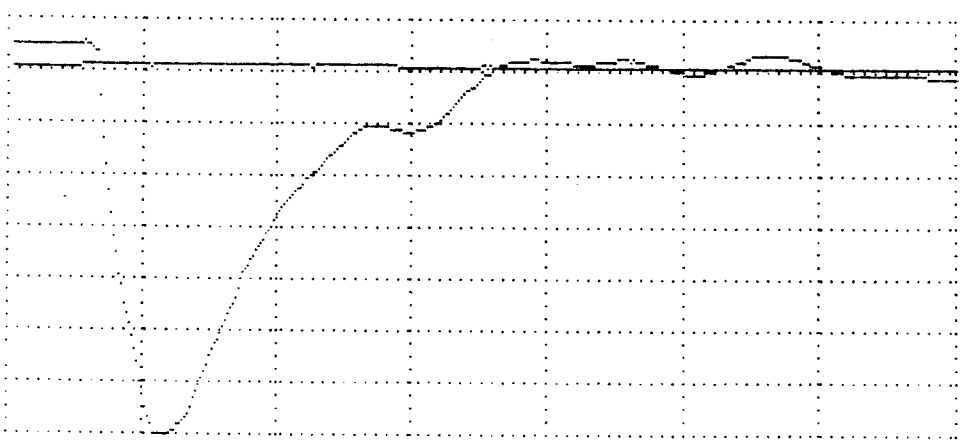

b)

Vertical	0.4 A/Division
Horizontal	100 nano seconds/Division
Streaming current	-1.17 μA
Specific charge	-15.9 μC kg^{-1}
Probe diameter	22.2 mm

Figure 4.22 (contd) Traces of some Typical Current Transients

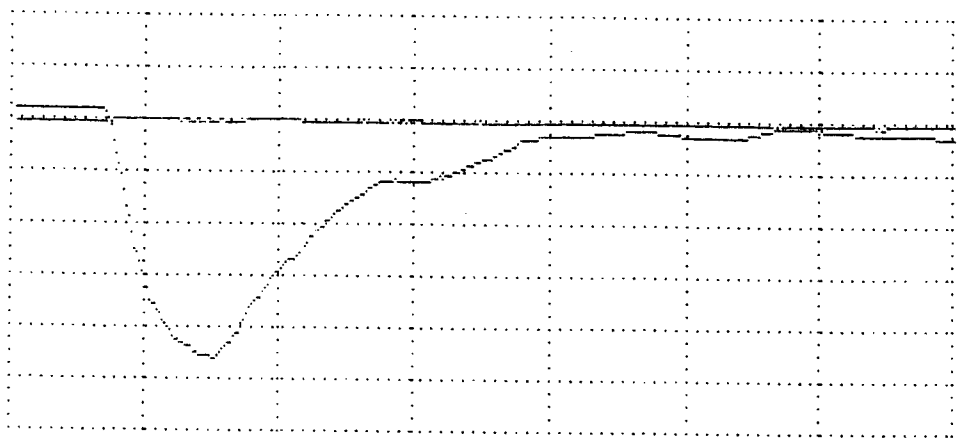

c)	Vertical	0.4 A/Division
	Horizontal	100 nano seconds/Division
	Streaming current	-1.61 μA
	Specific charge	-22.5 μC kg^{-1}
	Probe diameter	28.6 mm

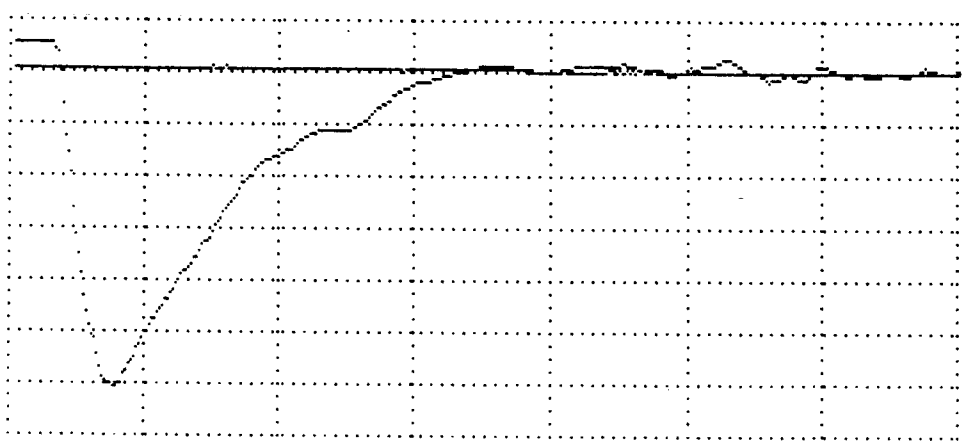

d)	Vertical	0.4 A/Division
	Horizontal	100 nano seconds/Division
	Streaming current	-3.56 μA
	Specific charge	-22.5 μC kg^{-1}
	Probe diameter	28.6 mm

Figure 4.22 (contd) Traces of some Typical Current Transients

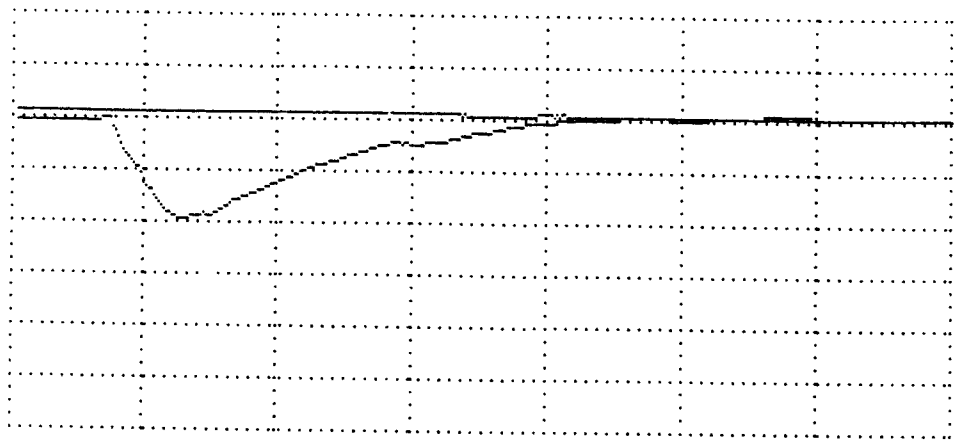

e)	Vertical	0.4 A/Division
	Horizontal	100 nano seconds/Division
	Streaming current	-3.56 μA
	Specific charge	-22.5 μC kg^{-1}
	Probe diameter	22.2 mm

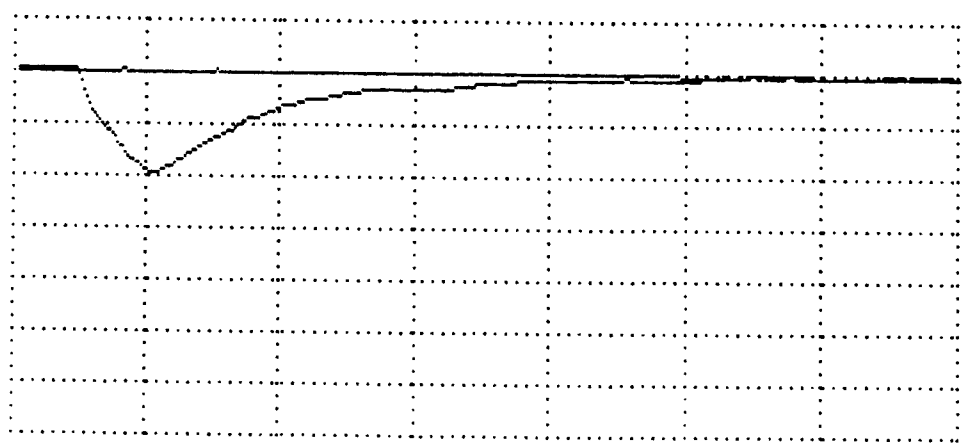

f)	Vertical	0.4 A/Division
	Horizontal	100 nano seconds/Division
	Streaming current	-0.68 μA
	Specific charge	-5.3 μC kg^{-1}
	Probe diameter	28.6 mm

Figure 4.22 (contd) Traces of some Typical Current Transients

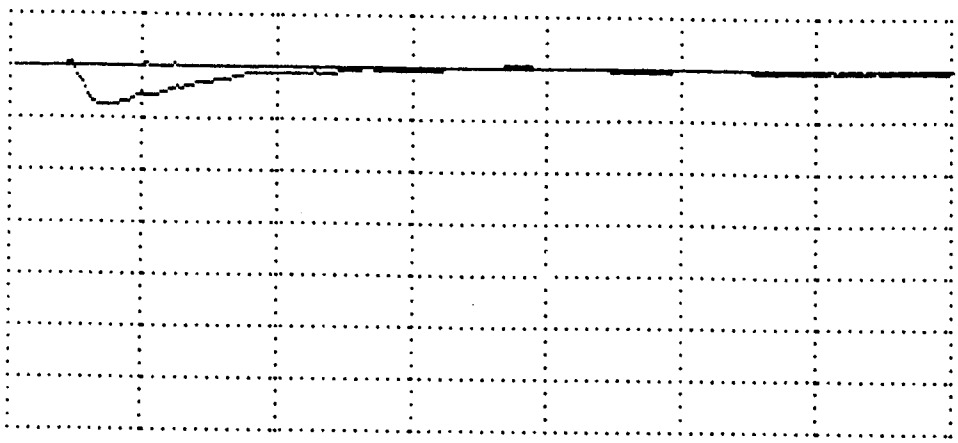

g)	Vertical	0.4 A/Division
	Horizontal	100 nano seconds/Division
	Streaming current	-0.68 μA
	Specific charge	-5.3 μC kg^{-1}
	Probe diameter	12.7 mm

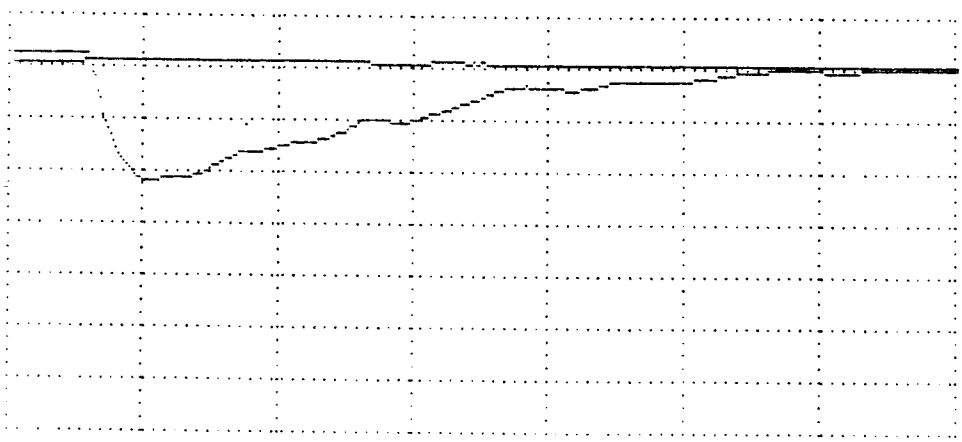

h)	Vertical	0.4 A/Division
	Horizontal	100 nano seconds/Division
	Streaming current	-3.56 μA
	Specific charge	-22.5 μC kg^{-1}
	Probe diameter	12.7 mm

Three electrodes with diameters 12.7 mm, 22.2 mm amd 28.6 mm were also used to measure the magnitude of total charge transfer. The total charge transfer for each probe insertion onto the surface of the bulked HDPE pellets was measured by reading the voltage rise on the capacitance which connected the electrode to earth (see Figure 2.10). The total charge transfer rather than charge transfer during individual discharges to the electrodes was measured for two reasons:

i) During each insertion a number of discharges to the electrode take place.

ii) In the event of an ignition it is not clear whether the first discharge to the probe ignites the propane/air/nitrogen mixture or the following discharges. The charge transfer cannot be measured when an ignition occurs because of the effect of the air ionisation by the flame.

The total charge transfer as a function of the specific charge density is shown in Figure 4.23. The data indicate that for the range of specific charge densities shown the total charge transfer increases as the electrode diameter decreases from 28.6 mm to 12.7 mm. This data, together with the current transient measurements, show that although the magnitude of individual discharges decrease for an electrode with a diameter of 12.7 mm, the number of discharges increase considerably.

4.4.2 Probability of Ignition of Gas Emitting Probe

a) Streaming Current Effect

Figure 4.24 shows the average probability of ignition as a function of pellets streaming current. A series of streaming currents (the charge on HDPE pellets entering the bottom hopper per unit time) were obtained by varying the corona injector potential and also the pellets mass flow rate. The average probability of ignition was obtained by calculating the average of the ignition probabilities for streaming current intervals of 0.5 μA. A spherical electrode with a diameter of 28.6 mm and a propane/air/

Figure 4.23 Total Charge Transfer to Spherical Probe

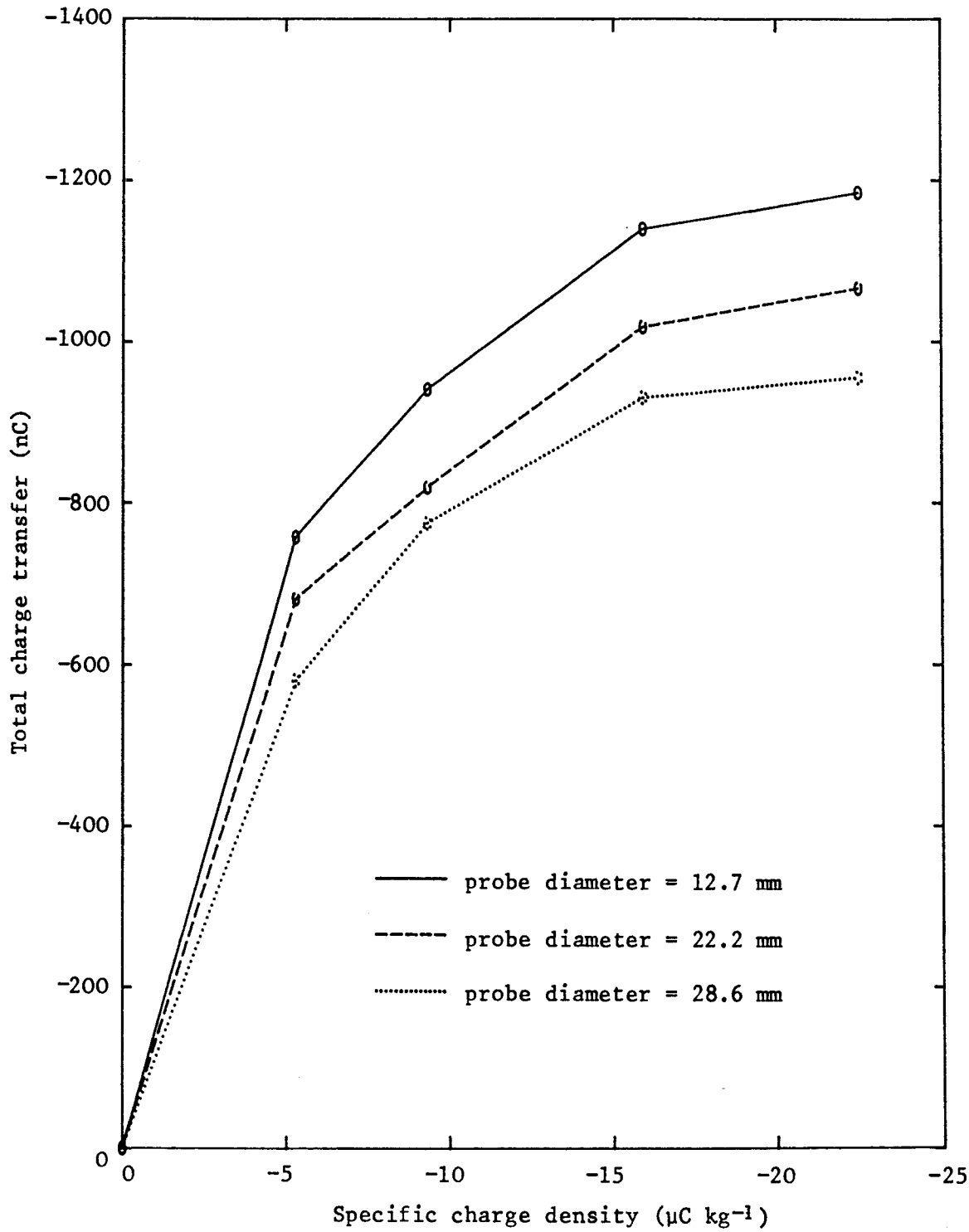

Figure 4.24 Probability of Ignition as a Function of Current

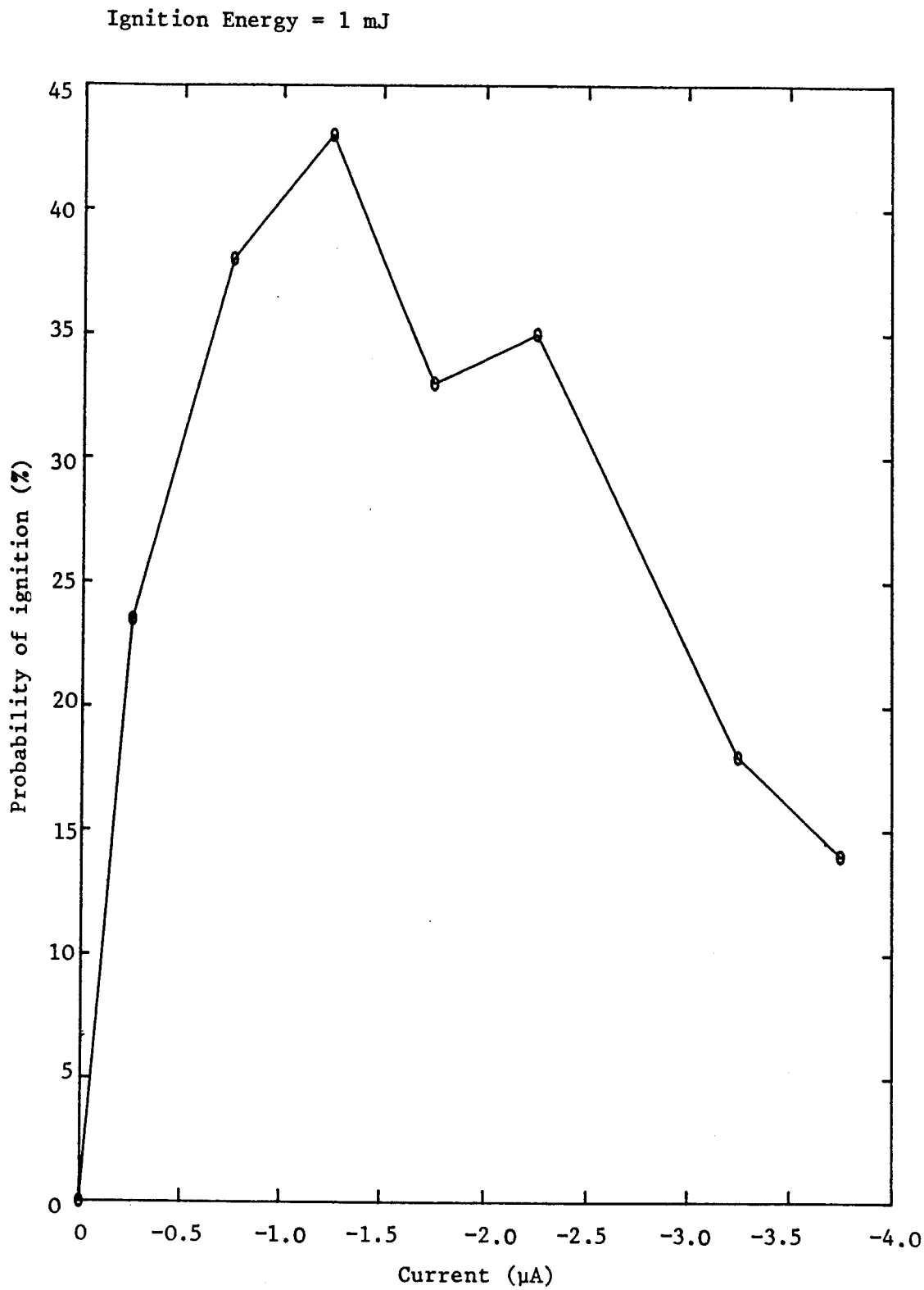

nitrogen mixture with an equivalent electrical energy of 1.0 mJ were used for this experiment. As can be seen from Figure 4.24, the probability of ignition increased to 43% at a streaming current of -1.25 μA and then decreased with further increases in current.

The probability of ignition as a function of streaming current for propane/air/nitrogen mixtures with higher minimum ignition energies than 1.0 mJ also showed that the largest probabilities of ignition were obtained for streaming currents of less than -1.5 μA (see Table 4.6).

Table 4.6 **Probability of Ignition of Propane/Air/Nitrogen Mixtures**

Streaming Current μA	Probability of Ignition %		
	MIE = 2.0 mJ	MIE = 3.6 mJ	MIE = 4.4 mJ
-0.19	0	0	0
-0.33	0	2	0
-0.40	0	0	0
-0.45	0	0	0
-0.58	0	0	0
-0.62	0	0	0
-0.64	2	0	0
-0.68	0	0	0
-1.00	2	2	2
-1.17	0	2	0
-1.50	10	2	0
-1.61	4	0	0
-2.22	4	2	0
-2.44	0	0	0
-3.39	4	2	0
-3.56	2	2	0

b) Specific Charge Density Effect

The dependence of the probability of ignition of two propane/air/nitrogen mixtures with minimum ignition energies of 1.0 mJ and 1.3 mJ as a function of pellets specific charge density is shown in Figures 4.25.a, 4.25.b, 4.25.c and 4.25.d. Two spherical electrodes with diameters 28.6 mm and 22.2 mm were used. The probability of ignition was, with a few exceptions, greatest for specific charge densities between -5 $\mu C\ kg^{-1}$ and -10 $\mu C\ kg^{-1}$. The probability of ignition fell as the specific charge density increased from about -10 $\mu C\ kg^{-1}$ to -22.5 $\mu C\ kg^{-1}$. The largest probabilities of ignition occurred when an electrode of diameter 22.2 mm was used.

As apparent from Figure 4.25.d, an exception to the above was the probability of ignition of a propane/air/nitrogen mixture with a minimum ignition energy of 1.3 mJ with pellets mass flow rates of 0.03 $kg\ s^{-1}$ and 0.07 $kg\ s^{-1}$. For these tests the maximum probabilities of 6% and 12% were achieved for specific charge densities of -22.5 $\mu C\ kg^{-1}$ and -15.9 $\mu C\ kg^{-1}$ respectively.

Although Figures 4.25.a and 4.25.d showed a general decrease in the probability of ignition with decreasing mass flow rate, this trend was not observed in Figures 4.25.b and 4.25.c. Specific charge density was shown in Figure 4.21 to be more or less independent of mass flow rate.

As shown in Table 4.7, the highest probability of ignition for propane/air/nitrogen mixtures with minimum ignition energies of 2.0 mJ, 3.6 mJ and 4.4 mJ were also obtained with a specific charge density of -9.3 $\mu C\ kg^{-1}$.

Figure 4.25a Probability of Ignition as a Function of Specific Charge Density

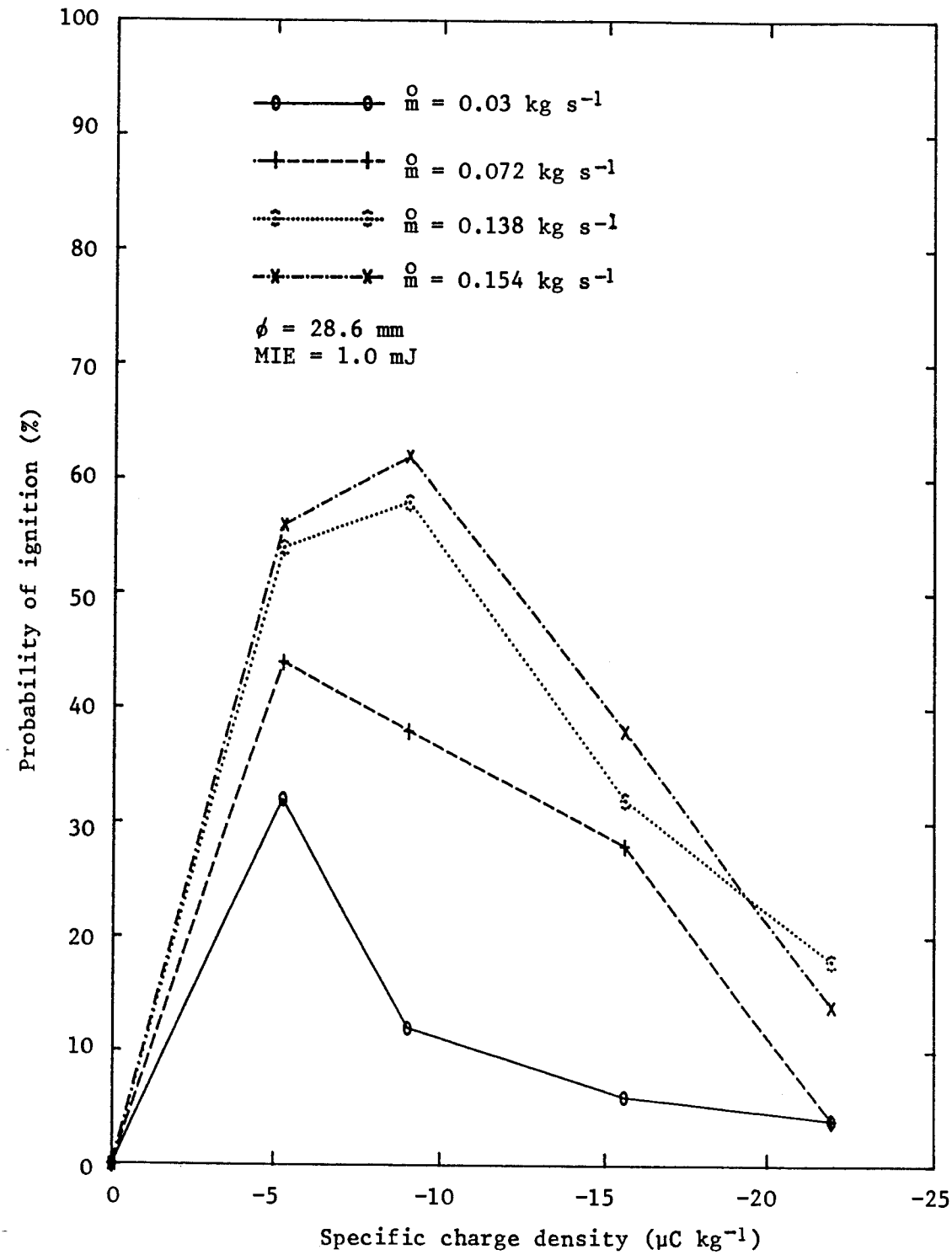

Figure 4.25b Probability of Ignition as a Function of Specific Charge Density

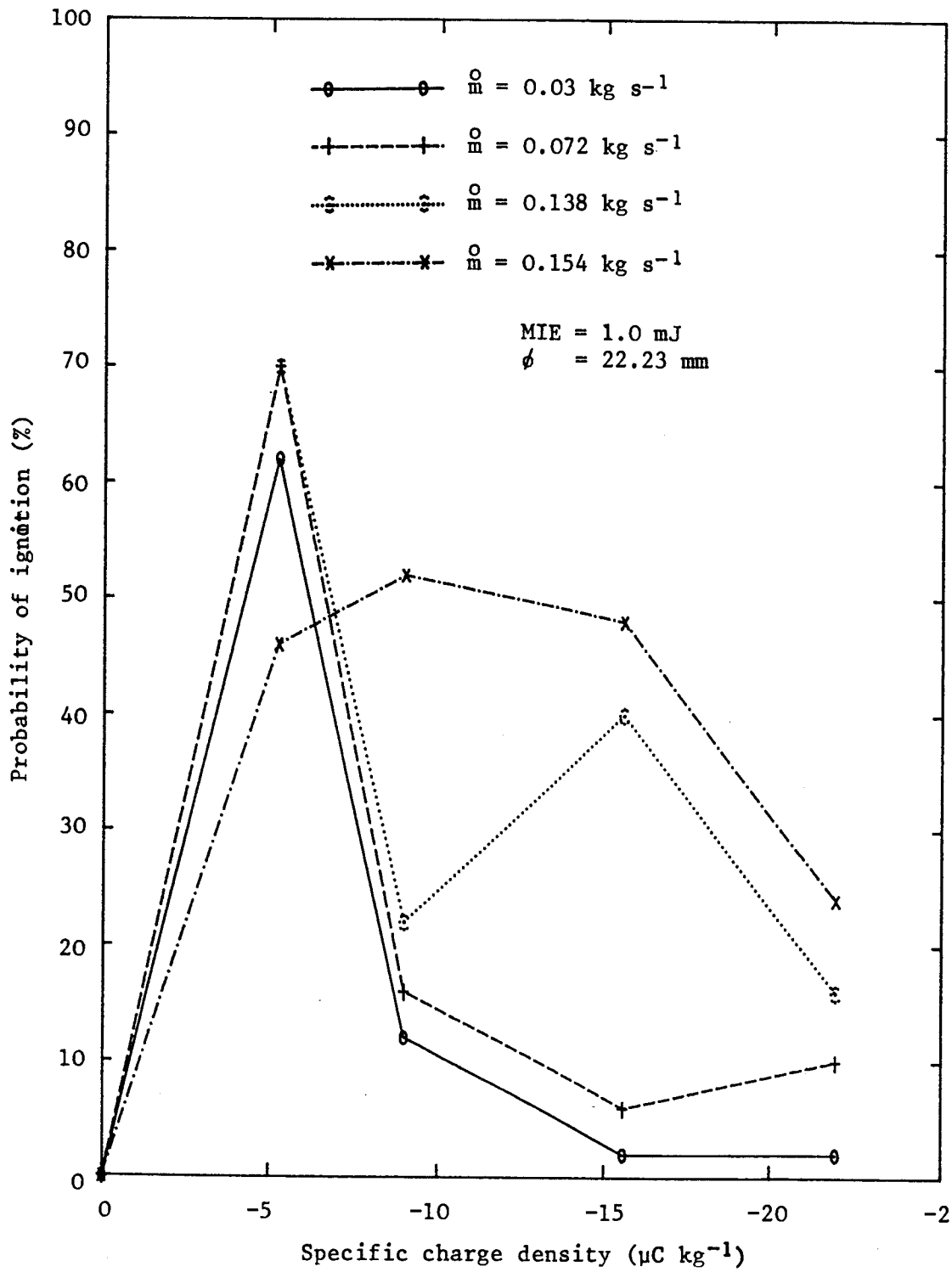

Figure 4.25c Probability of Ignition as a Function of Specific Charge Density

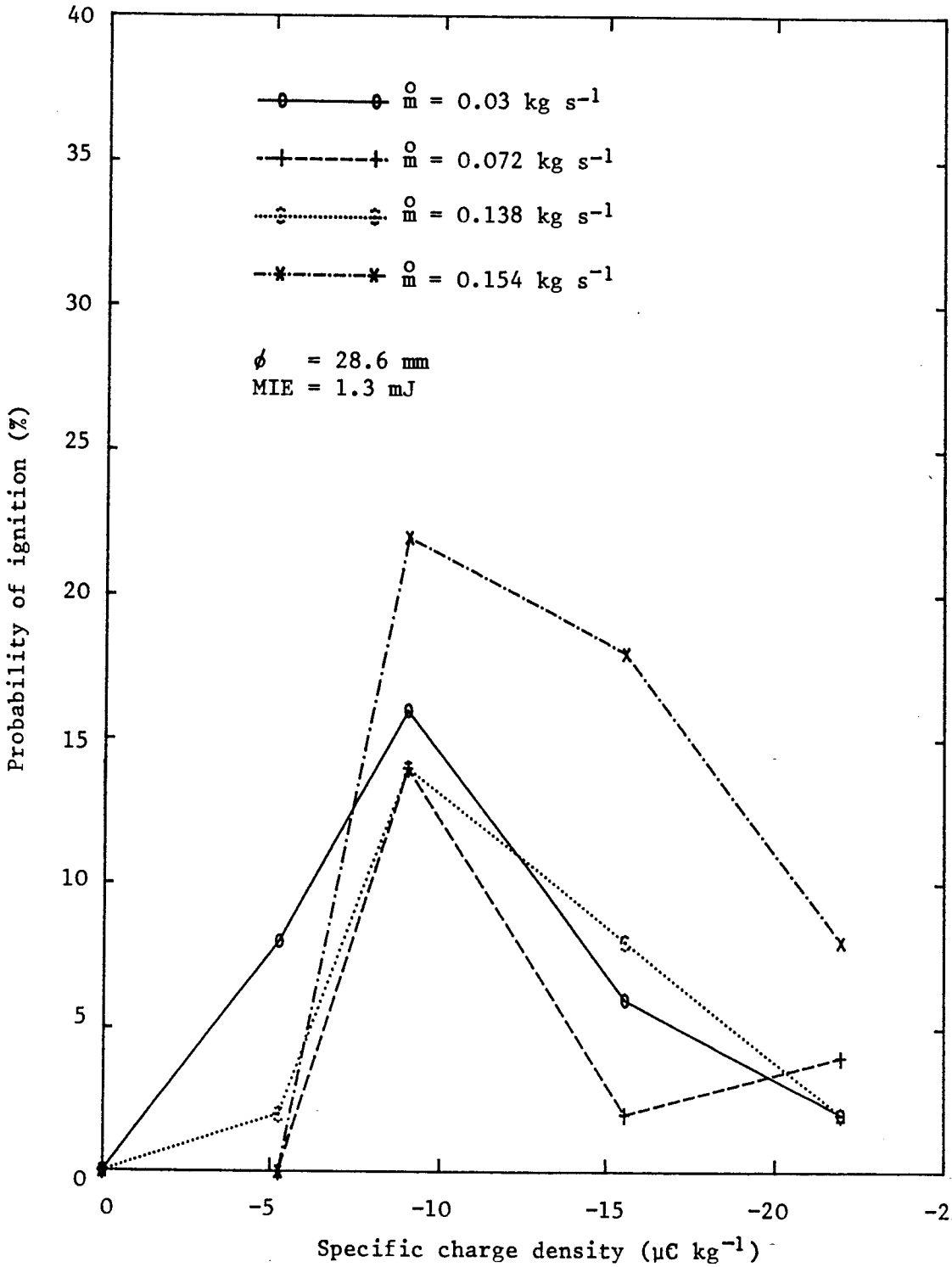

Figure 4.25d Probability of Ignition as a Function of Specific Charge Density

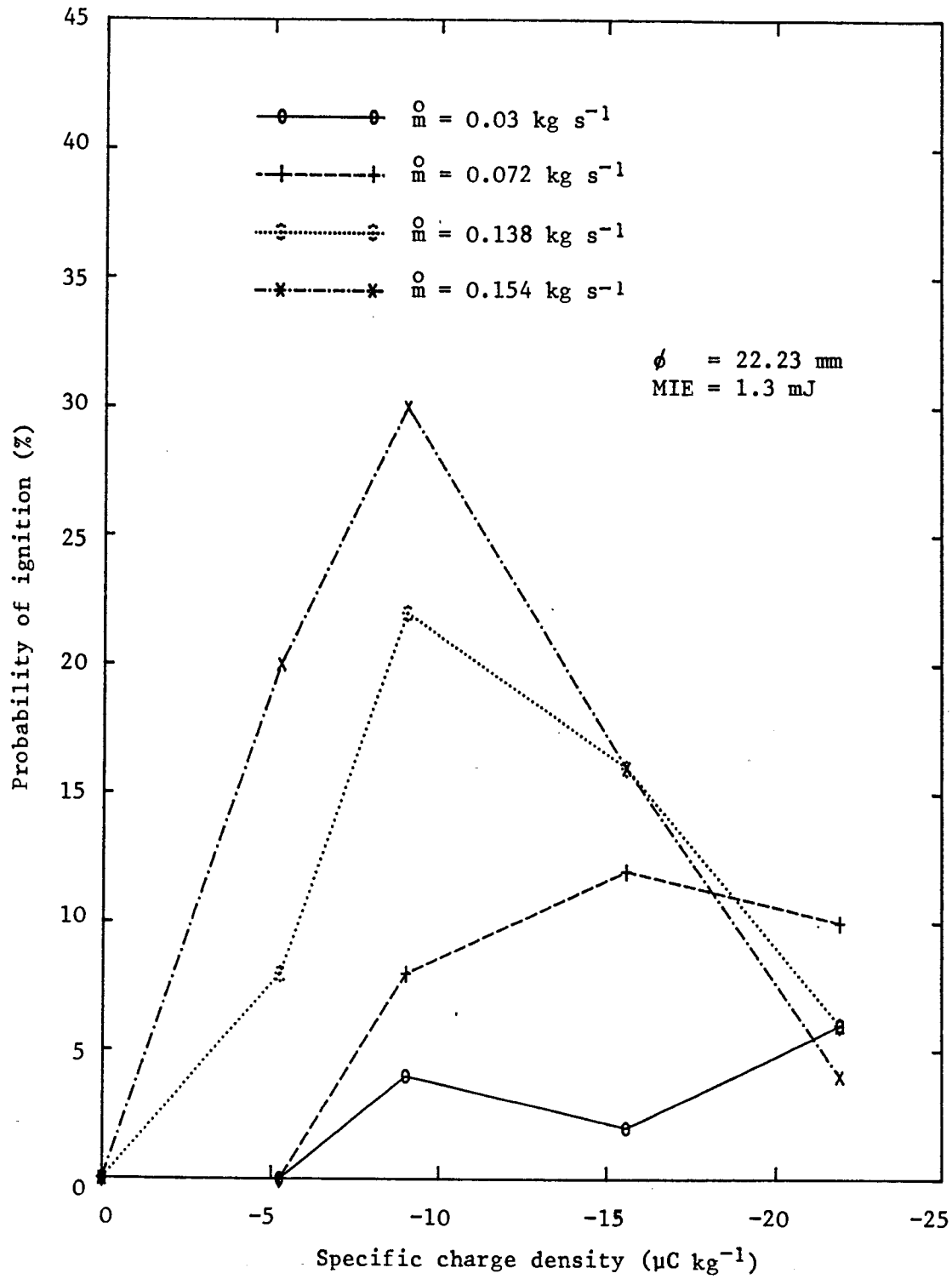

Table 4.7 Probability of Ignition of Propane/Air/Nitrogen Mixtures

Specific Charge Density $\mu C\ kg^{-1}$	Probability of Ignition %		
	MIE = 2.0 mJ	MIE = 3.6 mJ	MIE = 4.4 mJ
-5.3	0	0	0
-9.3	14	6	2
-15.9	4	4	0
-22.5	10	4	0

c) Mass Flow Rate Effect

Figures 4.26.a, 4.26.b, 4.26.c and 4.26.d illustrate the variation of the probability of ignition as a function of mass flow rate. The propane/air/nitrogen mixtures used for this experiment had minimum ignition energies of 1.0 mJ and 1.3 mJ. Ignitions were obtained with electrodes of 22.2 mm and 28.6 mm.

The probability of ignition generally increased with an increase in the mass flow rate. The largest probabilities were obtained with specific charge densities of -5.3 $\mu C\ kg^{-1}$ or -9.3 $\mu C\ kg^{-1}$.

The anomalous behaviour of the probability of ignitions as a function of mass flow rate in some of the figures could be due to the random character of the brush discharges. The random character of the branches can be very critical for the incendivity of this type of discharge. Figure 4.27 shows four traces of the current transients which illustrate the random character of the discharges. As can be seen, the ignition of the propane/air/nitrogen mixture did not always occur for discharges with the largest charge transfers to the gas emitting probe.

The highest equivalent electrical energy was achieved with discharges from the surface of HDPE pellets to a spherical electrode

Figure 4.26a Probability of Ignition as a Function of Powder Flow Rate

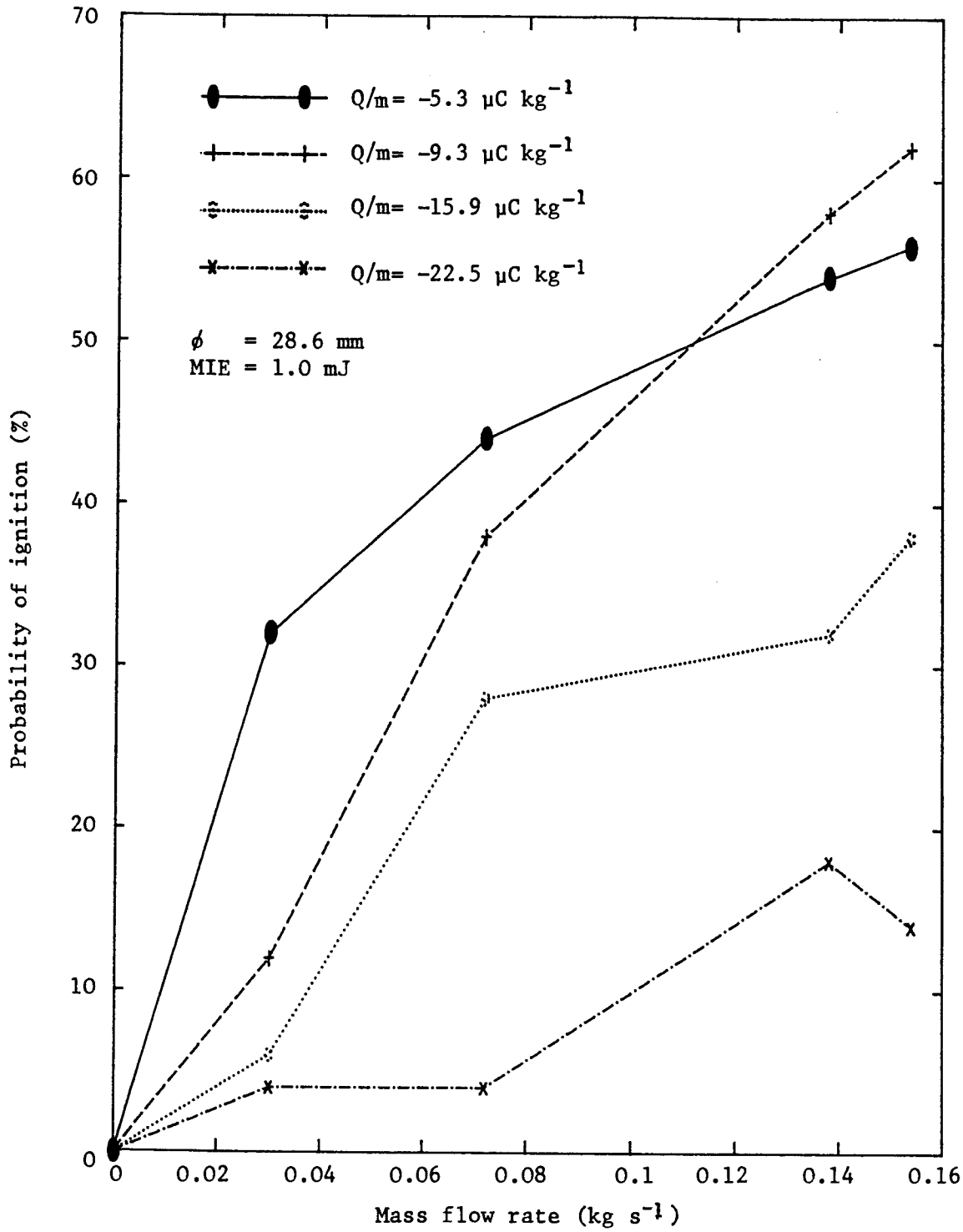

Figure 4.26b Probability of Ignition as a Function of Powder Flow Rate

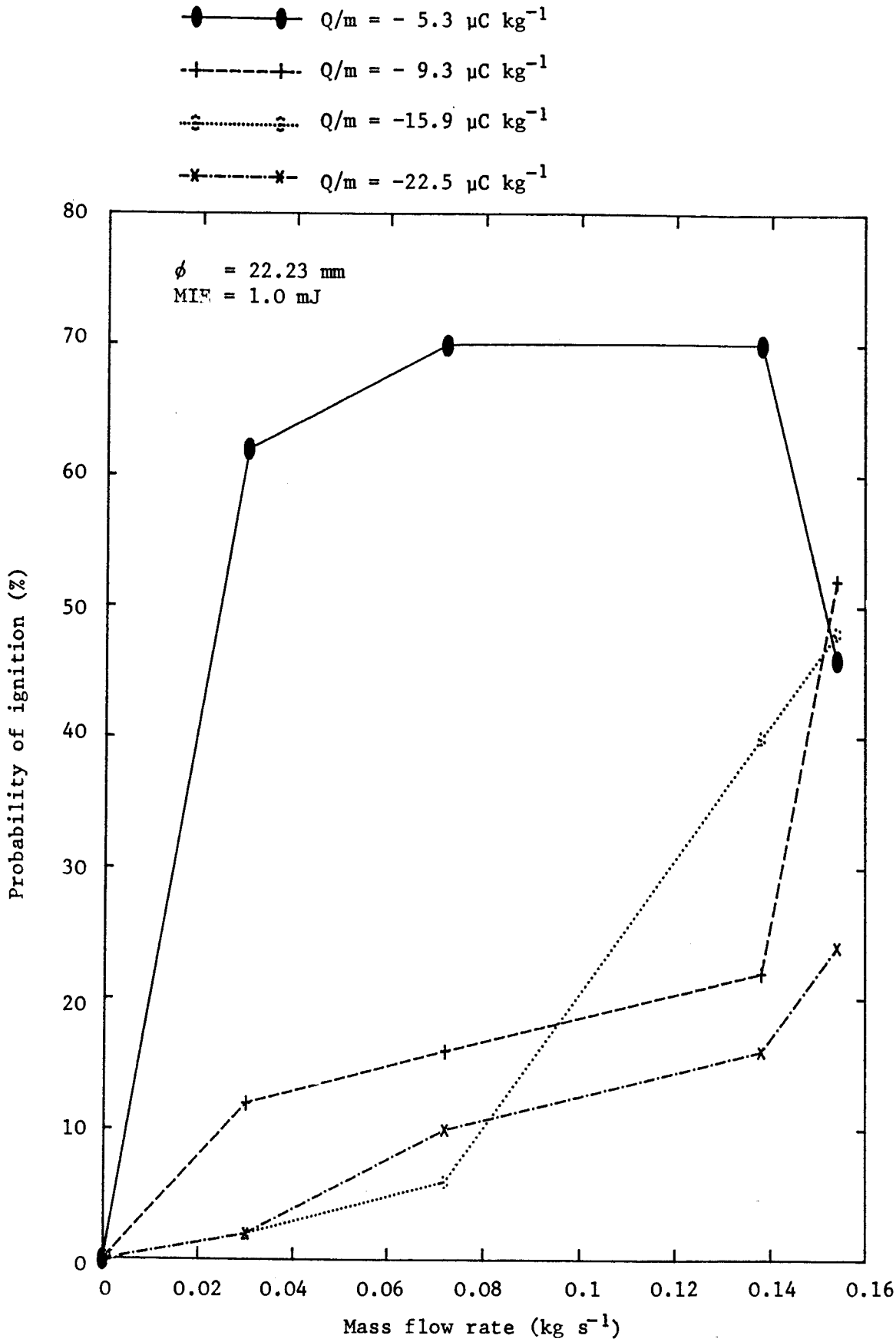

Figure 4.26c Probability of Ignition as a Function of Powder Flow Rate

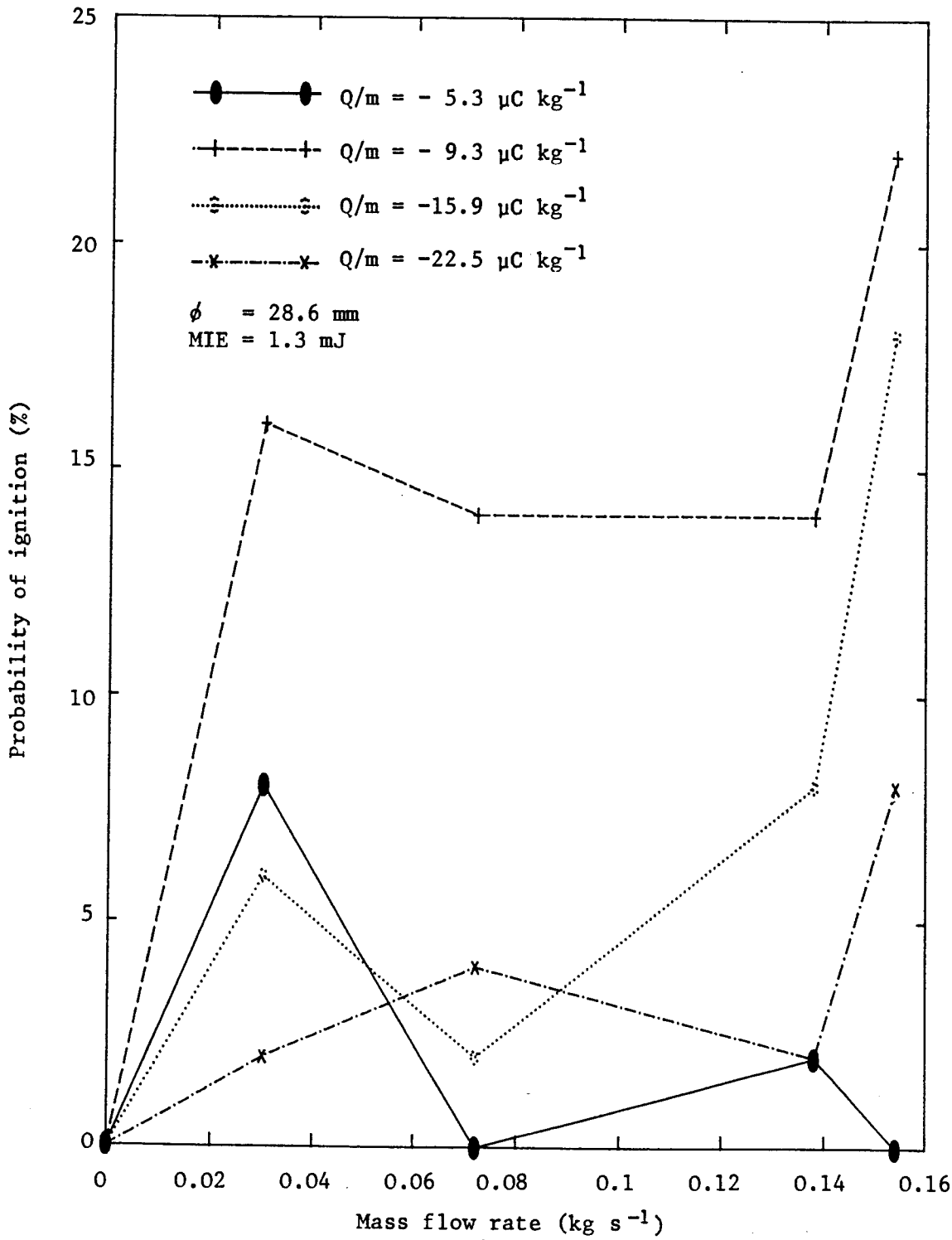

Figure 4.26d Probability of Ignition as a Function of Powder Flow Rate

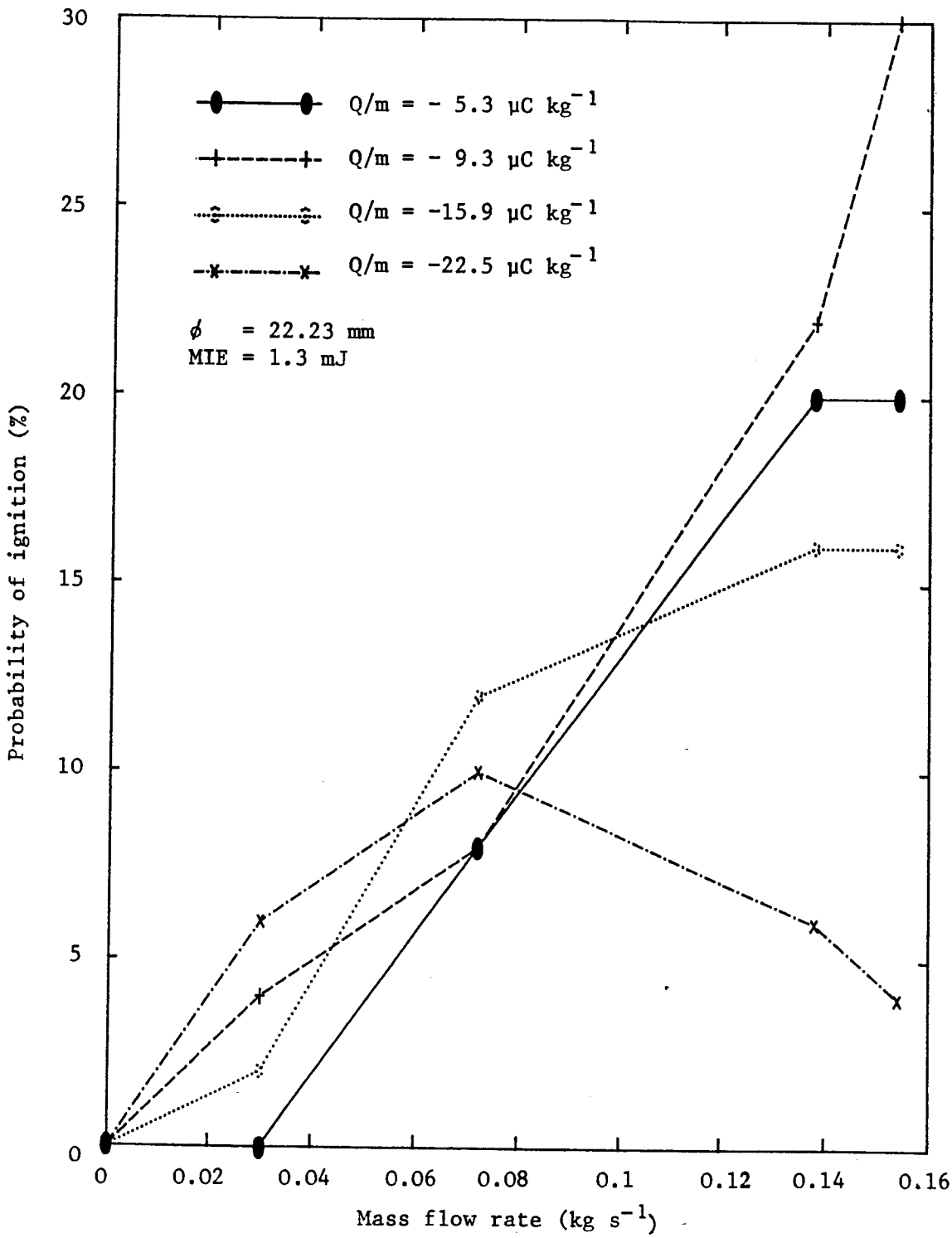

Figure 4.27 Comparison of the Current Transients of the Discharges which Did and Did Not Ignite the Gas Emitting Probe

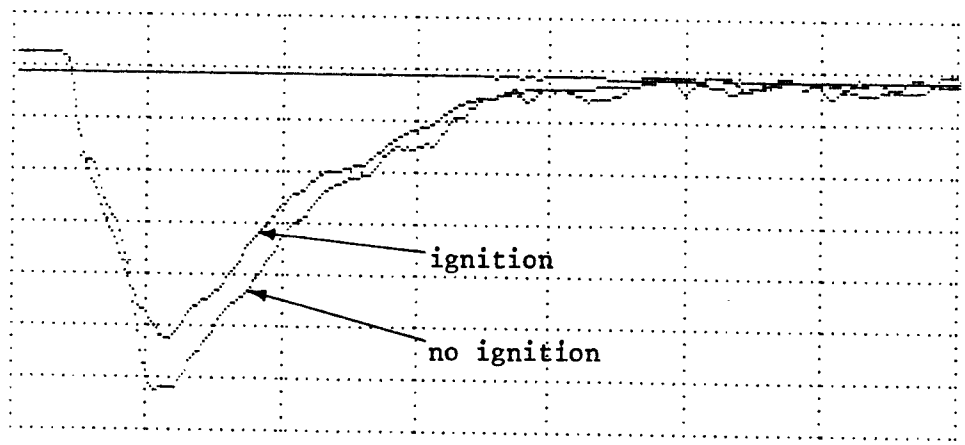

a)	Vertical	0.4 A/Division
	Horizontal	100 nano seconds/Division
	Streaming current	-0.33 μA
	Specific charge	$-9.3\ \mu C\ kg^{-1}$
	Probe diameter	28.6 mm

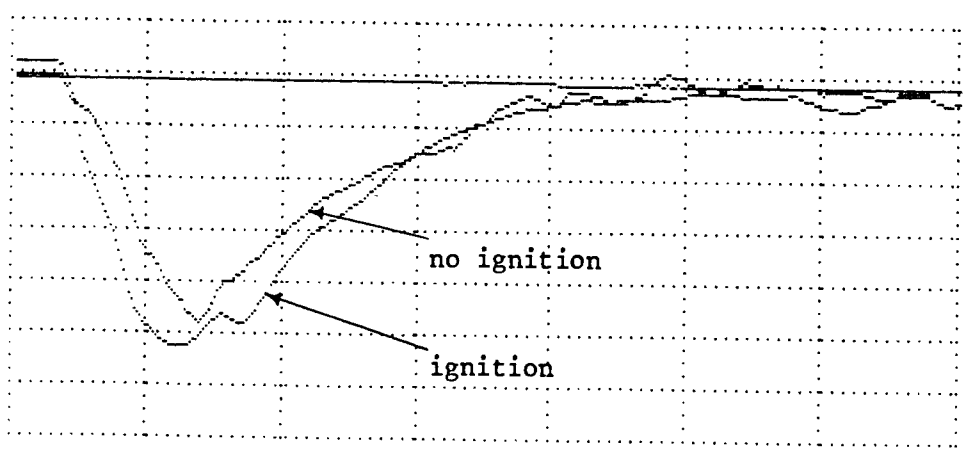

b)	Vertical	0.4 A/Division
	Horizontal	100 nano seconds/Division
	Streaming current	-0.33 μA
	Specific charge	$-9.3\ \mu C\ kg^{-1}$
	Probe diameter	28.6 mm

of 28.6 mm diameter. The ignition probability was 2%. The streaming current and the pellets flow rate were -1.0 μA and 0.138 kg s^{-1} respectively. The equivalent electrical energy was found to be 4.4 mJ.

4.4.3 Tests Carried out on Fine HDPE Powder

The cumulative mass distribution for the HDPE powder is shown in Figure 3.1. The mass median diameter of the powder is 500 μm. The solid density and bulk density of the HDPE fine powder are 950 kg m^{-3} and 470 kg m^{-3} respectively.

The charge on HDPE particles entering the bottom hopper per unit time, which constitute the streaming current as a function of powder flow rate, is shown in Figure 4.28. The maximum streaming current of -1.7 μA was achieved with a powder flow rate of 0.12 kg s^{-1} when a voltage of -17 kV was applied to the corona needles. Further increases in the corona voltage and the powder flow rate did not result in larger streaming currents.

Figure 4.29 shows the variation of the specific charge density of HDPE fine powder as a function of mass flow rate. The largest specific charge densities for all the corona potentials with the exception of -15 kV corona potential were obtained with a powder mass flow rate of 0.03 kg s^{-1}.

4.4.3.1 Total Charge Transfer to the Probes

The total charge transfer to three probes with diameters of 12.7 mm, 22.2 mm and 28.6 mm for each probe insertion onto the surface of bulking HDPE powder were measured. The range of the streaming currents and the specific charge densities for which these tests were carried out are shown in Figures 4.28 and 4.29 respectively. There was no clear dependence of the total charge transfer on parameters such as powder specific charge density, streaming current, powder mass flow rate and the probe diameter. The total charge transfers to the probes varied between about -200 nC and -660 nC.

Figure 4.28 Current as a Function of Mass Flow Rate

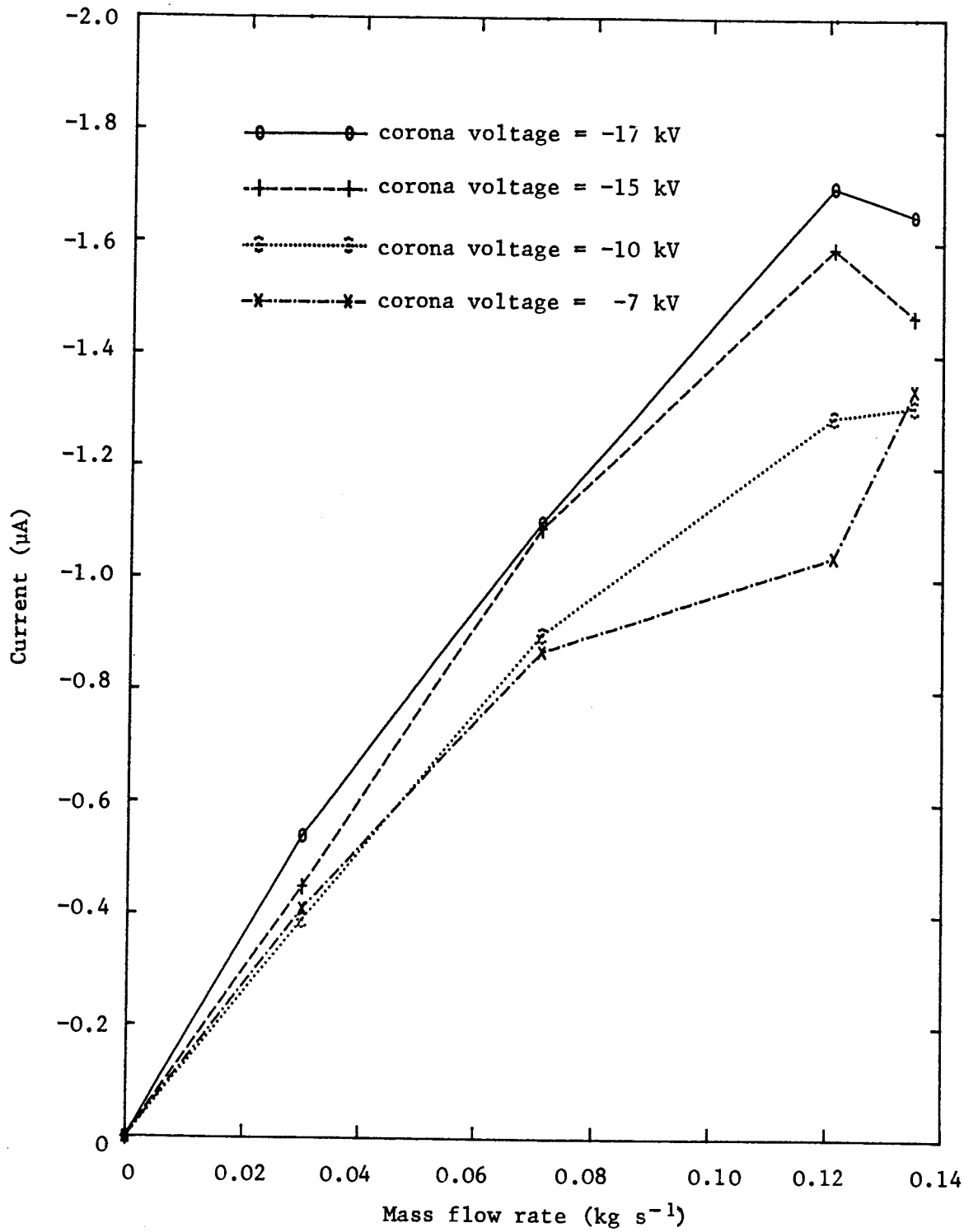

Figure 4.29 Specific Charge Density as a Function of Mass Flow Rate

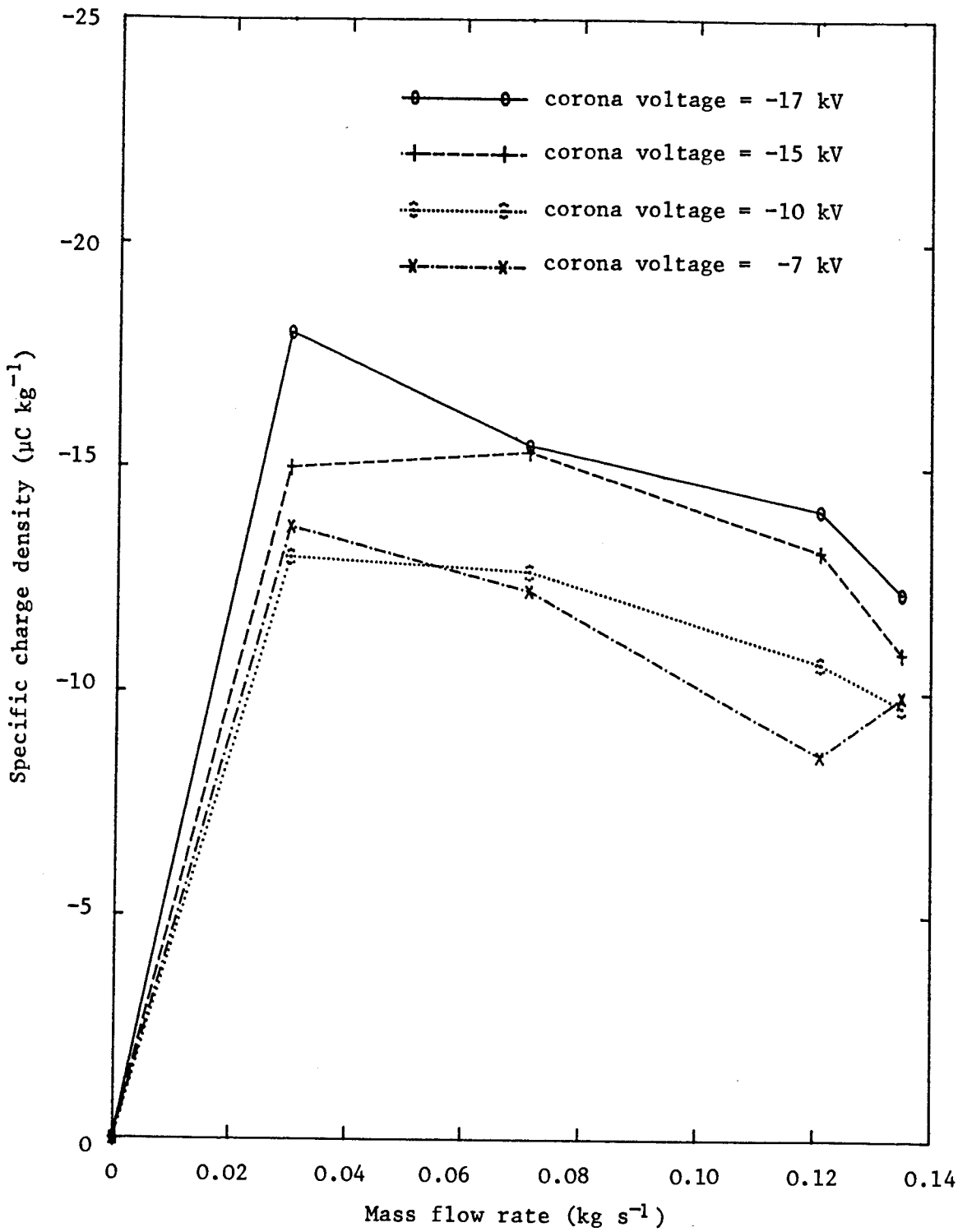

The current transients for some discharges are illustrated in Figure 4.30. The discharges were initiated by lowering two probes with diameters 12.7 mm and 28.6 mm towards the surface of the charged HDPE powder heap. With a few exceptions the total duration of the current flow for each discharge was about 300 nano seconds with a rise time of about 50 nano seconds. The magnitude of the discharges from the surface of bulked HDPE fine powder were considerably smaller than the discharges from the surface of HDPE pellets (see Figure 4.22).

4.4.3.2 Surface Potential Measurements

The potential on the surface of bulked HDPE powder was measured using an electric field meter which was calibrated to read surface potential. For the range of streaming currents (-0.4 μA - -1.7 μA) shown in Figure 4.28 the measured surface potential was -11.6 kV ± 3.2 kV. This indicates that the charge released as a result of fine HDPE powder particles bulking in the hopper, even for streaming currents of about -0.4 μA, is large enough to hold the surface potential to a value as low as -11.6 kV.

The surface potential values for fine HDPE are considerably lower than the surface potentials for bulked HDPE pellets (-78 kV - -40 kV) which confirms the earlier suggestions that a larger charge is released possibly in the form of corona discharges as a result of bulking of fine charged particles than pellets.

4.5 Discussion of the Results

The transfer and storage of charged powder into a container such as a silo or a hopper can be modelled by a capacitor representing the bulked charged powder in parallel with a resistor and a discharge gap representing the charge relaxation through the bulked powder and corona or more energetic discharges respectively. Figure 4.31 illustrates the model of the electrostatic mechanism which occurs during transfer and storage of charged particles.

Figure 4.30 Current Transient Traces

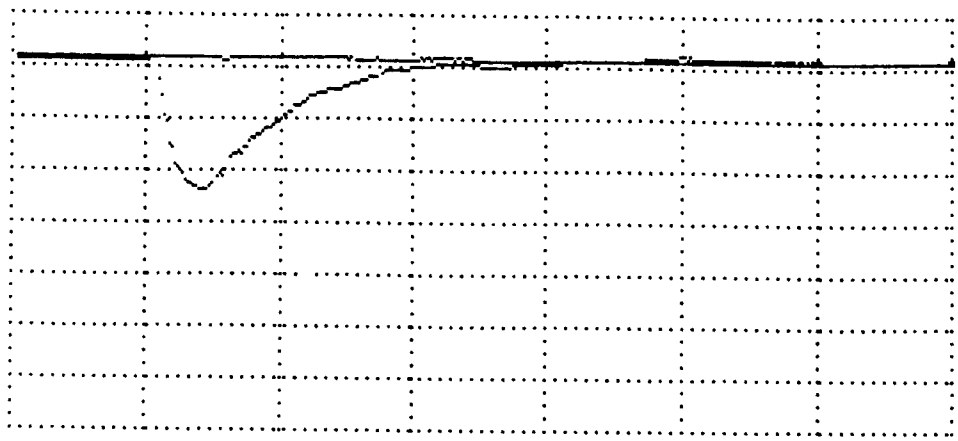

a)

Vertical	4 mA/Division
Horizontal	100 nano seconds/Division
Streaming current	-1.47 μA
Specific charge	-10.9 μC kg^{-1}
Probe Diameter	28.6 mm

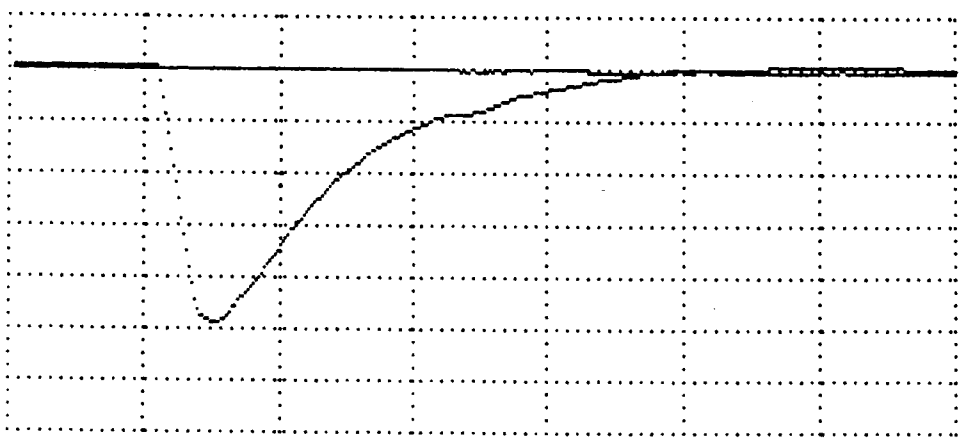

b)

Vertical	20 mA/Division
Horizontal	100 nano seconds/Division
Streaming current	-1.47 μA
Specific charge	-10.9 μC kg^{-1}
Probe diameter	12.7 mm

Figure 4.30 (contd) Current Transient Traces

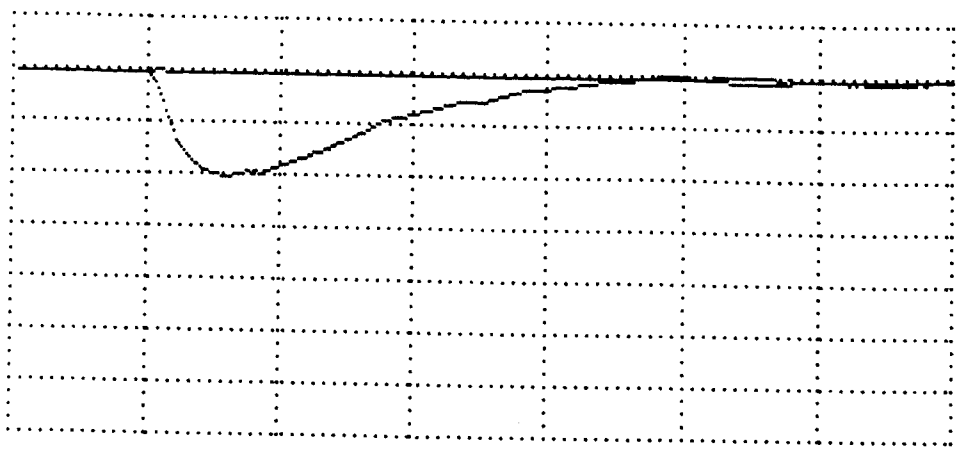

c)	Vertical	2 mA/Division
	Horizontal	100 nano seconds/Division
	Streaming current	-0.90 μA
	Specific charge	$-12.7\ \mu C\ kg^{-1}$
	Probe diameter	28.6 mm

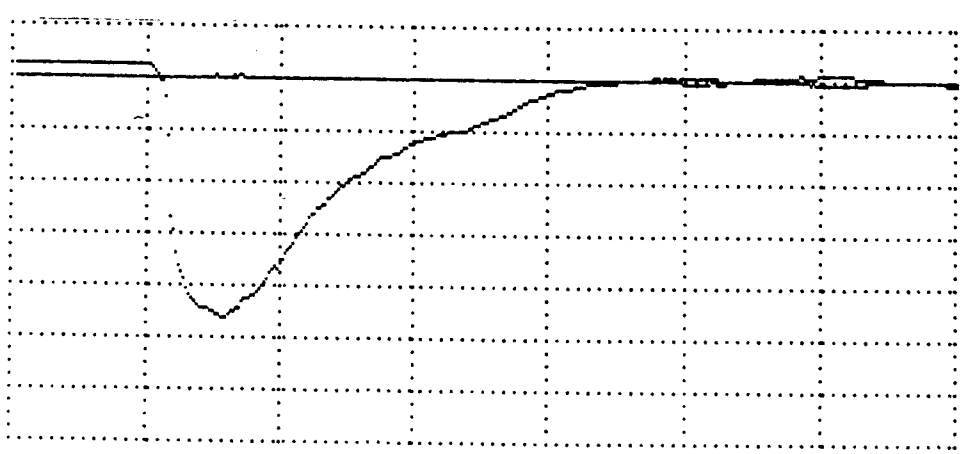

d)	Vertical	100 mA/Division
	Horizontal	100 nano seconds/Division
	Streaming current	-1.70 μA
	Specific charge	$-14.1\ \mu C\ kg^{-1}$
	Probe diameter	12.7 mm

Figure 4.30 (contd) Current Transient Traces

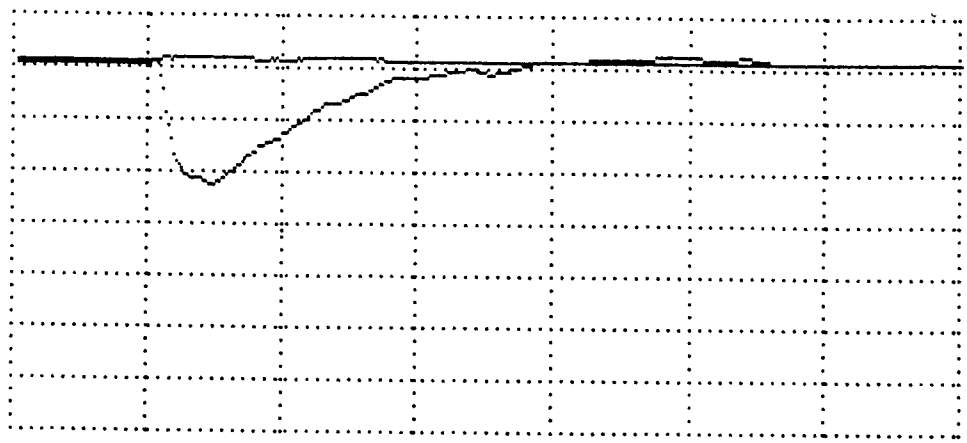

e)

Vertical	1 mA/Division
Horizontal	100 nano seconds/Division
Streaming current	-1.10 μA
Specific charge	$-15.5\ \mu C\ kg^{-1}$
Probe diameter	28.6 mm

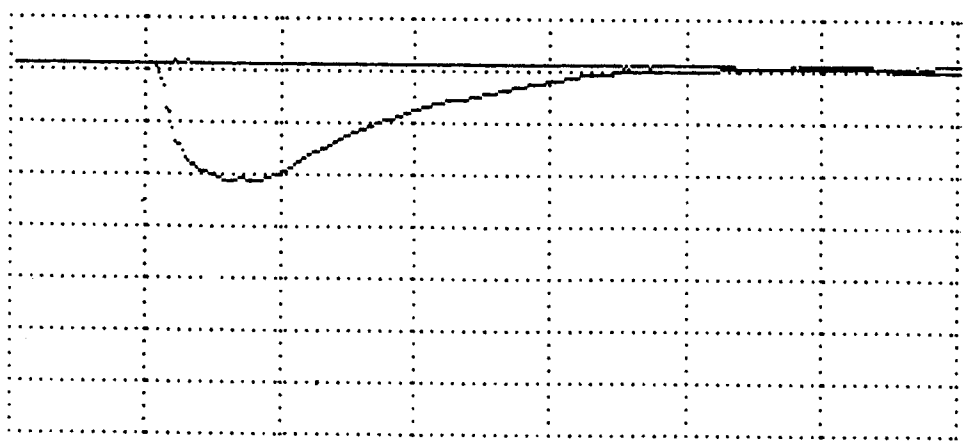

f)

Vertical	400 mA/Division
Horizontal	100 nano seconds/Division
Streaming current	-0.54 μA
Specific charge	$-18.0\ \mu C\ kg^{-1}$
Probe diameter	12.7 mm

Figure 4.31 Model of Electrostatic Processes that Occur During Filling of a Container

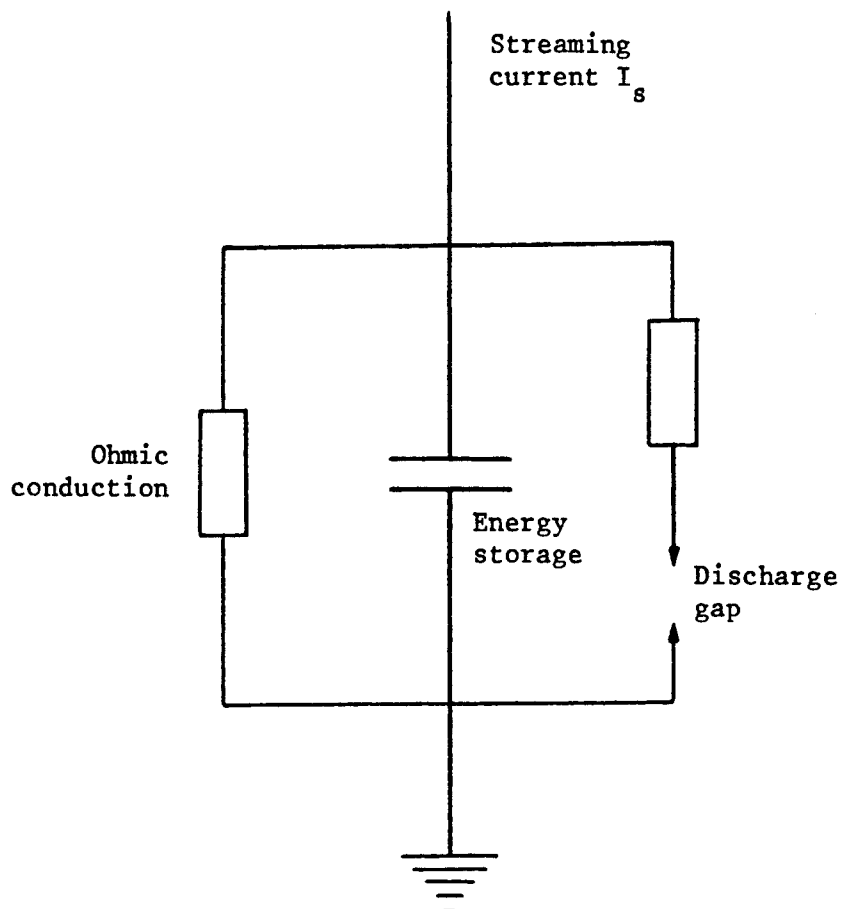

The streaming current charges the capacitor. The process of charging the capacitor cannot however take place indefinitely. A controlling factor is the dielectric breakdown strength of air. When highly charged particles are bulked together in a container, provided the powder is insulating enough, the electric field on the surface of bulked powder will exceed the breakdown limit causing ionisation of the air (see section 4.2). The air ions will partially neutralise the charged bulked powder until the field falls below the ionisation threshold again.

The powder relaxation time or the powder resistivity and the rate at which the charged powder enters the container (streaming current) govern the saturation time or the time for the commencement of the onset of air ionisation, as well as the magnitude of the ionisation. The electrostatic charges dissipate slowly if the relaxation time is large. The magnitude of the ionisation also depends on the particle size. For a small particle which is charged to its maximum level the full electric field is produced over only a small region near the surface. Therefore a higher surface charge density than that for a larger particle may be sustained. The amount of charge released during powder conglomeration increases the smaller the particle size becomes. This is because the effective surface area of the bulked powder is much smaller than the sum of the individual surface areas of all the incoming small particles (see section 3.3.3.4).

Suppose that the number of ion pairs produced in unit volume in unit time in the gas space above the powder heap is not affected by the flow of the current, the total current density, J, flowing in this case is given by equation (4.12):

$$J = n_o e \mu_+ E + n_o e \mu_- E \qquad (4.12)$$

μ_+ and μ_- are the corresponding ionic mobilities and E is the cumulative electric field generated in the air around the conglomerate. Equation (4.12) corresponds to Ohm's law and the conductivity of the gas is thus given by equation (4.13):

$$\sigma_c = \frac{J}{E} = n_o e (\mu_+ + \mu_-) \qquad (4.13)$$

The conductivity of the gas space above the bulked powder is therefore dependent on the equilibrium concentration (density) of ion pairs, n_o. The discharge gap representing the corona or more energetic discharges on the surface of bulked powder in Figure 4.31 may therefore be represented by a variable resistance. The magnitude of the ionisation determines the resistance value. The surface potential of the bulked powder for a particular streaming current depends on the resistance. If streaming current increases, the number of ion pairs produced increases and so the resistance decreases, which in turn results in a decrease in the surface potential. Glor et al (1989) found sudden decreases in the electric field strength on the surface of bulked HDPE pellets which coincided with surface discharges. It was also found that the frequency and magnitude of surface discharges increased with an increase in the streaming current.

Table 4.8 shows the surface potential values on the centre of the surface of bulked HDPE pellets, measured immediately after the finish of a run for a range of streaming currents.

Table 4.8 **Surface Potentials of Bulked HDPE Pellets**

Mass flow rate kg s^{-1}	Streaming current µA	Specific charge density µC kg^{-1}	Surface potential kV
0.030	-0.19	-6.3	-71.4
0.072	-0.64	-8.9	-69.4
0.138	-2.22	-16.1	-65.7
0.154	-3.56	-23.1	-39.7

The surface potential decreased from about -71 kV to about -40 kV for streaming currents of -0.19 µA and -3.56 µA respectively. The decrease in the surface potential indicates a larger air ionisation for a streaming current of -3.56 µA than for a current

of -0.19 μA. It was also shown previously that the probability of ignition decreased for streaming currents of greater than about -1 μA. The largest probability of ignition occurred for specific charge densities of between -5 μC kg^{-1} and -10 μC kg^{-1}. The probability of ignition was considerably lower for larger specific charge densities of about -22.5 μC kg^{-1}.

4.6 Summary

A theoretical model is presented to estimate the potential on the surface of bulked powder in a grounded conducting silo. The electrical resistance of the bulked powder is directly proportional to the volume resistivity of the bulked powder and inversely proportional to the capacitance of the geometry of the silo containing the powder (geometrical constant). The streaming current produces a constant surface potential across the resistance of the bulked powder. From the experimental observations the geometrical constant for the Marchwood silo was about 1, which suggests that surface potential of the bulked powder is equal to the product of the silo streaming current and the volume resistivity of the bulked powder. This model cannot estimate the potential on the surface of bulked powders having a volume resistivity larger than about 10^{12} Ωm because the excess charge is lost by low energy corona or brush discharges.

Electric field measurements above bulked HDPE powder surface and at different heights on the silo wall show that tribo-charging during pneumatic transfer of HDPE powder is bipolar. When the net charge on the powder entering the silo (silo current) is positive, the dust cloud which is formed by the fine particles is negatively charged and the coarse particles positively. With a negative silo current both the dust cloud and the bulked coarse particles are negatively charged.

Electric field strengths of about 150 kV m^{-1} are observed for HDPE near the surface of bulked powder towards the silo wall. Electric field strength of maize starch dust cloud on the silo wall

1.5 m from the top reaches a value of about 500 kV m^{-1}. The space potential measurements of the charged cloud of maize starch powder also show that the largest space potentials occur towards the centre of the silo and about 1 m to 2 m from the top of the silo. The space potential of maize starch dust cloud is much larger than for HDPE. This is due to the higher electrostatic charge on maize starch particles.

The discharge detection by radio frequency technique during transfer of HDPE in the test silo shows that the radio signal count rate increases as the specific charge density of HDPE increases. This is in sharp contrast with similar experiments during transfer of maize starch which show an increase in the radio signal count rate as the specific charge density of maize starch decreases. The detection of discharges by radio frequency method provides a high sensitivity to low energy electrostatic discharges, combined with a low sensitivity to corona discharges. This method has, however, the disadvantages of neither locating the point where discharges occur nor determining the energy of discharges. It may be possible that the discharges from the surface of bulked HDPE change from corona type discharges into more energetic discharges as the specific charge increases. In contrast the excess charge in the dust cloud of maize starch is dissipated in the form of low energy electrostatic discharges rather than corona discharges at low specific charge densities.

The magnitude of electrostatic discharges to probes in the regions within the silo where previous measurements have shown high electric field intensities are measured. Charge transfers of about -200 nC and -100 nC are obtained from the surface of bulked HDPE powder and maize starch dust cloud respectively. At high transport air relative humidities of about 70%, discharges of about -700 nC to the probes are obtained from the surface of bulked HDPE powder. The charge transfers to an earthed probe from the surface of a depression made in the bulked HDPE powder are larger in magnitude than the charge transfers from the surface of powder cone. There is

however no evidence that the ignition risk increases if such a depression is filled with charged powder.

The electrostatic discharges to the probes failed to ignite the dust cloud inside the test silo but on two occasions, once from the surface of bulked HDPE powder and another time from the maize starch dust cloud, the discharges did ignite the propane/air mixture. The equivalent electrical energy of these discharges is greater than 0.25 mJ.

A laboratory electrostatic powder handling rig is used to study the incendivity of electrostatic discharges from the surface of HDPE pellets. The pellets are charged using a corona charge injection device. The incendivity of electrostatic discharges is measured by passing discharges from the surface of bulked HDPE pellets through flammable propane/air atmospheres of different sensitivities. The minimum ignition energy of the propane/air mixture is increased by partially inerting it with nitrogen.

The current transients of the discharges which are initiated by lowering an earthed electrode towards the surface of charged bulked pellets are obtained using a transient digitiser. The current transients have a total duration of about 350 nano seconds with a rise time of about 50 nano seconds. With a few exceptions the discharges to an electrode with a diameter of 12.7 mm are the smallest in magnitude. The largest discharges occur with pellets charge densities of less than -15.9 $\mu C\ kg^{-1}$ and an electrode diameter of 22.2 mm.

The probability of ignition as a function of streaming current and specific charge of HDPE pellets show that the largest probabilities of ignition are obtained for streaming currents of less than -1.5 μA and for specific charge densities between $-5\ \mu C\ kg^{-1}$ and $-10\ \mu C\ kg^{-1}$. The probability of ignition increases to a maximum value and then decreases below and above the streaming currents and specific charge densities mentioned above. The probability of ignition generally increases with an increase in the

mass flow rate. There are however some exceptions to these observations. This anomalous behaviour may be attributed to the random character of the brush discharges. For example the study of some of the current transient traces show that the ignition of the propane/air/nitrogen mixture does not always occur for discharges with the largest charge transfers to the gas emitting probe.

The surface potential measurements on the centre of the bulked HDPE pellets surface show a decrease from about -71 kV to about -40 kV when the streaming current is increased from -0.19 μA to -3.56 μA.

When a highly charged powder having a volume resistivity larger than about 10^{12} Ωm is collected in an earthed conducting container, then the cumulative electric field generated in the air around the conglomerate will exceed the breakdown limit causing ionisation of the air. Comparison of the silo filling current and silo emptying current show that electrostatic discharges occurred during the bulking process. The excess charge could be released in the form of low energy corona discharges. The air ionisation will partially neutralise the charged bulked powder until the electric field falls below the ionisation threshold. Transfer and storage of charged powder into a container is modelled by a capacitor representing the bulked charged powder in parallel with a resistor and a discharge gap representing the charge relaxation through the powder and corona or more energetic discharges respectively. The conductivity of the gap space above the bulked powder is a function of the density of ions produced as a result of ionisation. The magnitude of the ionisation therefore determines the resistance of the discharge gap. If the charge per unit time entering the silo increases, the number of ion pairs produced increases and so the gap resistance decreases, which in turn results in a decrease in the surface potential. The decrease in the probability of ignition for streaming currents of greater than -1.5 μA and for specific charge densities greater than about -10 μC kg^{-1} can thus be attributed to the decrease in surface potential as a result of air ionisation during bulking of charged powder.

Chapter 5

Conclusions

CHAPTER 5

CONCLUSIONS

The efficiency and the ease with which powdered products can be transported and high transportation speeds of pneumatic conveying systems has resulted in the widespread use of such installations. In parallel with the use of pneumatic conveying, there have been many reports of dust explosions associated with industries handling particulate materials. The effects of a dust explosion can range from a small fire to considerable loss of production and operating confidence. The main sources of ignition of a combustible dispersed dust are flames, hot surfaces, welding and cutting operations, friction or impact sparks, electric sparks and electrostatic discharges. Among different types of ignition sources, electrostatic discharges account for about four percent of the recent dust explosions (1979-1984) in the UK [Abbott (1986)]. When considering hazards due to static electricity during pneumatic conveying and storage of powders and indeed during any other process, it is necessary to understand the mechanisms responsible for charge transfer and the occurrence and incendivity of the accompanying dissipation processes.

Electrostatic charges are usually generated/separated whenever two materials are rubbed together or simply touch and then separate, with one becoming negative and the other positive. In a metal the lower bands are full but the highest occupied band, the conduction band, is only half full. An electron in the conduction band can accept from an electric field the very small amount of energy it requires to be raised to a slightly higher energy level in the band. Conductors in general are characterised by having either a partly filled conduction-valence band, or an empty conduction band overlapping a filled valence band, so that there is in effect one continuous partly-filled band. In either case the electron is able to increase its energy within the band, and the material is a conductor. In most insulators the electrons lie in a full energy

band which is well below the Fermi energy of a metal while the empty conduction band of the insulator is at the vacuum level and is well above the Fermi energy. An insulator has a forbidden energy gap of up to 12 eV. Consequently, when a metal and an insulator are brought into contact, electrons ought not to transfer from the metal into the insulator or vice versa. An insulator, however, contains impurity atoms and the electrons associated with such atoms are in a slightly different environment to the other electrons in the insulator. An impurity atom may therefore give rise to an additional energy level which is outside the normally allowed range. This additional energy level may be occupied by an electron which will give rise to a filled energy level close to the conduction band, whereas the lack of an electron will give rise to an unoccupied energy level close to the valence band. When, therefore, two materials make and then break contact, charge transfer from one to the other occurs. For example, the charging of a freshly prepared film of polyethylene in contact with mercury was low. For films exposed to the laboratory air for a few hours, the contact charging increased by 2000 percent.

If small amounts of surface contamination, impurities or adsorbed materials significantly affect the contact charging process, it will be necessary to work under ultra-high vacuum conditions to achieve reproducible data. This is not of immediate practical relevance to most industrial situations because the solids and powders involved are not pure substances.

The impact charge and the impact area during a particle impact on a metal plate are linear functions of the vertical component of the impact velocity. The charge per unit area is independent of the impact velocity and angle and its value is only determined by the combination of the materials of the particles and the metal plate. The equilibrium value of charge is almost independent of the impact conditions and depends on the particle material and size and the plate material. The charge build-up on a polymeric pellet impacted to a metal target repeatedly follows an almost exponential growth.

The initial slope of the charging curve becomes steeper with an increase in the impact pressure which results in an increase in the contact area between the pellet and metal surface.

The static electrification of powder particles in a pneumatic conveying system is due to tribo-electrification caused by multiple collisions between powder particles and the pipe wall. The tribo-electrification of the particles in a pneumatic conveying system is affected by changes in the conditions of collision with the pipe wall, the material of the pipe and the atmosphere.

The phenomenon of electrostatic charging of powder particles during pneumatic conveying can be divided into two counteracting processes, charging and discharging. Charging occurs during contact and the subsequent separation of powder particles from the pipe wall. If a particle is charged after a previous impact then, as it approaches the pipe wall, opposite charges (image charge) will be induced on the pipe wall before impact, and a field is established acting in the opposite direction to that producing the charge transfer. In the absence of a large space charge field, this electric field determines any further charge transfer between the powder particle and the pipe wall and hence the saturation limit of the charge on the particle. Discharging occurs if the magnitude of the electric field due to the space charge of the powder entering or already in a pneumatic conveying pipework is made larger than the saturation space charge field level which can be acquired by powder in that particular conveying pipe under normal operating conditions. This can be caused by a change in the powder flow regime, for example, by changing from a dilute phase flow to a medium or dense phase flow. The excess charge on the powder particle will be dissipated after travelling through a short section of the conveying pipe.

The influence of the space charge field on the tribo-electrification of powders was investigated by using a corona charge injection device upstream of the first bend of the conveying pipe-work of the Marchwood silo rig. The specific charge density of

HDPE, wheat, sugar and maize starch powders was increased to levels between 2 times and 40 times larger than the specific charge which can be acquired by the powders in the same conveying pipework under normal pneumatic conveying conditions. The excess charge on the powder particles were lost almost completely by the time the particles had passed through the second bend.

In the small scale pneumatic conveying system, because of low mass flow rates and small pipe diameter, the charge on each particle must reach a higher level before an appreciable space charge field is set up in the conveying pipe. The saturation specific charge of HDPE in the small scale rig is much higher (10-40 $\mu C\ kg^{-1}$) than the saturation specific charge density of HDPE at the Marchwood full scale silo rig (0.6-6 $\mu C\ kg^{-1}$) where the mass flow rate is higher. The space charge field of the bulk of the powder travelling through a conveying pipe has therefore an influencing effect on the tribo-electrification of particles. It is thus quite possible to say that the magnitude of the tribo-charging of powders in a large scale pneumatic rig cannot be predicted by simply scaling up the results obtained from a laboratory size rig.

The charge build-up in a silo is related directly to the tribo-electrification of powder particles in the conveying pipework. Controlling the tribo-electric charging in the conveying pipework therefore offers a solution to the problem of charge build-up in silos. To this end the role of the space charge field on the tribo-electrification process was studied by applying a superimposed electric field to control the charging of powder particles colliding with the pipe wall in the presence of such a field.

A section of standard pipework of the Marchwood silo rig was modified by mounting a rod electrode along the axis, enabling a radial electric field to be set up between the rod surface and the inner walls of the pipe, either aiding or in opposition to the natural space charge field of the powder. The tribo-electrification of HDPE and maize starch powder can be controlled by a superimposed

electric field. The radial field at the surface of the rod electrode is higher than the field at the pipe wall, therefore the charge exchange between colliding particles and the rod surface are greater than charge exchanges at the pipe wall, the particle-rod exchange being dominant for the geometry and test conditions at Marchwood silo rig. By controlling the magnitude and sign of the voltage on the rod any charged powder entering the superimposed electric field region may be charged more highly, have its polarity reversed, or may be neutralised. When powder is neutralised the space charge field and the current of the silo drop to negligible levels.

As the influence of superimposed electric field on the charge transfer upon impact of HDPE and maize stach particles is in accordance with the theory of contact charging, where the electric field effectively changes the energy barrier between contacting materials, it is not unreasonable to assume that similar effects would be observed for all materials.

The saturation specific charge of powders in pipes during pneumatic conveying was investigated using both the Marchwood silo rig and the silo scale model. For both rigs, the specific charge of powder increases linearly with the velocity of the transporting air velocity for velocities between about 18 m s^{-1} and 35 m s^{-1}. The powder particles may be charged before entering the conveying pipe-work in which case a plot of specific charge density versus transport air velocity shows a non-zero charge on the powder at zero transport velocity. The specific charge of HDPE reaches a saturation level as the mass flow rate increases to about 5×10^{-4} kg s^{-1} using the small scale rig. At higher mass flow rates, the fall-off of specific charge with mass flow rate is observed. The specific charge of powder particles at Marchwood silo rig shows a trend with the specific charge decreasing as powder mass flow rate is increased.

As mentioned earlier, a scale model of a full size pneumatic conveying installation cannot be used to yield information regarding

the magnitude of the tribo-charging of powders transported in the full size rig. It is, however, possible to predict the trend of the tribo-electrification of powders by using a small scale rig.

A small scale pneumatic conveying rig can be used to compare the charging behaviour of different powders with any well defined powder which may be used as a standard test powder, keeping the operating conditions constant. The information obtained from such a test rig can be used as a guide in the electrostatic hazards analysis of a powder handling operation. For example, it can be inferred whether a particular powder is likely to charge to a higher or lower level compared with the standard test powder.

Transport air relative humidity has a noticeable effect on tribo-electrification of high density polyethylene powder. A plot of the specific charge density of HDPE as a function of the relative humidity of the transport air shows that a large relative humidity (RH $>\approx$ 50%) corresponds to a large negative specific charge and a small relative humidity corresponds to a positive specific charge density.

It is normally only when the powder enters a silo that a significant electrostatic hazard may arise. This is because the dispersed dust cloud of the powder in the silo normally requires less amount of energy to ignite. To evaluate the ignition risk of a dust cloud in a properly earthed conducting silo, the charge accumulated on and the incendivity of discharges from the surface of bulked powder and the dust cloud are studied.

The silo streaming current (charge on powder particles entering silo per unit time) produces a constant surface potential across the bulked powder resistance. The electrical resistance of the bulked powder is directly proportional to the volume resistivity of the bulked powder and inversely proportional to a geometrical constant. The geometrical constant is a function of silo dimensions, angle of response of bulked powder and the fill depth.

From experimental observations, the geometrical constant for Marchwood silo is about one, which implies that the surface potential is a product of silo streaming current and the powder volume resistivity. When the rate at which the charge enters the silo is larger than the rate at which the charge relaxes through the bulked powder, the electric field on the surface of bulked powder will increase and eventually will exceed the breakdown limit causing ionisation of the air. The excess charge is lost by low energy corona or brush discharges along the surface of the bulked powder. In the absence of any charge leakage, an approximate account of the quantity of charge released as a consequence of bulking of insulating powders can be given by comparison of the silo filling current and the silo emptying current.

The transfer and storage of charged powder in a grounded conducting container such as a silo can be modelled by a capacitor representing the bulked charged powder in parallel with a resistor and a discharge gap representing the charge relaxation through the bulked powder and corona or more energetic discharges respectively. The capacitor is charged by the streaming current. The process of charging the capacitor reaches a saturation limit when the dielectric breakdown strength of air is reached. The air ionisation as a result of bulking of charged insulating powders partially neutralises the charged bulked powder until the electric field falls below the ionisation threshold. The powder relaxation time and the streaming current govern the time for the commencement of the onset of air ionisation and the magnitude of the ionisation. The amount of charge released during powder bulking increases as the particle size decreases. The conductivity of the discharge gap space above the bulked powder is a function of the density of ionisation. If the charge per unit time entering a container increases, the number of ion pairs produced increases and so the gap resistance decreases, which in turn results in a decrease in the surface potential.

The surface potential values on the centre of the surface of bulked HDPE pellets in a laboratory powder handling rig for a range of streaming currents show a decrease in the surface potential from

-71.4 kV to -39.7 kV with an increase in the streaming current from about -0.2 μA to -3.6 μA respectively. The probability of ignition of a flammable propane/air/nitrogen atmosphere by discharges from the surface of charged HDPE pellets to metal probes increases to a maximum value at a streaming current of about -1.5 μA and then decreases for larger streaming currents. The largest probabilities of ignition are obtained for specific charge densities between -5 μC kg^{-1} and -10 μC kg^{-1}. The current transients of the discharges which are initiated by lowering an earthed spherical electrode towards the surface of charged HDPE pellets have a total duration of about 350 nano seconds with a rise time of about 50 nano seconds. The current transients show that the ignition of the flammable propane/air/nitrogen atmosphere does not always occur for discharges with the largest charge transfers to the probe. This anomalous behaviour may be attributed to the random character of the brush discharges.

With a few exceptions the discharges to an electrode with a diameter of 12.7 mm are the smallest in magnitude. It has been shown that for the range of specific charge densities between -5.3 μC kg^{-1} and -22.5 μC kg^{-1} the total charge transfer increases as the electrode diameter decreases from 28.6 mm to 12.7 mm. This data, together with the current transient measurements, show that although the magnitude of individual discharges are the smallest for an electrode with a diameter of 12.7 mm, the number of discharges increase considerably.

The highest equivalent electrical energy was achieved with discharges from the surface of HDPE pellets in the laboratory powder handling rig to a spherical electrode of 28.6 mm diameter. The ignition probability was 2%. The streaming current and the pellet flow rate were -1.0 μA and 0.138 kg s^{-1} respectively. The equivalent electrical energy was found to be 4.4 mJ.

Experimental results from the laboratory powder handling rig on HDPE fines showed no clear dependence of the total charge transfer to the probes on powder specific charge density, streaming

current, powder mass flow rate and the probe diameter (12.7 mm, 22.2 mm and 28.6 mm). The total charge transfer to the probes varied between about -200 nC and -660 nC. The magnitude of the discharges from the surface of bulked HDPE fines are considerably smaller than the discharges from the surface of HDPE pellets. For the range of streaming currents (-0.4 μA - -1.7 μA) the measured surface potential of HDPE fines was -11.6 kV ± 3.2 kV.

Electric field measurements of the HDPE fines dust cloud at different heights on the silo wall of Marchwood test rig and above bulked HDPE powder surface show that the tribo-electrification of HDPE powder is bipolar. Both the dust cloud and the bulked coarse particles are negatively charged when the silo streaming current is negative. When the silo streaming current is positive, the fine particle dust cloud is negatively charged and the bulked coarse particles are positively charged. There is, of course, no clear division between fines and coarse powder from a size point of view.

Electric field strengths of HDPE and maize starch dust clouds on the silo wall reached values of 150 kV m^{-1} and 500 kV m^{-1} respectively. The space potential of maize starch dust cloud is also much larger than for HDPE powder. This is due to the higher electrostatic charge on maize starch particles. Despite the relatively high electric field in maize starch dust cloud, however, only corona or brush type discharges were obtained.

The discharge detection by radio frequency techniques provides a method of detecting low energy electrostatic discharges. This method has, however, the disadvantage of neither locating the discharges nor determining the energy of discharges. Radio frequency count rate during transfer of HDPE powder in the Marchwood test silo increases as the specific charge density of HDPE increases. Radio frequency count rate for maize starch, however, shows a decrease in the radio signal count rate as the specific charge increases. Since corona discharges are unlikely to cause a dust cloud ignition, the radio frequency detection system was set to

provide a high sensitivity to low energy discharges (eg, brush discharges) and a low sensitivity to corona discharges. It may be possible that the discharges from the bulking HDPE powder change from corona type discharges into more energetic discharges as the specific charge increases. In contrast the excess charge in the dust cloud of maize starch is dissipated in the form of low energy electrostatic discharges rather than corona discharges at low specific charge densities.

The spherical probe and the gas emitting probe were inserted into the test silo in the regions where previous measurements had shown high electric fields to determine the magnitude and incendivity of the discharges. The charge transfers from HDPE dust cloud and the surface of bulked maize starch to the probes were very small. In comparison, charge transfers of about -200 nC and -100 nC were obtained from the surface of bulked HDPE powder and maize starch dust cloud respectively. Discharges of about -700 nC to the probes were obtained from the surface of bulked HDPE powder when the transport air relative humidity was about 70%. Electrostatic discharges from the surface of bulked HDPE powder and from the maize starch dust cloud ignited the propane/air atmosphere of the gas emitting probe. The minimum ignition energy of the propane/air atmosphere was 0.25 mJ.

Investigation of the relationship between the parameters which influence the electrostatic charging of powders and the ignition risks involved at Marchwood silo rig resulted in "Guidelines on Electrostatic Hazards During Pneumatic Conveying and Storage of Flammable Powders" (see Appendix B).

In summary, the following comments can be made concerning electrostatic explosion risks in earthed and conductive silos in the absence of flammable vapours or gases.

i) Unearthed metal items: There is no risk if no isolated metal can enter the silo.

ii) Bulk powder: There is no electrostatic risk identified from bulked powder with resistivity less than 10^9 Ωm. For powders having resistivity greater than 10^9 Ωm, no risk has been identified provided the minimum ignition energy of the powder exceeds 10 mJ.

iii) Dust cloud: There is a probability of obtaining ignition of a propane/air mixture with a minimum ignition of 0.25 mJ from discharges drawn from a dust cloud with powders of resistivity $\leq 10^9$ Ωm. It was not possible to ignite the dust cloud of powders with resistivity greater than 10^{15} Ωm or propane/air mixture of minimum ignition energy of 0.25 mJ from discharges drawn from the dust cloud.

Chapter 6

Recommendation for future study

CHAPTER 6

RECOMMENDATIONS FOR FUTURE STUDY

The present work has shown the relationship between streaming current, charge density and the probability of ignition of gas/air mixtures by discharges from the bulked high density polyethylene pellets. The following topics/questions which merit further study arise from some of the conclusions of the research.

The incendivity of discharges from the surface of bulked powder and the probability of ignition of gas/air mixtures having different minimum ignition energies should be investigated as a function of the following experimental parameters:

i) Streaming current
ii) Specific charge density
iii) Charge transfer
iv) Powder volume resistivity
v) Particle size.

The relationship between streaming current, specific charge and surface potential for powders with different particle sizes and volume resistivities can be investigated at the same time.

These experiments can be carried out using the electrostatic powder handling rig (see section 2.6) and the gas emitting probe (see section 2.6.5).

Further work is required to investigate the relationship between the charge transfer in a brush discharge and the incendivity of such a discharge.

It is recommended that the proposed experiments which involve flammable gases and powders should include steps to restrict the spread and effects of a possible explosion. It may therefore be

necessary to perform the experiments remotely and in a specially designated area.

It is believed that the above proposed experiments will lead to defining a range of streaming currents, specific charge densities, particle sizes and powder resistivities within which incendive brush discharges with a certain probabilty of occurrence are expected.

References

REFERENCES

Abbott, J.A. (1986) Survey of Dust Fires and Explosions in the United Kingdom 1979-1984, Warren Spring Laboratory, BHMB, Report No. LR 597 (MH).

Bailey, A.G. (1984) Powder Technology, 37, pp.71-85.

Bailey, A.G. (1986) Electrostatics Summer School, Southampton University, 10-12 Sept. 1986.

Bailey, A.G. (1987) Electrostatics 1987, Inst. Phys. Conf. Ser. No. 85, pp.1-12.

Bauser, H., Klopfler, W. & Robenhorst, H. (1970) Advances in Static Electricity, Auxilia, Brussels, Vol. 1, p.2.

Berta, I. & Gastanek, N. (1979) Electrostatics 1979, Inst. Phys. Conf. Ser. No. 48, p.67.

Blythe, A.R. (1979) Electrical properties of polymers, Cambridge University Press.

Blythe, A.R. & Reddish, W. (1979) Electrostatics 1979, Inst. Phys. Conf. Ser. No. 48, pp.107-114.

Boschung, P., Hilgner, W., Luttgens, G., Maurer, B. & Widner, A. (1977) J. Electrostatics, 3, pp.305-310.

Boschung, P. & Glor, M. (1980) J. Electrostatics, 8, pp.205-219.

Boyle, A.R. & Llewellyn, F.J. (1950) Trans. Chem. Ind. 69, p.173.

Butterworth, G. (1979) Electrostatics 1979, Inst. Phys. Conf. Ser. No. 48, pp.97-105.

Cartwright, P., Rose, L. & Singh, S. (1982) An Experimental Study of the Electrostatic Charging Properties of Polyethylene Powder During Pneumatic Conveying, British Petroleum Research Centre, Sunbury, Project No. 140, Report No. 20 956/M, 5 March 1982.

Cartwright, P. & Thorpe, D.G.L. (1982-1983) Silo Progress Annual Report, Wolfson Electrostatics Advisory Unit, Southampton University, Report No. 10/83, 1 January 1982 - 31 January 1983.

Cartwright, P. & Thorpe, D.G.L. (1983) Silo Progress Report, Wolfson Electrostatics Advisory Unit, Southampton University, 15 Dec. 1983.

Cartwright, P., Singh, S., Bailey, A.G. & Rose, L.J. (1985) IEEE Trans. on Industry Applications, Vol. 1A-21, No. 2.

Cartwright, P. (1986) Electrostatics Summer School, 10-12 Sept. 1986, Southampton University, pp.76-87.

Cho, A.Y.H. (1964) J. Appl. Phys., 35, No. 9, p.2561.

Chubb, J.N. (1974) IEE Conf. Gas Discharges, London, Sept. 1974. Publ. 118, p.448.

Chubb, J.N. & Butterworth, G.J. (1979) Electrostatics 1979, Inst. Phys. Conf. Ser. No. 48, pp.85-95.

Chubb, J.N., Erents, S.K. & Pollard, I.E. (1973) Nature, 245, 28 Sept. 1973, p.206.

Cole, B.N., Baum, M.R. & Mobbs, F.R. (1969-70) Proc. Inst. Mech. Engrs., 184, Pt. 3C, p.77.

Cottrell, G.A., Reed, C. & Rose-Innes, A.C. (1979) Inst. Phys. Conf. Ser. No. 48, p.249.

Coventry, P.F. (1984) Ph.D. Thesis, University of Southampton.

CPC/United Kingdom (1985) Bulk Storage of Powdered Starch, Guidance Notes for the manufacture and use of bulk starch silos, Revised Ed., Jan. 1985.

Cross, J. & Farrer, D. (1982) Dust Explosions, Plenum Press, New York.

Cunningham, R.G. (1966) J. Appl. Phys., 37, No. 4, pp.1734-1736.

Davies, D.K. (1967) Static Electrification, Inst. Phys. Conf. Ser. No. 4, p.29.

Davies, D.K. (1969) J. Phys. D.: Appl. Phys., 2, p.106.

Davies, D.K. (1970) Proc. 1st Int. Conf. on Static Electricity, Adv. Stat. Electrification, Vol. 1, p.10.

Davies, D.K. (1973) J. Phys. D.: Appl. Phys., 6, p.1017.

Dixon, G. (1981) Plastics Pneumatic Conveying and Bulk Storage, Ed. G. Butters, Applied Science Publishers Ltd.

Ebadat, V., Bailey A.G. & Singh, S. (1989), to be published in the Journal of Electrostatics.

Eckhoff, R.K. (1975) Combust. Flame, 24, p.53.

Eckhoff, R.K. & Enstad, G. (1976) Combust. Flame, 27, p.129.

Enstad, G.G. (1978) Bergen, Ref CMI No. 78001-1, April 1978.

Felstead, D.K., Rogers, R.L. & Young, D.G. (1983) Inst. Phys. Conf. Ser. No. 66, p.105, The Inst. Phys., Bristol & London.

Field, P. (1982) Handbook of Powder Technology, Dust Explosions, 4, Elsevier.

Field, R.F. (1946) J. Appl. Phys., 17, pp.31-38.

Flain, R.J. (1972) "Pneumatic conveying: how the system is matched to the material", Process Engineering, Nov. 1972, pp.88-90.

Gallo, C.F. & Lama, W.L. (1976) J. Electrostatics, 2, pp.145-150.

Gibson, N. & Lloyd, F.C. (1965) Brit. J. Appl. Phys., 6, pp.1619-1631.

Gibson, N. (1974) Measurement of the Incendivity of Electrostatic Discharges from Non-Conducting, Imperial Chemical Industries Ltd., Organics Division, Research Dept., April 1974.

Gibson, N. & Harper, D.J. (1981) J. Electrostatics, 11, pp.27-41.

Gibson, N. (1983) Inst. Phys. Conf. Ser. No. 66: Session I, Paper presented at Electrostatics 1983, Oxford, pp.1-11.

Gibson, N. (1986) Electrostatic Hazards in the Powder Handling Industries, Electrostatic Summer School, 10-12 Sept. 1986.

Glor, M. (1981) J. Electrostatics, 10, pp.327-332.

Glor, M., Luttgens, G., Maurer, B. & Post, L. (1989) J. Electrostatics, 23 (1989), pp.35-43.

Glor, M. (1984) Int. Symp. Electrostatics. Applications and Hazards, 26-28 Sept. 1984, Southampton.

Glor, M. (1985) J. Electrostatics, 16, p.175-191.

Greason, W.D. (1972) Effect of Electric Fields and Temperature on the Electrification of Metals in Contact with Insulators and Semiconductor, Ph.D. Thesis, The University of Western Ontario, London, Canada.

Harper, W.R. (1967) Contact and Frictional Electrification, Oxford University Press.

Hays, D.A. & Donald, D.K. (1971) Annual Report: Conf. on Electrical Insulation and Dielectric Phenomena (Nat. Acad. Sci., Washington DC, 1972), p.74.

Hays, D.A. (1974) J. Chem. Phys., 61, No. 4, 15 August 1974, p.1455.

Homewood, K.P. & Rose-Innes, A.C. (1979) Static Electrification, Inst. Phys. Conf. Ser. No. 48, p.233.

Homewood, K.P. (1981) J. Electrostatics, 10, p.299.

Huggett, M.R. (1987) Pneumatic, 3. 3rd Int. Conf. Pneumatic Conveying Tech., 24-26 March 1987, p.37.

Hughes, J.F. (1980) Trans. Ins. Marine Engineers, Vol. 92, TM6.

Hull, H.H. (1949) J. Appl. Phys., 20, p.1157.

John, W., Reischl, G. & Devor, W. (1980) J. Aerosol Science, 11, pp.115-138.

Kittaka, S., Murata, Y. & Masui, N. (1977) IEEE Trans. Electr. Insul., Vol. EI-12, No. 5, p.321.

Kornfeld, M.I. (1976) J. Phys. D.: Appl. Phys., 9, p.1183.

Kramer, H. & Asano, K. (1979) J. Electrostatics, 6, p.361.

Krupp, H. (1971) Proc. 3rd Conf. Static Electrification, Inst. Phys. Conf. Ser. No. 11, p.1., London.

Lees, P., Bright, A.W., Smith, J.R., McAllister, D. & Diserens, J. (1980) IEEE Trans. on Industry Applications, Vol. 1A-16, Nov/Dec 1980.

Lewis, B. & Von Elbe, G. (1961) Combustion, Flames and Explosions of Gases, Academic Press Inc., New York & London.

Linstrom, H.J. (1978) Elektrie Germany, 32, No. 3, pp.160-161.

Loeb, L.B. (1958) Static Electrification, Springer, Berlin.

Lovstrand, K.G. (1981) J. Electrostatics, 10, pp.161-168.

Mason, J.S. (1987) Pneumatic, 3. 3rd Int. Conf. Pneumatic Conveying Tech., 24-26 March 1987, p.53.

Masuda, H., Komatsu, T. & Linoya, K. (1976) AIChE Journal, 22, No. 3, pp.558-564.

Masui, N. & Murata, Y. (1983) Japanese J. Appl. Phys., 22, No. 6, pp.1057-1062.

Masui, N. & Murata, Y. (1984) Japanese J. Appl. Phys., 23, No. 1, pp.110-117.

Maurer, B. (1979) Ger. Chem. Eng. 4, pp.189-195.

Maurer, B., Glor, M., Luttgens, G. & Post, L. (1987) Inst. Phys. Conf. Ser. No. 85: Section 3, Paper presented at Electrostatics 1987, Oxford, pp.217-222.

Medley, J.A. (1953) Br. J. Appl. Phys., 4, Suppl. 2, p.528.

Mills, J.S. & Haighton, E.J. (1982) J. Electrostatics, 13, p.91.

Muller-Hillebrand, D. (1963) Investigation at Kopingebro in 1961, Socker-Handlingar II, 18, No.3.

Nordhage, F. & Bäckstrom, G. (1975) Static Electrification, Inst. Phys. Conf. Ser. No. 27, p.84.

Palmer, K.N. (1973) Dust Explosions and Fires, Powder Technology Series, Ed. J.C. Williams, Chapman & Hall Ltd.

Pollard, I.E. & Chubb, J.N. (1975) Static Electrification, Inst. Phys. Conf. Ser. No. 27, p.182.

Pooley, C.M. & Tabor, D. (1972) Proc. R. Soc. A., 329, p.251.

Ramackers, L. (1970) Advances in Static Electricity, Vol. 1, Proc. 1st Int. Conf. on Static Electricity, Austria, pp.370-377.

Robins, E.S., Rose-Innes, A.C. & Lowell, J. (1975) Static Electrification, Inst. Phys. Conf. Ser. No. 27, p.115.

Roff, W. & Scott, J. (1971) Fibers, Films, Plastics and Rubbers, A Handbook of Common Polymers, London, Butterworth.

Salaneck, W.R., Paton, A. & Clark, D.T. (1976) J. Appl. Phys., 47, No. 1, p.144.

Schumann, W.O. (1923) Elektrische Durchbruchfeldstarke von Gasen, Springer, Berlin.

Singh, S. (1983) International Workshop on Electrostatics - How to Manage Electrostatic Problems, Hazards and Applications, 28-30 Sept. 1983, Llandudno, North Wales, UK.

Singh, S. (1983) J. Powder and Bulk Solids Technology 7, 2, pp.13-16.

Singh, S., Ebadat, V. & Bailey A.G. (1987) Pneumat. 3, 3rd Int. Conf. on Pneumatic Conveying Technology, 24-26 March 1987, Jersey, Channel Islands.

Smith, J.R., Lees, P., McAllister, D. & Hughes, J.F. (1983) IEE Proc., Vol. 130, Pt. A, No. 7, November 1983, pp.369-378.

Sone, M., Toriyama, K. & Toriyama, Y. (1974) Applied Physics Letters, 24, No. 3, p.115.

Sprengling, G.R., (1971) Annual Report: Conf. on Electrical Insulation and Dielectric Phenomena (Nat. Acad. Sci., Washington DC, 1972).

Stoess, H.A. Jr. (1970) Pneumatic conveying, Wiley Interscience, New York.

Thorpe, D.G.L. & Cartwright, P. (1982) Silo Progress Report, Wolfson Electrostatics Advisory Unit, Southampton University, Report No. 6/82, 20 April 1982.

Thorpe, D.G.L. (1984) Silo Progress Report, Wolfson Electrostatics Advisory Unit, Southampton University, Report No. 15/84, Oct. 1984.

Thorpe, D.G.L., Singh, S., Cartwright, P. & Bailey A.G. (1985) J. Electrostatics, 16, pp.193-207.

Tolson, P. (1980) J. Electrostatics, 8, pp.289-293.

Tolson, P. (1981) J. Electrostatics, 11, pp.57-69.

Wilson, N. (1983) Inst. Phys. Conf. Ser. No. 66, Session I, Paper presented at Electrostatics 1983, Oxford, p.21.

Wilson, N. (1985) J. Electrostatics, 16, p.231.

Yamamoto, H. & Scarlett, B. (1986) World Congress Particle Technology, April 1986.

Yu, Y.F. (1985) J. Electrostatics, 16, pp.209-217.

Appendices

APPENDIX A

AN INVESTIGATION OF ELECTROSTATIC CHARGING EFFECTS IN HIGH SPEED GAS-SOLIDS PIPEWORK

[Cole, B.N., Baum, M.R., and Mobbs, F.R. (1969-1970)]

ANALYSIS OF ELECTROSTATIC CHARGING OF PARTICLES IN GAS-SOLIDS FLOW

The charging of a solid particle as a result of a collision with the wall of a pipe is assumed to be caused by the establishment of an 'effective' contact potential V_c between the particle and wall of dissimilar materials, and to their subsequent separation. Once the contact potential has been established, the two surfaces act as the plates of a capacitor carrying charges of opposite sign. If the plates are separated rapidly, as by the rebound of the particle from the wall surface, the charges remain on the surfaces leaving both the wall and the particle charged.

The collision between a particle and the wall is assumed to be a bounce and to involve no rubbing or sliding. No stipulation is made as to the means of charge transfer, which may be by electron or positive ion transfer. Metal to metal contact charging is known to be a result of electron transfer, and there is a possibility that charging involving an insulator may be caused by ion transfer. The generalisation is necessary in connection with the present experimental work since it is impossible to ensure that all the surfaces in question are not contaminated. Contamination has a considerable effect on charge transfer between surfaces during contact and separation.

Charge transfer takes place during contact and the subsequent separation of the two contacting surfaces. The charge transfer ceases when a critical distance of separation d_c is reached. This critical distance is assumed to be of the order of the inter-molecular distance of the materials in question. Beyond

the critical distance there is no further charge transfer and, therefore, capacitance magnification of the potential difference between the surfaces occur. Let the potential difference between the materials at separation d_c be V_c, then, assuming the system can be approximated to by a parallel plate capacitor, the total charge transferred during collision and separation is

$$Q_1 = CV_c \qquad (A.1)$$

where $C = \epsilon A/d_c$.

Equation (A.1) assumes that the two materials in contact have no initial charge, and also that there is no external electric field present. In gas-solids pipe flow the particle will have an initial charge owing to previous collisions with the duct wall.

By Gauss's law there will be no field inside the duct as a result of the charge on the duct wall if it is a conductor or a uniformly charged insulator, hence in the case we are considering we may assume an initial charge on the particle alone.

If the particle has taken a positive charge after a previous impact, then, as it approaches the other surface, negative charges will be induced on the previously uncharged wall surface before impact, and a field is established acting in the opposite direction to that producing charge transfer.

The charge transferred is now

$$\frac{\epsilon A}{d_c} (V_c - V_1) \qquad (A.2)$$

Potential Difference between Duct Wall and Particle Resulting from Charges Induced on the Wall of a Conducting Material

In the simple model shown in Figure A.1, it is assumed that the initially charged particle has a charge distribution over its surface which is equivalent to having the total charge concentrated at the centre of the spherical particle. The effect of the wall is

Figure A.1 Model for Establishing the Potential Difference Between the Duct Wall and a Particle, Arising from the Charge Induced on the Wall

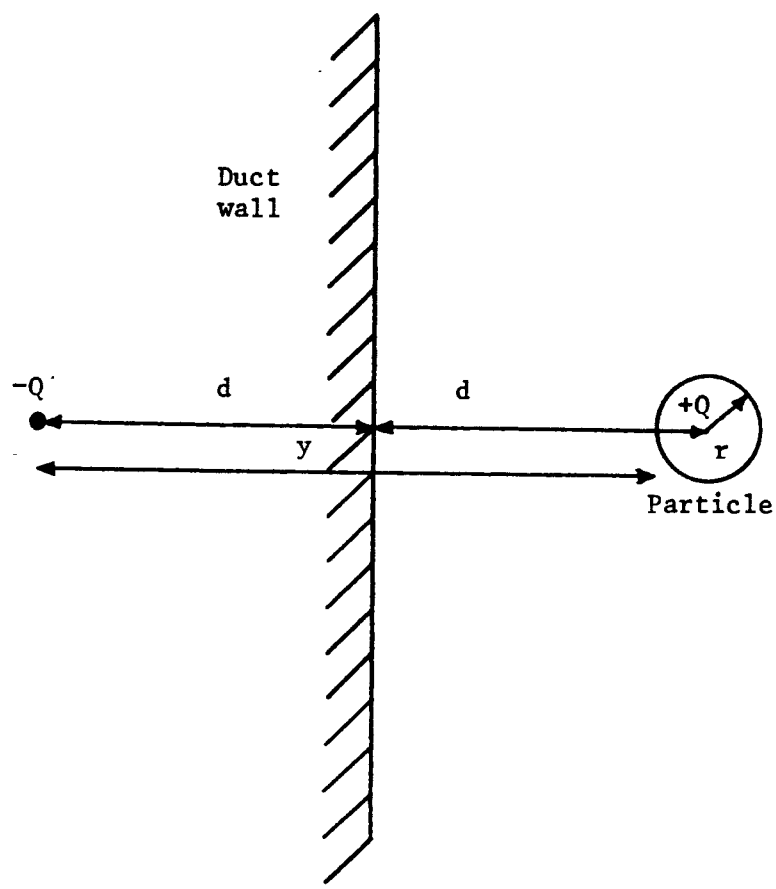

equivalent to the introduction of a mirror image of the charge in the wall.

The potential on the particle surface is, therefore,

$$V_y = \frac{Q_T}{4\pi\epsilon\ (2d-y)} - \frac{Q_T}{4\pi\epsilon y}$$

and the potential at the wall

$$V_{y = d} = 0.$$

At a wall-particle surface separation of d_c

$$V_{y = 2d-r} = \frac{Q_T}{4\pi\epsilon} \cdot \frac{2d_c}{r(d+d_c)}$$

and if $d_c \ll r$, then

$$V_{y = 2d-r} = \frac{Q_T\ d_c}{2\pi r^2 \epsilon} \qquad (A.3)$$

The potential difference between the particle surface and the wall at a separation of d_c is therefore

$$V_1 = \frac{Q_T\ d_c}{2\pi r^2 \epsilon} \qquad (A.4)$$

The contact region is defined as the maximum area over which charge transfer can take place. From Figure A.2 this area, A, is seen to be $\approx \pi a^2$, where

$$a^2 = 2rd_c - d_c^{\,2} \approx 2rd_c$$

In practice, neither the particle surface nor the wall surface will be perfectly smooth and the contact region must therefore be modified to account for surface roughness. The contact area should be modified by a factor f of the order of 10^{-7}, the true contact area being $2\pi\ f\ r\ d_c$. In our sample model this will be taken as the area of an equivalent parallel plate capacitor.

Figure A.2 Definition of Contact Region

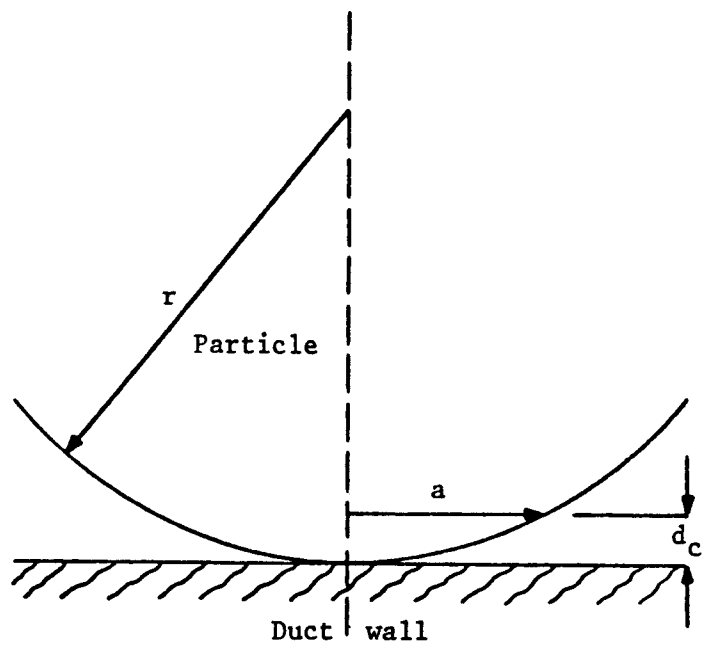

The Effect of the Field Produced by the Bulk of the Charged Particles Passing through the Duct

The potential difference between the particle and the wall may be further reduced by the field caused by the bulk of the charged particles flowing down the duct.

A uniform distribution of positively charged particles is assumed with N particles per unit volume of particle-gas mixture.

At any radius R in a circular pipe, the electric flux density will be

$$D = \frac{\pi R^2 N Q_T}{2\pi R} = \frac{Q_T N R}{2} \qquad \text{(A.5a)}$$

and the electric field strength

$$E = \frac{D}{\epsilon} = \frac{Q_T N R}{2\epsilon} \qquad \text{(A.5b)}$$

The potential difference between the wall and a point d_c from the wall is therefore

$$V_b = \int_{R-d_c}^{R} E\, dR = \int_{R-d_c}^{R} \frac{Q_T N R\, dR}{2\epsilon}$$

$$\approx \frac{Q_T N R d_c}{2\epsilon} \qquad \text{(A.6)}$$

Taking this additional factor into account, the potential difference during separation is now $V_c - (V_1 + V_b)$.

Charge Leakage

No account has so far been taken of the possibility of charge leakage during charging. It will be assumed that this leakage is by conduction while in contact with the wall, and not by gaseous discharge. The pressures involved in the experimental work are of the order of 3 atm, making gaseous discharge unlikely.

The charge at any point on the surface of the particle will have a greater potential with respect to the wall the further the point is from the wall. A potential gradient therefore exists across the particle, encouraging a flow of charge towards the wall. The potential difference across the particle is directly proportional to the charge on the particle. Assuming the time for an impact and separation to be fixed, the charge lost can be expressed as lQ_T, where l is a constant leakage factor related to the resistance of the leakage path.

In the absence of charge leakage the contact potential is $V_c - (V_1 + V_b)$ and the charge added to a particle per collision with the wall can be expressed as

$$\frac{dQ}{dn} = \frac{\epsilon Af}{d_c}\left[V_c - (V_1 + V_b)\right]$$

$$= \frac{\epsilon Af}{d_c}\left(V_c - \frac{Q_T d_c}{2\pi r^2 \epsilon} - \frac{Q_T NRd_c}{2\epsilon}\right) \qquad (A.7)$$

and hence $$\frac{dQ}{dn} = Q_1 - kQ_T$$

where $$Q_1 = \frac{\epsilon AfV_c}{d_c} \quad \text{and} \quad k = \frac{Af}{2\pi r^2} + \frac{NRAf}{2}$$

Introducing charge leakage

$$\frac{dQ}{dn} = Q_1 - kQ_T - lQ_T$$

In the general case where the particle has acquired a charge Q_o before the onset of charging by collisions with the duct wall, the total charge on the particle after a number of collisions is

$$Q_T = Q + Q_o$$

and hence $$\frac{dQ}{dn} = Q_1 - (k+1)(Q+Q_o) = Q_1 - K(Q+Q_o)$$

The solution of this equation is

$$Q = \left(\frac{Q_1}{K} - Q_o \right) (1-e^{-Kn}) \qquad (A.8)$$

and hence $$Q_T = Q+Q_o = \frac{Q_1}{K} (1-e^{-Kn}) + Q_o\, e^{-Kn}$$

The variation of the charge on the particle Q_T with the number of collisions is shown in Figure A.3. The cases considered are $Q_o = 0$, $Q_o > Q_1 K$ with the particle losing charge by leakage, and Q_o of opposite sign to Q.

Figure A.3 Variation of the Charge on a Particle with Number of Collisions

1. $Q_o = 0$
2. $Q_o = 2\frac{Q_1}{K}$
3. $Q_o = -2\frac{Q_1}{K}$

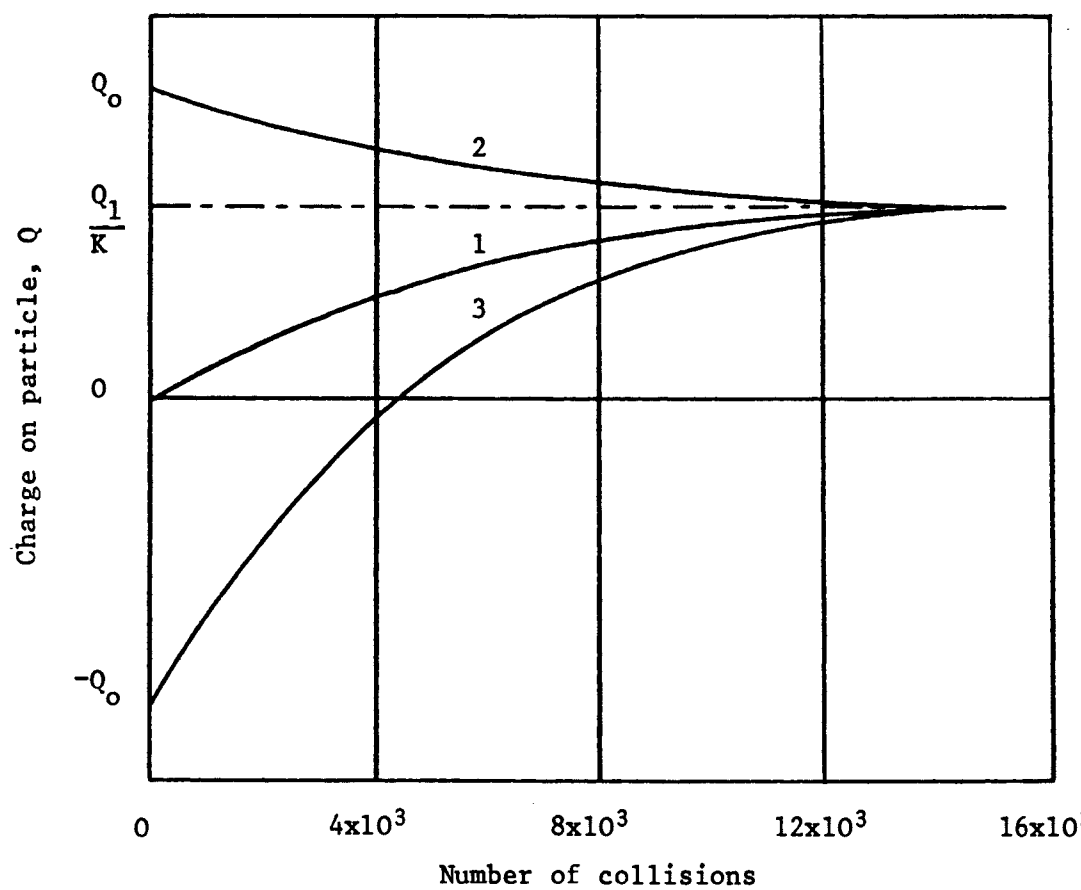

APPENDIX B

GUIDELINES ON THE ELECTROSTATIC HAZARDS DURING PNEUMATIC CONVEYING AND STORAGE OF FLAMMABLE POWDERS

SILO HAZARDS PROJECT

Supervisor : Dr Sampuran Singh
Scientist : Mr Vahid Ebadat
Technician : Mr Richard Ball
Consultant : Professor A G Bailey

INTRODUCTION

It is common practice in industry to pneumatically convey powdered materials into storage silos. In this operation, collisions of particles with other particles and with the conveying system pipework cause the particles to become electrostatically charged. This charging can lead to the production of electrical discharges which may be able to ignite flammable powders. A multi-sponsored (see Acknowledgement and List of Sponsors) research project ("The Silo Project") was undertaken at Southampton University aimed at specifying and determining the relationship between those parameters which influence the electrostatic charging of powders and the ignition risks involved. The experiment set up is described briefly in Appendix B.1.

Inside a silo, electrostatic charge is associated with:

i. unearthed metal items,
ii. the bulk powder,
iii. the dispersed dust cloud.

The research data have indicated that the rate of charge generation is affected by parameters such as:

powder transport speed,
solids loading,
mass flow rate,
relative humidity.

The spark incendivity hazard is affected by the rate of charge generation and by:

powder resistivity,
powder minimum ignition energy and minimum explosible concentration,
plant size and configuration.

The data obtained can be used to assess the ignition risk due to electrostatic charging. All comments apply to metal silos unless otherwise stated, which are of similar dimensions to the test silo (volume = 65 m^3, diameter = 4 m). However, limited measurements carried out on larger concrete silos [1,2] have shown that these recommendations may be extended to larger silos provided expert advice is sought. The electrostatic hazards associated with plastic silos and pipes were not studied, hence are not covered here.

DISCUSSION

i) Metal Items

Data confirm that unearthed metal plant and individual metal items can be a source of discharges that have the capability to ignite a wide range of powders.

Powder entering a silo can readily introduce 10 μC per second of charge (and possibly more with different conveying systems) which, depending on the nature of the powder, can create surface potentials and electrostatic space potentials in excess of observed

maximum values (maximum values observed were 20 kV and 100 kV respectively). If these potentials are allowed to appear on conducting objects which are not earthed, the energy stored (energy available to a subsequent discharge) is given by $\frac{1}{2} CV^2$, where

C = object capacitance
V = potential to which object is raised.

If the discharge energy is greater or equal ($\geq$) to the minimum ignition energy of the dust, an explosion risk results.

Some typical values of capacitance of common objects and the stored energy associated with these objects are listed in the following table:

Object	Capacitance (pF)	Possible Discharge Energy at 16 kV (mJ)	Possible Discharge Energy at 20 kV (mJ)
Major items of plant	100 to 1000	12.8 to 128	20 to 200
Metal drums	50 to 300	6.4 to 38.4	10 to 60
Metal bucket	10 to 100	1.3 to 12.8	2 to 20
Scoop, tin can etc	10 to 20	1.3 to 2.6	2 to 4

Table B.1 **Typical metal items encountered in industry with their capacitance and stored energy**

The data indicate that it is essential to ensure that metal plant is well earthed. The data also indicate the importance of ensuring that metal objects are kept out of the powder. It can be seen from Table B.1 that a small can, for example, sitting on the surface of a bulked insulating powder could, at 20 kV for example, have a stored energy of 2 to 4 mJ and any subsequent discharge would

have sufficient energy to ignite sensitive dusts, as well as the vapours of most flammable solvents, when present in flammable concentrations.

ii) **Bulk Powder**

The data have shown that it is only possible to produce discharges from a bulked powder surface when the product resistivity is high; reference to Table B.2 indicates bulk resistivity greater than 10^9 Ωm is required.

To produce discharges from the bulked powder capable of igniting common flammable solvents (a typical minimum ignition energy is 0.2 mJ) is likely to require product resistivities considerably higher than 10^9 Ωm. In spite of numerous ignition tests there has been only one ignition of the test gas (propane/air) [see Appendix B.1(ii)] and this was obtained from bulked HDPE fine powder (resistivity > 10^{15} Ωm) when using corona charge injection (a charge injection device was used in the transport loop to boost the charge on the powder in order to increase the electrostatic hazard) (see Appendix B.1). However, this one ignition does indicate that it is possible to ignite flammable vapours by means of discharges from the bulked powder and so until further information is available it is advisable to assume that a hazardous situation may arise where powders of resistivity > 10^9 Ωm are bulked especially in the presence of a flammable solvent atmosphere.

It was not found possible to produce a discharge from the bulked powder which was incendive to the dispersed dusts in the test silo. The most sensitive insulating powders tested were HDPE (fines) and phenolic resin, each with a minimum ignition energy of 10 mJ. The test results suggest that the production of a discharge of incendivity equivalent to 10 mJ from bulked powder may not be possible.

During emptying of silos, sometimes powder flow occurs within a channel surrounded by no-flowing material thus creating a

Table B.2 - Broad Summary of Test Results

Product	Powder Reaisitivity ρ (Ωm)	Particle Size Distribution	Minimum Ignition Energy (mJ)	Approx Max Silo Currents (no charge injection) (μA)	Non-incendive Discharges promoted from:		Vapour Ignitions (charge injection in use)	
					Bulk	Cloud/filling 'column'	Bulk	Cloud/filling 'column'
HDPE (fines)	$>10^{15}$	<75 μm	10	+3.5	YES	* (1)	YES (ONE)	* (1)
Wheat	(4 to 6) x 10^{7}	<500 μm	50	+11.0	NO	YES	NO	NO
Sugar	10^{8} to 10^{10}	<106 μm	30	+3.5	YES(2)	YES	NO	NO
Phenol	10^{13} to 10^{15}	* (1)	10	-8.0	YES	YES	NO	NO
Starch	(0.3 to 1.0) x 10^{9}	<50 μm	25	-13.5	NO	YES	NO	YES (ONE)

* (1) No data collected
(2) Very few observed

depression. There is no evidence that the ignition risk increases if such a depression is filled with charged powder.

iii) Dust Cloud

The results obtained show that the highest space potential values measured in the dust cloud of the test silo have occurred with starch and wheat (the two most conducting powders examined). Under tribo-charging, values in excess of 70 kV and 100 kV respectively have been recorded for these products. However, despite many attempts on these products, and using charge injection, only once has it been possible to initiate discharges from cloud to probe (see Appendix B.1) which has ignited a propane-air atmosphere of minimum ignition energy of 0.2 mJ and this was with the starch product. It should be noted that the space potential values obtained with charge injection to starch were similar to those obtained by tribo-charging alone with wheat. The above-mentioned result could be particularly significant where flammable solvent wet powders are introduced pneumatically into large storage silos.

Despite many tests no ignition of the dust clouds of the products tested occurred as a result of the discharges from the dust clouds to the probe.

Two types of discharge might originate from a dust cloud, ie, an incendive spark could be produced either by a lightning-like type of discharge or by an unusually high energy brush type discharge. Work performed by Boschung et al [3], in a larger volume silo than the test silo, suggested that a lightning-like type of discharge is unlikely to be possible. Brush type discharges, however, certainly occur but their incendivity to dust clouds is at present not known.

EFFECT OF PLANT SIZE AND CONFIGURATION

It should be stressed that the above-mentioned results originate from an all metal pneumatic transfer rig of fixed size and geometry.

However, the following comments can be made concerning larger metal and concrete silos.

i) Unearthed Metal Items: these are an electrostatic hazard in any size silo.

ii) Bulk Powder: the electrostatic hazard from bulk powder is expected to be independent of silo size. If powder resistivity is less than 10^9 Ωm, then dangerous surface potentials are unlikely to be produced.

iii) Dust Cloud: theoretical analysis indicates that an increase in silo size may lead to an increase in the probability of producing electrostatic incendive discharges from the dust cloud. However, data collected from limited measurements on large silos do not support this theory. The data support the view of other workers that incendive discharges from the dust cloud in large silos are extremely unlikely.

SUMMARY

An analysis chart of the electrostatic dust explosion hazard inside a metal storage silo similar to the test silo used at Southampton University is shown in Figure B.1.

The following items are considered to be particularly relevant:

i) Unearthed Metal Items: The principal hazard arises from conductors which are not earthed.

ii) Bulk Powder: Provided the silo is adequately earthed there is no risk identified from electrostatic ignition from bulked powder with resistivity less than 10^9 Ωm. For powders having resistivity greater than 10^9 Ωm no risk has been identified provided the minimum ignition energy of the powder exceeds 10 mJ. However, a hazardous situation may arise where powder

Figure B.1 **Electrostatic Ignition Analysis Procedure for Powders in the Absence of Flammable Vapours or Gases**

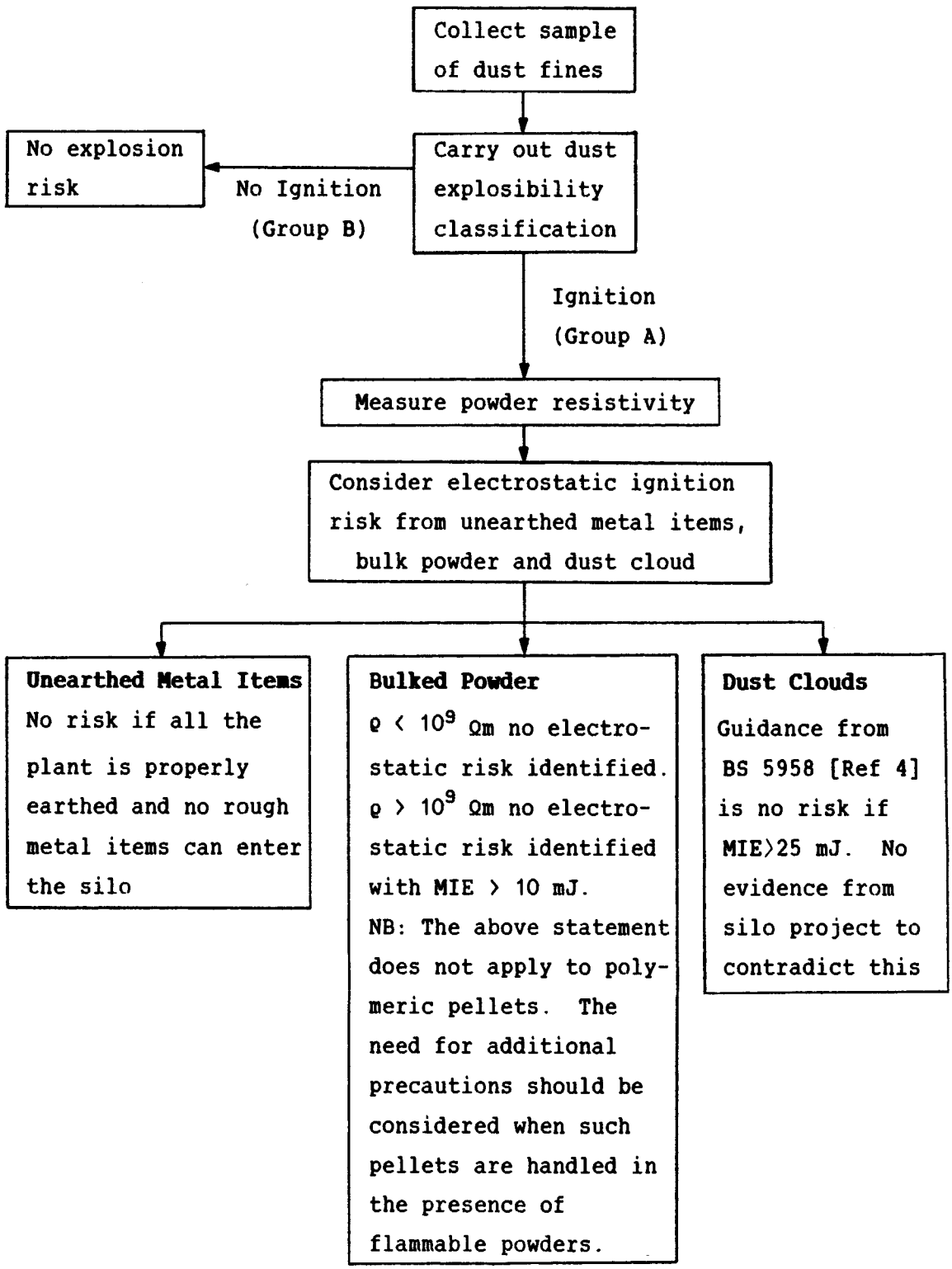

MIE is the minimum ignition energy of dust.

ρ is the product bulk resistivity (Ωm).

of resistivity greater than 10^9 Ωm is bulked in the presence of flammable solvent atmosphere (typical minimum ignition energy value is 0.2 mJ).

NB: The above statement does not apply to polymeric pellets. The need for additional precautions should be considered when polymeric pellets are handled in the presence of flammable powders.

iii) Dust Clouds: For insulating powders ($\rho > 10^{15}$ Ωm) it was not possible to ignite the dust cloud or propane/air mixture from discharges drawn from the dust cloud. The probability exists, however, of obtaining ignition of a propane/air mixture from discharges drawn from a dust cloud with powders of resistivity $\leq 10^9$ Ωm.

The evidence from this study does not contradict the guidance in BS 5958 [4] that there is no ignition risk from an electrostatically charged dust cloud if its minimum ignition energy is greater than 25 mJ.

REFERENCES

[1] Sampuran Singh and P. Cartwright "A Study of Electrostatic Activity in Grain Silos", IEEE Transactions of Industrial Applications Vol. IA-20 No. 4 (1984).

[2] D.G.L. Thorpe, Sampuran Singh, P. Cartwright and A.G. Bailey "Electrostatic Hazards in Sugar Dust in Storage Silos", Journal of Electrostatics, 16 (1985) p.195-207.

[3] Boschung et al, Journal of Electrostatics, 3 (1977) p. 303-310.

[4] British Standards Institute: Code of Practice for control of undesirable static electricity. BS 5958 Part 1:1980 and Part 2:1983.

ACKNOWLEDGEMENT

The silo project was supported by the Wolfson Foundation, the Health & Safety Executive and industrial sponsors. Their financial contribution and provision of test materials is very much appreciated.

Assistance with the experimental work was provided by D.G.L. Thorpe, R. Ball and P. Cartwright over different periods of this project. Technical discussions with P. Cartwright are also gratefully acknowledged.

This document was produced with the assistance of members of the Steering Committee comprising:

J. Abbott (Chairman)	)
J. Barton	) Health & Safety Executive
B. Porter	)
P. Tolson	)
G. Butters	) BP Chemicals Ltd
S. Cooke	)
D. McMahon	) CPC (UK) Ltd
R. Wray	)
B. Devlin	: British Ports Association
N. Gibson	: ICI (Organics) plc

None of this work would have been possible if it had not been for the hard work and dedication of the late Professor Bill Bright in gaining the support of the sponsors.

LIST OF SPONSORS

A list of all sponsors of this project is given below.

Wolfson Foundation, Heath & Safety Executive (UK), BASF (Germany), BP Chemicals (UK), British Ports Association (UK), Cadbury Schweppes (UK), CPC Ltd (UK), Dutch State Mines (Holland), ICI Organics (UK),

Insurance Technical Bureau (UK), National Grain and Feed Association (USA), Tate & Lyle Refineries (UK), United Biscuits (UK), Shell International (Holland), Nordson Corporation (USA), Glaxo Laboratories Ltd (UK), British Sugar plc (UK), Bestobell Mobrey Ltd (UK), Milk Marketing Board (UK).

APPENDIX B.1

EXPERIMENTAL FACILITIES

Figure B.2 shows a schematic of the experimental rig. It consists of two silos positioned side by side, which are linked by a closed system of steel pipes of internal diameter 10 cm. Pneumatic transport is used to transfer powder through about 41 m of conveying pipe from the storage silo to the test silo. Pipe bend radii are 1.5 m and the powder is lifted over a height of 10 m before entering the test silo. The return to the storage silo takes place through a short pipe section. The test silo is electrically isolated from ground and is normally earthed by connection to a micro-ammeter to enable measurement of streaming current. It is fitted with port-holes to accommodate test instrumentation. The system is explosion vented.

Many of the pipe sections can also be electrically isolated from the ground, and these may be earthed through micro-ammeters in order to measure their contribution to the total charge generated on the powder.

The pneumatic transport system operates with a variable speed blower capable of supplying up to 30 m^3 of air per minute. The system is capable of transporting materials at up to 8 kg s^{-1}. The relative humidity in the system can be reduced to 20%.

A corona charge injection device can be used in the transport loop. The injector can supply charge at a rate of up to 200 $\mu C\ s^{-1}$ at 30 kV. It comprises of a solid rod with protruding needles and

Figure B.2 Industrial Scale Electrostatic Hazards Investigation Experimental Rig

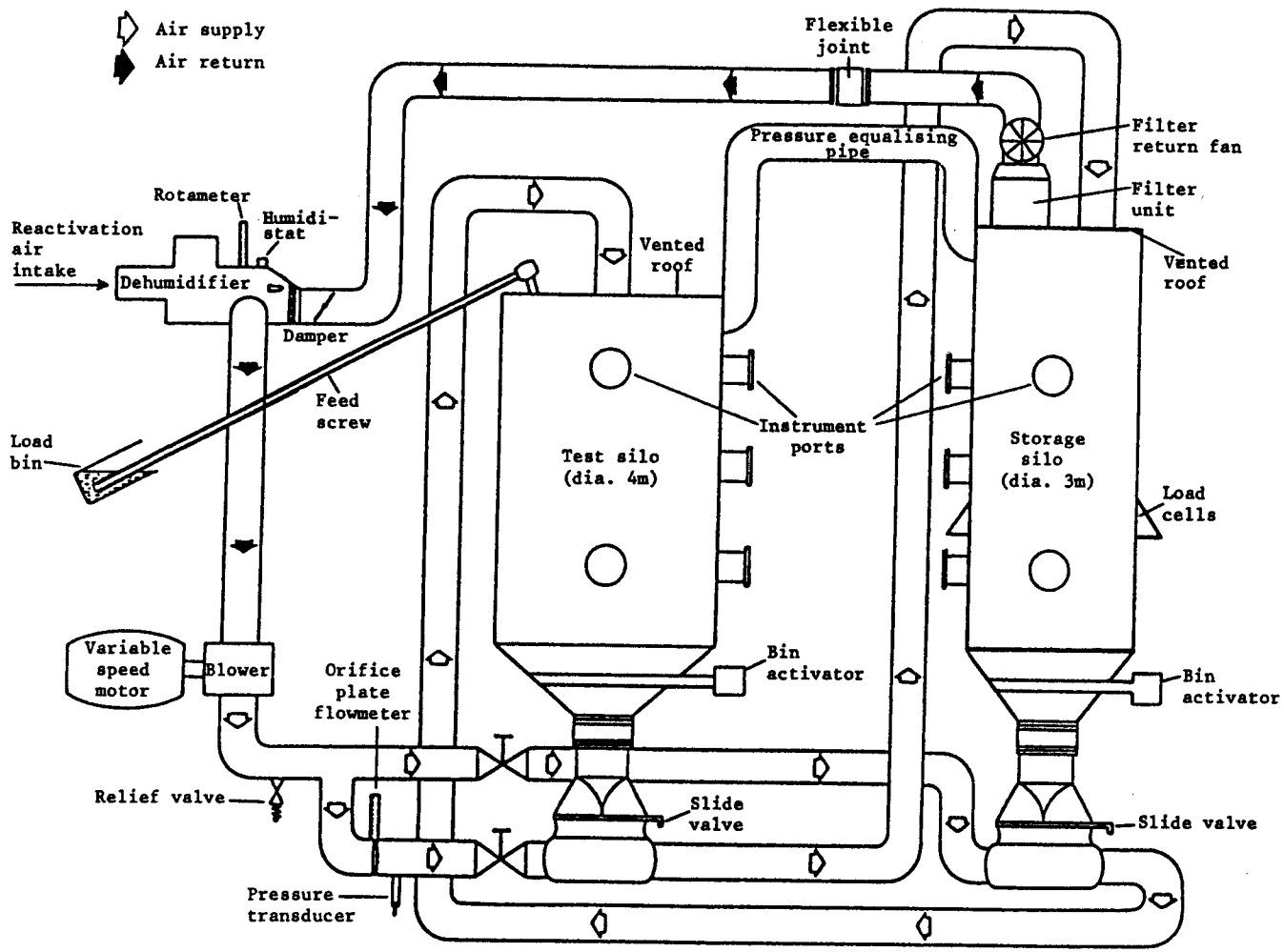

is mounted along the axis of a 45 cm pipe section of the transport loop. This was done to boost the charge entering the test silo above what could normally be achieved with the existing conveying system in order to increase the electrostatic hazard.

Two types of probe can be introduced remotely into the silo to promote discharges.

i) **A Spherical Probe:** Spheres of between 1 and 2 cm diameter are connected to an oscilloscope by a long length of coaxial cable. They are suspended in the air space above the bulked powder to induce discharges from the charged powder cloud. They can also be lowered to the bulked powder in attempts to induce discharges from the bulk.

ii) **A Gas Emitting Probe:** A gas shrouded probe was used to measure the incendivity of discharges. The principle of the measurement is that an earthed metal spherical electrode is immersed in a localised environment of propane/air mixture with a minimum ignition energy of 0.2 mJ. Any electrostatic discharge from the surface of the bulked powder or from the powder dust cloud which is capable of igniting this propane/air mixture is considered to have an equivalent electrical energy of at least 0.2 mJ.